Diss. ETH Nr. 12856

Synthesis and Investigation of Highly Functionalized Derivatives of Buckminsterfullerene

A dissertation submitted to the
SWISS FEDERAL INSTITUTE OF TECHNOLOGY ZÜRICH

for the degree of
Doctor of Natural Sciences

Presented by
Richard F. Haldimann
dipl. Chem. ETH

born July 6, 1969
from Les Brenets, NE

accepted on the recommendation of
Prof. Dr. François Diederich, examiner
Prof. Dr. Peter Chen, co-examiner

Zürich 1998

To my parents,
R.C. Haldimann and 'the true scientist' M.A. Haldimann,
for their support, love and being true friends.

Acknowledgements

I would like to thank Professor François Diederich for his financial and intellectual support of the work described in this dissertation. His visionary suggestions and contagious enthusiasm as well as the freedom in design and execution of the projects have made the past years a great learning experience.

A special thanks goes to Dr. Lyle Isaacs who taught me all the intricate secrets of fullerene chemistry and who showed me how to do scientific research.

Christian Fokas, for his friendship and his great work during his Diplomarbeit.

Ernst-Udo Wallenborn I thank for his perseverance and his chemical and computational brilliance which were instrumental in the theoretical analysis of the reaction mechanism described in chapter 5.

Dr. Marcos Gómez-López, Philipp Lustenberger and Dr. Jeanne Crassous are thanked for proof-reading and providing many valuable suggestions which substantially improved the manuscript.

I thank Prof. Dr. M. Saunders, A. Khong, and Dr. H. Jiménez-Vázquez for recording the ^{3}He-spectra.

I am grateful to all the members of the ETH staff for the outstanding services they provided. In particular I would like to thank Dr. Walter Amrein, Rolf Häfliger, Hans-Ulrich Hediger and Oswald Greter for measuring the mass spectra; Professor Bernhard Jaun, Brigitte Brandenberg, Dr. Monika Sebova, Muriel Hemmi, and Philipp Zumbrunnen for recording some of the NMR spectra.

I thank also Dr. Carlo Thilgen for his help naming the fullerene compounds.

Markus Rüttimann, Robert Epple, Thomas Carell, and in the latter stages of my thesis, Dr. Marcos Gómez-López and Dr. Marc Leduc made sure that working in the lab E39 a was often scientifically challenging but always fun experience.

I am particularly indebted to my mother, my sister Hélène, Markus Rüttimann and his familly, Robert Epple, Lars Burgdorf, and Marc-André (Tonci) Haldimann and the family in the U.S. who stood by me in the darkest period of my life.

A special thanks goes to Gabriela Bischofberger for her support in some of the synthesis, for two wonderful years, and simply for being.

I also would like to thank Prof. Dr. Jack Dunitz for the often amusing sometimes confusing but always very insightful discussions on chemistry and life.

Finally, my heartfelt thanks goes to wonderful Andrea Szekeres for her patience, support and love.

Parts of this thesis have been published or are submitted for publication:

- L. Isaacs R. F. Haldimann, F. Diederich, *Angew. Chem.* **1994**, *106*, 2434-2437; *Angew. Chem. Int. Ed. Engl.* **1994**, *33*, 2339-2342. Tether-Directed Remote Functionalization of Buckminsterfullerene.

- R. F. Haldimann, F.-G. Klärner, F. Diederich, *Chem. Commun.* **1997**, 237-238. Reactions of C_{2v}-Symmetrical C_{60} Pentakis-Adducts with Diazomethane: Regioselective Formation of Hexakis- to Octakis-Adducts and Mechanism of Methanofullerene Formation by Addition of Diazomethane Followed by Dinitrogen Extrusion.

- M. Rüttimann, R. F. Haldimann, L. Isaacs, F. Diederich, A. Khong, H. Jiménez-Vázquez, R.J. Cross, M. Saunders, *Chem. Eur. J.* **1997**, *3*, 1071-1076. π-Electron Ring-Current Effects in Multiple Adducts of $^3He@C_{60}$ and $^3He@C_{70}$: A ^3He NMR Study.

- L. Isaacs, F. Diederich, R. F. Haldimann, *Helv. Chim. Acta* **1997**, *80*, 317-342. Multiple Adducts of C_{60} by Tether-Directed Remote Functionalization and Synthesis of Soluble Derivatives of New Carbon Allotropes $C_{n(60+5)}$.

- F. Cardullo, P. Seiler, L. Isaacs, J.-F. Nierengarten, R. F. Haldimann, F. Diederich, *Helv. Chim. Acta* **1997**, *80*, 343-371. Bis- through Tetrakis-Adducts of C_{60} by Reversible Tether-Directed Remote Functionalization and Systematic Investigation of the Changes in Fullerene Properties as a Function of Degree, Pattern, and Nature of Functionalization.

- E.-U. Wallenborn, R. F. Haldimann, F.-G. Klärner, F. Diederich, *Chem. Eur. J.* **1998**, *in press*. Theoretical Investigation of the Origin of Regioselectivity on Methanofullerene Formation by Addition of Diazo Compounds: A Model Study

Parts of this thesis were presented at international conferences.

- R. F. Haldimann, F.-G. Klärner, F. Diederich, oral presentation held at the *1997 Joint International Meeting* - The 192nd Meeting of *The Electrochemical Society,* Inc. and the 48th Annual Meeting of *The International Society of Electrochemistry* - "Fullerenes: Chemistry, Physics, and New Directions", Paris, 31. August - 5. September, 1997. Reactions of C_{2v}-Symmetrical C_{60} Pentakis-Adducts with Diazomethane: Regioselective Formation of Hexakis- to Octakis-Adducts and Mechanism of Methanofullerene Formation by Addition of Diazomethane Followed by Dinitrogen Extrusion.

- R. F. Haldimann, E.-U. Wallenborn, F.-G. Klärner, F. Diederich, poster presentation at the *36th IUPAC Congress*, Genf, 17. - 22. August, 1997. Regioselective Formation of Hexakis- to Octakis-Adducts and Mechanism of Methanofullerene Formation by Addition of Diazomethane Followed by Dinitrogen Extrusion.

Table of Contents

Table of Contents i
Abbreviations v
Summary viii
Zusammenfassung xi

1. Introduction to Buckminsterfullerene 1

1.1 The Discovery of the Fullerenes 2

1.2 Separation and Characterization of C_{60} and the Higher Fullerenes 3

1.3 Purification of C_{60} 4

1.4 Structural Aspects of the Fullerenes 6
1.4.1 The Isolated Pentagon Rule (IPR) 6
1.4.2 The Molecular Structure of C_{60} 8
1.4.3 The Electronic Structure of C_{60} 9

1.5 The Physical Properties of C_{60} 12
1.5.1 The Heat of Formation 12
1.5.2 Solubility 13
1.5.3 The UV/VIS Spectrum of C_{60} 15
1.5.4 The Ring Currents and Magnetic Properties of C_{60} 17
1.5.5 The ^{13}C NMR Spectrum of C_{60} 20
1.5.6 The IR Spectrum of C_{60} 21
1.5.7 Photophysical Properties 21

2. The Principles of Reactivity of C_{60} 24

2.1 General Considerations of the Reactivity of C_{60} 24

2.2 Charge and Spin Densities in Nucleophilic and Radical Reactions of Buckminsterfullerene 25
2.2.1 Nucleophilic Additions Part 1: Charge Distribution 25
2.2.2 Radical Additions: Spin Localization 27

2.3 Establishing the Reactivity of C_{60} as an Electron Deficient Alkene by Metal Complexation 29
2.3.1 Nucleophilic Additions Part 2: The Bingel Reaction and Related Nucleophilic Cycloaddition Reactions of C_{60} 31
2.3.2 [4+2] Cycloadditions: Diels-Alder Reactions with C_{60} 33
2.3.3 [3+2] Cycloadditions: Additions of Diazo and Azide Derivatives 36
2.3.4 [2+1] Cycloadditions 43

2.4 Multiple Functionalization of C_{60} 46
2.4.1 Nomenclature for Multiple Adducts of C_{60} 46
2.4.2 Octahedral Addition Patterns 47
2.4.2.1 Reversible Multiple Functionalization with Sterically Demanding Addends 47
2.4.2.2 Irreversible Multiple Functionalization with Sterically Demanding Addends 48
2.4.3 Selective Crystallization: The Special Case of the *trans*-1 Addition Pattern and a *cis*-1,*cis*-1,*cis*-1 Tris-Adduct 53
2.4.4 6-5 Open and 6-6 Open Bis-Adducts 55

2.5 *Multiple Radical Additions* 60

3. Investigation of the Chemical Properties of Highly Functionalized Buckminsterfullerene 65

3.1 Tether-Directed Remote Functionalization of C_{60} 65
3.1.1 Introduction 65
3.1.2 Application of the Tether-Directed Remote Functionalization Methodology to a High Yield Synthesis of an *e*-Bis-Adduct of C_{60} 67
3.1.3 Extension of the Tether-Directed Remote Functionalization of C_{60}: from Tris- to Hexakis-Adducts 68

3.2 Investigation of the Chemical Properties of the C_{2v}-Symmetrical Pentakis-Adduct **90** 71
3.2.1 Introduction 71
3.2.2 Exploiting the Confinement of the Reactivity of C_{2v} Symmetrical Pentakis-Adducts of C_{60} to a Single Double Bond: Synthesis of Highly Functionalized Homofullerene Derivatives 73
3.2.2.1 Preliminary Remarks 73
3.2.2.2 Synthesis of a C_s-Symmetrical Monopyrazolino-Hexakis-Adduct of C_{60} 73
3.2.2.3 Establishing the Regioselectivity of the Dinitrogen Extrusion of Highly Functionalized Fullerene-Pyrazoline Derivatives. Part 1: Regiospecific Synthesis of a C_1-Symmetrical Homofullerene Hexakis-Adduct of C_{60} *via* Thermal Dinitrogen Extrusion from a Pyrazoline Precursor 75
3.2.2.4 Establishing the Regioselectivity of the Dinitrogen Extrusion of Highly Functionalized Fullerene-Pyrazoline Derivatives. Part 2: Photolysis of the Monopyrazolino-Hexakis-Adduct of C_{60} 77
3.2.2.5 Regiospecific Synthesis of a Tris-Homofullerene Octakis-Adduct of C_{60} 81
3.2.2.6 Regioselective Synthesis of a Bis-Homofullerene Heptakis-Adduct of C_{60} 84
3.2.2.7 Treatment of the Heptakis-Adduct with Diazomethane: The "Geminal"-Heptakis-Adduct is Not an Intermediate in the Formation of the Octakis adduct 86
3.2.2.8 Attempted Synthesis of a C_{2v}-Symmetrical Tetrakis-Homofullerene Nonakis-Adduct of C_{60} 88
3.2.2.9 Attempted Oxidative Opening of the Fullerene Sphere 89
3.2.2.10 Synthesis of a Bis-Homofullerenediol Heptakis-Adduct of C_{60} 91

3.2.2.11 Attempted Oxidative Cleavage of the Bis-Homofullerenediol Heptakis-Adduct 93

3.3 Investigation of the Influence of the Nature of the Addends on the Chemical Behavior of Highly Functionalized Fullerene Derivatives 94
3.3.1 Template Directed Synthesis of an All Cyclopropanated C_{2v}-Symmetrical Pentakis-Adduct of C_{60} 94
3.3.2 Reaction of an All Cyclopropanated C_{2v}-Symmetrical Pentakis-Adduct with Diazomethane 98
3.3.3 Synthesis of a Five-Fold Cyclopropanated Homofullerene Hexakis-Adduct 99
3.3.4 Synthesis of a Five-Fold Cyclopropanated Bis-Homofullerene Heptakis-Adduct 100
3.3.5 Synthesis of a Five-Fold Cyclopropanated Bis-Homofullerenediol Heptakis-Adduct 102
3.3.6 Attempted Oxidative Cleavage of the Five-Fold Cyclopropanated Bis-Homofullerenediol Heptakis-Adduct 103

3.4 Comparison of the Chemical Reactivity of the Two C_{2v}-Symmetrical Pentakis-Adducts **47** and **90** 104
3.4.1 Theoretical and Experimental Considerations 104
3.4.2 Results and Discussion 107

3.5 Conclusions 109

4. Investigation of the Physical Properties of Highly Functionalized Buckminsterfullerenes 110

4.1 Investigation of π-Electron Ring Current Effects in Multiple Adducts of $^3He@C_{60}$ by ^3He NMR Spectroscopy 110
4.1.1 Prelude: ^1H NMR as a Probe of the Fullerene Chromophore 110
4.1.2 Introduction 112
4.1.3 Experimental Considerations 114
4.1.4 ^3He NMR Results in the Series of the C_{60} Multiple Adducts **124–129** 116
4.1.5 Conclusions 118

4.2 Spectroscopic Analysis of Highly Functionalized Homofullerene Derivatives 119
4.2.1 ^1H NMR Analysis of the Homofullerene and Methanofullerene Derivatives : Effect of the Addition Pattern on the Ring Currents of Highly Functionalized C_{60} Adducts 119
4.2.2 Electronic Absorption Spectroscopy 123

4.3 Conclusions 126

5. Investigation of the Origin of Regioselectivity in Homofullerene Formation by Addition of Diazo Compounds 127

5.1 Introduction: Thermal Dinitrogen Extrusion from a Diazopropane-Xylene- and a Diazopropane-Toluene-Adduct 127

5.2 Determination of the Arrhenius Parameters for the Thermal Dinitrogen Extrusion from a Highly Functionalized Fullerene-Pyrazoline Derivative 130

5.3 Theoretical Investigation of the Thermal Dinitrogen Extrusion From a Diazomethane Benzene Adduct 134
5.3.1 Results and Discussion 135
5.3.1.1 Transition State Geometries and Energies 135
5.3.1.2 Magnetic Properties 140
5.3.1.3 Larger Model System 145
5.3.2 Conclusions 147

6. Experimental Part **149**

6.1 Instrumentation 149

6.2 Materials and General Techniques 150

6.3 Nomenclature 151

6.4 General Procedures for Kinetic Measurements (Sections 3.4 and 5.2) 151

6.5 Experimental Details 152

6.6 Kinetic Data for the Dinitrogen Extrusion from **95a** 180

7. Literature **183**

Abbreviations

Ac	acetyl
AM1	Austin model 1
B3LYP	Becke 3 functional with Lee, Yang, Parr parametrization
br.	broad
calc.	calculated
CAS	Chemical Abstract Service
CASSCF	complete active space SCF
CC	column chromatography
conc.	concentrated
CSGT	continuous set of gauge transformations
d	day, doublet (NMR)
DBU	1,8-diazabicyclo[5.4.0]undec-7-ene
o-DCB	ortho-dichlorbenzene
dec.	decomposition
DFT	density functional theory
DMA	9,10-dimethylanthracene
DMSO	dimethylsulfoxide
eq.	equivalent
ESR	electron spin resonance
FAB	fast atom bombardment
fcc	face centered cubic
GIAO	gauge independent atomic orbital
h	hour
hfi's	hyperfine interactions
HMO	Hückel molecular orbital
HOMO	highest occupied molecular orbital
HPLC	high performance liquid chromatography
IPR	isolated pentagon rule
IR	infrared spectroscopy
ISC	intersystem crossing
LDI	laser-desorption-ionization
LSDA	local spin density approximation
LUMO	lowest unoccupied molecular orbital

M	molarity (moles l^{-1})
m	medium IR band, multiplet (NMR)
max	maximum
$MEMN_3$	methoxyethoxymethyl azide
min	minute
mM	milli-molar (10^{-3} moles l^{-1})
MM2	molecular mechanics method 2
MM3	molecular mechanics method 3
MNDO	modified neglect of differential overlap
MO	molecular orbital
m.p.	melting point
MP2, MP4	first and fourth order Møller-Plesset perturbation
NMR	nuclear magnetic resonance
PAHs	polycyclic aromatic hydrocarbons
Ph	phenyl
Piv	pivaloyl
PM3	parametric method 3
q	quartet (NMR)
RT	room temperature
ref.	references
R_f	retention factor (TLC)
RHF	restricted Hartree-Fock
s	strong IR band, singlet (NMR), second
sat.	saturated
sc	simple cubic
SCF	self-consistent field
$SEMN_3$	trimethylsilylethoxymethyl azide
sh	shoulder (UV/VIS)
soln.	solution
t	triplet (NMR)
TBAI	tetrabutylammonium iodide
THF	tetrahydrofurane
TLC	thin layer chromatography
TOF	time-of-flight
TsOH	toluene-4-sulfonic acid
UPS	ultraviolet photoelectron spectroscopy

UV	ultraviolet
VIS	ultraviolet/visible
vs.	versus
w	weak IR band
ZPE	zero point energy

Summary

Chapter 1 introduces the reader to the fullerenes. A short historical account of the discovery of C_{60} and the higher fullerenes is given. This Section is followed by a description of the molecular and electronic structure of C_{60} which presents the basis for understanding its chemical behavior. The chapter closes with a description of the most important physical and spectroscopic properties of buckminsterfullerene.

Chapter 2 gives an overview of the chemical behavior of C_{60}. The chapter is divided into two sections: in the first section, some examples of monofunctionalizations of the fullerene core are presented. The main focus is on the types of reactions which are relevant for the work described in the chapters 3 – 5. In the second part of the chapter, the formation of higher adducts of C_{60} is presented and some simple frontier orbital arguments which explain the formation of certain preferred addition patterns are presented.

Chapter 3 presents the results of the investigation of the chemical reactivity of highly functionalized adducts of C_{60} such as pentakis-adduct **90a**. The investigations revealed that the thermal and photolytical dinitrogen extrusion from the highly functionalized fullerene pyrazoline **95a** exhibits the same regiochemical behavior as the parent fullerene pyrazoline $C_{61}N_2H_2$. In particular, thermal dinitrogen extrusion from **95a** proceeds regiospecifically producing exclusively the corresponding 6-5 open homofullerene derivative. Exploiting both the high regioselectivity of the thermal dinitrogen extrusion from **95a** as well as the fact that the reactivity of the fullerene chromophore in C_{2v}-symmetrical pentakis adducts such as **90a** is confined to a single double bond, allowed the synthesis of a series of highly functionalized homofullerene derivatives including the octakis-adduct **98a**. The final part of the Chapter discusses the influence of the nature of the addends on the reactivity of the fullerene towards 1,3-dipolar cycloaddition with diazomethane. It was found that replacing the two fused cyclohexene moieties of **90a** with cyclopropane addends results in a more pronounced dienophile character of the reactive double bond of the residual fullerene chromophore.

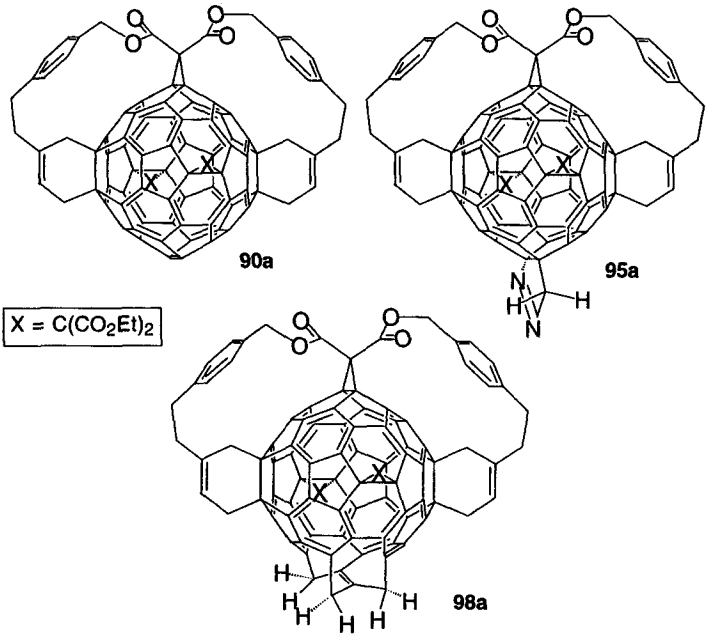

Chapter 4 presents the results of the investigation of the spectroscopic changes which occur upon increasing functionalization of the fullerene sphere. The first Section gives an account of the effect of multiple functionalization of the fullerene core on the magnetic properties of the respective $^3He@C_{60}$-derivatives, as revealed by ^3He NMR spectroscopy of a series of bis- to hexakis-adducts of C_{60}. It was found that the ^3He resonances of the endohedral fullerene complexes are strongly shielded with respect to the resonance of $^3He@C_{60}$. However, whereas the shielding of the endohedral ^3He atom increases strongly upon mono- and bis-functionalization of $^3He@C_{60}$, it is not substantially enhanced by further functionalization. The results were interpreted in terms of π-electron ring current effects based on theoretical work of *Haddon et al.* The second and third Section of the Chapter presents a ^1H NMR and UV/VIS spectroscopic analysis of highly functionalized homofullerene derivatives, respectively. The change in the chemical shifts of the protons placed atop former five and six membered rings, respectively, can be rationalized with the same ring current model used for the interpretation of the ^3He NMR study.

In Chapter 5, the origin of the regioselectivity of the thermal dinitrogen extrusion from fullerene diazoadducts of fullerenes is investigated. A concerted orbital symmetry controlled [$2\pi_s + 2\pi_s + 2\sigma_a + 2\sigma_s$] mechanism is proposed to be responsible for the observed high regioselectivity of such reactions. The mechanistic hypothesis is based on the strong similarity between the thermal and photochemical reactivity of fullerene-fused pyrazolines, such as **95a**, and diazopropane-xylene and -toluene adducts investigated previously by *Klärner et al.* (Section 1 and 2 of the Chapter). The final Section of the Chapter presents a thorough theoretical investigation of such a mechanism on a model system by *ab initio* and density functional methods. The calculations indicate that the thermal dinitrogen extrusion from the model system, namely, the cycloadduct of diazomethane and benzene, proceeds *via* an aromatic transition state rather than a diradical intermediate.

Zusammenfassung

In Kapitel 1 wird die Stoffklasse der Fullerene vorgestellt. Als erstes wird ein kurzer historischer Überblick über die Entdeckung von C_{60} und der höheren Fullerene gegeben. Im weiteren folgt die Beschreibung der molekularen und elektronischen Struktur von C_{60}, welche die Grundlage für das Verständnis der chemischen Reaktivität dieses Moleküls darstellt. Abschliessend werden die wichtigsten physikalischen und spektroskopischen Eigenschaften von Buckminsterfulleren diskutiert.

Kapitel 2 gibt eine Übersicht über die chemischen Eigenschaften von C_{60}. Das Kapitel wurde in zwei Unterkapitel aufgeteilt. Im ersten Teil des Kapitels werden einige Monofunktionalisierungen des Fullerens vorgestellt. Es werden dabei hauptsächlich Reaktionen diskutiert, welche für die in den Kapiteln 3 – 5 vorgestellten eigenen Arbeiten relevant sind. Im zweiten Teil des Kapitels wird die Synthese von höheren Addukten von C_{60} beschrieben. Die bevorzugte Entstehung gewisser Additionsmuster wird anhand von einfachen Grenzorbitalbetrachtungen diskutiert.

Im Kapitel 3 werden Untersuchungen zur Reaktivität von hochfunktionalisierten C_{60}-Addukten, wie z. B. Pentakis-Addukt **90a**, vorgestellt. Es zeigte sich, dass die thermische und photolytische Stickstoffabspaltung des hochfunktionalisierten Fullerenpyrazolins **95a** mit der gleichen Regiochemie erfolgt wie diejenige des entsprechenden Mono-Adduktes $C_{61}H_2N_2$. Insbesondere die thermische Stickstoffextrusion von **95a** erfolgt regiospezifisch und führt ausschliesslich zum entsprechenden 6-5 offenen Homofullerenderivat. Die hohe Regioselektivität der thermischen Stickstoffextrusion von **95a** einerseits, und die Tatsache, dass die Reaktivität des Pentakis-Adduktes **90a** auf eine Doppelbindung reduziert ist andererseits, ermöglichte die Synthese einer Serie von hochfunktionalisierten Homofullerenderivaten, wie z. B. des Oktakis-Adduktes **98a**. Im letzten Teil des Kapitels wird der Einfluss der chemischen Natur der Addenden auf die Reaktivität der entsprechenden Fullerenderivate in 1,3-dipolaren Cykloadditionsreaktionen mit Diazomethan untersucht. Es stellte sich dabei heraus, dass der Ersatz der anellierten Cyklohexenringe von **90a** durch Cyklopropanringe den dienophilen Charakter der reaktiven Doppelbindung des verbleibenden Fullerenchromophors erhöht.

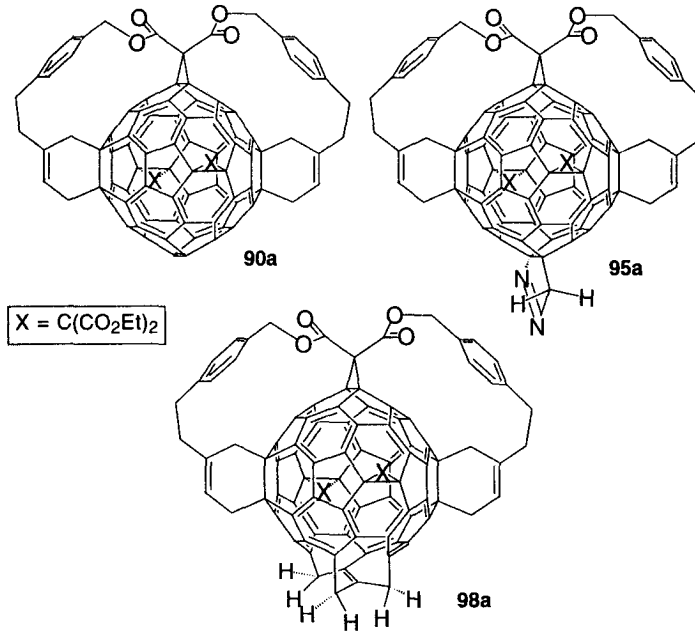

Kapitel 4 beschäftigt sich mit den Veränderungen der spektroskopischen Eigenschaften von Fullerenderivaten, welche durch zunehmende Funktionalisierung des Fullerens auftreten. ^{3}He-NMR-spektroskopische Analyse einer Serie von Bis- bis Hexakis-Addukten von ^{3}He@C_{60} (endohedraler ^{3}He Komplex von C_{60}) zeigte den Einfluss mehrfacher Funktionalisierung auf die magnetischen Eigenschaften des Fullerens auf. Dabei zeigte sich, dass die ^{3}He-Kerne im Innern der untersuchten endohedralen Fullerenkomplexe im Vergleich zu ^{3}He@C_{60} stark abgeschirmt sind. Doch während Mono- und Bis-Funktionalisierung von ^{3}He@C_{60} zu einer starken Abschirmung des endohedralen ^{3}He-Kerns führt, erfährt die ^{3}He-Resonanz der höher funktionalisierten endohedralen Fullerenaddukte kaum eine weitere Hochfelverschiebung. Diese Beobachtungen wurden basierend auf einem von *Haddon et al.* entwickelten Ringstrommodel für C_{60} erklärt. Im zweiten und dritten Teil des Kapitels werden die Resultate von ^{1}H-NMR und UV/VIS spektroksopischen Untersuchungen von hochfunktionalisierten Homofullerenderivaten vorgestellt. Die Veränderung der chemischen Verschiebung der Protonen, die sich über den fünf- bzw. den sechsgliedrigen Ringen der entsprechenden Fullerenderivate befinden, konnte

anhand des gleichen Ringstrom-Models erklärt werden, welches für die Interpretation der ^{3}He NMR Untersuchung verwendet worden war.

In Kapitel 5 wird der Mechanismus der thermischen Stickstoffextrusion von Diazo-Addukten von Fullerenen untersucht. Ein konzertierter, orbitalsymmetrisch kontrollierter [$2\pi_s + 2\pi_s + 2\sigma_a + 2\sigma_s$] Mechanismus wird vorgeschlagen, um die beobachtete hohe Regioselektivität solcher Reaktionen zu erklären. Diese mechanistische Hypothese basiert auf der grossen Ähnlichkeit des photolytischen und thermischen Verhaltens von Fullerenpyrazolinen, wie z. B. **95a**, mit jenem der Diazoalkan-Addukte von Xylol und Toluol, die von *Klärner et al.* untersucht worden sind (Teil 1 und 2 des Kapitels). Im letzten Teil des Kapitels wird der vorgeschlagene Mechanismus anhand eines Modelsystems in einer theoretischen Studie mittels *ab initio*- und Dichtefunktionalrechnungen untersucht. Die Resultate dieser Rechnungen weisen darauf hin, dass die thermische Stickstoffabspaltung vom gewählten Modellsystem (dem Cykloaddukt von Diazomethan und Benzol) bevorzugt über einen aromatischen Übergangszustand und nicht über ein diradikalisches Zwischenprodukt verläuft.

1. Introduction to Buckminsterfullerene

Organic chemists have had a long standing affection towards highly symmetrical molecular structures. Many man years of intense research went into the synthesis of cubane [1] and later into the synthesis of dodecahedrane [2] (Figure 1a) and b). However, it was not by the means of a carefully planned design and long synthesis but by simple laser vaporization of graphite in an inert atmosphere that an icosahedral cluster of 60 carbon atoms, now called buckminsterfullerene (Figure 1c), was discovered joining graphite and diamond as the smallest member of a third form of pure carbon: the fullerenes.

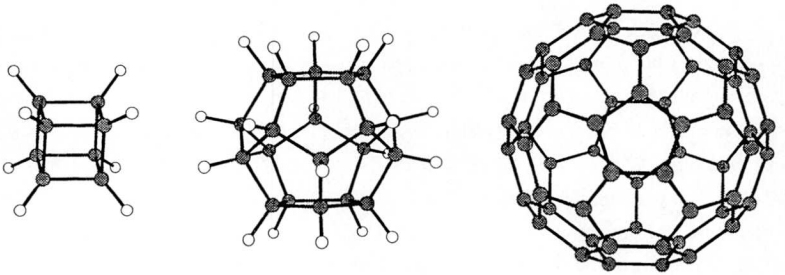

Figure 1. Structures of the caged hydrocarbons a) cubane, b) dodecahedrane, and c) the carbon allotrope buckminsterfullerene, with their respective symmetry.

The fascinating physical and chemical properties of buckminsterfullerene such as the discovery of the superconductivity of alkali metal doped C_{60}[1] [4], and the possibility of chemical functionalization of the fullerene core have made C_{60} to arguably the most interesting single molecule of the past years and has led to the publication of thousands of scientific papers on its physical and chemical behavior. To the organic chemist, the unique structure of C_{60} make this molecule ideal for exploring and understanding the chemical reactivity of this new carbon allotrope, and, taking advantage of its physical properties, to synthesize new materials and derivatives for biological applications.

[1]The superconductivity in doped C_{60} will not be discussed in this thesis, for a review on the topic see refs. [3].

The following Chapter gives a short historical account of the discovery of C_{60} and the higher fullerenes. Some emphasis is put on the description of the molecular and electronic structure of C_{60}, which is necessary for the understanding of its chemical behavior. This Section is followed by a description of its most important physical and spectroscopic properties. How the organic functionalization of the fullerene core can alter some of the properties of C_{60} will be discussed. This aspect is of the foremost importance in order to comprehend the properties of fullerene derivatives presented in later Chapters.

1.1 The Discovery of the Fullerenes

The discovery of the fullerenes began in 1984 when *Kaldor* and co-workers produced carbon clusters by laser vaporization of graphite followed by cooling of the resulting plasma by high pressure helium [5]. The carbon clusters were photoionized by a second UV laser and analyzed by laser desorption (LD) time of flight (TOF) mass spectrometry. Clusters with up to 190 carbon atoms could be detected. In the range of n = 1-30, an ion signal was detected for each C_n. However, above n = 40 only clusters containing an even number of carbons were observed. To explain this even only feature of the spectrum in the range C_n $40 \leq n \leq 100$, the authors proposed the formation of carbyne, a high temperature form of carbon [5]. Interestingly, the peaks corresponding to C_{60} and C_{70} were slightly dominant, but were not specifically mentioned in the paper. In 1985, *Kroto et al.* carried out experiments aimed at understanding the mechanism by which long-chained carbon molecules are formed in interstellar space [6]. Using a very similar experimental setup to the one utilized by *Kaldor* and co-workers, they found that under certain clustering conditions the peak corresponding to the C_{60}^+-ion completely dominated the spectrum, the next most prominent peak being the C_{70}^+-ion. In order to explain the apparent stability of the cluster containing 60 carbon atoms, the authors suggested a truncated icosahedral structure containing 12 pentagons and 20 hexagons (Figure 1c). They argued that only a spherical structure with all carbon sp^2-valences satisfied could account for the apparent stability of this carbon cluster. It was decided to name C_{60} Buckminsterfullerene after the American architect *R. Buckminster Fuller* whose geodesic domes are constructed on the same principle, solely with pentagons and hexagons, and had inspired the authors to propose the soccer-ball structure of C_{60}. However, laser vaporization of graphite did not allow to produce macroscopic quantities of this new carbon allotrope, necessary for the investigation of its physical and chemical properties. Nevertheless,

Buckminsterfullerene C_{60} was discussed widely in the literature and rapidly became the subject of many theoretical investigations.

Five years after the discovery of C_{60} was reported [6], the astrophysicists *Krätschmer, Huffman* and co-workers developed a simple method for the production of macroscopic amounts of fullerenes [7]. By evaporating graphite through resistive heating in an inert atmosphere of helium (~ 100 Torr), they were able to produce carbon soot containing a few weight per cent of C_{60}. The infrared (IR) spectrum of the fullerene containing graphitic soot showed four absorptions [8] in good agreement with the previously calculated values for I_h-C_{60} [9-12] indicating the presence of C_{60} in the soot mixture. The fullerenes were subsequently separated from the soot by extraction with benzene and filtration, removing the insoluble soot particles. The extract was analyzed by mass spectrometry which showed a strong peak at *m/z* 720, the mass required for C_{60}, and a less intensive peak at *m/z* 840 corresponding to C_{70} [7].

1.2 Separation and Characterization of C_{60} and the Higher Fullerenes

Soon after the first report of the macroscopic production of fullerenes [7], pure samples of C_{60} and C_{70}[2] were isolated from the soot mixture after column chromatography on neutral alumina [14,15]. The ^{13}C nuclear magnetic resonance (NMR) spectrum of C_{60} showed only one peak [14,15] giving further evidence for the proposed I_h-symmetrical structure of C_{60}. A mixture of C_{60} and C_{70} produced an additional five lines in the ^{13}C NMR spectrum supporting the previously proposed [16,17] D_{5h}-symmetrical rugby ball structure of C_{70} (Figure 2).

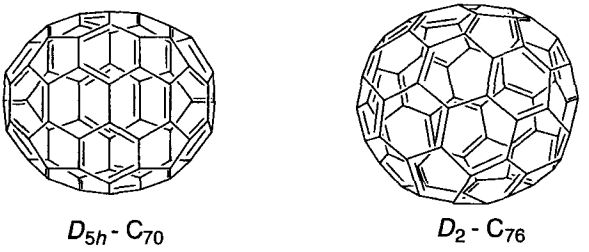

Figure 2. Structures of D_{5h}-symmetrical C_{70} viewed perpendicular to the C_5-axis, and of one enantiomer of the D_2-symmetrical C_{76} viewed along one of the three C_2-axes.

[2]The ratio of C_{60} to C_{70} in the raw fullerene extract produced by resistive heating of graphite is around 85:15 [13].

Further investigation of crude fullerene extracts produced by resistive heating of graphite, by *Diederich et al.*, revealed the presence of C_{76}, C_{84}, C_{90}, and C_{94} in a total amount of 3 to 4% by weight [18]. Subsequently, the isolation of pure samples of C_{76} and of two isomers of C_{78} by reversed phase HPLC was reported by *Diederich* and co-workers [19]. Analysis of the ^{13}C NMR spectrum of the C_{76} sample showed the presence of a single D_2-symmetrical isomer (Figure 2).

The two C_{78} fractions were shown to contain a C_{2v}- and a D_3-symmetrical isomer, respectively, in a 5:1 ratio (Figure 3) [20]. A third isomer of C_{78}, the C_{2v}'-C_{78} isomer was later identified by *Kikuchi et al.* in a mixture with the D_3- and C_{2v}-isomers of C_{78} [21][3] . Recently a D_2-C_{80} isomer was isolated. It is the least abundant isomer of the higher fullerenes C_{76} to C_{96} [25]. A mixture of at least three C_{82} isomers was also isolated, which contained a C_2-symmetrical isomer [21]. The D_2- and D_{2d}-symmetrical isomers of C_{84} were originally characterized as a mixture [18,21] and have been very recently separated by recycling HPLC [26]. The structure of D_{2d}-C_{84} has been confirmed by X-ray analysis of an iridium complex of the isomer (Figure 3) [27].

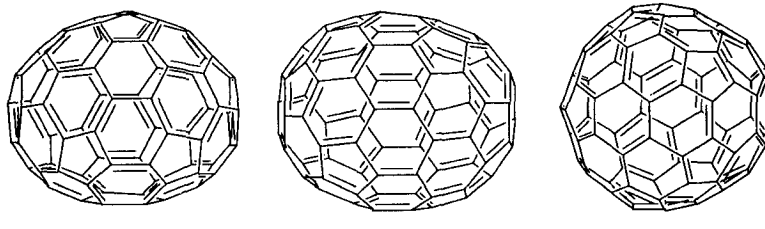

Figure 3. Structures of the two characterized isomers of C_{78}, (only one enantiomer of the minor, D_3-symmetrical, isomer is depicted), and of one isomer of C_{84}, with their respective symmetry.

1.3 Purification of C_{60}

The earliest separations of C_{60} from C_{70} and the higher fullerenes were achieved by column chromatography of the crude fullerene extract on neutral alumina using either pure hexane [14,15] or mixtures of hexane and toluene (95:5 *v/v*) as eluant [18]. However, the low solubility of fullerenes in these solvent mixtures severely limited the

[3]The C_{2v}'-C_{78} isomer as well as the C_{82} isomers are not or hardly present in the crude fullerene mixture obtained by resistive heating of graphite [20] but are found in the soot produced by the arc vaporization method (for arc vaporization methods see [22-24]).

amount of material that could be processed. Addition of as little as 10% of toluene to the mobile phase caused C_{60} and C_{70} to elute together [28]. The use of pure toluene as eluant in which C_{60} is about 60 times more soluble (see 1.5.2.) than in hexane was first reported by *Meier et al.* who used an automated high pressure gel permeation chromatography setup, thus allowing larger scale isolation of C_{60} with a purity >95% [28]. The most powerful chromatographic separation of C_{60} from the higher fullerenes was reported by *Isaacs et al.* [29] based on a procedure previously reported by *Tour* and co-workers [30]. Using a mixture of silica (SiO_2) and activated charcoal as the stationary phase and pure toluene as eluent allowed the isolation of 1.5g C_{60} by plug filtration (Figure 4) starting from 2.5g of crude fullerene extract in 15 min. with 1-3% $C_{60}O$ as the only detectable impurity [29].

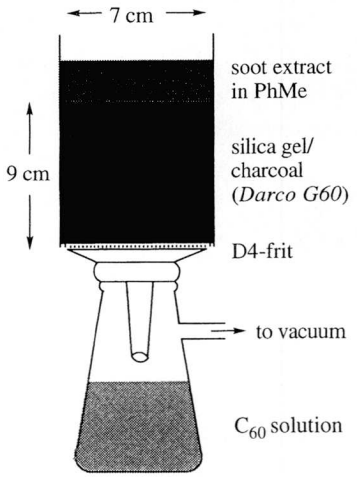

Figure 4. Plug filtration setup for C_{60} purification on activated charcoal/silica gel using PhMe as the eluent.

Large scale purification of C_{60} is also possible by crystallization exploiting the different temperature dependencies of C_{60} and the higher fullerenes [31] (see 1.5.2).

The improved purification techniques and optimized production conditions [13,32] have lowered the price of pure C_{60} from ~1200 \$/g in 1991 to ~35 \$/g in 1997[4], and pure C_{60} (purity > 99.5%) is now routinely purchased in larger quantities for laboratory use.

[4] *Material and Electrochemical Research Corp. (MER Corp.)* Tuscon, Arizona (AZ) 85706, USA.

1.4 Structural Aspects of the Fullerenes

1.4.1 The Isolated Pentagon Rule (IPR)

All fullerenes isolated and characterized so far are constructed solely by five- and six membered rings. According to the *Euler theorem*, a spherical structure is obtained by introducing 12 pentagons into a plane of hexagons. Thus, all carbon clusters with twelve pentagons which fulfill the equation $n = 20 + 2k$ ($k \neq 1$) in which n is the number of carbons and k the number of hexagonal faces can lead theoretically to spherical fullerene type structures. Furthermore, all fullerenes must have an even number of carbon atoms, since enlarging a fullerene by the addition of a hexagon adds two carbons to the structure. For C_{60} there are 1812 [33] and for C_{70} there are 8149 [34] distinct structural isomers which obey the above equation, yet only I_h-C_{60} and D_{5h}-C_{70} are formed. Analysis of all the structural possibilities of C_{60} and C_{70} reveals that the ones found are the only isomers which do not require two or more fused pentagons as a structural subunit. In fact, in all the fullerenes characterized so far[5] the 12 pentagons are isolated from another (*i.e.* they are surrounded by hexagons), leading to corannulene type substructures (Figure 5).

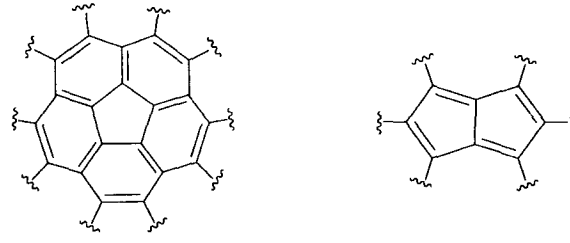

Figure 5. Illustration of a) the corannulene substructure which is a basic motif in C_{60}, and b) a pentalene substructure which violates the isolated pentagon rule and has not been observed in any of the isolated fullerenes.

This rule has been identified as structural requirement for stable fullerene structures and has been termed the *isolated pentagon rule* (IPR) [17,36,37]. C_{60} is the

[5]Very recently the isolation of the D_{6h}-symmetrical isomer of C_{36} which has twelve abutting pentagons has been reported. However, electron diffraction of crystallites of C_{36} implied an intermolecular 'bond length' of 1.7 Å, indicating that it exists as polymer in the condensed phase and is only in the gas phase a discrete molecule [35].

smallest fullerene which can obey the IPR. The next larger IPR-fullerene is C_{70}, which explains the absence of isolable fullerenes between C_{60} and C_{70}. For C_{76+2n} ($n \geq 0$) the number of IPR satisfying isomers rises sharply [38], leading to the possibility of having more than one low energy structure for a fullerene of a given size [34]. The rationalization of the *isolated pentagon rule* is that fused pentagons in a fullerene structure lead to high local curvature in which the bonding geometry of the carbon atoms involved deviates strongly from the ideal planar sp^2-hybridization geometry (Figure 6).

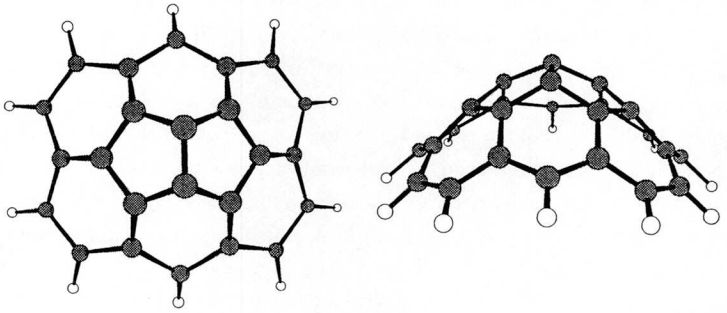

Figure 6. Illustration of the curvature enforced on the central sp^2 carbons by the IPR violating motif of two fused pentagons surrounded by six hexagons a) viewed from the top, and b) from the side. (MM2 [39] minimized structure)

This leads to large σ-strain as well as reduced π-overlap and therefore to high energy structures [36,40]. Furthermore, it has been suggested that abutting pentagons will lead to antiaromatic pentalene type substructures (Figure 5b) further decreasing the thermodynamic and kinetic stability of such isomers[6] [37,45-47]. Recent calculations have indicated that the absence of fused pentagons is probably primarily due to σ-strain[7] which amounts to at least 30 kcal mol^{-1} per pentalene subunit [34,40,46-48].

[6]This argument must be treated with caution since it was based on Hückel calculations which have not been very successful at describing the aromaticity (or the lack thereof) of C_{60} [36,37,41-44].

[7]*Fowler* and co-workers have found a linear relationship between the total energy of fullerene isomers and the energy arising solely from pyramidalization of the carbons of the respective isomers, indicating that electronic destabilization of non-IPR fullerene isomers plays only a minor role for their thermodynamic stability [34,40].

1.4.2 The Molecular Structure of C_{60}

Attempts to determine the precise geometrical structure and bond lengths of unfunctionalized C_{60} by X-ray analysis were challenging due to the fast isotropic rotation of the nearly spherical C_{60} molecules in the face centered cubic (fcc) crystal lattice at room temperature as well as long range disorder in the crystals [49,50]. The first X-ray structures were obtained from C_{60} derivatives in which the addend prevented rotation of the C_{60} core in the crystal [51,52]. Structural information of pristine C_{60} was obtained by low temperature X-ray analysis [53-55], by gas phase electron diffraction [56], by solid state ^{13}C NMR measurements [57] and by X-ray analysis of C_{60} solvates[8] [58-60]. These measurements confirmed the nearly spherical icosahedral structure of C_{60} with a mean atom to atom diameter of ≈7.1 Å. Taking into account the *van der Waals* radius of the carbon atoms, the diameter is ≈10.4 Å and the cavity is ≈3.5 Å (Figure 7). Even though the high symmetry of C_{60} makes all carbon atoms chemically equivalent, there are two different types of bonds by which they are connected, namely, those fusing two six membered rings (6-6 bonds) and those fusing a six and a five membered ring (6-5 bonds). The 30 6-6 bonds of C_{60} are found to be significantly shorter (between 1.385 Å [55] and 1.401 Å [56]) than the 60 6-5 bonds (between 1.455 Å [54] and 1.467 Å [53]) resulting in a mean bond length alternation of ≈0.06 Å.

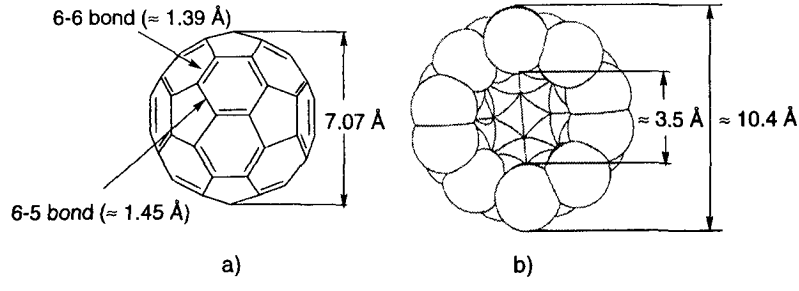

Figure 7. Representation of a) the two different types of bonds in C_{60}, their respective bond lengths, nucleus-to-nucleus diameter, and b) the diameter of the cavity and of the molecule taking into account the *van der Waals* radius of the carbon atoms shown in a space filling model of C_{60} cut in half.

[8] Intercalation of suitable molecules such as ferrocene [58] into the interstices of the C_{60} crystal lattice slows the isotropic rotation of the C_{60} molecules and thus allows X-ray analysis at room temperature.

This highly anisotropic distribution of the π-electrons is reflected in the low temperature X-ray structures of C_{60} [53-55]. Orientational ordering occurs below 261 K resulting in a simple cubic structure in which the C_{60} molecules are packed in such a way that the π–electron rich 6-6 bond faces the center of an electron poor pentagonal ring [54,55].

1.4.3 The Electronic Structure of C_{60}

When describing the electronic structure of C_{60} two obvious features must be considered: i) the spherical shape of the non-planar conjugated system will force the rehybridization of the 60 sp^2 carbon atoms, increasing the *s*-character of the hybrid π-orbitals, and ii) the high I_h symmetry of the molecule will lead to highly degenerate molecular orbitals. The second of these features relates to the topological properties of the π-system and is conveniently treated with Hückel molecular orbital (HMO) theory [61].

i) First the effect of the pyramidalization of the sp^2 fullerene carbon atoms shall be discussed. The POAV1 (*p* orbital axis vector) analysis [62] of C_{60} yields an angle between the σ and *p* atomic orbitals ($\Theta_{\sigma p}$) of 101.6°, leading to a $s^{0.093}p$ hybridization for the *p* orbital and $sp^{2.278}$ hybridization for the three σ orbitals [63], which is in part responsible for the high electron affinity of C_{60} [3a,64-67]. This can be visualized with the help of simple MO analysis (Figure 8): Upon pyramidalization of a carbon-carbon double bond, the overlap of the *p* AO's decreases which raises the energy of the HOMO, but, because the AO's of in the LUMO are out of phase, lowers the energy of the LUMO, and the magnitude of the change in its energy is greater than that in the HOMO. In addition, as the *p* AO's acquire *s* character on pyramidalization, the energy of the hybrid AO's decreases, since *s* orbitals are lower in energy than *p* orbitals. This effect stabilizes both the HOMO and the LUMO. In the case of the HOMO, this latter effect works in the opposite direction from the decreased overlap between the hybrid AO's, thus accounting for its small energy increase. In contrast, in the case of the LUMO the two effects are additive, thus leading to a large decrease of its energy (Figure 8) [68,69].

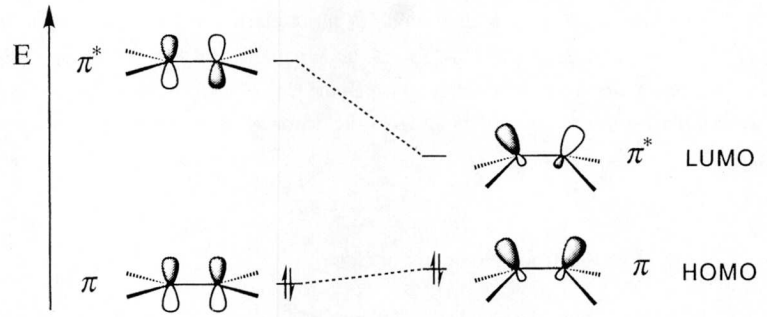

Figure 8. Simplified MO representation of the effect of pyramidalization of the frontier orbitals of a carbon-carbon double bond.

Rehybridization through pyramidalization also changes the shape and orientation of the π orbitals of buckminsterfullerene, such that the larger lobes of the *p*-orbitals are directed towards the outer surface[9] and are tilted away from both the five- and six-membered rings of C_{60} [72]. Furthermore, the reduced overlap of the *p* AO's forming the π-bonds in C_{60} might be in part responsible for the poor delocalization of its double bonds. Localization of the π-electron density to the 6-6 bonds of C_{60}, already apparent from the structural analysis of C_{60} (Section 1.4.2.), is also reproduced in calculations at all levels of theory[10] [73]. Thus, the best Kekulé structure of C_{60} is that in which all double bonds are placed exocyclic to the five membered rings, producing [5]radialene and 1,3,5-cyclohexatriene substructures, respectively, within the fullerene sphere (Figure 9).

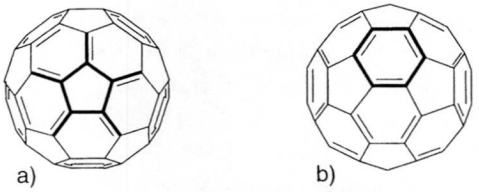

Figure 9. Illustration of a) the [5]radialene substructure, and b) the 1,3,5-cyclohexatriene substructure in C_{60}.

[9]The rehybridization due to pyramidalization of the benzene carbon atoms in [2.2]paracyclophane shifts the π–electron density to the outside face of the molecule [70] and, similar to C_{60}, readily undergoes addition reactions with carbenes [70,71].

[10]For example, simply taking the ratio of *Kekulé* structures which place a double bond at a 6-6 junction and 6-5 junction respectively, to the sum of all *Kekulé* resonance structures of C_{60} produces π-bond orders of 11/25 for the 6-6 bonds and 7/25 for the 6-5 bonds, respectively [43].

Violating this structural motif in C_{60} derivatives by placing a double bond into a five membered ring has been calculated to cost 8.5 kcal mol^{-1} [74,75]. Considering both the effects of the pyramidalization of the fullerene carbon atoms as well as the strong tendency for bond localization, C_{60} is best described as conjugated, highly strained, electron deficient polyalkene; a description which explains many aspects of its chemical reactivity discussed in Chapter 2.

ii) A more general picture of the electronic structure of C_{60} is obtained by simple HMO analysis, which produces 30 bonding and 30 antibonding π molecular orbitals allowing to fill all the 60 π electrons into the bonding orbitals producing a closed shell electron configuration. Approximate energy levels of the π–like orbitals are obtained directly by diagonalization of the Hückel Hamiltonian, which yields a fivefold degenerate h_u HOMO separated by a substantial energy gap from the energetically low lying triply degenerate t_{1u} LUMO and the triply degenerate t_{1g} LUMO+1 (Figure 10) [63,76-78]. This picture of the frontier orbitals is upheld at more sophisticated, all electrons including levels of theory with the exception that the h_g and g_g molecular orbitals which are degenerate within the Hückel approximation become the HOMO–1 and the HOMO–2, respectively, but remain closely spaced [79-81] . The closed shell electron configuration of C_{60} combined with the HOMO-LUMO energy gap of 1.5-2.0 eV [82], are the main electronic reasons for the kinetic stability of buckminsterfullerene.

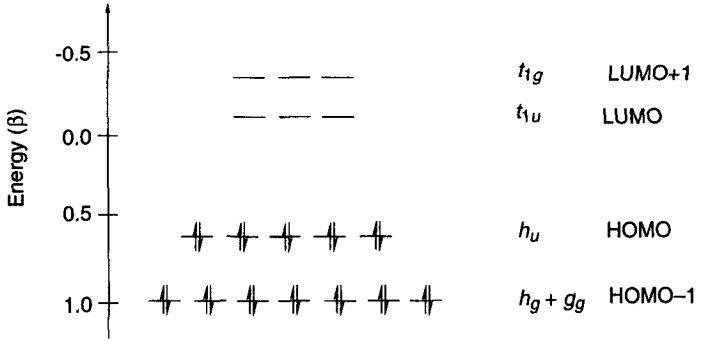

Figure 10. Representation of the *Hückel* molecular orbitals for C_{60} (in units of β) showing the HOMO–1, HOMO, LUMO, LUMO+1 and their respective symmetries

Simple HMO treatment of I_h-C_{60} also correctly predicts the high electron affinity and electrochemical behavior of buckminsterfullerene. As a result of the non-alternant nature of C_{60}, the HOMO and the LUMO are placed unsymmetrically around the origin of energy ($\beta = 0$), indicating facile reduction by adding an electron into the energetically low lying LUMO but difficult oxidation, since this necessitates the removal of electrons from the closed shell system with a significantly stabilized HOMO (Figure 10). Indeed, in accord with this description, C_{60} shows a high gas phase electron affinity of 2.666±0.001 eV [83,84] and can undergo 6 electrochemically reversible, one electron reductions, producing C_{60}^{6-}, thereby filling the triply degenerate t_{1u} LUMO [85-87]. In contrast, the gas phase ionization potential lies at ≈7.6 eV [88-91] and only one reversible single electron oxidation of C_{60} at the very positive potential of +1.26 V *vs.* ferrocene is possible [92,93].

1.5. The Physical Properties of C_{60}

1.5.1 The Heat of Formation

Combustion experiments have allowed to determine the heat of formation of the two most abundant fullerenes C_{60} and C_{70} [94-98] providing benchmark data against which the accuracy of theoretical predictions can be judged. When combined with the experimentally determined enthalpy of sublimation [99,100], four measurements [94,96-98] yielded values of ΔH_f°(g) of approximately 600 kcal mol^{-1}. With a heat of formation ΔH_f°(g, C) of 10.16 kcal mol^{-1} per carbon atom [98] C_{60}, is thermodynamically much less stable than the other two carbon allotropes graphite (ΔH_f°(g, C) = 0.0 kcal mol^{-1}) and diamond (ΔH_f°(g, C) = 0.4 kcal mol^{-1}). Calculations by *Schmaltz et al.* [37] indicate that about 80% of the heat of formation is due to rehybridization of the sp^2-carbons in C_{60} as a result of the non-planar nature of the molecule. The ΔH_f°(g, C) value of C_{70} (9.65 kcal mol^{-1})[11] is lower by 0.51 kcal mol^{-1} per carbon atom compared to that of buckminsterfullerene [98] which can be rationalized by reduction of the strain induced by the twelve five membered rings through incorporation of five additional six membered rings. However, C_{60} is kinetically very stable: Ion beam experiments of C_{60} ions showed no evidence for impact induced fragmentation on silicon or graphite surfaces at impact energies greater than 200 eV, which by far exceeds the energy at which benzene and naphthalene have already completely fragmented [101][12]. C_{60} may therefore be best described as a high

[11] A lower value (9.03 kcal mol^{-1}) for ΔH_f°(g, C) of C_{70} has been reported [96].

[12] At 90 eV the parent ion of naphthalene is less than 5% of the scattered ion intensity [101]

energy structure which is located in a deep potential well on the energy hypersurface. The kinetic stability of C_{60} is primarily due to the caged σ-structure. This becomes apparent in the mass spectra of highly functionalized fullerenes which tend to loose their addends regenerating C_{60}.

Comparison of the calculated values for the heat of formation of C_{60} produce very diverging results with differences of up to *ca.* 690 kcal mol^{-1} (for MMP2 and AM1). Inspection of Table 1 reveals a rather poor performance of the semiempirical methods: MNDO, PM3, and AM1 give extremely large values for $\Delta H_f^\circ(g)$ by overestimating the strain energy of C_{60} by a wide margin, whereas the molecular mechanics method MM3 [102] reproduces the experimental value very well. The good performance of MM3 in fullerene chemistry is quite general, illustrating that σ-strain parameters determine both the energy and geometry of the respective molecules. *Ab initio* calculations with a modest size basis set at the HF/STO-3G level also yield reasonable estimates for the standard enthalpy of formation of C_{60}.

Table 1. *Calculated and experimental heat of formation of C_{60}.*

Method	$\Delta H_f^\circ(g)$ (kcal mol^{-1})	Method	$\Delta H_f^\circ(g)$ (kcal mol^{-1})
MMP2 [103]	286	AM1 [104,105]	973
PM3 [74,105]	812	MNDO [106,107]	869
MM3 [108]	574	HF/STO-3G [105]	582
HF/STO-3G [108][a)]	625	Exp. [96]	597.5 ± 4.0
Exp. [94]	599.6 ± 2.1	Exp. [97]	598.7 ± 3.8
Exp. [95]	633.1 ± 3.8	Exp. [98]	609.6 ± 3.6

a) Single point calculation using MM3 optimized geometry of C_{60}.

1.5.2 Solubility

The solubility of C_{60} has been systematically investigated in a wide variety of solvents [109-117]. The solubility is generally quite low, because solvation of C_{60} requires disruption of many solvent-solvent interactions[13] which is not adequately compensated by the interaction of the solvent with C_{60}, since the latter has a rigid

[13]The molar volume of crystalline fcc-C_{60} (429 cm^3 mol^{-1}) is significantly larger than the molar volume of any of the investigated solvents [109].

geometry and no permanent dipole moment. Some general trends for the solubility of C_{60} have been established, which are apparent upon inspection of Table 2. In polar or H-bonding solvents like methanol, acetonitrile, tetrahydrofurane (THF), and dimethylsulfoxide (DMSO), C_{60} is almost completely insoluble. It is sparingly soluble in alkanes like pentane, hexane, and decane, with the solubility increasing with the number of carbon atoms. The solubility in chloroalkanes is generally higher than in alkanes, 1,1,2,2-tetrachloroethane being the best among the halogenated hydrocarbons [117]. Aromatic solvents are generally substantially better, and solubility can be further increased by substitution with electron donating groups such as methoxy and methyl groups. Substitution with electron withdrawing groups such as nitro and nitrile groups, reduces the solubility. Generally, enhanced solubility can be achieved by increasing the molecular size of the solvent; thus electron rich naphthalenes are among the best solvents for C_{60}. A notable exception to these trends is CS_2, which C_{60} solubilizes quite well but is neither very large nor does it show any strong interaction with the C_{60} chromophore, which is a frequently observed effect of good solvents of C_{60} (see Section 1.5.3).

Table 2. Solubility of C_{60} in different solvents at 25 °C [117].

Solvent	Concentration (mg ml^{-1})	Solvent	Concentration (mg ml^{-1})
Polar solvents		*Aromatic Hydrocarbons*	
water	1.3×10^{-11}	benzene	1.70
methanol	3.5×10^{-5}	*Benzene-derivatives*	
acetonitrile	0.000	benzonitrile	0.41
ethanol	0.001	nitrobenzene	0.80
acetone	0.001	benzaldehyde	0.41
tetrahydrofuran	0.06	toluene	2.90
Alkanes		anisole	5.60
n-pentane	0.005	chlorobenzene	7.00
cyclohexane	0.036	1,2,3,5-tretramethylbenzene	20.80
n-hexane	0.043	1,2-dichlorobenzene	27.00
n-decane	0.071	*Naphthalene-derivatives*	
Haloalkanes		1-methylnaphthalene	33.00
chloroform	0.16	1-chloronaphthalene	51.00
dichloromethane	0.26	*Miscellaneous*	
carbon tetrachloride	0.32	carbon disulfide	7.90
1,1,2,2-tetrachloroethane	5.30	pyridine	0.89

C_{60} shows an anomalous temperature dependency of its solubility [31,111,113,114,116,118]. In solvents like hexane, toluene, CS_2, and *o*-xylene the solubility increases upon heating reaching a maximum between 0 °C and 30 °C.

Further heating to the respective boiling points of the solvents reduces the solubility by a factor of 2-3 [111,116]. In contrast, the solubility of C_{70} does not decrease upon heating in the mentioned solvents [116]. As a practical consequence, almost pure C_{60} precipitates out of a saturated solution of crude fullerenes upon heating providing a very simple method for the large scale purification of C_{60} [31].

1.5.3 The UV/VIS Spectrum of C_{60}

Due to the I_h-symmetry of C_{60}, only electronic transitions between the closed shell ^1A_g ground state to upper electronic states of ^1T_u symmetry are allowed [80,119,120]. The energetically lowest, symmetry allowed excitations are from the HOMO to the LUMO+1 and from the HOMO–1 to the LUMO, respectively (*cf.* Figure 10). The singlet-singlet HOMO-LUMO transition is forbidden, but can be induced by molecular vibrations of the proper symmetry (for an excellent detailed analysis of the UV/VIS spectrum of C_{60} see [119]). The UV/VIS spectrum of C_{60} in n-hexane [14,15,119] is dominated by the orbitally allowed HOMO-LUMO+1 excitations giving rise to strong absorptions in the 190 - 410 nm region with three broad main bands at 211 nm ($\varepsilon \approx 158000\ M^{-1}\ cm^{-1}$), 256 nm ($\varepsilon \approx 174000\ M^{-1}\ cm^{-1}$), and 328 nm ($\varepsilon \approx 52500\ M^{-1}\ cm^{-1}$) and a weaker band at 404 nm ($\varepsilon \approx 2950\ M^{-1}\ cm^{-1}$). In the visible region, the spectrum shows a highly transparent region between 420 and 440 nm which is followed by a weak broad band ($\varepsilon \leq 750\ M^{-1}\ cm^{-1}$) between 440 to 635 nm with two main maxima at 598 and 543 nm. The weak absorptions in the visible region have been assigned to the forbidden HOMO-LUMO transitions [119,120]. The highly resolved UV/VIS spectrum recorded by *Leach et al.* [119] in hexane shows a very weak absorption maximum at 620 nm which they have assigned to the energetically lowest singlet-singlet HOMO-LUMO transition, corresponding to 2.0 eV for the solution HOMO-LUMO gap[14].

The combination of transparency in the blue (420 - 440 nm) and in the red region (> 635 nm) is responsible for the characteristic purple color of diluted C_{60} solutions. The color and UV/VIS spectrum is solvent and, to a lesser degree, concentration dependent [122]. This phenomenon originates mainly from differences in the absorption intensity in the 400 - 500 nm range and is most pronounced for solvents which interact with C_{60} (*i.e.* solvents in which C_{60} is very soluble like electron rich

[14]The optical band gap does not directly correspond to the calculated HOMO-LUMO gap of the unperturbed C_{60} due to configuration interaction [121]

aromatics) [123,124]. Very similar effects have been observed in guest-host complexes of C_{60} with calix[5]arene derivatives [125].

Removing a double bond from C_{60} through functionalization has a strong influence on the color and the UV/VIS spectrum, producing wine red (for cyclopropanated structures such as **1** (Figure 11) to brown solutions (for larger ring fused fullerene derivatives) of the respective fullerene derivatives. The symmetry allowed intense absorptions in the UV range of their spectra (at 257 and 329 nm) are hardly shifted by the functionalization but are less intense, consistent with going from a 60 to a 58 π electron system [126]. Very characteristic for all 6-6 closed monoadducts is the appearance of a sharp band at $\approx$ 430 nm and a weak absorption band at $\approx$ 695 nm [29,127,128]. According to calculations, the band at $\approx$ 430 nm corresponds to the absorption at 404 nm of the unfunctionalized C_{60} and the band at $\approx$ 695 nm arises from the formerly symmetry forbidden HOMO-LUMO transition which becomes allowed due to the reduction of the symmetry of the molecule [129]. In contrast, the UV/VIS spectrum of the 6-5 open homofullerene[15] which retains the 60 π electron system in the expanded structure **2** (Figure 11) is practically superimposable to that of C_{60} [131] indicating that the electronic structure is very similar to that of the parent fullerene.

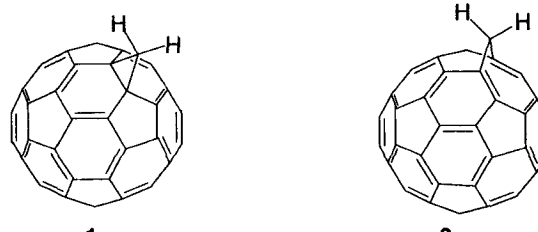

1 **2**

Figure 11. Structure of the 6-6 closed C_{60} monoadduct **1** in which the methylene moiety bridges a former 6-6 double bond and of the 6-5 open isomer **2** in which the methylene moiety bridges a former 6-5 bond retaining the 60 π-electron chromophore of C_{60}.

Indeed, this is supported by density functional calculations at the local density approximation level (LDA) which suggest that, despite the lowering of the molecular

[15]Fullerene derivatives in which a carbon atom bridges a 6-6 bond in a cyclopropane-type fashion are called methanofullerenes, and 6-5 open derivatives, in which the methano group bridges the open junction between a 6- and a 5-membered ring are called homofullerenes [130]. When stressing the fact of the open nature of the 6-5 bond of homofullerene derivatives and of the cyclopropane type bonding in the methanofullerene derivatives, respectively, the prefix 6-5 open, and 6-6 closed, respectively, shall be used in this thesis.

symmetry of **2** compared to C_{60}, the character of the molecular orbitals is hardly affected, so that the electronic transitions from the ground state to the t_{1u}-derived triplet remain dipole forbidden [132]. Furthermore, electrochemical studies by *Echegoyen* and co-workers suggest that the LUMO of 6-5 open homofullerenes such as **2** remain approximately triply degenerate, whereas those of the 6-6 closed isomers are about doubly degenerate, further supporting the interpretation that the electronic structures of 6-5 open fullerene derivatives are virtually identical to those of the parent carbon sphere [133].

1.5.4 The Ring Currents and Magnetic Properties of C_{60}

In their original publication describing the first experimental evidence for buckminsterfullerene, *Kroto et al.* described C_{60} as aromatic, being covered on its inner and outer surface by a sea of π-electrons [6]. If indeed the 60 π-electrons of C_{60} were free to flow around the fullerene sphere, it would have 41 times the ring-current magnetic susceptibility of benzene, and thus would be strongly diamagnetic [65,134]. *London* calculations by *Elser* and *Haddon* [65], however, predicted C_{60} to be only weakly diamagnetic, and they were confirmed by measurements of the magnetic susceptibility of bulk C_{60} [65,135] (for an excellent account of the magnetic properties and ring currents in fullerenes, see the review article by *Haddon* [134]). In fact, the magnetic susceptibility of buckminsterfullerene (χ (C_{60}) = –260 CGS ppm mol^{-1} = –4.3 CGS ppm per mol C [135a-b]) is smaller than that of diamond (χ (diamond) = –5.5 CGS ppm per mol C) and is comparable to that found in materials for which it is known that the electronic currents are confined to the atoms [134]. Nevertheless, substantial ring currents are present in C_{60}. Calculations [136-138] revealed that strong paramagnetic currents flow within the pentagons, whereas weaker diamagnetic currents extend around the fullerene sphere (Figure 12).

The overall vanishingly small magnetic susceptibility of bulk C_{60} results from a cancellation of diamagnetic and paramagnetic ring current contributions [136]. Protons of C_{60}-adducts, which are rigidly placed atop the fullerene surface are suitable probes for testing these *local* magnetic fields generated by the ring currents. Indeed, ^{1}H NMR spectroscopy has shown that protons located above pentagons of homofullerene

derivatives[16] are strongly deshielded (Figure 12) [29,131,139,140] in agreement with the paramagnetic ring currents in the five membered rings of C_{60}.

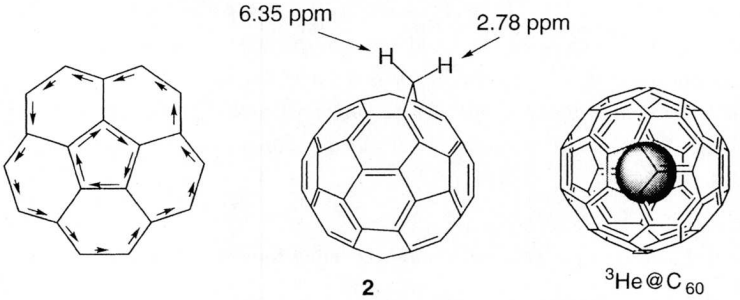

Figure 12. Electronic ring currents in a corannulene substructure of C_{60} for a magnetic field oriented perpendicular to a plane containing the pentagon (left) showing the strong paramagnetic ring current in the central pentagon and a weaker diamagnetic current extending around the perimeter of the substructure. Furthermore, the ^{1}H chemical shifts of the parent homofullerene $C_{61}H_2$ are shown [131], as well as a depiction of the endohedral compound ^{3}He@C_{60}.

Further insight into the magnetic properties of C_{60} was provided by *Saunders* and co-workers, who synthesized ^{3}He@C_{60} (Figure 12) by heating samples of C_{60} to 600–650 °C at a pressure of *ca* 3000 atm. [141], where X@C_{60} denotes an atom X within (endohedral to) C_{60}. The helium inside the fullerene cage experiences the sum of the magnetic fields generated by all ring currents of the fullerene chromophore and therefore ^{3}He NMR spectroscopy allows to probe the magnitude of the resultant magnetic field at the center of the molecule [142]. The ^{3}He NMR chemical shift for ^{3}He@C_{60} is –6.36 ppm relative to the resonance of free ^{3}He dissolved in 1-methylnaphthalene [141]. The chemical shift of ^{3}He@C_{60} (and of endohedral fullerene complexes in general) is not solely due to π-electron ring currents but also to the shielding by the σ-bonds of the fullerene cage, which contributes –5.2 ppm to the total shielding of the endohedral ^{3}He in ^{3}He@C_{60} [134,143]. *London* calculations predicted that reduction of C_{60} to C_{60}^{6-} results in the disappearance of the paramagnetic ring currents in the five-membered rings and appearance of diamagnetic currents in the same rings resulting in an expected strong upfield shift [135,136]. These results were subsequently supported by *ab initio* calculations by *Cioslowski* [144,145] and *Bühl et*

[16]It is assumed that the ring currents of the homofullerene-derivatives are comparable to those of pristine C_{60}, which seems to be a reasonable assumption in view of the electronic similarity of homofullerenes to unfunctionalized C_{60} (see Section 1.5.3).

al. [143] and are in good agreement with the recently determined value of –48.7 ppm for the chemical shift of $^3He@C_{60}^{6-}$ relative to free helium [146].

Mono-functionalization of the fullerene core leads to an upfield shift of the ^3He resonance. The magnitude of the shift is dependent on the nature of the addition (6-5 open *vs.* 6-6 closed), as well as on the nature of the addend (Figure 13). The ^3He shifts of 6-6 closed monoadducts appear *ca.* 3 ppm upfield compared to $^3He@C_{60}$ [142]. An exception are the endohedral ^3He methanofullerene derivatives such as **3** which are shielded by only *ca.* 2 ppm. Apparently the magnetic properties of the fullerene are less perturbed in the mono-adducts with a fused cyclopropane ring than in those in which larger rings have been fused to the fullerene sphere (for example the monoadduct **4** with a fused cyclohexene ring). This can be understood considering the well established double bond-like behavior of cylopropane rings in conjugation with a π-system, which results in a smaller perturbation of the electronic structure of the π-chromophore of **3** compared to **4** [147].

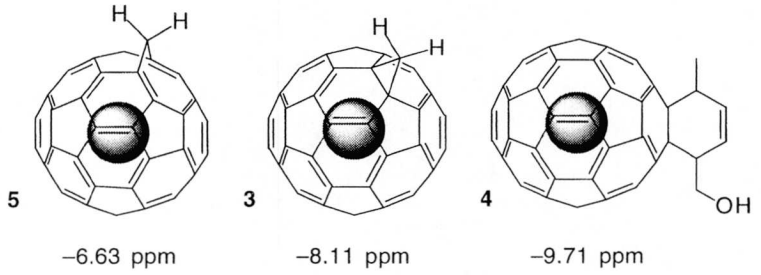

Figure 13. Representative examples of endohedral ^3He mono-adducts of C_{60} and their ^3He NMR chemical shift [142,148].

In comparison, the ^3He resonance of the 6-5 open $^3He@C_{61}H_2$ (**5**) is hardly shifted upfield *versus* $^3He@C_{60}$ ($\Delta\delta \approx -0.2$ ppm). This comparatively small shift may be seen as the result of the high similarity of the electronic structure of homofullerene **2** and of pristine C_{60}, which is also apparent in their respective electronic absorption spectrum (Section 1.5.3).

1.5.5 The ^{13}C NMR Spectrum of C_{60}

As a result of the I_h-symmetry of C_{60}, all Carbon atoms are chemically equivalent giving rise to a single resonance in the ^{13}C NMR spectrum at 143.2 ppm in C_6D_6 [14]. The chemical shift is comparable to the ^{13}C NMR shifts of the strained polyaromatic hydrocarbons (PAH's) pyracylene and corannulene [149] which constitute structural motifs of C_{60}. In the large fullerene fragment triacenaphthotriphenylene $C_{36}H_{12}$ (Figure 14 c) the ^{13}C resonances are located between 152.2 and 125.4 ppm [150], comparable to the range for the sp^2 fullerene carbon atoms of C_{60} derivatives (Figure 14).

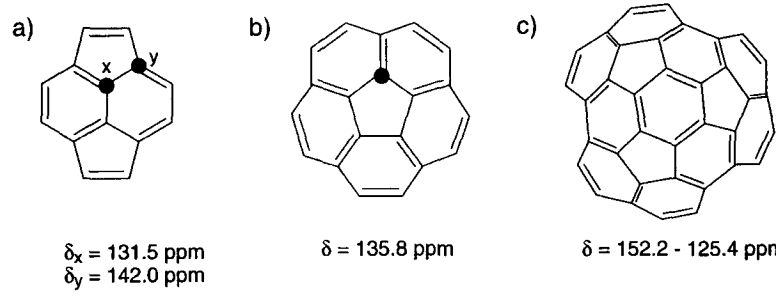

Figure 14. Structures of some PAHs which are structural motifs in C_{60} and selected chemical shifts for the quaternary Carbon atoms: in a) pyracylene [149], b) corannulene, [151] and the fullerene fragment $C_{36}H_{12}$ [150].

Simple rationalization of the chemical shift in C_{60} and strained PAH's is not possible since both ring current effects and strain induced rehybridization of the sp^2 Carbon atoms have an influence on the chemical shift [149,152]. Although no quantitative relationship between strain induced rehybridization and the resonance of the sp^2 carbons has been established [152], increased pyramidalization generally leads to a downfield shift of the carbon NMR resonances [69b]. Furthermore, a correlation of the ^{13}C resonances of C_{70} and the degree of pyramidalization of the respective carbon atoms allowed the assignment of the resonances in the ^{13}C NMR spectrum[17][15], which was later confirmed by 2D-NMR experiments [153]. At any rate, the chemical shift of the fullerene sp^2 carbon atoms is very sensitive to distortions in the cage geometry,

[17]*It is interesting to note that the chemical shift of the most pyramidalized carbons at the C_{70} poles with a* POAV angle of 102.5° give rise to a signal at 150.07 ppm which is very close to the value of 152.2 ppm which is probably the resonance of the carbons of the central 6-membered ring of the $C_{36}H_{12}$ fullerene fragment with almost the same POAV angle of 102.4° (Figure 14c).

often leading to surprisingly well resolved spectra of C_{60} derivatives in the fullerene sp^2-region, making ^{13}C NMR spectroscopic analysis (combined with symmetry considerations) the single most important criterion for the structural assignment of fullerene derivatives.

1.5.6 The IR Specturm of C_{60}

Out of the 174 vibrational modes for C_{60} only 46 correspond to distinct mode frequencies. Of these, 10 are Raman active ($2A_g + 8H_g$) and 4 (T_{1u}) are IR active and the remaining 32 are optically silent. The 4 IR bands of highly pure C_{60} deposited on a KBr pellet appear at 526, 576, 1183, and 1429 cm^{-1}, respectively [154]. The vibrational modes can be decomposed into a radial (displacement of an atom parallel to the radial axis of the C_{60} sphere) and two tangential components (displacement of an atom along a double bond and displacement perpendicular to both the double bond and the radial axis) [11]. This allows to divide each vibrational mode into percentage contributions from the three directions. The low frequency band at 526 cm^{-1} corresponds to the IR active breathing mode resulting almost exclusively (93%) from the radial displacement of the carbon atoms [11] and as a result remains relatively unperturbed upon functionalization of the fullerene core [155]. The three remaining higher frequency vibration bands have an increasing tangential contribution [11] and, as a consequence, are shifted strongly upon functionalization of the fullerene double bonds and/or are obscured by the absorption bands arising from the functional groups of the addends.

1.5.7 Photophysical Properties

Irradiation of C_{60} with light produces the singlet excited $^1C_{60}^*$ state which has a very short life time (~1.3 ns) and decays to the triplet state ($^3C_{60}$) nearly quantitatively (Scheme 1) [156-159]. The high triplet quantum yield is due to very weak fluorescence[18] of $^1C_{60}^*$ and the very high efficiency of the intersystem crossing from the singlet to the triplet state of C_{60} resulting from the small singlet-triplet splitting (≈10 kcal mol^{-1}) [161] and a large spin-orbital interaction [162]. Phosphorescence of $^3C_{60}$ is rarely observed, despite the high triplet yield[19]. The triplet state energy of C_{60} was

[18]The fluorescence quantum yield of $^1C_{60}^*$ in toluene is $3.2 * 10^{-4}$ [160].
[19]Heavy atom induced phosphorescence of $^3C_{60}$ has been observed [163].

determined to be 36.3 kcal mol^{-1} [163-165], allowing $^3C_{60}$ to produce $^1O_2$ (E ($^1O_2$) = 22.5 kcal mol^{-1}) *via* energy transfer to molecular oxygen with almost 100% efficiency [161,164]. The produced singlet oxygen does neither react with C_{60} nor is it efficiently quenched by the fullerene, making C_{60} a powerful singlet oxygen sensitizer. Triplet C_{60} is a fairly strong oxidizing agent[20] and is readily reduced by electron donors such as amines[21] *via electron transfer to form the* C_{60} *radical anion and the donor cation* [156,166].

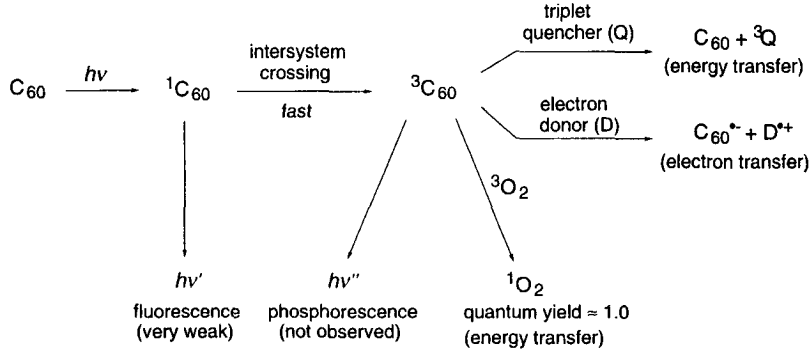

Scheme 1. Photophysical processes of C_{60} after excitation with light.

Quenching of the triplet state of C_{60} can also be achieved by energy transfer to rubrene in a diffusion controlled process which yields ground state C_{60} and triplet rubrene [161].

The photophysical behavior of monofunctionalized C_{60} derivatives such as **6** and **7** (Figure 15) is very similar to the that of the parent fullerene [126,129,167]. Values near unity were determined for the quantum yield of $^1O_2$ production for the cyclopropanated fullerene derivative **6** [126] and only slightly lower values (5–10%) for the cyclohexane fused alcohol **7** [128].

[20]The reduction potential of $^3C_{60}$ has been estimated to be 1.56 V [166].

[21]Reduction of the triplet state by hydroquinone by abstraction of a hydrogen atom has also been reported [156].

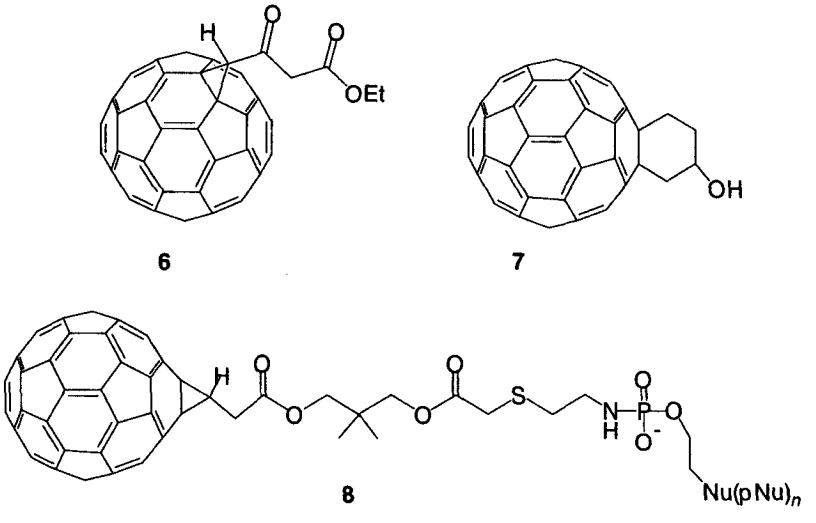

Figure 15. Structure of the cyclopropanated monoadduct **6** and the cyclohexane fused alcohol **7** which were used for photophysical studies (cf. [126] and [128]), and of the fullerene oligonucleotide conjugate **8** which was used for photoinduced sequence specific cleavage of DNA ($Nu(pNu)_n$ = T(3')CTTCCTCTTCTT(5')) [168].

Polar side chains greatly enhance the solubility of fullerene derivatives in hydrogen bonding and other polar solvents, making them amenable to biological applications [169]. For example, the fullerene oligonucleotide **8** was shown to bind to single stranded DNA, double stranded DNA, and double stranded DNA with a hairpin [168]. In each case, the fullerene conjugate cleaved the DNA strand specifically at guanine residues proximal to the fullerene moiety upon exposure to light, either through oxidation by $^1O_2$ or through direct oxidation of the guanosin nucleotides by electron transfer [170].

2. The Principles of Reactivity of C_{60}

In this Chapter, some of the basic characteristics of the reactivity of C_{60} will be discussed and illustrated with examples from the literature. The main focus will be on the types of reactions which are relevant for the work described in the following Sections. For a more comprehensive treatment of the chemistry of buckminsterfullerene, the reader is referred to an excellent monograph by *Hirsch* [171] which covers the chemistry of C_{60} until the beginning of 1994 and many reviews [172-177], the most recent ones being those by *Diederich* and *Thilgen* [178] and by *Samal* and *Sahoo* [179]. The Section is divided into two Sections: in the first part, some examples of monofunctionalization on the fullerene core will be given illustrating the transformations of relevance for the work described later. In the second part of the Section, the regioselective formation of higher adducts of C_{60} will be discussed. A brief look at the change in the chemical behavior of higher adducts of C_{60} will be taken.

2.1 General Considerations of the Reactivity of C_{60}

i) The combination of the pyramidalized double bonds and the energetically low lying triply degenerate LUMO of buckminsterfullerene make it a good electron acceptor (see Section 1.4.3 on the electronic structure of C_{60}) and thus susceptible to nucleophilic and radical additions. Its reactivity is similar to the that displayed by electron deficient alkenes.

ii) As a result of its spherical structure and of the pyramidalization of its double bonds, C_{60} is a highly strained molecule (see Section 1.5.1). Functionalization of double bonds of C_{60} changes the hybridization of the respective carbon atoms in the fullerene sphere from sp^2 to sp^3. This reduces both the local strain of the functionalized carbon atoms as well as that of the entire molecule [64] and generally increases the energy of the LUMO[22]. Therefore the reactivity of the remaining double bonds of fullerene chromophore towards nucleophiles and cycloadditions is reduced. This often enables to control the degree of functionalization by carefully choosing the reaction conditions and the stoichiometry of the reagents.

[22]However, a direct correlation of the global strain of the molecule and the energetic position of the LUMO is not possible.

iii) Mono- and oligo-adducts of C_{60} will lead to addition patterns which minimize the number of double bonds at 6-5 junctions, since this is associated with a cost of 8.5 kcal mol^{-1} per 6-5 double bond [74,75].

iv) C_{60} displays significant bond length alternation (see Section 1.3.3) in which the 30 6-6 bonds display a higher double bond character than the longer 6-5 bonds. The localization of the double bonds at the 6-6 junctions is reflected in the chemical behavior of buckminsterfullerene: cycloadditions lead exclusively to adducts bridging 6-6 bonds and both addition reactions as well as radical reactions of sterically non-demanding reagents occur preferentially across 6-6 bonds. For the latter two reaction types, the observed regioselectivity is a direct consequence of the charge and spin-density localization of the intermediate fullerene anion and fullerene radical, respectively (see Section 2.2).

2.2 Charge and Spin Densities in Nucleophilic and Radical Reactions of Buckminsterfullerene

Considering the conjugated nature of buckminsterfullerene, one might assume that the incoming charge of a nucleophile or the unpaired electron of a radical, respectively, will be evenly distributed over the entire fullerene sphere in order to achieve maximum stabilization of the fullerene based anion and radical, respectively. However, both experimental evidence and calculations indicate very little delocalization and place the negative charge or the radical in close proximity to the addend.

2.2.1 Nucleophilic Additions Part 1: Charge Distribution

Controlled addition of lithium and *Grignard* reagents RM (R = alkyl [180], phenyl [181], alkynyl [182]) as well as NaCN [183] yielded the corresponding monoanionic fullerene derivative $C_{60}R^-$, which could be quenched by acid giving rise to the respective $C_{60}HR$ derivatives. ^{13}C NMR spectroscopy showed that all the derivatives displayed C_s-symmetry indicating that the products were the result of a 1,2 addition across a 6-6 bond Scheme (2). In contrast, when the sterically demanding *t*-BuLi was added to C_{60} followed by protonation of the intermediate fullerene anion, a mixture of the 1,2-adduct **9e** and 1,4-adduct (±)-**10** was obtained (85:15 in favor of the 1,4-adduct) [184].

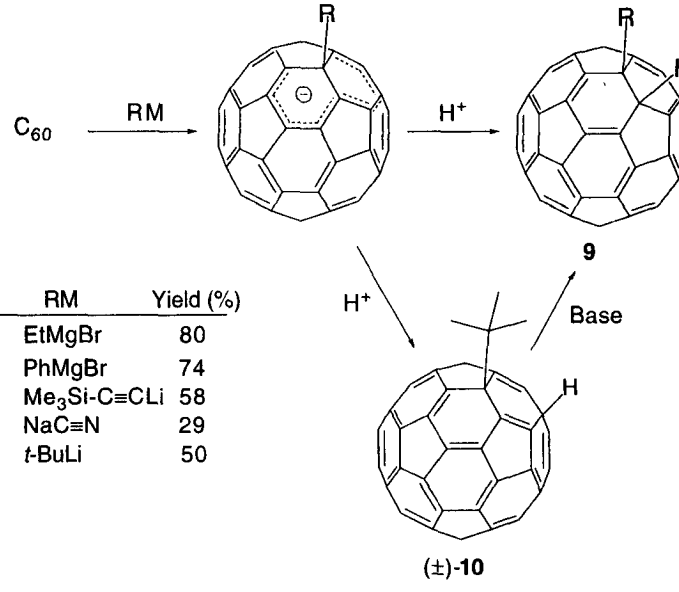

9	RM	Yield (%)
a	EtMgBr	80
b	PhMgBr	74
c	Me_3Si-C≡CLi	58
d	NaC≡N	29
e	*t*-BuLi	50

Scheme 2. Synthesis of hydroalkylated, hydroarylated, hydroalkynylated, and hydrocyano fullerene derivatives. They lead exclusively to the 1,2 addition pattern upon protonation of the intermediate fullerene anion **9a-d** with the exception of the *t*-Butyl-derivative which produces a mixture of the 1,4-adduct (±)-**10** and 1,2-adduct **9e**.

Treatment of the isomeric mixture with base led to the rearrangement of the kinetic product, namely the 1,4-adduct (±)-**10**, to the thermodynamically more stable 1,2-derivative **9e** [184]. These observations can be rationalized by analysing the charge distribution of the intermediate fullerene anions: The ^{13}C NMR spectrum of a pure sample of the anion *t*-Bu$C_{60}^-Li^+$ in THF-d_8 showed the pattern of a C_{60} derivative with C_s-symmetry and variable temperature ^1H NMR spectroscopic investigations revealed the hindered rotation of the *tert*-butyl group ($\Delta G^{\neq}$ = 9.3 (±0.1) kcal mol^{-1} at –60 °C) [180b]. AM1 calculations of the electron densities (Mulliken charges) on the fullerene sphere of the *t*-BuC_{60}^- anion provided a clearer insight (Figure 16)[23] [180a,182b,186].

[23]Similar single point calculations at the HF/3-21G level of theory using AM1 optimized geometries suggest far more delocalization of the negative charge over the fullerene sphere [185]; in view of the experimental evidence (*vide supra*) it is assumed that these calculations overestimate the degree of delocalization.

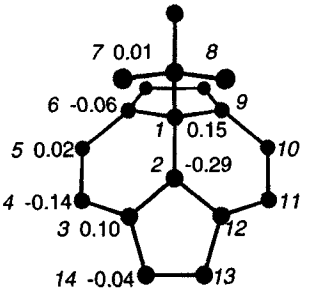

Figure 16. Mulliken charges of the affected pyracylene subunit of the intermediate *t*-BuC_{60}^- obtained from AM1 calculations [180a] (the numbering of the fullerene atoms are in italics)

These calculations showed that the charge is not evenly distributed over the fullerene sphere but rather localized. The highest partial charge was found on the C-atom next to the sp^3 carbon across the 6-6 bond (at the 2-position), followed by the 4-position (in a *para*-relationship to the *t*-Bu moiety). And only substantially smaller charges were found at the 6- and 9-position[24]. Thus protonation or quenching of the intermediate anion will preferentially occur at the 2-position if the steric requirements of the nucleophile or the electrophile are not very great. 1,-4 Additions will only take place when the steric repulsion between the addends does not allow a 1,-2 addition pattern [186] (for a stable 1,-4 addition pattern which was obtained by nucleophilic addition of *t*-BuLi followed by quenching of the intermediate anion with the very bulky 1,4-dicyclopropyltropylium cation see ref. [187]).

2.2.2 Radical Additions: Spin Localization

Upon addition of radicals to C_{60}, the observed distribution of the unpaired spin density in the $RC_{60}^{\bullet}$ monoadducts is very similar to the calculated charge distribution in the RC_{60}^- anions: The organic radical species R$^{\bullet}$ which is to be added to the fullerene, can be generated *in situ* either photochemically or thermally by established radical reactions from suitable precursor molecules [188-197]. Probably most informative was the addition of *t*-Bu$^{\bullet}$ to C_{60}, which was obtained by photolysis of equimolar di-*tert*-butylmercury and C_{60} in toluene and yielded the rather persistent *t*-Bu$C_{60}^{\bullet}$ radical [188,191]. Variable temperature ESR measurements of the fullerene radical revealed a hindered rotation of the *t*-Bu-moiety with an estimated 7.3 ± 0.5 kcal mol^{-1} for the enthalpy barrier for the rotation around the C—C_{60} bond [191,198].

[24]The numbering of the fullerene is not according to the IUPAC recommendations, but is used very frequently in the fullerene literature (see ref. [174c]) as proposed by *Godly* and *Taylor* [130] and has been applied here so the reader can identify the respective regioisomers when mentioned in the literature.

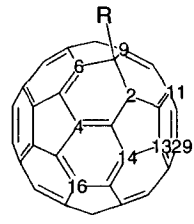

C#	Spin Density
2	0.41
4, 11	0.20
6, 9	0.05
13, 14	0.03
16, 29	0.08

Figure 17. Unpaired spin density distribution over the fullerene sphere according to non-local DFT calculations on PM3 optimized geometry of the fullerene radical $HC_{60}^{\bullet}$ [199]; similar spin densities have been calculated for R=H with semi-empirical methods [200,201] and for R=CH_3 (DFT-BLYP) [202], which are all in good agreement with the ESR-spectra of the respective radicals [203].

The ESR spectrum of the *t*-Bu$C_{60}^{\bullet}$ radical was intense enough to allow the detection of hyperfine interactions (hfi's) with the ^{13}C isotopes of the C_{60}-adduct in natural abundance, thus, permitting to estimate the spin density distribution on the fullerene [188,190]. Based on the spectra, the largest spin density was assigned to the C(2) carbon atom, across the 6-6 bond adjacent to the *t*-Bu moiety. The two next-largest spin densities were originally assigned to the symmetry equivalent C(4), C(11) and to C(6), C(9), respectively [188,190] (Figure 17). However, based on quantum-chemical computations of spin densities [199,201,202,204], and of the ESR spectrum of MuC_{60} [205][25] it was later established that the unpaired spin on C(6) and C(9) in $RC_{60}^{\bullet}$ monoadducts is in fact very small[26]. Thus, the unpaired electron is primarily located at C(2) and at the symmetry equivalent carbon atoms C(4) and C(11) and is hardly found across the 6-5 bond from the addend at C(6) and C(9), respectively (Figure 17).

Thus, in both the fullerene anion RC_{60}^{-} as well as the fullerene radical $RC_{60}^{\bullet}$, negative charge and the unpaired electron, respectively, are located primarily at the C(2) carbon atom followed by C(4) and C(11), and are hardly found at C(6) and C(9). The very similar behavior of the fullerene anion and radical can be rationalized by inspection of the resonance structures in Figure 18. Only the resonance structure placing the negative charge or the unpaired electron at the C(2) position on the fullerene does not involve placing a double bond in a five membered ring, which occurs only at a cost of 8.5 kcal mol^{-1} [74,75].

[25]Mu is the symbol for muonium, a short-lived isotope of hydrogen. Its nucleus has a mass one-ninth that of that of a proton, a nuclear spin $I = 1/2$, and a magnetic moment 35 times that of a proton.
[26]These experiments were carried out with a highly ^{13}C enriched sample of C_{60} [205]

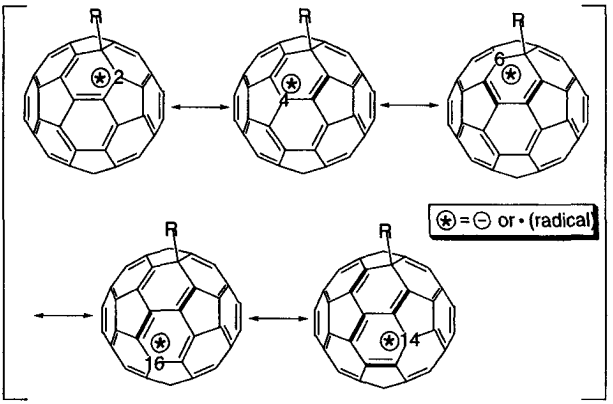

Figure 18. Depiction of the resonance structures placing a negative charge or an unpaired electron at the indicated sites. The importance of the respective resonance structure decreases with the number of double bonds (shown in bold) which have to be introduced into a five membered ring.

The importance of the respective resonance structures decreases parallel to the number of the double bonds which are forced into the five membered rings, in good agreement with both the calculated charge density as well as the unpaired spin density on the respective carbon atoms of the fullerene. Such a simple analysis describes the reactivity of fullerene anions as well as fullerene radicals in a very satisfactory way.

2.3 Establishing the Reactivity of C_{60} as an Electron Deficient Alkene by Metal Complexation

A key experiment for elucidating the chemical behavior of C_{60} was carried out by *Fagan et al.* in 1991 (Scheme 3) [52,206]. At that time, the only reactions that had been carried out with buckminsterfullerene were the oxidation of C_{60} with OsO_4 by *Hawkins et al.* [51,207] and a Birch reduction by *Smalley* and co-workers which had led to the formation of an isomeric mixture of predominantly $C_{60}H_{36}$ [23]. However, these experiments did not allow to determine whether C_{60} was best described as a rather unreactive aromatic molecule with benzene like rings or if it was indeed more reactive. It was therefore decided to react C_{60} with an excess of $[Cp^*Ru(MeCN)_3]^+$ $F_3CSO_3^-$ which is known to give strong η^6-binding with planar arenes displacing three acetonitrile ligands, and to form η^2-complexes with electron deficient alkenes upon displacement of only one coordinated acetonitrile ligand.

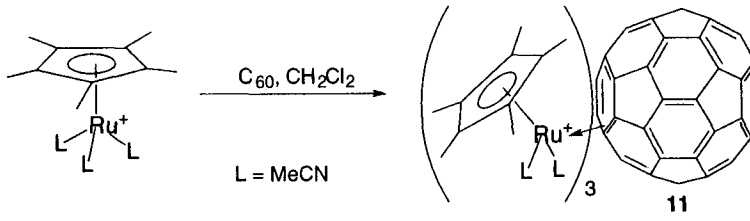

Scheme 3. Reaction of C_{60} with $[Cp^*Ru(MeCN)_3]^+ F_3CSO_3^-$ which showed the preference of C_{60} to react as an electron deficient polyene [52].

The reaction product **11** showed that three ruthenium atoms were attached to C_{60} and that two acetonitrile ligands were retained on each ruthenium, indicating η^2-complexation and electron deficient olefin type behavior of C_{60}[27]. This result was confirmed by the reaction of C_{60} with platinum, palladium, and nickel complexes [52,206,209]. Low-valent complexes of these metals are known to easily undergo complexation with electron deficient olefins. The reaction of C_{60} with one eq. of $[Pt(Ph_3P)_2(\eta^2\text{-}C_2H_4)]$ allowed the isolation of the complex **12**, the X-ray crystal structure determination of which showed that the reaction had taken place at a 6-6 bond (Scheme 4) [52,210].

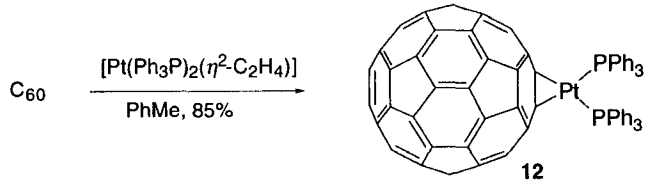

Scheme 4. Reaction of C_{60} with the Pt(0) complex $[Pt(Ph_3P)_2(\eta^2\text{-}C_2H_4)]$ to give the C_{2v}-symmetrical square planar complex [52].

These experiments allowed two very important conclusions:

i) The chemical behavior of C_{60} resembles that of an electron deficient alkene rather than that of a planar arene.

ii) The reactions take place across 6-6 bonds and not across 6-5 bonds.

Considering the discussion of the physical properties in Section 1, these results might not seem terribly surprising, but they were the first indication of the chemical

[27] It is interesting to note that complexation of $[Cp^*Ru(MeCN)_3]^+ F_3CSO_3^-$ with corannulene gave a η^6-complex, indicating that the chemical behavior (and therefore the electronic structure) of C_{60} is significantly different than that of its isolated structural subunits (*i.e.* corannulene) [208].

behavior of this highly conjugated molecule and influenced heavily the way organic chemists would view C_{60} and choose the chemical reactions to be carried out.

2.3.1 Nucleophilic Additions Part 2: The Bingel Reaction and Related Nucleophilic Cycloadditon Reactions of C_{60}

The cyclopropanation of C_{60}, based on a nucleophilic addition-elimination reaction, was first introduced by *Bingel* using the commercially available diethylbromomalonate [211]. The reaction mechanism is believed to be a two step process in which first a stabilized *α-halocarbanion* adds to C_{60} producing the fullerene anion **13**, which in a second step displaces the halogen in an intramolecular nucleophilic substitution yielding a methanofullerene (Scheme 5).

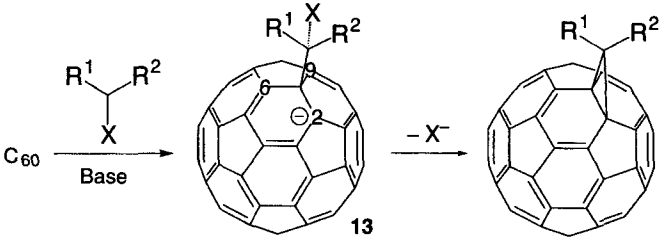

R^1	R^2	X	Product	Yield (%)
CO_2Et	CO_2Et	Br	**15**	45
COPh	Ph	Cl	**16**	25
NO_2	H	Br	**17**	19
CO_2Et	C≡N	Br	**18**	31
C≡CSiMe$_3$	C≡CSiMe$_3$	Br	**14**	55
CO_2Et	COMe	I	**19**	30

Scheme 5. Nucleophilic addition of α-halocarbanions to C_{60} followed by displacement of the halide as reported by *Bingel* [211], *Diederich* and co-workers [182a,218], *Wudl* and co-workers [217], and *Nierengarten* and co-workers [219].

This mechanistic hypothesis is supported by the fact that methanofullerenes can also be obtained using phosphonium ylides [212] and sulfonium ylides [213] *via* the nucleophilic addition of the ylide to C_{60} followed by elimination of PPh_3 or Me_2S. The

α-halomalonates have been generated *in situ* from the corresponding malonates by using two eq. of base in the presence of I_2 or CBr_4 [214-216].

The *Bingel* reaction can be extended to the preparation of a large variety of functionalized methanofullerenes: α-Chloroketones, α-bromonitromethane and α-bromocyanoacetates have consequently been added to C_{60} [217]. Diethynylmethanofullerenes such as **14** can also be prepared by this method from the corresponding 3-bromopenta-1,4-diynes (Scheme 5) [182a,218]. The reaction is fast, clean, and proceeds in fair to good yields. The difference in polarity of the products generally makes it easy to separate the mono-adduct from unreacted C_{60} or bis-adducts. In addition, since many malonate derivatives are commercially available or are easily synthesized, the *Bingel* reaction is extensively used for the preparation of stable fullerene derivatives.

It is noteworthy, that no 6-5 open products have been detected in these types of reactions, which supports the calculations that the negative charge of the intermediate fullerene anion **13** is essentially confined to the 2-position across a 6-6 bond and not at the 6 and 9 positions across 6-5 bonds.

Recently, the synthesis of the fullerene dimer **20** has been reported (Scheme 6) [220]. The formation of the [2+2] adduct **20** was carried out in the solid state in a KCN-mediated mechanochemical reaction of C_{60}, by the use of a 'vibrating mill' [221][28]. The reaction is believed to occur by first addition of CN^- to C_{60} to form $C_{60}(CN)^-$, which then reacts with a closely located C_{60} molecule in a 1,4-addition mode. The cyano moiety is subsequently eliminated in an intramolecular S_N2' reaction of the intermediate anion **21** producing the dimer **20** (Scheme 6) [220][29].

[28]Polymeric adducts of C_{60} can be obtained *via* photopolymerization [222] or by pressure-induced polymerization [223] in the solid state by [2+2] reaction between double bonds of adjacent molecules.

[29]It is worthwhile to mention some of the physical properties of this first carbon allotrope obtained by the means of 'classical' organic synthesis: the UV spectrum of **20** exhibits absorption maxima at 328, 434 and 698 nm, which are typical for 1,2 dihydro-fullerene monoadducts (see Section 1.5.4.) however the shape of the spectrum is quite different, possibly indicating some electronic interaction between the fullerene spheres. The dimer is thermally and electrochemically labile and reverts to C_{60} upon heating between 150 and 175°C and also upon uptake of one electron. Interestingly, the positive-ion Fourier-transform ion cyclotron resonance mass spectrum of **20** shows next to the base peak due to C_{60} (100%) and the molecular ion peak for C_{120} (1.0%) a series of peaks corresponding to C_{120} - C_{2n} (n = 1 - 5) with intensities ranging from 1.0 to 2.3% showing that the C_{120} does not only dissociate into C_{60}, but also reduces its size by extruding C_2 units and, presumably, rearranges into even numbered fullerenes C_{118} to C_{110} [220].

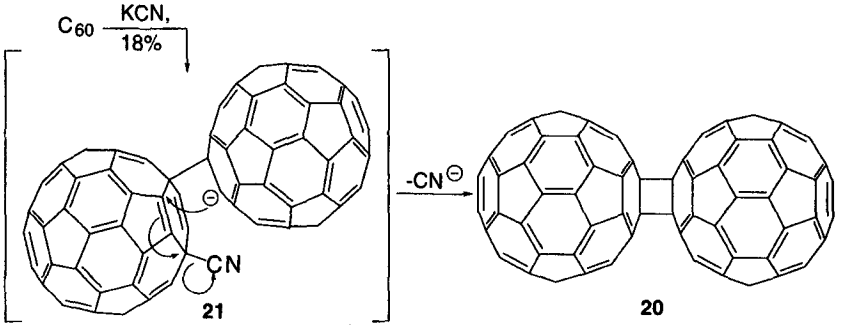

Scheme 6. Formal [2+2] cycloaddition of C_{60} to yield the dumbbell-shaped dimer C_{120} (**20**), as reported by *Wang et al.* [220].

2.3.2 [4+2] Cycloadditions: Diels-Alder Reactions with C_{60}

Among the most widely used chemical transformations of electron deficient alkenes are *Diels-Alder* reactions. It is therefore no surprise that this reaction has been utilized by many groups for the functionalization of C_{60}, and has been extensively reviewed [171,175b,178], most recently by *Sliva* [224]. The reaction with 1,3-dienes occurs at a 6-6 bond, with C_{60} acting as the dienophile, which gives rise to 1,2-addition products in which a cyclohexene ring has been fused to the fullerene core. To date, no reactions where C_{60} acts as the diene, or in which the reaction has occurred across a 6-5 bond[30] of C_{60} have been reported[31].

The reaction of C_{60} with cyclopentadiene or with anthracene gave the cycloadducts **22** and **23a**, respectively (Figure 19) [227,227b,228]. The adducts were found to be stable enough to allow isolation and characterization, but reverted to the starting materials upon heating [227a-b,229]. The high thermal lability of the cycloadducts **22** and **23a**, is most likely due to steric repulsion between the addend and the fullerene sphere. Increasing the steric demand of the diene by introducing substituents at the C(9) and C(10) positions of the anthracene moiety was shown to enhance the retro-*Diels-Alder* reaction in **23b** and **23c** [230,231].

[30]Very recently, benzyne has been reported to add across a 6-5 bond in C_{70} [225].

[31]Diels-Alder reactions across 5-6 bonds or in which C_{60} acts as a diene have been calculated to be disfavored by 17 and 60 kcal mol^{-1}, respectively, compared to reactions across 6-6 bonds [226].

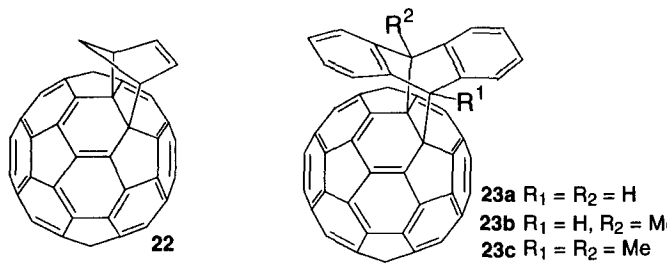

Figure 19. Cycloadducts of C_{60} with cyclopentadiene and anthracene derivatives.

In order to increase the thermal stability of *Diels-Alder* adducts of C_{60}, the groups of *Müllen* and *Rubin* used dienes which gave compounds **24a-c**, that were stabilized towards the retro-reaction, since cycloreversion would have to overcome the stabilization energy provided by the aromatic system of **24** producing high energy *o*-quinodimethane intermediates [232] (Scheme 7). Thus, **24a** was obtained by addition of a norbornenone derivative after *in situ* decarbonylation [232], and **24b** was produced by reacting C_{60} with *o*-quinodimethane generated *in situ* from α,α'-dibromo-*o*-xylene in the presence of KI and [18]crown-6 or tetrabutylammonium iodide (TBAI) [233,234]. X-ray crystal structure determination of compounds **24a** [232,235] and **24c** [233,236] showed that the fullerene 6-6 bond at the fusion is substantially longer than the normal sp^3-sp^3 C-C distance of 1.54 Å (1.59 Å in **24a**, 1.62 Å in **24c**).

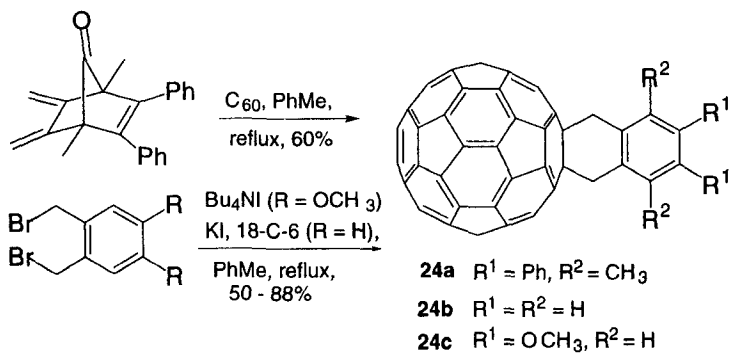

Scheme 7. Syntheses of the *Diels-Alder* adducts stabilized with respect to cycloreversion, as reported by the groups of *Rubin* (**24a**) [232], *Müllen* (**24b**) [234], and *Diederich* (**24c**) [233].

Of particular relevance for the work presented later is that *Diels-Alder* cycloadditions of acyclic buta-1,3-dienes, which do not have sterically demanding

groups at the 1 or 4 position of the diene moiety, lead to thermally stable adducts with C_{60} [128,227a,237]. For example, *Kräutler* and *Puchberger* reacted C_{60} with 1000 eq. of 2,3-dimethyl-buta-1,3-diene at room temperature to yield **25a** (Scheme 8) [237a], and *Rubin* and co-workers prepared a series of fullerene cycloadducts in yields between 30 and 60% with 1-substituted, 2-substituted, or 2,3-disubstituted buta-1,3-dienes by refluxing C_{60} with a small excess of the diene (between 1 and 3 eq.) in PhMe (Scheme 8) [237c]. The cycloadducts of C_{60} with buta-1,3-dienes showed no propensity to undergo retro-*Diels-Alder* reaction, even upon heating.

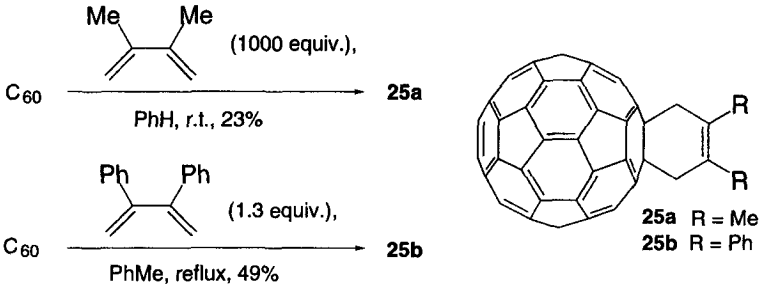

Scheme 8. Two examples of *Diels-Alder* adducts of C_{60} with acyclic buta-1,3-diene derivatives as reported by the groups of *Kräutler* [237a] and *Rubin* [237c].

However, unless strict exclusion of air and light was maintained throughout the reaction and purification steps, the adducts were always contaminated with, or completely converted to more polar products [237a]. *Rubin* and co-workers have shown that allylic hydroperoxides are readily formed by a self-sensitized $^1O_2$ ene reaction at the cyclohexene rings of the fullerene [4+2] cycloadducts (Scheme 9) [237c,238].

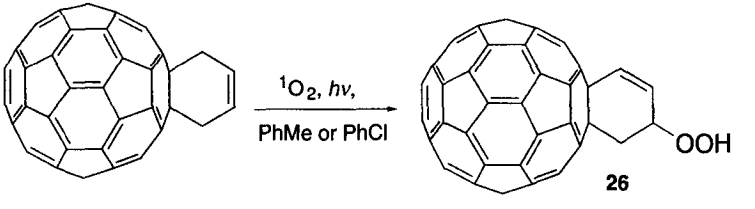

Scheme 9. Self-sensitized $^1O_2$ ene reaction at the cyclohexene ring of the C_{60} cycloadduct with buta-1,3-diene to give hydroperoxide **26** [238].

2.3.3 [3+2] Cycloadditions: Additions of Diazo- and Azide Derivatives

Since the reactivity of the 6-6 bonds of C_{60} is similar to that of electron deficient alkenes, buckminsterfullerene can potentially react with any 1,3-dipoles in a [3+2] cycloaddition fashion. A wide variety of 1,3-dipoles have indeed been shown to add to C_{60}. These include trimethylenemethane derivatives [239,240], azomethine ylides [241], carbonyl ylides [242], nitrile oxides [243], nitrilimines [244], buta-2,3-dienolates [245], and sulfinimides [246]. In all these cases, the isolated mono-adducts are bridged at a 6-6 ring junction as a result of 1,2-addition resulting in five-membered rings fused to the fullerene skeleton and are thermally stable.

Diazo compounds were discovered to react with C_{60} by *Wudl* and co-workers [228a,247,248] and they have been widely investigated by *Diederich* and co-workers [29,173,249].

1,3-Dipolar addition of diazo compounds followed by thermal dinitrogen extrusion produces the 6-5 open homofullerene as the major product which is often accompanied by a minor amount of the 6-6 closed isomer (Figure 20). However, in theory, four structures with a single C-atom bridging two neighboring fullerene carbon atoms are possible (Figure 20). As there are two different kinds of bonds in C_{60}, two possible regioisomers can arise, namely those bridging a 6-6 junction and those bridging a 6-5 junction. Furthermore, by analogy to methanoannulenes [250], each of these two isomers could potentially exist in either the σ- or π-homoaromatic form, respectively, called 'closed' and 'open', thus leading to a total of four possible isomers. In the 6-6 open and 6-5 open isomers, the bridged carbon atoms are at nonbonding distance, whereas in the 6-6 closed and 6-5 closed isomers, they are connected by a transannular bond.

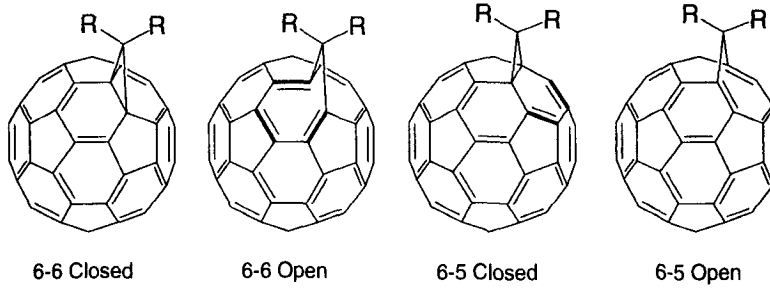

Figure 20. The four possible isomeric structures having a single C-atom bridging two neighboring fullerene carbon atoms. Double bonds which are forced into 6-5 ring junctions in the 6-6 open and 6-5 closed isomers are highlighted in bold.

No 6-6 open and 6-5 closed methanofullerene isomers have been observed so far. The reason for these experimental findings can be seen upon inspection of Figure 20. In the 6-6 closed methanofullerene and in the 6-5 open isomer, the favorable bonding pattern of C_{60} is conserved, in which all the double bonds are placed exocyclic to the five-membered rings at 6-6 ring junctions. In contrast, in the 6-6 open and 6-5 closed valence isomers three respectively two double bonds are forced into 6-5 ring junctions which is known to be energetically costly [74,75] (see also Section 2.1.1.) and therefore, the 6-6 open and the 6-5 closed valence isomers are strongly disfavored relative to the 6-6 closed and 6-5-open structures[32] [132,249].

Very instructive in describing the chemical behavior of additions of diazo-derivatives to C_{60} is the reaction of diazomethane with fullerenes which was first carried out by *Wudl et al.* [131] and later further investigated by *Smith III* and co-workers (Scheme 10) [139,251].

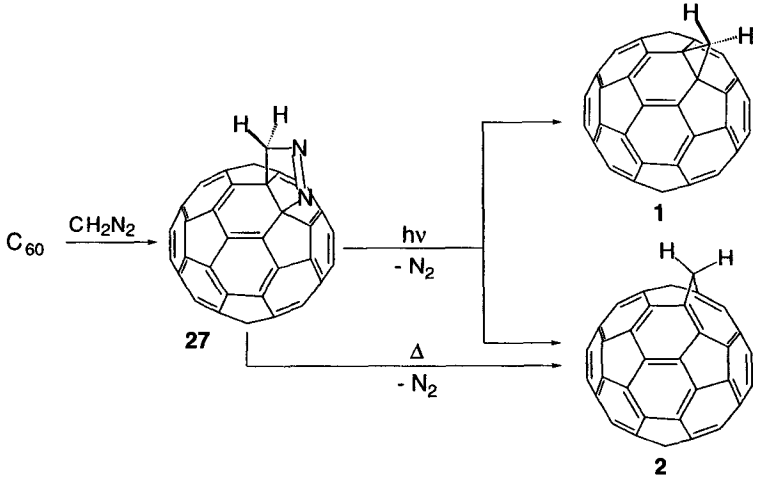

Scheme 10. Synthesis of the 6-5 open and of the 6-6 closed fullerene derivatives **2** and **1**, respectively, as reported by the groups of *Wudl* and *Smith III* [131,139,251a].

The 1,3-dipolar cycloaddition of diazomethane to C_{60} at 0 °C gave the pyrazoline intermediate **27**, which could be isolated and characterized. It was found to be thermally instable and to readily lose dinitrogen upon heating in a highly regioselective reaction, forming the parent homofullerene $C_{61}H_2$ **2** virtually quantitatively with only traces of **1** [131,251a]. In contrast, photolysis of the

[32]In addition to forcing three double bonds into five membered rings in the 6-6 open valence isomer, two of those double bonds are located at the bridgehead carbon atoms of the isomer, and are distorted from planarity further decreasing its stability [249].

intermediate pyrazoline produced a mixture of the 6-6 closed isomers **1** and **2** in ratios between 2:1 and 1:4, depending on the concentration of the solution of **27** [139,251a]. The two isomers were found to be stable and could not be mutually rearranged in one another, neither photolytically nor thermally [230,251a]. The homofullerene derivatives **28a,b** obtained by thermal N_2 elimination and rearrangement from the pyrazoline intermediates (Scheme 11), are the kinetic products. They are less stable than the 6-6 closed isomer (**29**), most likely due to the double bonds located at the bridgehead carbon atoms which, due to distortion from non-planarity, are energetically costly (*Bredt's rule*). In the 6-6 closed isomer **29**, the structural distortion is less important and energetically less costly. The higher stability of the 6-6 closed isomer compared to that of the 6-5 open isomers[33], and is supported by calculations at different levels of theory [132,249,252].

In contrast to the parent homofullerene $C_{61}H_2$ **2**, the homofullerene derivatives $C_{61}R^1R^2$ (R^1 and/or $R^2 \neq H$) **28** can be rearranged to the more stable methanofullerene derivatives **29** thermally [29,248,253], photochemically [254], electrochemically (Scheme 11) [87,133,255], and in one case, under acid catalysis [253].

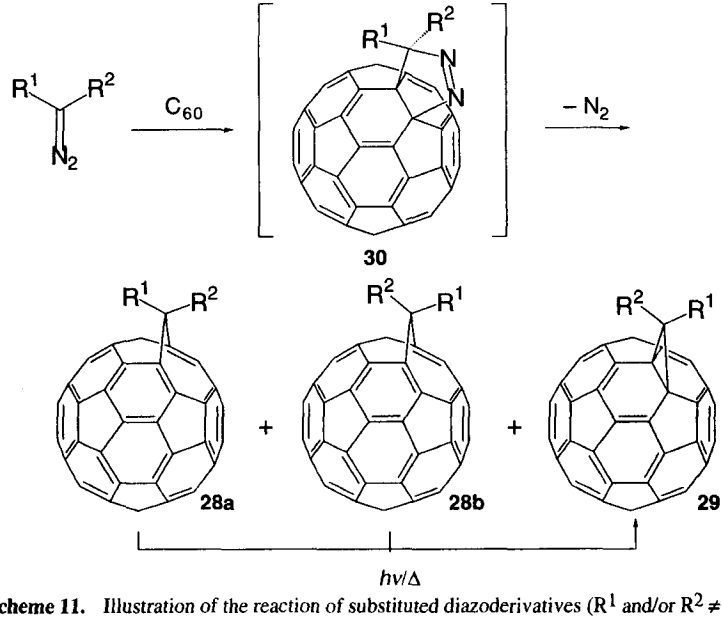

Scheme 11. *Illustration of the reaction of substituted diazoderivatives (R^1 and/or $R^2 \neq H$) with C_{60}.*

[33]In the case of the parent methanofullerene $C_{61}H_2$ the energy difference at the semi-empirical RHF/PM3 level between the 6-5 open and the 6-6 closed isomers is significantly smaller than in the methanofullerenes $C_{61}RR'$ (R and/or R' ≠ H) [249].

The thermal rearrangement of the initially formed homofullerene derivative **28** to the 6-6 closed isomers was initially proposed to occur *via* a two step mechanism, first involving an electrocyclic ring closure to the 6-5 closed isomer, followed by a [1,5] shift to the 6-6 closed isomer [249]. However, measurements of the kinetics of the rearrangement revealed a zero-order reaction [139,256,257], implicating a more complex mechanism.

Li and *Shevlin* proposed that the rearrangement of **28** to **29** is light promoted and proceeds as shown in Scheme 12[34]. The first step is the photochemical conversion of **28** to the singlet excited state, ^{1}**28***, which undergoes very efficient inter-system crossing to the triplet ^{3}**28** (see also Section 1.5.7, for a more detailed account on the photophysical properties of C_{60} and some derivatives). The step requiring thermal activation is postulated to be the rearrangement of ^{3}**28** to the biradical **31**. Radical recombination then leads to the thermodynamic product **29**.

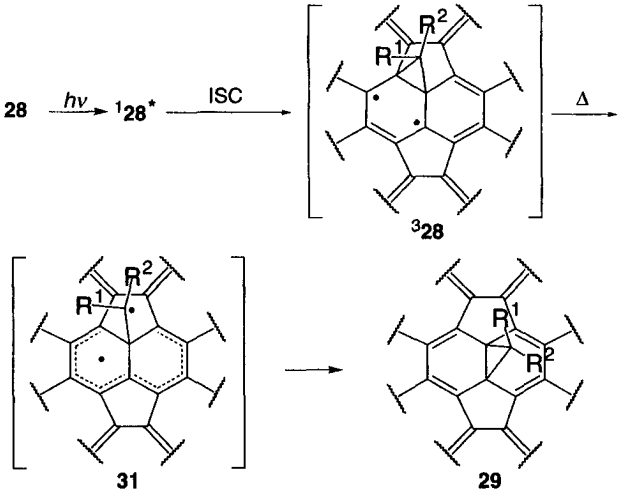

Scheme 12. Mechanism for the light-promoted thermal rearrangement of the 6-5 open isomer **28** to the 6-6 closed **29** ($R^1$and/or $R^2 \neq H$) as proposed by *Li* and *Shevlin* [257].

[34]The mechanism is identical to the di-π-methane (Zimmerman) rearrangement which was proposed previously by *Wudl* and co-workers for the photochemical homofullerene-methanofullerene rearrangement [254].

The mechanism is supported by the following observations:

i) The rearrangement is significantly slower in the presence of dioxygen[35], most likely due to the efficient quenching of the triplet intermediate ^{3}**28** by $^3O_2$ (Scheme 12) [254,257] (see also Section 1.5.2).

ii) The thermal reaction is almost completely absent when carried out in the dark [257].

iii) Substituents (R^1, R^2) at the bridging carbon atom of the homofullerene which are known to stabilize radicals in α-position facilitate the rearrangement. *Wudl* and co-workers found that the ease of thermal isomerization of homofullerenes to the corresponding methanofullerenes decreased in the order diaryl, arylalkyl, and dialkyl homofullerenes[36] [256].

The addition of unsymmetrically substituted diazomethane derivatives proved to be not only regio-, but also diastereoselective (Table 3) [29,255,256,258-260]. The degrees of regioselectivity 6-5 open (**28**) *vs.* 6-6 closed (**29**)) and as diastereoselectivity (**28a** *vs.* **28b**) depend on the nature of the diazo compound as well as the reaction conditions: Electron rich diazo-derivatives add very easily to C_{60} and the reaction can be carried out under mild conditions (T < 60 °C), which seems to strongly limit the formation of the 6-6 closed methanofullerenes **29** [261]. However, when the diazo moiety is attached to electron withdrawing substituents, the 1,3-dipole addition to C_{60} is less facile[37] and higher temperatures and longer reaction times are necessary to carry out the addition, resulting in a lower regio- and diastereoselectivity of the overall reaction (Table 3). In general, the intermediate pyrazoline **30** formed in the first step of the reaction can't be isolated as it readily looses dinitrogen under the reaction conditions used (Scheme 11).

[35]The rearrangement was 11.6 times faster when carried out in a rigorously degassed solution compared to that of an oxygen containing solution under otherwise identical conditions [257].
[36]Substituents at the bridging carbon of the homofullerenewhich are capable of stabilizing radicals can lower the energy barrier for the conversion of ^{3}**28** to the diradical **31**, thus enhancing the rate of the overall rearrangement.
[37]Electron withdrawing substituents of diazo compounds will lower the HOMO energy of the dipole and will slow down the reaction with electron poor dipolarophiles, such as C_{60} [262].

Table 3. Comparison of the isomer distribution upon thermal reaction of diazoderivatives with C_{60}.

			Isomer Distribution			
R^1	R^2	Δ, time	**28a**	**28b**	**29**	Ref.
Ph	$(CH_2)_3CO_2Me$	65 °C, 22 h	95	n.r.[a]	n.r.[a]	[256]
p-MeO_2CPh	H	25 °C, n.r.[a]	95	n.r.[a]	n.r.[a]	[255]
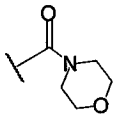	H	110 °C, 48 h	9	1	5	[259]
CO_2Et or CO_2t-Bu	H	110 °C, 24 h	3	1	1	[29]

[a]not reported.

Methanofullerenes are thermally stable compounds and constitute a very versatile class of compounds. For example, methanofullerenes **32** and **33** can be converted under acidic conditions to the carboxylic acid **34** (Scheme 13) which can in turn be easily condensed with amines and alcohols [127]. Methanofullerene adducts have been extensively used for the preparation of fullerene containing polymers [263] and functional derivatives [264-269] which retain most of the fullerene like properties [178] and for the preparation of biological conjugates [168,169a,270].

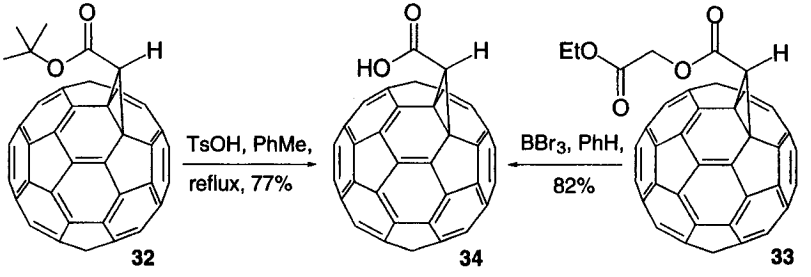

Scheme 13. Syntheses of the versatile synthon **34** as reported by the group of *Diederich* [127]. TsOH = Toluene-4-sulfonic acid.

The addition of organic azides to C_{60} has shown to be a further powerful method for functionalization of the fullerene core and is the only other method besides the addition of diazo compounds to produce 6-5 open monoadducts [271]. Thermal reaction of azides with fullerenes proceeds *via* a 1,3 dipolar addition to produce the thermally labile triazoline which could be isolated if the reaction was carried out at temperatures below 60 °C [272-275]. The structure of **35b** was confirmed by X-ray analysis [273]. At temperatures above 80 °C, the triazolines loose N_2 and rearrange to the regioisomeric 6-5 open azahomofullerenes **36** and to traces of the 6-6 closed aziridin derivatives[38] **37**.

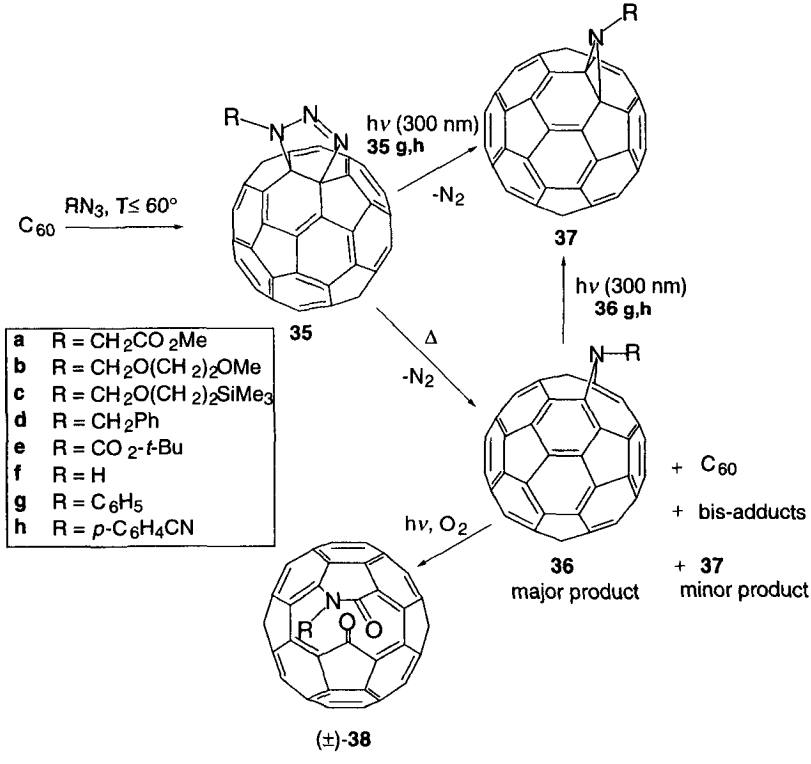

Scheme 14. Addition of azides to C_{60} and thermal as well as photolytical dinitrogen extrusion from the intermediate triazoline. Note that photolytical rearrangement of **36** has only been achieved when R = aryl, with R ≠ aryl the azahomofullerene does not rearrange but reacts with O_2 to yield **38** [271-273,275,276].

[38]The systematic name for 6-6 closed nitrogen bridged fullerenes is epiminofullerenes [130].

A major side reaction in the thermal extrusion of dinitrogen from **35** is the cycloreversion of the triazoline moiety producing C_{60} in 20 to 55% [272,273,275]. From a mechanistic standpoint, this is of some relevance, since the 6-6 closed aziridine derivatives **37** may be formed by [2+1] addition of nitrenes produced under reaction conditions through partial decomposition of the free azide which is present due to cycloreversion, rather than by direct rearrangement of the triazoline **35**.

In analogy to their carbon counterparts, 6-6 closed aryl-epiminiofullerenes **37g,h** can be obtained by photolysis of the triazolines **35g,h** and of the 6-5 open azahomofullerenes **35g,h**, respectively [275]. In contrast, irradiation of the alkyl-azahomofullerene **36b** under similar conditions did not yield the isomeric 6-6 closed form, but produced the ketolactam (±)-**38b**[39,40], indicating the very high efficiency of $^1O_2$ sensitization by **36b** of traces of residual $^3O_2$ [276]. However, unlike the homofullerenes (except the parent homofullerene $C_{61}H_2$), none of the azahomofullerenes **36** could be rearranged thermally to the 6-6 closed isomers [271,272,275,282] and seem to be in general less inclined to rearrange than the homofullerenes **28**, thus making them very powerful derivatives in which the physical properties parent fullerene remain essentially unchanged due to the preservation of the 60 π-electron system of the C_{60} core (see Section 1.5.3). In addition, as the synthesis of the azide starting materials is often quite simple (usually obtained in a one step reaction by nucleophilic substitution of alkyl or benzyl halides by N_3^-), diverse 6-5 open azahomofullerene monoadducts such as a dendritic fullerene [283], a self assembling amphiphilic fullerene [284], a fullerene dipeptide [285], and a calix[8]arene-C_{60} conjugate [286] have been reported in the literature.

2.3.4 [2+1] Cycloadditions

C_{60} undergoes [2+1] cycloaddition reactions with divalent species such as carbenes, nitrenes, and silylenes [287]. In all these cases, the addition of the reagents occurs at a fullerene 6-6 double bond in a single step. Addition of carbenes was first accomplished by *Vasella, Diederich* , and co-workers who prepared optically active fullerene-sugar conjugates by thermal decomposition of sugar diazirines producing the nucleophilic glycosylidene carbenes which readily added to C_{60} (Scheme 15) [288]. The assignment of the methanofullerene structure of **39** was based on analysis of the ^{13}C-NMR spectra which showed three resonances of quaternary carbon atoms in the sp^3

[39]Very recently the partial optical resolution of (±)-**38b** has been reported [277].
[40]The ketolactam fullerene derivative (±)-**38b** has been used for the synthesis of the heterofullerene $C_{59}N$ as its dimer [278], for the parent hydrazafullerene $C_{59}NH$ [279], and its benzyl derivative [280] as well as arylated derivatives [281].

region of the spectrum in agreement with the presence of a cyclopropane ring in **39** [289].

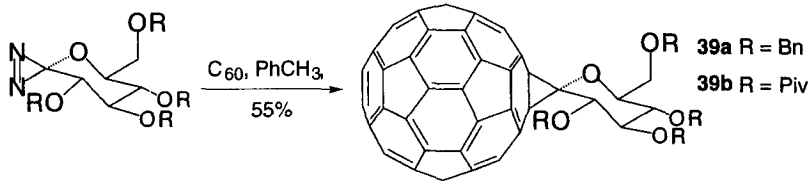

Scheme 15. Synthesis of fullerene-sugar conjugates obtained by carbene addition to C_{60} as reported by the groups of *Diederich* and *Vasella* [288]. Bn = Benzyl, Piv = pivaloyl.

In principle, any method which generates carbenes could be used for the functionalization of C_{60}. For example, additions of dihalocarbenes [290,291], dimethoxycarbene [127,292], diethynyl carbenes [182a,218,293], dicyanocarbene [217], vinyl carbenes [240b], and *Fischer* carbenes [294] to C_{60} have been reported (Scheme 16). Since in general the reactions proceed cleanly and only the products of 1,2-addition at the 6-6 ring junction form, contrarily to the addition of diazo compounds, the carbene addition is a very useful method for the synthesis of methanofullerene derivatives.

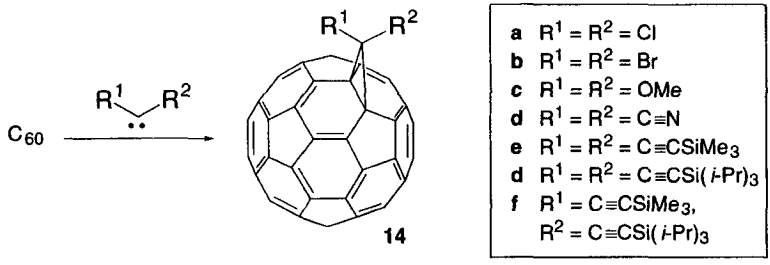

Scheme 16. Some examples of methanofullerenes that can be prepared by addition of carbene intermediates to a C_{60} double bond [127,182a,217,218,290,291,292,293].

Analogous to the addition of carbenes, the addition of nitrenes produces almost exclusively 6-6 closed epiminofullerene derivatives[41], in which the highly reactive nitrene has added to a 6-6 bond in a [2+1] cycloaddition reaction [295,298-302]. The

[41] A small amount of a 6-5 open azahomofullere derivative is obtained in the thermal generation of the nitrene by N_2-elimination of azidoformate [295], which was probably formed by cycloaddition of the starting material followed by N_2 extrusion of the initially formed triazoline [296], rather than by direct insertion of the nitrene into a 6-5 bond of the fullerene, in agreement with this observation is the fact that no 6-5 open adducts were found when the nitrene of the azidoformate was generated photochemically [297].

parent epiminofullerene[42] $C_{60}NH$ **40**, could be obtained easily by addition of *tert*-butyl azidoformate to a boiling solution of C_{60} in 1,1,2,2-tetrachloroethane and refluxing the resulting mixture for five hours[43] [299,300].

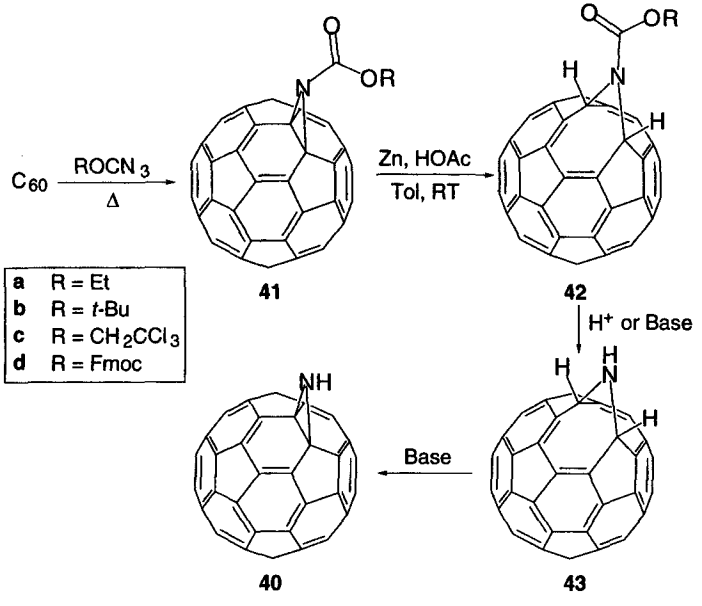

Scheme 17. Synthesis of the 6-6 open fullerene monoadducts **42** and **43** as reported by *Banks et al.* [305].

Shorter reaction times (30 min) produced the urethane **41**, which upon treatment with zinc and glacial acetic acid provided the ring expanded homofullerene **42** in virtually quantitative yield possessing a bridged 10 membered ring orifice in which a 6-6 bond had been reductively opened (Scheme 17). Elimination of the nitrogen protecting group provided access to the parent ring expanded compound $C_{60}H_2NH$ **43**, which was stable as a solid and in solution under acidic and neutral conditions, but underwent oxidative ring closure to **40** when treated with base [305]. The compounds **42** and **43** are the only monoadducts with an open 6-6 bond reported in the literature to date.

[42]The epiminofullerene **40** can be used as nucleophile for the synthesis of urethano-, amido and sulfonamido fullerenes [299,303].

[43]Under mass-spectrometric conditions, using desorptive-chemical-ionization **40** fragments to $C_{59}NH^{+\bullet}$ and $C_{59}NH_2^+$ [304].

2.4 Multiple Functionalization of C_{60}

Considering the presence of 30 equivalent double bonds at 6-6 junctions and the 60 single bonds at 6-5 junctions of C_{60}, multiple functionalization can give rise to a large number of regioisomers. At the beginning of the work presented in the next Sections, very few higher adducts with a defined addition pattern had been prepared and characterized, and a controlled synthesis towards defined addition patterns in acceptable yield was practically limited to the tether directed remote functionalization method, which shall be described in the following Section. Controlled synthesis of multiple adducts of C_{60} is still very challenging and subject to current research, and the discovery of reactions which lead to defined addition patterns is more often than not the product of chance rather than design. Nevertheless, certain trends which show a preference for particular functionalization patterns have emerged and shall be discussed. Surprisingly, despite the increasing number of well characterized multiple adducts of C_{60}, no review has been published on the topic to date.

2.4.1 Nomenclature for Multiple Adducts of C_{60}

In the case of multiple 1,2-adducts in which the addends are located at 6-6 ring junctions, eight descriptors indicating the relative position of the addends on the fullerene have been introduced by *Hirsch* and co-workers [306]. In order to describe also multiple adducts which contain addends bridging 6-5 junctions, the original bond labelling algorithm was modified and extended [307]. As the first system is still used in the literature and is very much more intuitive than the latter, it will be used in this thesis. In this system, the C_{60} sphere of a mono-adduct is divided into three areas: the hemisphere containing the addend (*cis*), the equatorial region (*equatorial*), and the opposite hemisphere (*trans*) (Figure 21). Three different sets of double bonds can then be discerned within the hemisphere of the first addend (*cis*-1, *cis*-2, *cis*-3), four different sets of them in the hemisphere opposite to the one possessing the addend (*trans*-1, *trans*-2, *trans*-3, *trans*-4), and two different sets of double bonds are located at the equator (e_{face}, e_{edge}) [306,308]. In order to describe a multiple adduct [230], one starts with the first addend and determines the relative location of the second, and in the next step, the location of the third relative to the second is determined. This process is repeated up to the last addend, the position of which relative to the first addend is finally determined. This generates a combination of descriptors[44] containing the same

[44] In some cases, more than one combination of descriptors is possible for a given structure. Thus, the order of priority cis > e > trans, is employed all along this thesis.

number of constituents as the number of addends (except for the bis-adducts which have only one descriptor component).

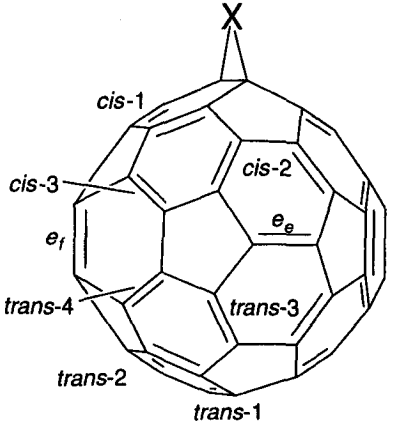

Figure 21. Position of the nine different double bonds in a C_{60} mono-adduct relative to the 6-6 bond carrying the first addend X. In the case of bis-adducts bearing identical addends, the two regioisomers e_{face} and e_{edge} are the same.

2.4.2 Octahedral Addition Patterns

2.4.2.1 Reversible Multiple Functionalization with Sterically Demanding Addends

The first functionalization of C_{60} which led to a defined multiple adduct was carried out by *Fagan* and co-workers [309]. By reacting C_{60} with an excess (≈ 10 eq.) of $[Pt(Et_3P)_4]$ in benzene, it was possible to obtain the air sensitive hexakis-adduct **44** in 88% yield (Scheme 18). The spectroscopic characterization and the X-ray crystal structure determination of **44** showed that the addends are placed in an octahedral pattern on the fullerene sphere (*e,e,e,e,e,e*), the molecular symmetry of the complex being T_h [45]. Later, the analogous Ni and Pd hexakis-adduct complexes could also be prepared [206].

In this addition pattern, the residual fullerene chromophore is reduced to eight benzenoid rings connected by biphenyl type bonds. Analysis of the X-ray crystal structure of **44** revealed that the 6-6 and 6-5 bond length alteration (≈ 0.04 Å) within the benzenoid rings was significantly reduced with respect to C_{60} or its mono-adducts (≈ 0.06 Å) [309]. Synthesis of bis-adducts $\{[Pt(Et_3P)_2]_2C_{60}\}$ showed the formation of three regioisomers, the *trans*-1 and two other isomers which are not direct precursors of

[45] As the octahedral point group is not a subgroup of I_h the molecular symmetry will be lower than O_h.

44, indicating that during the formation of **44** a mixture of many isomers was present, which upon increased functionalization in the presence of an excess of $[Pt(Et_3P)_4]$ equilibrated to form the thermodynamic product **44**. The reversibility of the metal complexation to C_{60} explains the formation of only one, isomerically pure, multiple adduct in excellent yield. The steric requirements and the 'aromatization' of the benzenoid substructures with a higher π delocalization were believed to be the driving force in the formation of **44** [206]. Interestingly, the addition of 1 eq. of diphenylacetylene to a benzene solution of **44** afforded the pentakis-adduct **45** upon loss of one $Pt(Et_3P)_2$ addend (Scheme 18) [206].

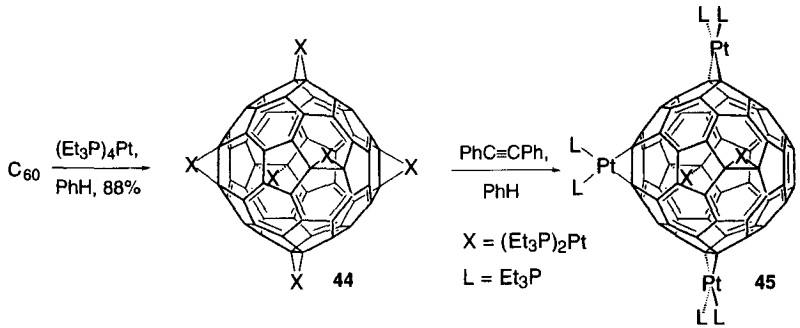

Scheme 18. Reaction of C_{60} with an excess of $[Pt(Et_3P)_4]$ leading to the formation of the hexakis-adduct **44** under thermodynamically controlled conditions, and the removal of an $Pt(Et_3P)_2$ addend, as reported by the group of *Fagan* [206,309].

2.4.2.2 Irreversible Multiple Functionalization with Sterically Demanding Addends

Although these initial studies by *Fagan* and co-workers indicated that under thermodynamic control multiple 1,2-additions to the fullerene sphere might generally proceed to give T_h-symmetrical hexakis adducts, it was unclear if irreversible 1,2 additions to C_{60} would show a preference for certain addition patterns or if such reactions would produce a statistical distribution of all possible regioisomers. This question was addressed by *Hirsch* and co-workers who have since carried out the most comprehensive study on the reactivity of C_{60} in multiple sequential 1,2-functionalization reactions [306,307,310-312]. The first reaction to be studied was the nucleophilic cyclopropanation of C_{60} (*Bingel* reaction) using diethyl α-bromomalonate and NaH as the base at room temperature [306,310]. The mono-adduct **15** was first prepared and then further reacted under the same conditions to give a mixture of isomeric bis-adduct. HPLC separation allowed the isolation of seven regioisomeric bis-

adducts **46a-46g** in yields of 0.9, 2.5, 15.5, 3.7, 12.0, 5.3, and 0.8%, respectively[46] (Scheme 19) [306].

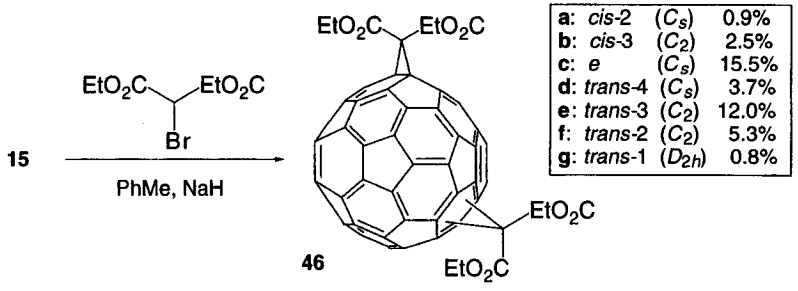

Scheme 19. Nucleophilic cyclopropanation of mono-adduct **15** yielding a mixture of seven bis-adducts **46** as reported by the group of *Hirsch* [306].

Seven out of the eight possible bis-adducts were isolated by HPLC. The structural assignment of the respective isomers was based on NMR spectroscopic techniques which allows to determine the symmetry of the respective isomers[47]. Furthermore, comparison of the HPLC elution order with the calculated dipole moments (AM1) permitted structural assignment. The formation of the *cis*-1 bis-adduct was ruled out due to severe steric interactions between the addends which are forced into close proximity in that addition pattern. Inspection of the relative product distribution (Scheme 19) clearly showed the preference of nucleophilic reagents for the *e*, and *trans*-3 locations. Since the cyclopropanation reaction with bromomalonates is not reversible, the regioselectivity can't be explained by product stability of certain addition patterns[48]. It must be due to the different reactivity of the eight distinct types of 6-6 bonds in the C_{60}-mono-adduct resulting from the cage distortion which occurs upon addition of the first addend (*i.e.* lowering of the symmetry of the C_{60} cage from I_h to C_{2v}). The regioselectivity, therefore, must be of kinetic origin. This conclusion was supported by frontier orbital calculations (AM1) on mono-adduct **15** which showed enhanced LUMO coefficients at the e_{face} location, followed by the *trans*-3 and *cis*-2 positions, consistent with the relative yields of the nucleophilic bis-cyclopropanation

[46] Direct bis-cyclopropanation of C_{60} with diethyl α-bromomalonate and NaH gave **46a-46g** in the same yields.

[47] From ^1H and ^{13}C NMR studies alone only the *trans*-1 isomer and the C_s-symmetrical *e*-isomer can be unambiguously assigned. (The *trans*-1 isomer is the only bis-adduct with D_{2h}-symmetry and the *e*-isomer is the only one which will show three signals for the ethyl groups of the addends; all others will display only two).

[48] This is supported by AM1 calculations which revealed only very small differences in the heat of formation of the respective isomers. Only the *cis*-1 isomer was found to be significantly less stable (*ca.* 18 kcal mol^{-1}) than the others, due to steric repulsion between the addends.

reaction, and enhanced LUMO+1 coefficients for the e_{edge} locations, followed by *cis*-1 and *trans*-2 [307,310].

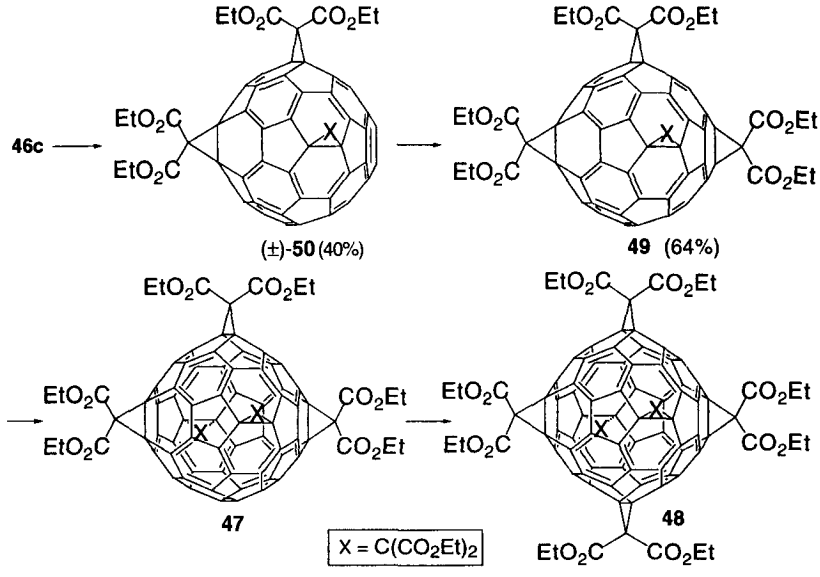

Scheme 20. Stepwise multiple nucleophilic cyclopropanation of C_{60} showing increased regioselectivity with increasing number of addends in *e* relationship, as reported by the groups of *Hirsch* [306,310].

An increase of the regioselectivity in the nucleophilic cyclopropanation was found in the further cyclopropanation reaction of certain bis-adducts. Thus, when isomerically pure *e* bis-adduct **46c** or *trans*-3 bis-adduct (±)-**46e** was used for a further reaction, the *e,e,e* tris-adduct (±)-**50** and the *trans*-3,*trans*-3,*trans*-3 tris-adduct, respectively, could be obtained in 40% yield after HPLC separation (Scheme 20). The regioselectivity further increased dramatically along the series: (±)-**50** → **49** → **47** → **48**, with hexakis-adduct **48** being the only regioisomer formed in the final step (Scheme 20) [310].

The one pot reaction of C_{60} with 8 eq. diethyl bromomalonate and DBU, respectively, yields the hexakis-adduct **48** in approximately 14% [231]. The reaction produces a significant amount of regioisomeric multiple adducts which do not arise from additions to *e*-double bonds, indicating that a pronounced proportion of the successive cyclopropanation of C_{60} proceeds along different channels. This is plausible, as the least regioselective step is the formation of the bis-adducts **46a-46g** (Scheme 19). Eventhough the *e*-isomer **46c**, a precursor molecule of **48**, is the main

product (relative yield 38%), 60% of the bis-adducts are five isomers from which **48** can not be formed.

The yield of the hexakis adduct **48** can be significantly increased by reversible template-directed activation of the *e*-double bonds introduced by *Hirsch* and co-workers [231]. The strategy takes advantage of the reversible addition of a template precursor forming a mixture of multiple adducts. Under thermodynamic control, adducts with incomplete octahedral addition patterns predominate, which can serve as template for subsequent irreversible *e*-additions with increased regioselectivity (see Scheme 20).

9,10-Dimethylanthracene (DMA) was found to be a suitable template precursor since it adds reversibly to C_{60} already at room temperature (see also Section 2.3.2). Addition of 10 eq. of DMA to C_{60} resulted in the formation of predominantly bis- and tris-adducts with an incomplete octahedral addition pattern. Subsequent treatment of the mixture with 8 eq. of DBU and bromomalonate, respectively, yielded the hexakis-adduct **48** in 37%, which is a threefold increase compared to the reaction without template activation [231].

The crystal structure of **48** [231], similarly to that of the hexaplatinum complex **44**, shows a reduction of the bond length alteration by half (≈ 0.03 Å) within the benzenoid rings in the residual chromophore of the fullerene in comparison to C_{60}.

However, when the nucleophilic cyclopropanation reaction was carried out on the mono-adduct **41b**, (see Scheme 17) having a sterically less demanding addend compared to **15**, addition at the *cis*-1 bond also occurred. The *e*, *cis*-1 ((±)-**51**)[49] and *trans*-3 bis-adducts were in that order the most abundant regioisomers isolated (Figure 22) [312]. AM1 calculations showed that in this case, the *cis*-1 bis-adduct (±)-**51** is thermodynamically the most stable isomer, followed by the *e* bis-adduct[50].

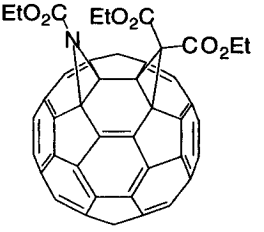

(±)-**51**

Figure 22. Bis-adduct with a *cis*-1 addition obtained pattern by nucleophilic cyclopropanation of **41b** [312].

[49]It is noteworthy, that hydrogenation of 1,2-$C_{60}H_2$ with BH_3 led predominantly (50%) to the *cis*-1-isomer of $C_{60}H_4$ followed by equal amounts (20%) of the *e* and an unidentified isomer [313] (probably (±)-*trans*-3 as later the (±)-*trans*-3,*trans*-3,*trans*-3 $C_{60}H_6$ could be isolated and characterized [314]).

[50]The *cis*-1 bond in C_{60}-monoadducts has been found in various X-ray crystal structures (see for example [265,312]) to be significantly shorter (followed by the e_{edge}-bond) than the other 6-6 bonds of C_{60}. And it has been argued that the shortest double bonds in a fullerenes in general and in fullerene derivatives should be the most reactive [265,315-317]. However, the reactive *trans*-3 bond of C_{60} monoadducts is hardly perturbed upon monofunctionalization [312], making a direct correlation between bond length and reactivity implausible.

The preference for multiple functionalization in the *e*-position in the case of sterically demanding addends, which prevent the formation of the *cis*-1 isomer explains the isolation of the hexakis-adduct **52** from a one-pot reaction in good yields (Scheme 21). *Kräutler* and *Maynollo* allowed C_{60} to react with 1000 eq. of 2,3-dimethylbuta-1,3-diene in *ortho*-dichlorobenzene (*o*-DCB) at 110 °C for 10 days [318]. After column chromatography, the T_h-symmetrical hexakis-adduct **52** was isolated in 26% yield for which the structure could be unambiguously assigned by NMR spectroscopy. The extremely high regioselectivity of this six-fold [4+2] cycloaddition reaction with C_{60} is due to a combination of the steric requirements of the cyclohexene rings which effectively prevent additions in *cis* positions relative to the other addends, and to the *e*-directing effect once at least two addends are bound in an *e* relationship and which increases parallel to the degree of functionalization.

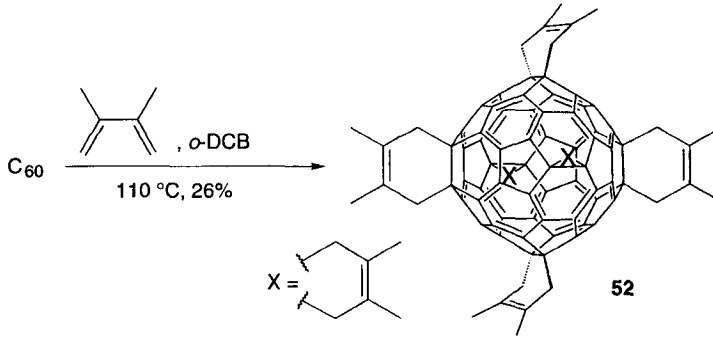

Scheme 21. Six-fold [4+2] cycloaddition of 2,3-dimethylbuta-1,3-diene to C_{60} showing high regioselectivity [318].

These examples established that both reversible as well as irreversible 1,2-additions to C_{60} with sterically demanding addends show a preference to form an octahedral addition pattern on the fullerene sphere. Furthermore, it could be shown that the increased selectivity which is observed in the sequential *e*-addition pattern can be well understood by inspection of the LUMO coefficients (RHF-SCF-AM1) of the respective adducts **46c** to **47** [307].

2.4.3 Selective Crystallization: The Special Case of the *trans*-1 Addition Pattern and a *cis*-1, *cis*-1, *cis*-1 Tris-Adduct.

Among the eight regioisomeric bis-adducts, the most symmetrical *trans*-1 is the kinetically most disfavored, and, in the cases experienced so far, it is the least soluble isomer. This insolubility has allowed the isolation of some *trans*-1 bis-adducts from reaction mixtures containing many regioisomers. The method is applicable only in the case of reversible reactions in which the precipitation of the *trans*-1 isomer drives the equilibrium toward its formation. In contrast, kinetically controlled irreversible reactions lead to a large number of isomers in the reaction mixture (*vide supra*) and equilibration is not possible.

The reaction of C_{60} with $Ir(CO)Cl(PMe_2Ph)_2$ (1 - 3 eq.) in benzene led to the precipitation of a deep violet material [319], consisting of obelisks, plates, clumps of needles, and amorphous material. X-ray crystallographic analysis showed that the obelisks and plates were conformational isomers of the *trans*-1 C_{2h}-symmetrical bis-adducts **53a** which had selectively crystallized from the reaction mixture (Figure 23). In an attempt to prepare higher multiple adducts by the use of less bulky and more reactive reagents, the *trans*-1 bis-adducts **53b** and **53c** also precipitated selectively [320]. Complex **53c** was soluble enough to allow ^{31}P-NMR spectroscopic studies which indicated extensive dissociation in solution and the coexistence of **53c** with a variety of other bis-adducts.

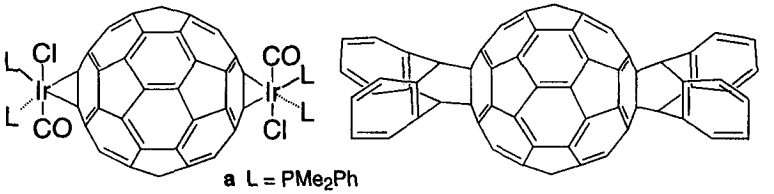

53 **54**

Figure 23. *Trans*-1 bis-adducts **53** [319,320] and **54** [227a] isolated through selective crystallization by the groups of *Balch* and *Nogami*, respectively.

Reaction of C_{60} with anthracene in refluxing benzene produced next to the mono-adduct **23** (25% yield) (Figure 19), a bis-adduct fraction in 24% yield [227a]. As a result of the low solubility of the D_{2h}-symmetrical **54**, separation from other bis-

adduct regioisomers was possible by repetitive precipitation from CS_2 with hexane. Its structure could be unambiguously assigned by NMR spectroscopy (Figure 23).

In a variation of the theme, *Kräutler* and co-workers were able to obtain the *trans*-1 bis-adduct **54** by heating a sample of the crystalline mono-adduct **23a** at 180 °C for 10 min [321]. Analysis of the crystal structure of **23a** had shown that the monoaddcts are aligned linearly, in such a way that the anthracene moiety of one molecule faces the *trans*-1 bond of the next. Thus, heating of the crystal resulted in a topochemically controlled intermolecular anthracene-transfer reaction in the solid state affording 48% each of C_{60} and the bis-adduct **54** (Scheme 22). The reaction is believed to be entropy driven, due to the additional rotational freedom of the C_{60} in the crystal upon the anthracene transfer to its neighbor [321].

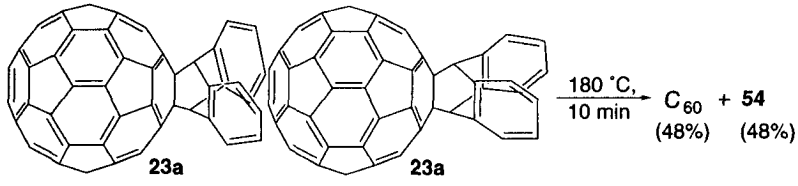

Scheme 22. Topochemically controlled regioselective functionalization of C_{60} by *Kräutler* and co-workers [321].

By use of the selective crystallization method, two other unique addition patterns were realized in the complexes **55** and **56**. The C_{2h}-symmetrical **55** was obtained by mixing benzene solutions of C_{60} and $[Ir_2Cl_2(1,5\text{-}COD)_2]$ in a 1:1 molar ratio (Figure 24) [322]. In tetrakis-adduct **55**, *cis*-1 bis-addition is combined with *trans*-1 addition. The C_{3v}-symmetrical complex **56** was prepared by heating a hexane mixture of C_{60} and $Ru_3(CO)_{12}$ in a 1:2 molar ratio (Figure 24) [323]. The formed precipitate was separated from residual C_{60} by thin layer chromatography and characterized by X-ray analysis. C_{60} displays a coordination behaviour toward the triruthenium cluster which is similar to that of benzene. Tris-adduct **56** is the only case in which the *cis*-1,*cis*-1,*cis*-1 pattern within a six-membered ring is realized[51].

[51] Bis-adducts with direct Ru-Ru bonding and *cis*-1 addition pattern have also been reported [324].

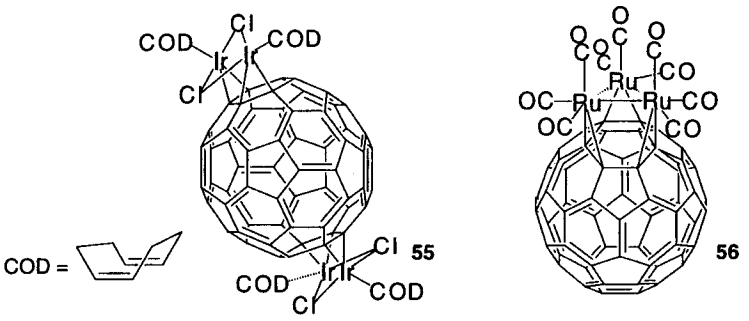

Figure 24. The two unique addition patterns in tetrakis-adduct **55** [322] and tris-adduct **56** [323] as reported by the groups of *Pakkanen* and *Shapley*, respectively.

2.4.4 6-5 Open and 6-6 Open Bis-Adducts

The 6-5 open bis-adducts which will be discussed in this Section were all discovered during the work of this thesis presented in the following Sections.

The first 6-5 open bis-adduct was reported by *Hirsch*, *Wudl* and co-workers [272]. They found that the dominant bis-adduct which had been formed as a side product in the synthesis of **36** [271] (see Scheme 14) was the bis-azahomofullerene **57**[52] in which two adjacent, open 6-5 junctions are bridged by nitrogen atoms (Scheme 23). The regioselectivity of the bis-addition is quite remarkable: when C_{60} and an excess of trimethylsilylethoxymethyl azide ($SEMN_3$) in chlorobenzene was heated to reflux for approximately 12 h, **57b** was formed as the main product (60%), in which the bridging nitrogenatoms are arranged in a geminal relationship on the shared 6-6 bond of C_{60}, along with the mono-adducts **36b** (30%) and **37b** (10%) [272]. In order to obtain information on the origin of the regioselective formation of **57** a concentrated solution of **36a** was treated with methyl azidoacetate at room temperature which led to the formation of only one mixed triazoline/azahomofullerene **58**. Dinitrogen extrusion upon heating gave rise to **57** and a small amount of another bis-adduct **59**, whose structure could not be unambiguously assigned.

[52]The bisazahomofullerene **57a** fragments under FAB mass spectroscopic conditions to $C_{59}N^+$ and C_{60}^+ in an approximate ratio of 5:4 [325], and **57** (with R = $CH_2O(CH_2)_2OCH_3$) can be transformed to the heterofullerene dimer $(C_{59}N)_2$ [326], although in lower yield than if starting from the ketolactam **38b** (*ca.* 12-15% *vs.* 85-95%) (see Scheme 14).

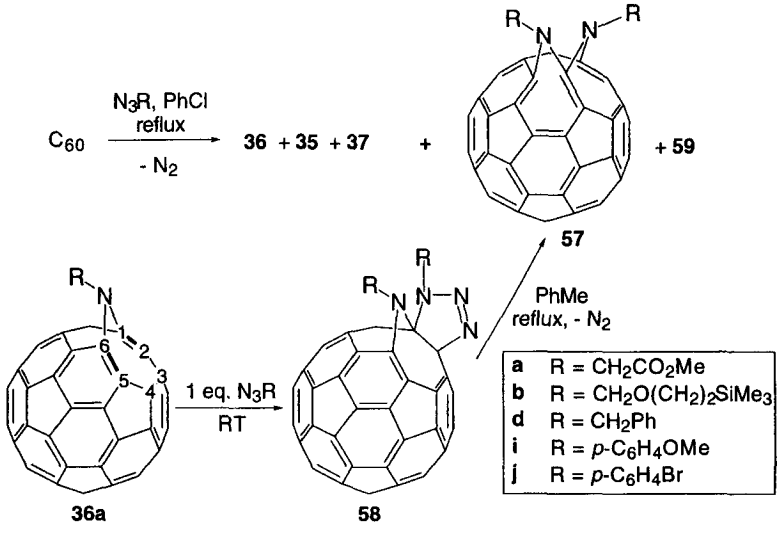

Scheme 23. Synthesis of the bis-azahomofullerene **57** as reported by *Hirsch, Wudl,* and co-workers [272].

The regioselectivity of the addition of the azide to the mono-adduct **36a** was explained by the polarization of the enamine-type double bonds in **36** (shown in bold), which according to calculations[53], showed the highest positive partial charges at the C(1) and C(6) and the highest negative partial charges at C(2) and C(5), respectively. As alkyl-azides have the highest negative partial charge at the alkylated nitrogen and only a very small negative charge at the terminal nitrogen, the [3+2] cycloaddition will preferably produce the observed product **58**[54]. An analogous addition pattern was obtained by *Shinkai* and co-workers, who used a bisazide tethered by a partial fragment of a crown ether to attach a cone-calix[4]arene close to the fullerene sphere [327].

By using short alkyl tethers, *Luh* and co-workers and *Chan* and co-workers were independently able to synthesize the bis-azahomofullerenes **60**, **61** and **62** in which the nitrogen atoms that bridge the open 6-5 junctions of a five membered ring are separated by a 6-5 bond (Figure 25) [282,328-330].

[53]The partial charges are Mulliken charges, calculated with the semiempirical AM1 method [272].
[54]The regioselectivity of the addition of alkyl azides to **36** can also be readily understood in terms of frontier orbital analysis, and is generally observed in the addition of alkyl-azides to enamine- or enol-double bonds [262].

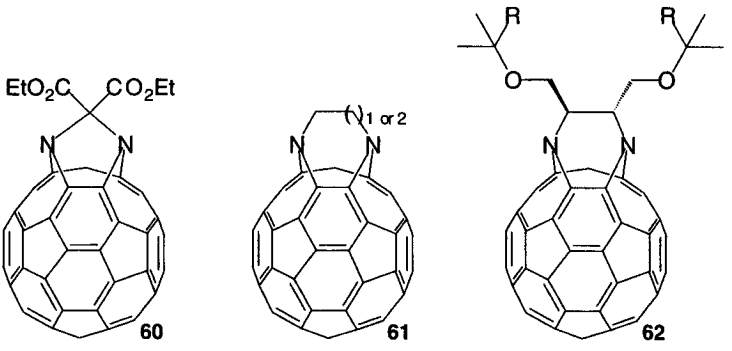

Figure 25. Depiction of the tethered bisazahomofullerenes **60**, **61**, and of the chiral, C_2-symmetrical derivative **62**, as reported by *Luh* and co-workers and *Chan* and co-workers [328-330].

The synthesis of the bisadducts was achieved by refluxing a solution of C_{60} with an excess (1.2 - 1.5 eq.) of the corresponding bisazides in chlorobenzene or xylene, producing the bisazahomofullerenes in yields between 49 and 65% [328-330]. The exact reason for the high regioselectivity in the formation of the bisazahomofullerenes **60**, **61** and **62** is not entirely understood, but quite obviously the tether of the bisazide starting compounds prevents the two azide moieties to adopt a conformation which could lead to the formation of mixed triazoline/azahomofullerenes such as **58**, thus preventing the formation of the addition pattern found in **57**.

A possible reaction pathway was proposed by *Luh* and co-workers, who were able to isolate the bistriazoline **63** which shows a *cis*-1 addition pattern [282]. Based on the NMR spectra alone, it was not possible to rule out **64**, but only **63** is compatible with the products obtained upon thermal dinitrogen extrusion. However, in contrast to the synthesis of **60** - **62**, the bisazahomofullerene **65** and the bisepimino compound **66** are formed in a 1:1 ratio upon thermolysis of **63** (Figure 26). It is therefore not sure if *cis*-1 bistriazoline compounds analogous to **63** are key intermediates in the highly regioselective formation of **60** - **62** [55].

[55]It is also not clear which influence the tether has on the regioselectivity of the thermal dinitrogen extrusion from the intermediate pyrazolines.

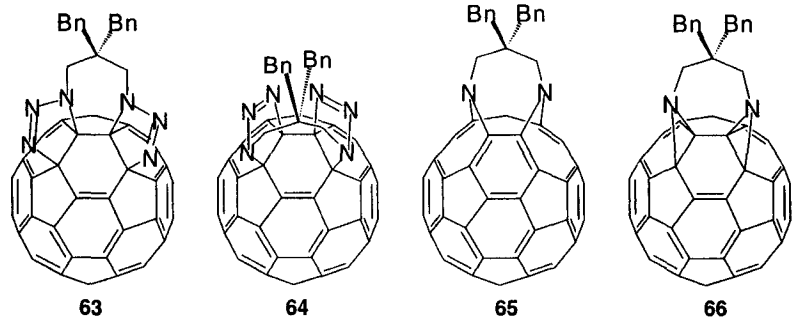

Figure 26. Structures of the bis-azahomofullerene **65** and of the bis-epiminofullerene **66** which are obtained upon thermolysis of the *cis*-1 bistriazoline **63** or **64** as proposed by *Luh* and co-workers [282].

Hirsch and co-workers investigated the regioselectivity of the addition of nitrenes generated *in situ* from ethyl azidoformate at 145 °C to the epimino fullerene monoadduct **41a** (see Scheme 17). The regioselectivity was similar to the one observed in the nucleophilic cyclopropanation of mono-adduct **15** and gave seven regioisomeric bis-epiminofullerenes which are isostructural to **46** (Scheme 19) in addition to the green *cis*-1 bis-adduct **67a** [56] (Figure 27) [311]. The yield of **67a** could be increased substantially (to 50%) by reacting **41a** with a twofold excess of the corresponding azide at 60°C for four days and then heating the reaction mixture for 30 min to 110°C.

In this case, the formation of **67a** is believed to proceed *via* the mixed epimino/trazolinofullerene **58**. Interestingly, of the eight bis-adduct regioisomers produced in the nitrene addition at high temperatures the *cis*-1 isomer is the only one which has two 6-6 open bonds. This can be understood considering the principle of minimizing the number of energetically unfavorable 6-5 double bonds: whereas **67** forces three double bonds into five membered rings, the other regioisomers would require six double bonds at 6-5 junctions.

[56]The regioselectivity was slightly lower than in the nucleophilic bis-cyclopropanation of C_{60}, most likely due to the higher temperatures which are necessary to generate the nitrene (145°C for the addition of nitrenes *vs.* RT for the *Bingel* cyclopropanation reaction); it nevertheless exhibits preference for the *cis*-1 and *e* adduct formation.

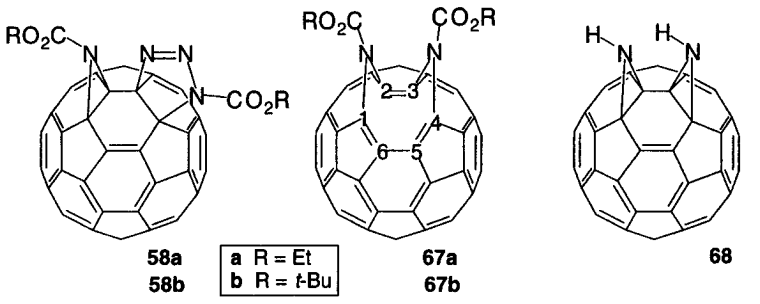

Figure 27. Depiction of the bis 6-6 open fullerene **67**, which rearranges to the bis-epimino fullerene **68** upon removal of the nitrogen protecting groups and can be synthesized either by twofold nitrene addition or *via* the proposed mixed epimino/triazoline derivative **58** as reported by *Hirsch* and co-workers [311].

Besides the addition pattern, the nature of the imino addend is also important: upon deprotection of **67b** with trifluoracetic acid at room temperature, the parent *cis*-1 bisepiminofullerene **68** was obtained which has closed transannular 6-6 bonds. B3LYP/3-21G density functional calculations produced structures in which the carbamate units of **67** are almost planar with a C(1)-N-C(2) bond angle of 107.8° allowing good overlap of the free electron pairs of the nitrogen with the π^* of the carbonyl moiety. The corresponding bond angle in the 6-6 closed *cis*-1 structure is about 65° and the N-atoms of the carbamates are pyramidalized, indicating a reduced conjugation between the lone pairs of the nitrogens and the π^* of the carbonyl. Thus, the balance between two competitive effects, namely, introduction of unfavorable 6-5 double bonds and the possibility of sp^2-hybridization in the case of amides or carbamates determines whether the transannular 6-6 bonds are open or closed. Structures **67** are the only known fullerene derivatives besides **42** and **43** (see Scheme 17) with open transannular 6-6 bonds.

Besides the homofullerenes discussed in the following Section, only one example of a carbon bridged bishomofullerene has been reported in the literature. *Rubin* and co-workers found that the diene **69** [238] underwent a very facile photochemically promoted rearrangement to the stable bis-homofullerene **70** [331]. The process is assumed to occur *via* the initial [4 + 4] photoadduct **71** which is not isolable and immediately undergoes a thermally allowed [4 + 2] cycloreversion to afford the bishomofullerene **70**. The structure of **70** could be proven by X-ray analysis of its cobalt complex **72**. Interestingly, the crystal structure of the cobalt complex **72** revealed that besides coordinating in a η^2-fashion to the ethylene bridge the cobalt had inserted oxidatively into the 6-5 bond opposite of the ethylene bridge of **70** [331]

(Scheme 24). In contrast to the 6-5 open bisazahomofullerenes discussed above, which bridge 6-5 junctions in one five membered ring, the bishomofullerene **70** bridges two 6-5 junctions in a six membered ring in a *cis vicinal* relationship to the common 6-6 bond (Scheme 24).

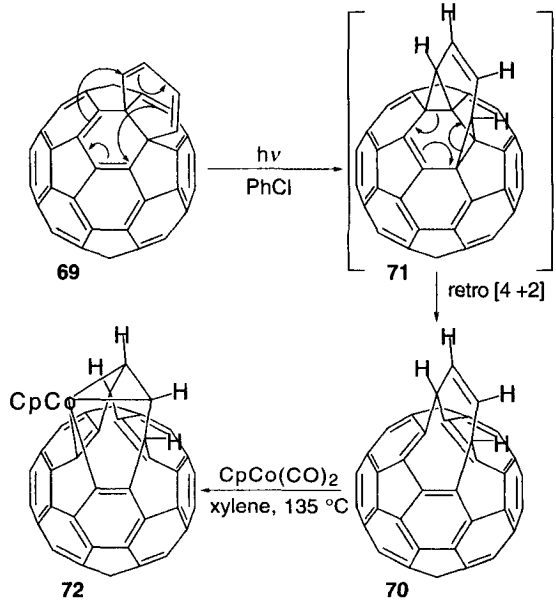

Scheme 24. Synthesis of the bishomofullerene **70** and its cobalt complex **72** according to *Rubin* and co-workers [331].

2.5 Multiple Radical Additions

Radicals readily react with C_{60} most often producing multiple adducts. For example, photochemically generated benzyl and methyl radicals produced radical and nonradical adducts R_nC_{60} (R = $C_6H_5CH_2$) with n = 1 - 15, and $(CH_3)_nC_{60}$ with n = 1 to at least 34, warranting characterization of C_{60} as a radical sponge which readily mops up almost any free radicals [203,332]. Defined multiple radical adducts R_nC_{60} (R = $C_6H_5CH_2$) with n = 3 and 5 were obtained by addition of benzylic radicals generated *in situ* by photolysis of saturated PhMe solutions of C_{60} containing di-*tert*-butylperoxide at 50 °C. At that temperature, the less stable radical adducts decayed which led to a narrowing of the ESR lines. The ESR spectra of the dominant radical species were consistent with the formation of radicals **73** and **74** (Scheme 25) [332]. The unusual

stability of these species was attributed to steric shielding of the fullerene based radical provided by the benzylic groups. The addition patterns in **73** and **74** result from repetitive radical 1,4-additions, as expected from the presence of sterically demanding groups and spin density calculations (see 2.1.1.), and their formation is driven by the generation of stable allylic and ultimately cyclopentadienyl radicals.

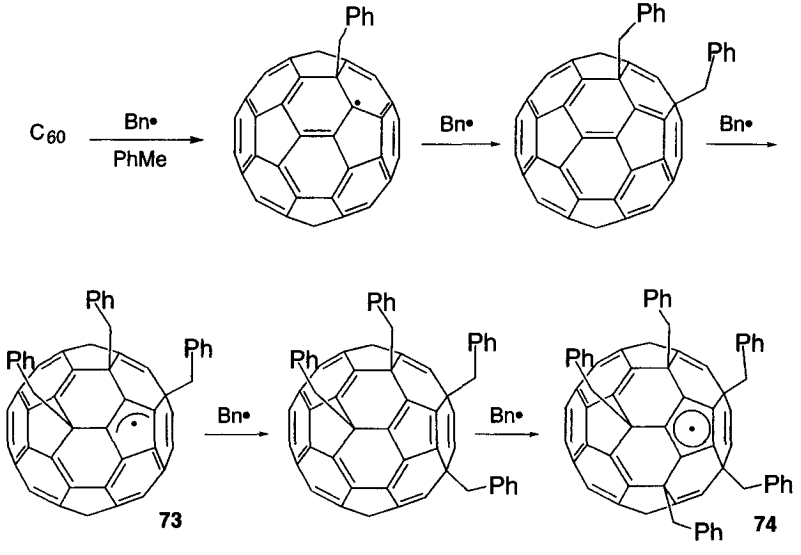

Scheme 25. The addition patterns for multiple benzyl radical addition to C_{60} as reported by *Krusic* and co-workers [332].

C_{60} undergoes multiple additions of halogens [333]. Although in several cases mixtures of structurally unassigned compounds have been obtained, well defined multiple adducts were produced as the major products in other cases and they were isolated mostly by precipitation from the reaction mixture. Due to the similarity of the addition patterns to those exhibited in the above mentioned radical additions, it is likely that halogen addition (X = Cl, Br) to C_{60} occurs *via* a radical mechanism. The pattern observed in the halogenated fullerenes with X = Cl, Br is the result of multiple 1,4-additions. In the case of X = F, the observed addition pattern[57] is consistent with multiple 1,2-additions. The two different addition modes are consistent with calculations for $C_{60}X_2$ at the AM1 level which predict the products of 1,2- and 1,4-

[57]Defined highly fluorinated fullerene derivatives (not discussed explicitly in this thesis) such as the C_{3v} symmetrical $C_{60}F_{18}$ [334], $C_{60}F_{36}$ (mixture of four isomers, one with *T*- and another with T_h-symmetry) [335] and the *T*-symmetrical $C_{60}F_{48}$ [336] have been prepared. Structural assignments were based on 2D (COSY) ^{19}F-NMR spectroscopy.

addition to be the most stable isomers for X = F, and X = Cl, Br, respectively [75]. This is the result of a balance between the electronic effect of introducing a double bond into a five-membered ring in the 1,4-addition mode, and the steric effect of eclipsed groups in the 1,2-mode, which is particularly unfavorable in the case of the sterically demanding Br groups.

When C_{60} was brominated in CCl_4 or benzene, magenta plates of $C_{60}Br_6$ (**75**) precipitated from the reaction mixture. Bromination of C_{60} in CS_2 or $CHCl_3$ yielded dark brown crystals of $C_{60}Br_8$ (**76**) (Scheme 26) [337]. When the bromination was carried out in neat bromine, yellowish-orange microcrystals of the bromine solvate of $C_{60}Br_{24}$ (**77**) precipitated (Scheme 26) [337,338]. All the structures **75**, **76**, and **77** were established by X-ray crystallography. A closer analysis of structure **75** shows that the addition pattern is very similar to that observed for sterically demanding radicals (see radical **74**). Therefore, it was concluded that successive 1,4-additions of bromo radicals occur, with the sixth addend quenching the final cyclopentadienyl radical.

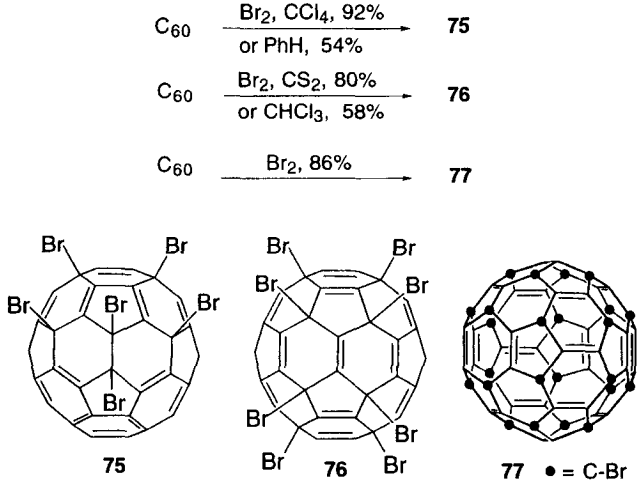

Scheme 26. Addition of Br_2 to C_{60} yielding multiple adducts with a different degree and pattern of addition depending on the reaction conditions as reported by *Birkett et al.* [337] and *Tebbe et al.* [338].

The corresponding chlorinated derivative **78** was obtained by treatment of a benzene solution of C_{60} with ICl and proven to be isostructural to **75** by spectroscopic methods (Scheme 27) [339]. Electrophilic aromatic substitution reaction of **78** with benzene gave **79** which was dechlorinated with an excess of PPh_3 most likely yielding an intermediate cyclopentadienyl anion which was subsequently quenched by traces of

water in the solvent producing **80** [340]. The regioselectivity of the addition and the possibility of further transformations makes the halogenation of C_{60} a valuable reaction for fullerene multiple adduct preparations[58].

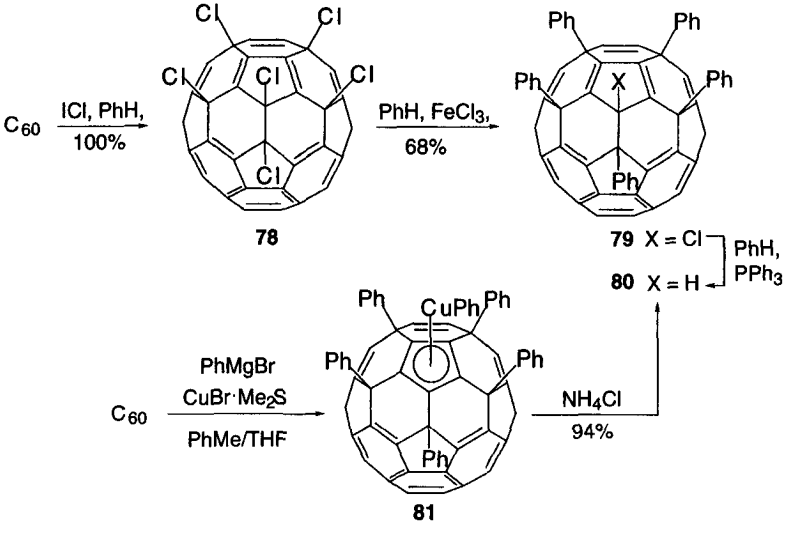

Scheme 27. Chlorination of C_{60}, and electrophilic aromatic substitution reaction of benzene with **78**, and direct synthesis of **80** *via* the η^5-complex **81** [339,340] [342].

Synthesis of **80** was also achieved directly by reaction of C_{60} with an excess of organocopper reagent prepared *in situ* from PhMgBr and CuBr•Me_2S followed by quenching with aqueous NH_4Cl producing the pentaphenyl adduct $C_{60}Ph_5H$ **80** in 94% yield [342]. Treatment of a THF-d_8 solution of **80** with LiO*t*-Bu or KO*t*-Bu led to a conversion of the C_s-symmetric **80** to a species showing C_{5v} symmetry concluded from the ^1H NMR and ^{13}C NMR spectra of the complexes, in accordance with a structure in which the lithium and potassium ion, respectively, were coordinated in a η^5 fashion to the cyclopentadienyl moiety in the C_{60} sphere, similar to the copper intermediate **81**. Indeed, treatment of **80** with TlOEt in THF-d_8 produced thallium(I) complex [Tl(η^5-$C_{60}Ph_5$)] which gave crystals suitable for X-ray analysis proving the η^5-coordination of the metal to the isolated five membered ring of the pentaphenyl C_{60} derivative [342]. The particular significance of these findings was that the addition pattern of a fullerene derivative can produce substructures within the fullerene framework (in this case an isolated cyclopentadiene ring) which show a similar chemical behavior to their

[58]The hexachloroadduct **78** reacts with allyltrimethylsilane in the presence of $TiCl_4$ to form the corresponding hexaallyl-C_{60} derivative [341].

monocyclic counterparts. The reactivity of such isolated substructures within the fullerene chromophore may differ substantially from the chemical behavior of the parent fullerene[59].

In structures **75** and **76**, two and four bonds, respectively, are located within five-membered rings. The double bonds in **75** are in a cyclopentadiene substructure and no longer part of the C_{60} π-system as all adjacent carbon atoms are sp^3-hybridized. In **76**, two of the double bonds at the 6-5 ring junctions are also surrounded by sp^3-carbon atoms. The deconjugation of these double bonds from the fullerene chromophore may also be responsible for the observed addition patterns. The tetrakis-adduct **76** was also obtained, together with intact C_{60}, by disproportionation of **75** upon heating in benzene or carbon tetrachloride. The relative instability of **75** compared to **76** is a consequence of the eclipsing interaction between the two Br-atoms in 1,2 position: In **76** all Br-atoms are in a 1,4- or 1,3-arrangement. Probably the conversion of **75** into **76** involves a sequence of 1,3-shifts initiated by the weakly bound central bromine atom[60]. Three-fold repetition of the addition pattern in **76** gives rise to the T_h-symmetrical pattern of **77**.

Halogen addition to C_{60} is reversible, and equilibration to the most stable products is possible. Compounds **75-78** all revert to the intact fullerene upon heating in the absence of solvent; of the brominated C_{60} derivatives, **77** is the most stable. The formation of diverse derivatives in different solvents most likely arises from selective precipitation of the least soluble fullerene derivatives, which inhibits further reactions to take place.

[59]Fourfold addition of fluoernyl to C_{60} produces a fulvene ring substructure (isostructural to $C_{60}Ph_4$, see Scheme 25) has been reported [343]. Interestingly, the fulvene type substructure of the adduct shows the same chemical behavior as fulvene itself.

[60]The crystal structure of **75** produces a longer C-Br bond for the central bromine compared to the peripheral bromine atoms, indicating that it is less strongly bound to the fullerene core [337].

3. Investigation of the Chemical Properties of Highly Functionalized Buckminsterfullerenes

The emphasis of this chapter is on the investigation of the chemical changes which occur upon increasing functionalization of the fullerene sphere. The chapter is divided into five sections:

-Section 3.1 is an introductory section, which describes in detail the synthesis of bis- to hexakis-adducts of C_{60} with a defined addition pattern *via* tether directed remote-functionalization of C_{60} developed in our group by *Dr. Isaacs* [344]. This methodology represents the basis for the investigations and synthetic efforts carried out in this thesis.

-Section 3.2 describes the synthesis of defined mono- to tris homofullerene derivatives taking advantage of the confinement of the reactivity of the fullerene chromophore to a single double bond in C_{2v}-symmetrical pentakis-adducts of C_{60}.

-In Section 3.3, the influence of the nature of the addends on the regiochemistry of highly functionalized fullerene derivatives is investigated.

-In Section 3.4, the influence of the nature of the addends of C_{2v}-symmetrical pentakis-adducts of C_{60} on the reactivity towards 1,3-dipolar cycloaddition of diazomethane is investigated.

-Section 3.5 gives a brief summary of the key findings of the Sections 3.2 to 3.4.

3.1 Tether-Directed Remote Functionalization of C_{60}

3.1.1 Introduction

A rich variety of methods for the preparation of covalent mono-adducts of buckminsterfullerene have been developed in many laboratories worldwide (see Section 2.3, and for a more comprehensive review, refs. [171-173,174a-c,175a-c,176a-d,177-179]). Initially, the controlled synthesis of defined multiple adducts in acceptable yields was limited to reversible reactions with transition metal complexes leading to the thermodynamically most stable isomer (see 2.4.2.1), to radical additions (see 2.5), or to those derivatives which, by chance, would selectively crystallize from the reaction

mixture (see 2.4.3). Irreversible, stepwise functionalization of the fullerene core, on the other hand, produced mixtures of regioisomers, and purification was subsequently accomplished by often tedious chromatographic separations (see 2.4.2.2).

A more rational approach to the synthesis of a single desired regioisomer in multiple-functionalization reactions was developed in our laboratories in 1994 by *Isaacs et al.* [344]. The concept of tether-directed remote functionalization was applied in order to achieve regioselective multiple additions (Figure 28). Such an approach had originally been developed by *Breslow* for the regioselective derivatization of steroids and long-chain alkanes [345,346].

The principle of the tether-directed remote functionalization of C_{60} is schematically depicted in figure 28. The key aspect of the method is that a tether (T) is designed in such a way that upon addition of an anchor[61] (A), the geometric constraints imposed by the tether force the subsequent functionalization by a reactive group (RG) to take place at a single defined double bond of the residual fullerene chromophore producing only one regioisomer.

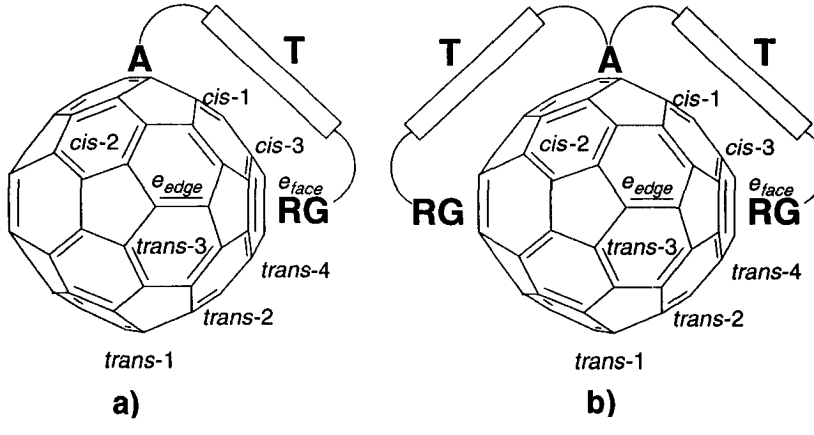

Figure 28. Schematic representation of the tether-directed remote bis-functionalization (**a**) and tris-functionalization (**b**) of C_{60}. The bonds have been labeled relative to the anchor. A = anchor, T = tether, RG = reactive group.

[61]The reactive group to add first to the fullerene was termed anchor, to emphasize that the first addition irreversibly attaches (anchors) the tether-reactive group conjugate to the fullerene sphere.

3.1.2 Application of the Tether-Directed Remote Functionalization Methodology to a High Yield Synthesis of an *e*-Bis-Adduct of C_{60}

An *e*-bis-adduct was identified by *Dr. Isaacs* as the first target molecule. The reasons for choosing the *e* addition pattern were twofold: on the one hand *Hirsch* and co-workers had previously shown that, from an *e*-bis-addition pattern, nucleophilic cyclopropanation with 2-bromomalonate proceeds with enhanced regioselectivity in an *e* position relative to the addends already in place [310] (see 2.4.2.2). On the other hand, it was envisaged that once a suitable tether and reactive group had been developed for the synthesis of the *e*-bis-adduct the use of the same tether reactive group-conjugate could be used to synthesize a tris-adduct in which the second reactive group adds to the other, symmetry equivalent, e_{face}-double bond (Figure 28 b). A particularly intriguing aspect of the addition pattern of a tris-adduct such as b in Figure 28 where the two reactive groups are in an *e* relation to the anchor and in a *trans*-1 relation to each other is, that it is unique to the tether methodology and can't be obtained by other methods[62].

The cyclopropane ring of a methanofullerene was identified as a suitable anchor since it is conformationally rigid and directs substituents at the methano bridge directly towards the e_{face} double bonds (see Scheme 28). As the reactive group, a 2-substituted buta-1,3-diene - known to undergo irreversible *Diels-Alder* reactions with 6-6 double bonds of C_{60}[63] [232,234,237a] (see 2.3.2) - was chosen, as it preserves the plane of symmetry passing through the anchor-cyclopropane moiety, allowing unambiguous identification of a C_s-symmetrical *e*-bis-adduct[64]. The selection of the correct tether connecting the anchor with the reactive group was essential for the regioselectivity of the intramolecular *Diels-Alder* addition, since it had to favor attack at the e_{face} bond (Figure 28) over attack at the second equatorial e_{edge} or the *cis*-3 and *trans*-4 bonds located close to the equator. Molecular model investigations revealed that a *para*-xylylene fragment was the ideal tether to readily differentiate between the desired position of attack (e_{face}) and the e_{edge} and *trans*-4 bonds. A semi-empirical RHF-SCF-PM3 computational study [249,347] predicted that a *para*-xylylene tether would furthermore lead to a large energetic preference (6.5 kcal mol^{-1}) for the targeted e_{face}

[62]The cyclopropanation of an *e*-bis-adduct leads to a D_3-symmetrical *e,e,e*-tris-adduct (see Section 2.4.2.2).

[63]Initial attempts using 9-substituted anthracene derivative as the reactive group were unsuccessful due to facile *retro Diels-Alder* reaction [230].

[64]All other additions to double bonds besides the e_{face} and *trans*-1 double bonds (the latter addition pattern can be prevented by adjusting the length of the tether) would lead to C_1-symmetrical bis-adducts.

bis-adduct **82** over a *cis*-3 regioisomer [344,348][65]. Indeed, the synthesis proved to be very powerful producing the *e*-bis-adducts **82a** and **82b** as the only regioisomers (Scheme 28) [344,348].

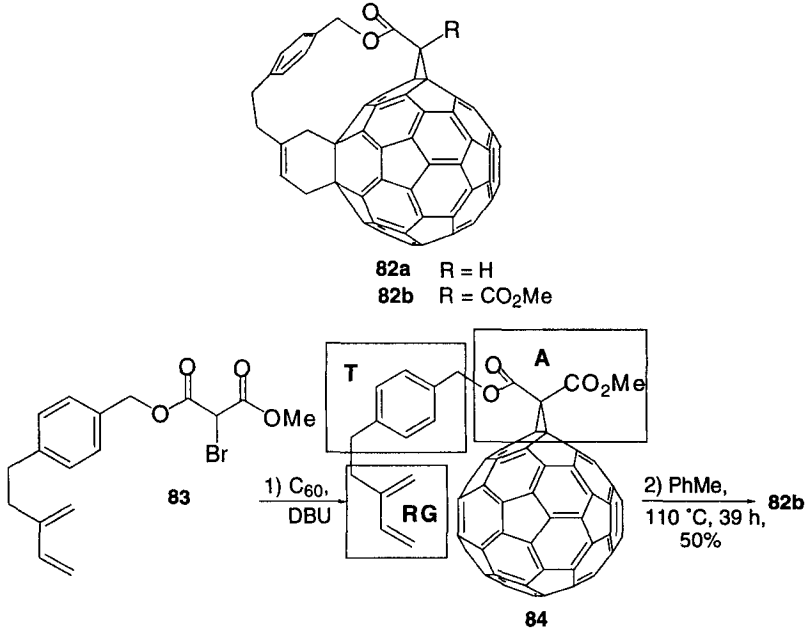

Scheme 28. Depiction of the molecular structures of the bis-adducts **82a** and **82b**, the synthesis of **82b** upon *Bingel* addition followed by intramolecular *Diels-Alder* cycloaddition [348,350].

3.1.3 Extension of the Tether-Directed Remote Functionalization of C_{60}: from Tris- to Hexakis-Adducts

As anticipated, the regiospecific synthesis of the C_{2v}-symmetrical tris-adduct **85** could be achieved in good yield by using the symmetrical, doubly tethered precursor **86** (Scheme 29), which was obtained by bromination of **87**. *Bingel* addition of **86** to an excess of C_{60} (2 eq.) afforded the wine-red methanofullerene **88**. Twofold *Diels-Alder* cycloaddition of the butadiene reactive groups took place upon heating a deoxygenated

[65]The evaluation of the e_{face} and the *cis*-3 regioisomers was based on the respective relative product stability, which showed that the e_{face} bis-adduct was preferred by 6.5 kcal mol^{-1} over the *cis*-3 regioisomer. The assumption made there was that the geometry and energy of the respective transition states were similar to the products implying a late transition state for the reaction. This assumption was shown to be justified by calculations by *Friedman* and *Kenyon* [349] who found that the geometry and energy of the activated complexes leading to the respective isomers were indeed fairly well represented by the respective products.

solution of **88** (*ca.* 0.6 mM) in PhMe to 110 °C in the dark for 39 h, which furnished the brown C_{2v}-symmetrical tris-adduct **85** in good yield (Scheme 29).

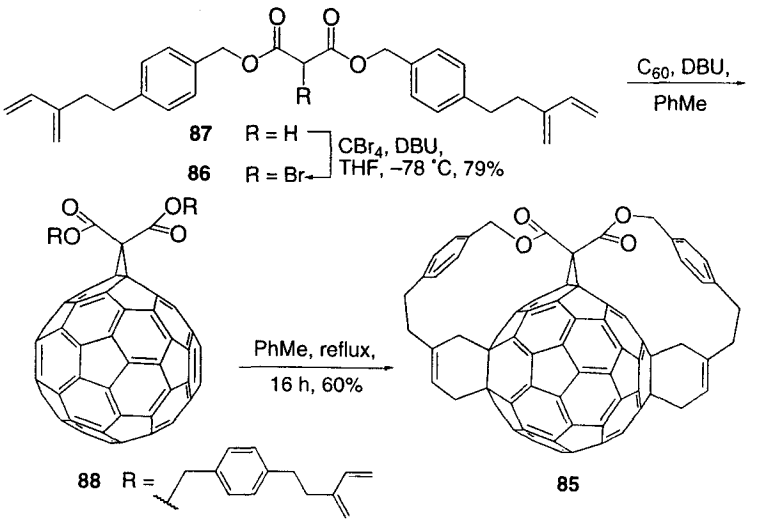

Scheme 29. Synthesis of the tris-adduct **85** according to *Isaacs et al.* [348].

Further functionalization of the tris-adduct **85** was feasible by *Bingel* addition of untethered 2-bromomalonate derivatives providing the C_s-symmetrical tetrakis-adducts **89a,b** in very good yields (≥ 70%) (Figure 29) [308,344,348]. The high regioselectivity of the nucleophilic cyclopropanation reaction[66] is in accord with the frontier orbital calculations by *Hirsch* and co-workers [307,310,312] which yielded enhanced LUMO coefficients at the *e*-bonds. Furthermore, the transition states of the addition leading to **89** might be further lowered in energy by the generation of two isolated benzenoid rings as shown in Figure 29; addition to any other 6-6 bonds in **85** fails to generate such benzenoid ring substructures.

The following *Bingel*-addition with diethyl 2-bromomalonate led to the formation of a mixture of the two isomeric pentakis-adducts **90a** and **91a** in ratios

[66]Starting from the tris-adduct **85**, addition of diethyl 2-bromomalonate in the presence of DBU produced **89a** as the only regioisomer. Using the larger bis(2-ethoxy-2-oxoethyl) 2-bromomalonate for the *Bingel* addition led to a slight contamination of **89b** with three other tetrakis-adducts resulting from addition to less activated double bonds. The lower selectivity in the formation of **89b** compared to **89a**, is probably due to increased steric interactions of the bulkier new addend with the three already in place, which offset the intrinsic electronic preferences of the system [348].

between 80:20 (in PhCl) and 91:9 (in CCl_4)[67] in a combined yield of 70%. Separation of **90a** and **91a** by crystallization or chromatography initially failed, preventing the isolation of pure **90a**. However, complete separation of the formed pentakis-adducts was possible if the fourth and fifth addends were bis(2-ethoxy-2-oxoethyl) malonates which generate larger differences in the R_f values of the isomeric bis-adducts **90b** and **91b**, which were obtained in a 78:28 ratio upon *Bingel* addition of the corresponding bromomalonate in PhCl.

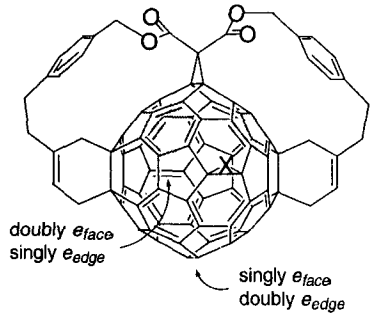

89a X = $C(CO_2Et)_2$
89b X = $C(CO_2CH_2CO_2Et)_2$

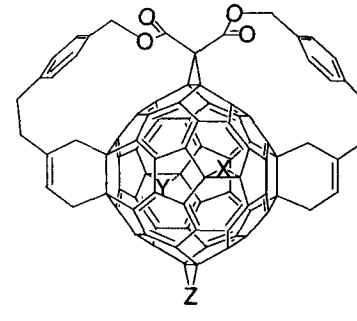

90a X = Y = $C(CO_2Et)_2$, Z = ——
90b X = Y = $C(CO_2CH_2CO_2Et)_2$, Z = ——
91a X = Z = $C(CO_2Et)_2$, Y = ——
91b X = Z = $C(CO_2CH_2CO_2Et)_2$, Y = ——

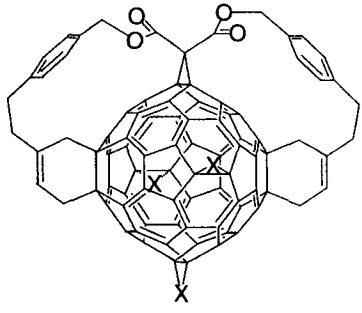

92a X = $C(CO_2Et)_2$
92b X = $C(CO_2CH_2CO_2Et)_2$

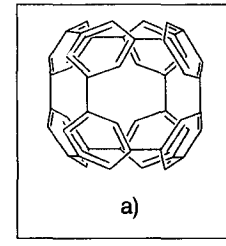

Figure 29. Structures of the tetrakis-, pentakis- and hexakis-adducts obtained with high regioselectivity by *Bingel* addition of untethered malonates to the tris-adduct precursor **85** (Scheme 29). The isolated benzenoid rings in the tetrakis-adducts **89** are highlighted in light gray. Also depicted at the bottom right hand corner of the figure is a), a schematic illustration of the benzenoid 'cubic' cyclophane substructure in **92**.

[67]The enhanced preference for the formation of the C_{2v}-isomeric pentakis-adduct **90a** over the C_s-symmetrical regioisomer **91a** when using CCl_4 compared to PhCl indicated that the selectivity of the *Bingel* addition increases when using increasingly apolar solvents.

The regioselectivity observed for attack at one triply *e*-6-6 bond of **89**, leading to **90**, over attack at another triply *e*-6-6 bond, leading to **91**, was quite remarkable. Inspection of the molecular structure of the tetrakis-adduct **89** revealed that the more reactive bond is doubly e_{face}, with regard to the fused cyclohexene rings of **89** and singly e_{edge} to the anchor cyclopropane (Figure 29), whereas the less reactive 6-6 bond is doubly e_{edge}, relative to the fused cyclohexene and singly e_{face} to a cyclopropane. The selectivity is in agreement with the computational studies by *Hirsch* and co-workers who had predicted enhanced reactivity of e_{face} bonds over e_{edge} bonds [307,310,312][68].

Synthesis of the hexakis-adduct **92** possessing a pseudo-octahedral *e,e,e,e,e,e*-addition pattern was achieved either directly by reacting the tris-adduct **85** with an excess diethyl 2-bromomalonate in the presence of base producing **92a** in 73% yield, or by reacting the C_s-symmetrical pentakis-adduct **91b** with a twofold excess of the appropriate bromomalonate anion, providing **92b** in 85% yield. The residual π-chromophore of **92** consists of eight formally benzenoid rings arranged in a 'cubic' cyclophane structure (Figure 29 a). X-ray crystal structure analysis of **92a** revealed that the bond length alteration typically observed for C_{60} and lower adducts (see Section 1.4.2) is significantly reduced (by *ca.* 0.02 to 0.03 Å) in the eight 'aromatic' rings of this chromophore [308,351] (see also Section 2.4.2) [231,309].

3.2 Investigation of the Chemical Properties of the C_{2v}-Symmetrical Pentakis-Adduct 90

3.2.1 Introduction

The tether directed remote-functionalization methodology provided access to isomerically pure C_{2v}-symmetrical pentakis-adduct **90b** in a fairly good overall yield. In such a pentakis-adduct, the reactivity of the residual chromophore is confined to a single double bond (the last double bond in an *e*-position with regard to the addends already in place), allowing to explore the chemical behavior of such highly functionalized fullerene derivatives and compare it to the parent C_{60}.

[68]However, synthesis of bis-cyclopropanated adducts revealed a preference for the formation of e_{edge} bis-adducts over the e_{face} isomers [312], in apparent discrepancy with the theoretical predictions. Therefore, it is probable, that not only the relative position of the attack (e_{face} *vs.* e_{edge}) but also the nature of the addends already in place (cyclopropane *vs.* cyclohexene) and the addition pattern on the fullerene (mono- *vs.* C_s-symmetrical tetrakis adduct) must be taken into consideration.

The first insight into the change of the reactivity of the C_{2v}-symmetrical pentakis-adduct **90b** compared to pristine C_{60} was gained in the synthesis of **93**, which had been targeted by *Dr. Isaacs* for the construction of derivatives of fullerene-acetylene hybrid carbon allotropes [308]. Initial attempts to synthesize **93** under the same conditions which readily led to a cyclopropanation of C_{60} [218], by *Bingel* addition of the brominated alkyne derivative **94** to **90b** in the presence of DBU in PhCl failed, and solely unreacted starting material could be recovered. Only when the reaction was carried out in Me_2SO, in which the intermediate 3-bromopenta-1,4-diynyl anion is much more nucleophilic[69], a clean conversion to the dialkynylmethanofullerene **93** could be observed (Scheme 30) [348].

The reduced electrophilicity of pentakis-adduct **90b**, compared to C_{60}, is also reflected in its reduction potential[70], which showed that the first one electron reduction of pentakis-adduct **90b** was cathodically shifted by 0.68 V with respect to C_{60} (-1.66 *vs.* -0.98 V) [350,352].

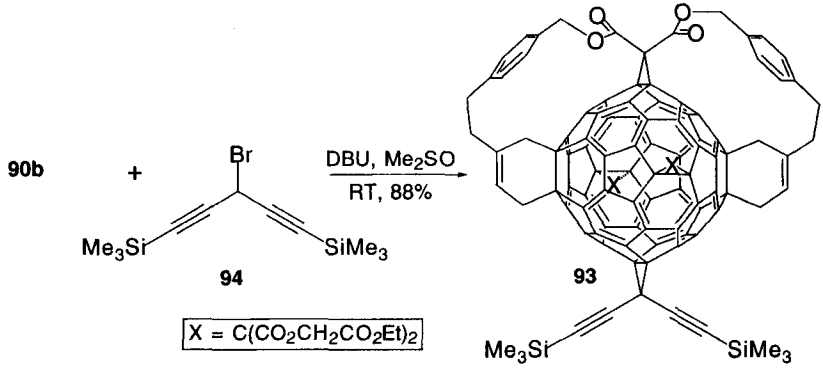

Scheme 30 Synthesis of the dialkinyl-methanofullerene **93** according to *Isaacs et al.* [308,348].

[69]The aprotic polar solvent Me_2SO is well capable of solvating cations leading to free anions which, in turn, are not well stabilized by the solvent, thus, increasing the nucleophilicity of the anions.
[70]As nucleophilic additions (*e.g.* the *Bingel*-reaction) should be favored by the electrophilicity of the fullerene or fullerene derivative and in return, the more electrophilic species should be more readily reduced, the ease of nucleophilic attack should parallel that of the electrochemical reduction.

3.2.2 Exploiting the Confinement of the Reactivity of C_{2v}-Symmetrical Pentakis-Adducts of C_{60} to a Single Double Bond: Regioselective Synthesis of Highly Functionalized Homofullerene Derivatives

3.2.2.1 Preliminary Remarks

The syntheses described below were carried out with both the pentakis-adduct **90b** with the bis(2-ethoxy-2-oxoethyl) malonates as well as with **90a** containing diethyl malonate moieties. As discussed in Section 3.2.2.4, it turned out that the diazomethane adduct of **90b** proved to be unstable under photolytical reaction conditions, whereas under similar reaction conditions, the product of the diazomethane addition to a mixture of the pentakis-adducts **90a** and **91a** led to an isolable amount of products, making the synthesis of isomerically pure **90a** necessary for the photochemical investigations. As the syntheses of the products described below (except for the photolysis experiments) are identical when starting from either **90a** or **90b**, they shall be discussed together.

Synthesis of a mixture of **90a** and **91a** was carried out according to the published procedure described above. [308,344,348]. Pure **90a** could be obtained by column-chromatographic separation (SiO_2-*H*, CH_2Cl_2/hexane 90:10) of the mixture of **90a** and **91a** (Figure 29). However, the separation was very tedious and only **90a** could be isolated in pure form.

3.2.2.2 Synthesis of a C_s-Symmetrical Monopyrazolino-Hexakis-Adduct of C_{60}

In view of the reduced electrophilicity and therefore also of the reduced dienophile character of the pentakis-adduct **90b** (*vide supra*), it was decided to use a large excess of diazomethane for the synthesis of the pyrazolines **95a** and **95b**[71]. Thus, a solution of **90a** or **90b** in $CHCl_3$ was reacted with a *ca.* 60-fold excess of etheral CH_2N_2 at 0 °C (Scheme 31). After 90 min, the color of the solution had changed from orange to a bright yellow (typical of hexakis-adducts with a pseudo-octahedral addition pattern), indicating that the 1,3-dipolar cycloaddition had taken place at the desired double bond, and TLC analysis confirmed the disappearance of the starting material and the formation of a new product with a lower R_f value. Column chromatography (SiO_2-*H*) allowed the isolation of **95a** and **95b** in 71 and 93% yield, respectively.

[71] As the reactivity of **90b** is limited to a single double bond, the formation of a mixture of multiple CH_2N_2 addition products is not a problem.

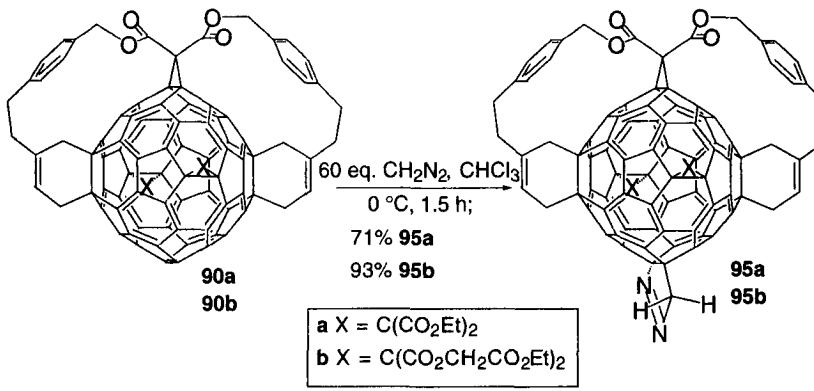

Scheme 31. Synthesis of the hexakis-adducts **95a,b**, *via* 1,3-dipolar cycloaddition of diazomethane to the central double bond in the remaining pyracylene subunit of the pentakis-adducts **90a,b**.

The pyrazolines **95a** and **95b** were found to be thermally quite unstable and rearranged at room temperature within a few days to a new orange, product both in solution as well as in the solid. Prolonged storage in the solid state at –20 °C under N_2 led to decomposition of **95b** to more polar products, probably due to slow oxidation of **95b** with residual O_2. Thus, the characterization of both **95a** and **95b** had to be carried out immediately after their syntheses.

The ^{1}H NMR spectra of **95a** and **95b** show no diastereotopic protons and a single resonance around 5.7 ppm for the enantiotopic pyrazoline-methylene protons. This strongly suggests that **95a** and **95b** posses C_s-symmetry on the NMR time scale, which is only compatible with the addition of CH_2N_2 to the remaining double bond in a pseudo-octahedral position, since addition to any other double bond in **90** would lead to a C_1-symmetrical compound. The C_s-symmetry of **95a** and **95b** is additionally supported by their respective ^{13}C NMR spectra which show 28 (for **95a**) and 30 (for **95b**) out of the 32 sp^2-carbon resonances expected for the C_s-symmetry of the proposed structures. Furthermore, the shape of their UV/VIS spectra strongly resembles that of hexakis-adduct **92** [344,348] which has the same addition pattern (see Section 4.2.2). The expected N=N stretching vibration is weak but clearly visible in the IR spectrum around 1570 cm^{-1}. The instability of the pyrazoline moiety is apparent in the FAB-mass spectra of both **95a** and **95b** which shows only a weak peak for the molecular ion of **95a** (17%) at *m/z* 1521.5, and no signal for M^+ of **95b**. The base peak for both products arises from $[M - N_2]^+$ resulting from loss of dinitrogen from **95a** and **95b**.

3.2.2.3 Establishing the Regioselectivity of the Dinitrogen Extrusion of Highly Functionalized Fullerene-Pyrazoline Derivatives. Part 1: Regiospecific Synthesis of a C_1-Symmetrical Homofullerene Hexakis-Adduct of C_{60} *via* Thermal Dinitrogen Extrusion from a Pyrazoline Precursor

The thermal dinitrogen extrusion from **95** was investigated. The main interest of this experiment was to see if the reaction would proceed with the same high regioselectivity for the highly functionalized fullerene derivative **95** as originally observed for the thermal dinitrogen extrusion from the parent fullerene-pyrazoline $C_{61}H_2N_2$ (see Section 2.3.3 and refs. [131,139,251a-b]) and thus provide access to the homofullerene **96**.

Heating a solution of **95a** or **95b** in CCl_4 under reflux (Scheme 32) led within 15 min to a color change from bright yellow to orange, very similar to the color of the pentakis-adduct **90**. The conversion was very clean producing **96a,b** as the only products according to TLC analysis. Thus, **96a** and **96b** could be obtained in almost quantitative yield (in both cases 93%) after filtration through SiO_2 and recrystallization.

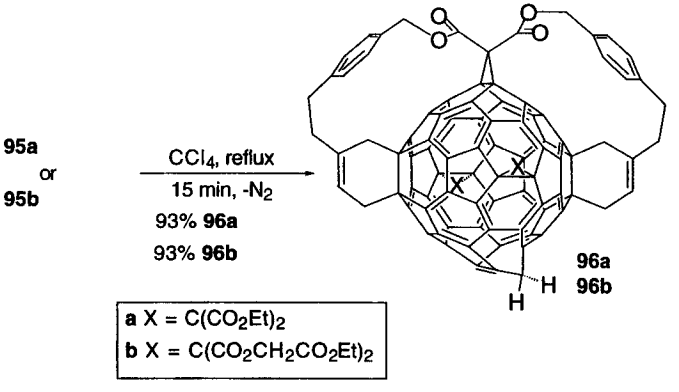

Scheme 32. Synthesis of the 6-5 open C_1-symmetrical hexakis-adducts **96a,b** *via* regioselective dinitrogen extrusion from the respective pyrazoline precursors **95a** and **95b**.

Analysis of the ^1H NMR and ^{13}C NMR spectra showed that the reaction had indeed proceeded highly regioselectively yielding only a C_1-symmetrical product consistent with the structures of **96a** and **96b**, respectively. The loss of symmetry in both **96a,b** is apparent in the signals arising from the diastereotopic alkene-protons of

the cyclohexene rings which are split into two overlapping triplets around 6.2 ppm (see Figure 30). The protons of the methylene group bridging the open 6-5 junction in **96a** resonate as an AX system with a geminal coupling constant of 9.9 Hz at 4.71 and 2.13 ppm[72], respectively.

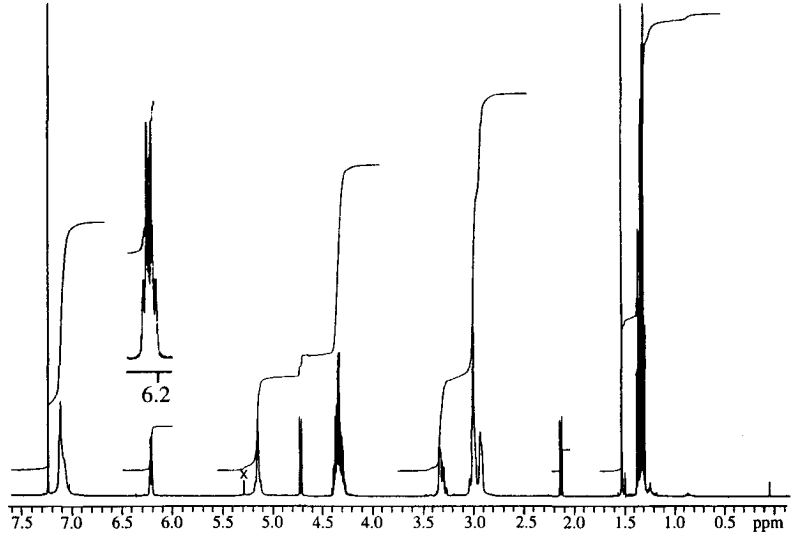

Figure 30. ^1H NMR spectrum (400 MHz, $CDCl_3$) of the C_1-symmetrical hexakis-adduct **96a**. The expansion shows the overlapping triplets arising from the two diastereotopic alkene protons of the tether-cyclohexene moieties.

The ^{13}C NMR spectrum of **96a** shows all six resonances for the carbonyl moieties and both **96a** and **96b** exhibit 55 signals in the sp^2 region confirming the C_1 symmetry of the products. The UV/VIS spectra of **96a** and **96b** are very similar to that of pentakis-adduct **90b**, which was the first indication that also highly functionalized homofullerenes such as **96b** retain much of the optical properties of the corresponding structure lacking the methano bridge (*i.e.* of **90b**), similar to what had previously been observed for the parent homofullerene $C_{61}H_2$ (see Section 1.5.3).

[72]In **96b**, the doublet at lower field falls in the range of 4.75-4.85 ppm and is masked by the resonances of the diastereotopic protons $C(CO_2CH_2CO_2Et)$ of the malonate addends.

3.2.2.4 Establishing the Regioselectivity of the Dinitrogen Extrusion of Highly Functionalized Fullerene-Pyrazoline Derivatives. Part 2: Photolysis of the Monopyrazolino-Hexakis-Adduct of C_{60}

The regioselectivity of the thermal dinitrogen extrusion from **95a,b** forming the 6-5 open **96a,b** (Scheme 32) is analogous to what had been previously observed in the synthesis of the parent homofullerene $C_{61}H_2$. Photolytical dinitrogen extrusion from the pyrazoline $C_{61}H_2N_2$, on the other hand, had led to the formation of a mixture of the homofullerene and the 6-6 closed methanofullerene (see section 2.3.3 and [131,139,251a-b]). We decided to investigate if the photolysis of the highly functionalized pyrazoline **95a,b** would similarly produce a mixture of the 6-5 open and 6-6 closed derivatives.

Initial photolysis experiments were carried out with solutions of the pyrazoline **95b** in degassed benzene in an NMR tube or a Pyrex test tube at concentrations between 13.1 and 0.6 mM. Photolysis of the solutions with a medium pressure 250 W Hg lamp, however, invariably led to complete decomposition of the starting material. In order to further evaluate the conditions necessary for the photolysis it was decided to prepare the pyrazolines from a mixture of the pentakis-adducts **90a** and **91a** (Figure 29) in order to investigate if the bis(2-ethoxy-2-oxoethyl) malonates were responsible for the apparent instability of **95b** under photolytical conditions. Thus, a mixture of the pentakis-adducts **90a** and **91a** was treated with diazomethane as described above (Section 3.2.2.2) and the resulting mixture of the corresponding pyrazolines[73] was photolyzed. Indeed, photolysis of a *ca.* 2 mM solution of the pyrazoline mixture in C_6D_6 was successful. The reaction was continuously monitored by TLC. After eight minutes the starting material had disappeared and besides a considerable amount of baseline material, the formation of a new product with a higher R_f value was visible.

It was therefore decided to repeat the experiments with pure **95a**. The following experiments revealed that the yield of isolable products of the photolysis of **95a** is highly concentration dependent. For example, photolysis of a 0.7 mM or a 23.0 mM solution of **95a** in C_6D_6 without cooling led to complete decomposition of the starting material. Best results were achieved (Scheme 33) at a concentration of 9.6 mM and repeatedly cooling the reaction mixture by holding the NMR tube into ice water for *ca.* 15 s, in order to limit the thermal dinitrogen extrusion from **95a**. After *ca.* 8 min, TLC

[73]The regioisomeric pyrazolines, which arise from the 1,3-dipolar addition of CH_2N_2 to the mixture of the C_{2v}- and C_s-symmetrical pentakis-adducts **90a** and **91a**, respectively, could not be separated chromatographically.

analysis showed only two spots: one at the baseline and an orange one at the same R_f value as the C_1-symmetrical hexakis-adduct **96a**.

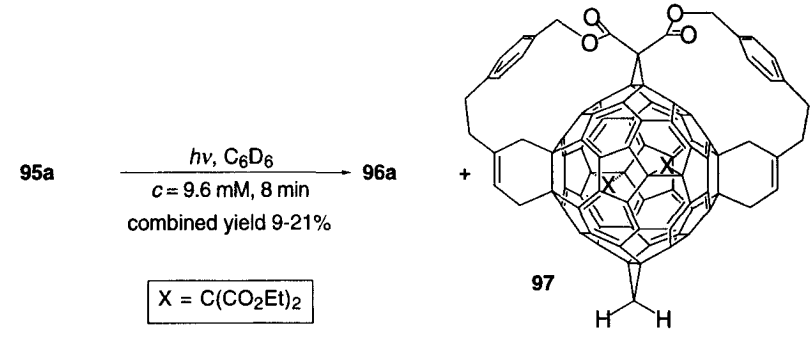

Scheme 33. Photolysis of the pyrazoline **95a** producing a mixture of the C_{2v}-symmetrical methanofullerene **97** and the C_1-symmetrical homofullerene **96a**.

After removing the products arising from decomposition of **95a** by filtration through a pad of SiO_2, the C_{2v}-symmetrical hexakis-adduct **97** and the C_1-symmetrical regioisomer **96a** were obtained in a combined yield between 9 and 21%. The ratio of **96a** and **97** was determined by comparison of the integrals of the resonances corresponding to the enantiotopic protons of the CH_2 bridge of **97** (labeled a in Figure 31) and of those corresponding to the diastereotopic protons of **96a** (labeled b and b' in Figure 31), respectively.

The isomeric mixture could not be separated by column chromatography. Therefore, **97** was purified by adding CH_2N_2 at 0 °C to the mixture in CH_2Cl_2 which transformed **96a** into the octakis-adduct **98a** (see below, Section 3.2.2.5) while leaving **97** unchanged. Chromatographic purification (SiO_2-*H*, CH_2Cl_2) was subsequently feasible, yielding **97** as a bright yellow solid.

The structure of **97** was conclusively established on the basis of its spectroscopic data. Its C_{2v}-symmetrical structure is supported by the number and multiplicity of the resonances in the ^1H NMR spectrum. In particular, the homotopic protons of the CH_2 bridge (Figure 31) give rise to a singlet at 2.57 ppm. Further support for C_{2v} symmetry comes from the ^{13}C NMR spectrum which shows 15 of the 17 expected resonances of the fullerene C-atoms and three carbonyl resonances of equal intensity.

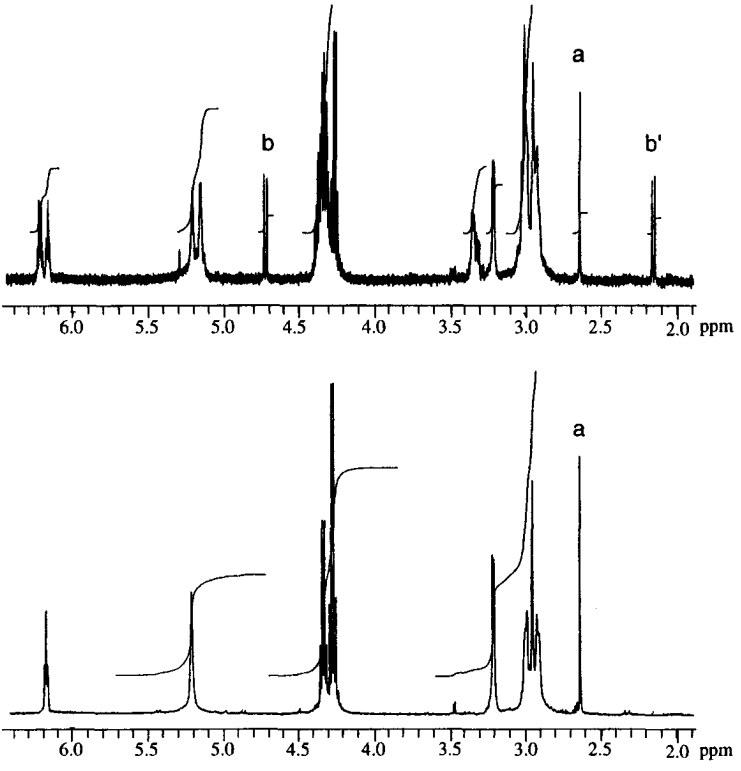

Figure 31. Expansion of the ^1H NMR spectrum (500 MHz, $CDCl_3$) of a mixture of **96a** and **97** (top) as obtained after photolysis of the pyrazoline **95a** and the corresponding expansion of the pure C_{2v}-symmetrical hexakis-adduct **97** (bottom). The singlet arising from the two enantiotopic protons of the CH_2 bridge of **97** is labeled a, and the two doublets corresponding to the two diastereotopic protons of **96a** are labeled b and b', respectively.

The isomer distribution and combined yield of the two regioisomers was found to be strongly dependent on the intervals between cooling the reaction mixture during the photolysis. Longer periods between cooling increased the formation of the 6-5 open isomer **96a**, whereas shorter intervals enhanced the relative yield of the 6-6 closed isomer **97** (Table 4).

These results indicate that at least part of the 6-5 open isomer **96a** in the runs I and II (Table 4) could be formed by thermal dinitrogen extrusion and not *via* the photolytical pathway. However, more frequent cooling of the reaction mixture decreased the yield of the isolable products and attempts to increase the relative yield of **97** by photolysis of frozen solution of **95a** in C_6D_6[74] led to complete decomposition of the starting material.

Table 4. Influence of the time between cooling the samples in the photolysis experiments on the isomer distribution of **96a** and **97** and the combined yield.

Run [a]	Time between Cooling in min. [b]	Ratio **96a**:**97**	Combined Yield in %
I	3.5; 2; 2 x 1.	2:1	21
II	3.5; 1.5; 3 x 1.	1.6:1	11
III	3; 5 x 1.2.	1:1.8	9

[a] Runs I–III were carried out with 9.6 mM solutions of **95a** in C_6D_6.

[b] Cooling of the samples was achieved by holding the NMR tube into ice water for *ca.* 15 s.

As discussed in section 2.3.3, the photolysis of the parent fullerene pyrazoline $C_{61}H_2N_2$ was found to be concentration dependent producing the 6-6 closed isomer **1** and the 6-5 open isomer **2** in ratios between 2:1 at low concentrations up to 1:4 at high concentrations of the pyrazoline precursor [139,251a].

Thus, the photolysis of highly functionalized fullerene-pyrazoline **95a** ultimately yielded similar results to those previously obtained with the pyrazoline $C_{61}H_2N_2$.

[74]The sample of **95a** in solid C_6D_6 was obtained by freezing the corresponding 9.6 mM solution in an ice bath.

3.2.2.5 Regiospecific Synthesis of a Tris-Homofullerene Octakis-Adduct of C_{60}

Treatment of **96a** and **96b** with *ca.* 60 equiv. of CH_2N_2 in $CHCl_3$ at 0 °C (Scheme 34) led almost immediately to a color change from orange to yellow, indicating that **96** is more reactive towards diazomethane than **90**. After purification by column-chromatography and recrystallization, **98a** and **98b** were isolated in 85 and 90% yield, respectively.

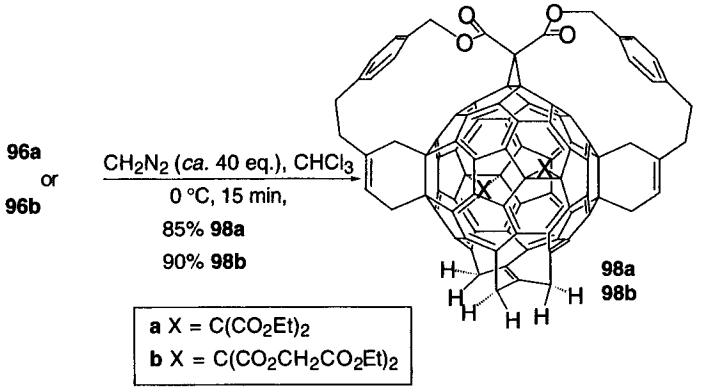

Scheme 34 Synthesis of the octakis-adducts **98a,b**. The high yield of the four step reaction is noteworthy.

The FAB mass spectra showed the respective masses for the molecular ions of **98a** and **98b** at *m/z* 1521.2 and 1753.3 as the base peaks. The ^1H NMR spectra are consistent with the C_1-symmetrical structures of **98a** and **98b** showing six doublets for the diastereotopic methylene protons of the CH_2 moieties bridging the 6-5 open junctions which are grouped into two sets of three doublets at low field between 4.53 and 4.06 ppm and three at high field between 3.49 and 2.02 ppm (Figure 32). In analogy to the bridge CH_2 proton resonances of hexakis-adducts **96a**, the three protons giving rise to the signals at low field were assigned to those located over former five membered rings, whereas the other three are assumed to be located above former six membered rings and appear therefore at higher field.

The ^{13}C NMR spectra of **98a** and **98b** show all six (**98a**) and ten (**98b**) expected carbonyl resonances for the C_1-symmetrical compounds. As a consequence of signals overlapping, only 56 of 66 (**98a**) and 53 of 66 (**98b**) signals are visible in the sp^2 region. As a result of their C_1 symmetry and the overlapping of some signals in the respective

^{13}C NMR spectra, it is not possible to deduce the molecular structures of the octakis-adducts **98a** and **98b** based solely on the spectroscopic data.

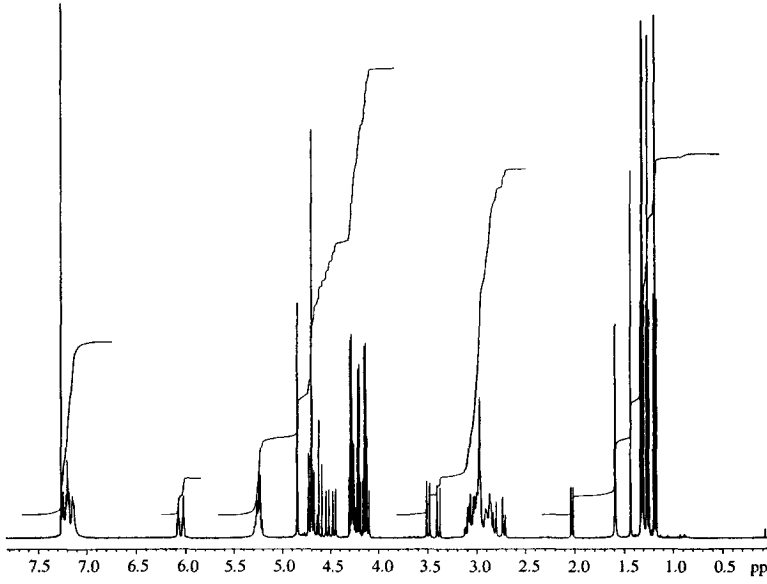

Figure 32. ^{1}H NMR spectrum (500 MHz, $CDCl_3$) of the C_1-symmetrical octakis-adduct **98b**. The resonances of the alkene protons of the cyclohexene moieties are split into two triplets between 6.1 and 6.0 ppm. The protons of the three methano groups bridging 6-5 open junctions appear as six doublets, two around 4.5 ppm, one at ~4.1 ppm (obscured), two around 3.5 ppm, and one around 2.0 ppm.

However, the high regioselectivity of the reaction (reflected in the high yield of **98**) indicated that the reactivity of each of the precursor molecules (*i.e.* **96** and **99** and/or **100**; see Scheme 35) must be limited to a single double bond. If this were not the case, one would expect the formation of more than one product. Taking this into consideration, the following assumptions were made upon which the structures of **98a** and **98b** were proposed:

i) 1,3-Dipolar cycloaddition of CH_2N_2 can only occur at the double bonds in the pyracylene subunit of the fullerene depicted in Scheme 35. This may be assumed since all other double bonds are sterically not accessible as they are in a *cis*-1 relationship to addends already in place.

ii) The reactivity of the hexakis-adduct **96** is confined to the double bond in a pseudo-octahedral position[75] (the double bond highlighted in bold in Scheme 35).

iii) Dinitrogen extrusion of the intermediate pyrazolines **101** or **102** proceeds regioselectively to the bis-homofullerenes **99** or **100**, respectively.

iv) The reactivity of the heptakis-adducts **99** and **100** is limited to the geminally and vicinally bis-functionalized double bond, respectively.

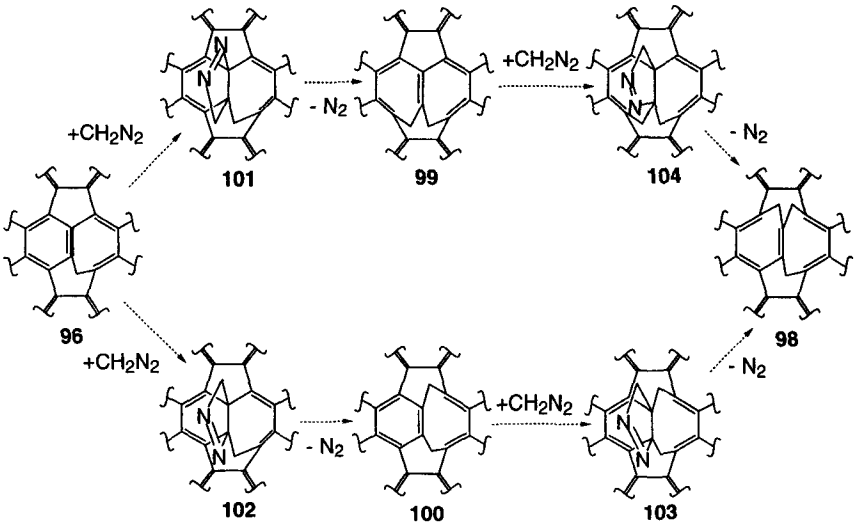

Scheme 35. Illustration of the possible reaction pathways leading to the octakis-adduct **98** *via* the heptakis-adduct **99** and/or *via* **100**. The reactive double bond of the C_1-symmetrical hexakis-adduct **96** is highlighted in bold. For clarity, the fullerene is shown only in part.

If the assumptions proved to be true, then the reaction sequence to the octakis-adduct **98** can proceed *via* the pyrazolines **101** and/or **102** and the bis-homofullerenes **99** and/or **100**. Once the pyrazolines **104**[76] or **103** are formed, the final dinitrogen

[75]This assumption is supported by semi-empirical MO calculations (RHF-SCF-AM1 [353] and RHF-SCF-PM3 [347]) which yield the largest coefficients in the LUMO at the carbon atoms of the double bond highlighted in bold in Scheme 35.

[76]The addition of CH_2N_2 to the central double bond of **99** could lead to a regioisomer of **104** (not shown) in which the carbon atom of CH_2N_2 is attached to the carbon atom carrying the two methylene moieties. However, upon dinitrogen extrusion the methylene group would have to bridge the central 6-6 bond of **99** leading to a C_s-symmetrical compound, which can be ruled out based on the spectroscopic data of the octakis-adduct **98**.

extrusion *must* proceed regioselectively to the tris-homofullerene **98**, since if the methylene moiety bridged the central 6-6 bond of heptakis-adduct **99** or **100**, the respective products would be C_s-symmetrical which is incompatible with the spectral data of **98**.

3.2.2.6 Regioselective Synthesis of a Bis-Homofullerene Heptakis-Adduct of C_{60}

In order to prove assumptions i) through iii), it was necessary to synthesize the intermediate heptakis-adduct **99** and/or **100**. Therefore, it was decided to react the hexakis-adduct **96b** with an excess of diazomethane at low temperatures. It was assumed that at low temperatures the intermediate pyrazoline(s) **101** and/or **102** would be stable (Scheme 35) and would prevent further addition of diazomethane by blocking the reactive double bond. Subsequent quenching of excess CH_2N_2 and warming the reaction mixture to room temperature would allow the isolation of the resulting heptakis-adduct(s) after extrusion of N_2 from the intermediate pyrazolines.

Diazomethane (*ca.* 20-fold excess) was added to a solution of **96a** and **96b**, respectively, in CH_2Cl_2 at –80 °C (Scheme 36). The reaction mixture was then allowed to warm within 10 min to –60 °C. At that point, the color of the solution had changed from pale orange to yellow, indicating that the cycloaddition of CH_2N_2 had taken place, and the excess reagent was immediately quenched with acetic acid. Indeed, the reaction showed a high regioselectivity producing only the heptakis-adducts **99a** and **99b** in 83 and 79% yield[77], respectively. The selective formation of the bis-homofullerenes **99a** and **99b** proved assumptions i) through iii), namely that the 1,3-dipolar cycloaddition of diazomethane occurs only at the central double bond of the pyracylene subunit depicted in Scheme 35 (assumptions i and ii) and that the dinitrogen extrusion proceeds regioselectively to form a bis-homofullerene derivative (assumption iii).

[77]The selective formation of the heptakis-adduct **99** implies that the 1,3-dipolar cycloaddition of CH_2N_2 proceeds highly regioselectively forming as the only the intermediate the pyrazoline **101** (Scheme 35). The regioselectivity of this reaction can be understood upon inspection of the semi-empirically calculated (RHF-SCF-AM1 [353]) frontier orbitals of diazomethane and of the hexakis-adduct **96**. According to frontier orbital theory, the dipole and the dipolarophile will react in such a way that the atoms with the large orbital coefficients in the HOMO (dipole) and LUMO (dipolarophile), respectively, and those with small orbital coefficients in the HOMO (dipole) and LUMO (dipolarophile), respectively, will combine. The calculation of the HOMO of CH_2N_2 yields the largest coefficient (0.580) at the carbon atom of the molecule followed by the terminal nitrogen (0.396). The largest coefficients of the LUMO of **96** are found at the bridgehead C-atom (0.121) followed by the adjacent C-atom (0.084) of the double bond highlighted in bold in Scheme 35. Therefore, both the most dipolarophile double bond of **96** as well as the selective formation of **99a,b** is correctly predicted by frontier orbital theory using semi-empirical MO calculations.

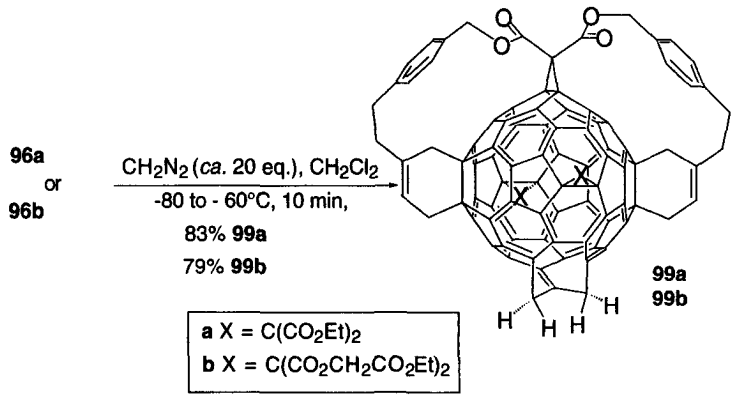

Scheme 36. Synthesis of the heptakis-adducts **99a,b**.

The C_s symmetry of **99a,b** allows the unambiguous assignment of their molecular structure based on the spectroscopic data. ^{1}H NMR spectroscopic studies show that the two pairs of enantiotopic protons of the methano bridges give rise to two doublets at 4.44 and 2.76 ppm for **99a** (Figure 33) and 4.48 and 2.75 ppm for **99b**, respectively. The alkene protons of the cyclohexene moieties appear as one triplet, which is consistent with the C_s symmetrical structure of **99a**[78].

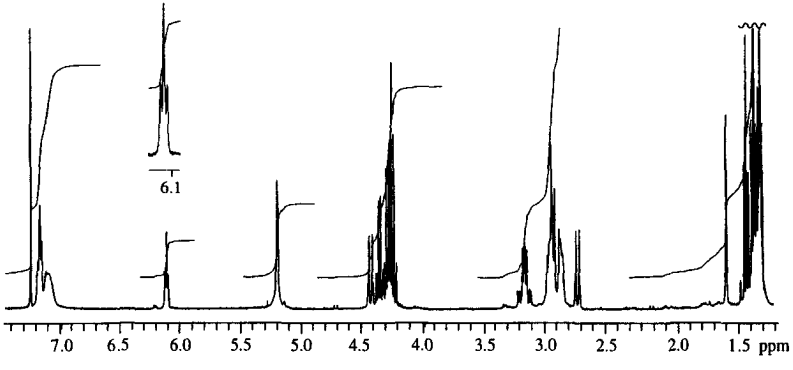

Figure 33. ^{1}H NMR spectrum (400 MHz, $CDCl_3$) of the C_s-symmetrical heptakis-adduct **99a**. The expansion shows the triplet arising from the two enantiotopic alkene protons of the tether-cyclohexene moieties.

[78]For the other C_s-symmetrical heptakis-adduct **100** (Scheme 35), the cyclohexene alkene protons would be diastereotopic and therefore one would expect signal to split into two triplets similar to what was observed in the C_1-symmetrical hexakis-adducts **96a,b** (*vide supra*).

The ^{13}C NMR spectra further support the molecular structures of **99a,b**. The diastereotopic carbonyl carbon atoms of the malonate addends which lie in the plane of symmetry give rise to four (**99a**) and eight (**99b**) resonances, respectively, of single intensity whereas the two enantiotopic carbonyl carbon atoms of the anchor malonate produce one peak of double intensity, which is only compatible with the proposed geminal relationship of the two methylene bridges in **99a,b**. Furthermore, the sp^2-region of the ^{13}C NMR spectrum shows 30 (**99a**) and 31 (**99b**) resonances of the 34 expected for the C_s symmetry of the structures.

3.2.2.7 Treatment of the Heptakis-Adduct with Diazomethane: The "Geminal"-Heptakis-Adduct is Not an Intermediate in the Formation of the Octakis adduct.

In order to prove assumption iv) it was decided to proceed in two steps. First, react the heptakis-adduct **99b** with an excess of diazomethane at 0 °C *i.e.* under the same conditions that had produced the octakis-adduct **98b** starting from the C_1-symmetrical hexakis-adduct **96b**. If exclusively **98b** was formed it would strongly suggest that the 'geminal' heptakis-adduct **99b** is the intermediate product in the reaction sequence from the hexakis-adduct **96b** to the octakis-adduct **98b** (Scheme 36). In a second step, it was envisaged to synthesize the intermediate pyrazoline **104** by adding diazomethane at low temperatures to a solution of **99b**. By virtue of the C_s symmetry of **104** (Scheme 35), its structure could be deduced by low temperature NMR spectroscopy, thus proving assumption iv).

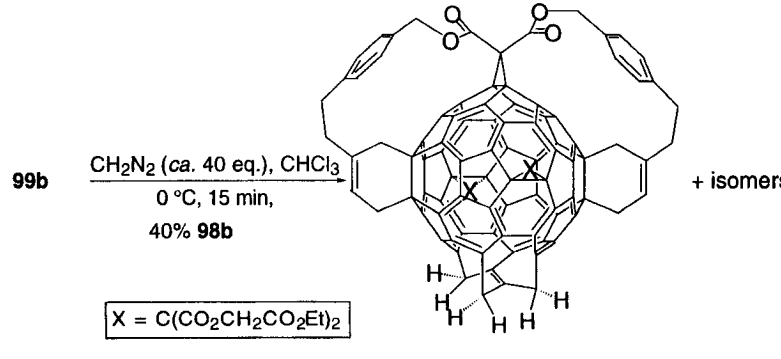

Scheme 37. Attempted synthesis of the octakis-adduct **98b** starting from the heptakis-adduct **99b** using the same conditions as in the synthesis of **98b** when starting from the hexakis-adduct **96b** (see Scheme 32).

Surprisingly, treatment of **99b** with diazomethane at 0 °C produced the octakis-adduct **98b** only in *ca.* 40% in a mixture with at least one other C_1-symmetrical adduct as determined by ^{1}H NMR (Scheme 37). The reduced yield of the octakis-adduct **98b** in the reaction of diazomethane with the heptakis-adduct **99b**, compared to the reaction of diazomethane with the hexakis-adduct **96b** under the same conditions, shows that **99b** can not be the intermediate leading to **98b** (Scheme 38). As it is plausible to assume that at 0 °C the double bond of **96b** in a pseudo-octahedral position remains the most reactive one, and in view of the fact that the geminal heptakis-adduct **99b** is not the intermediate, the reaction at 0 °C must proceed *via* the vicinal heptakis-adduct **100** (see Scheme 38).

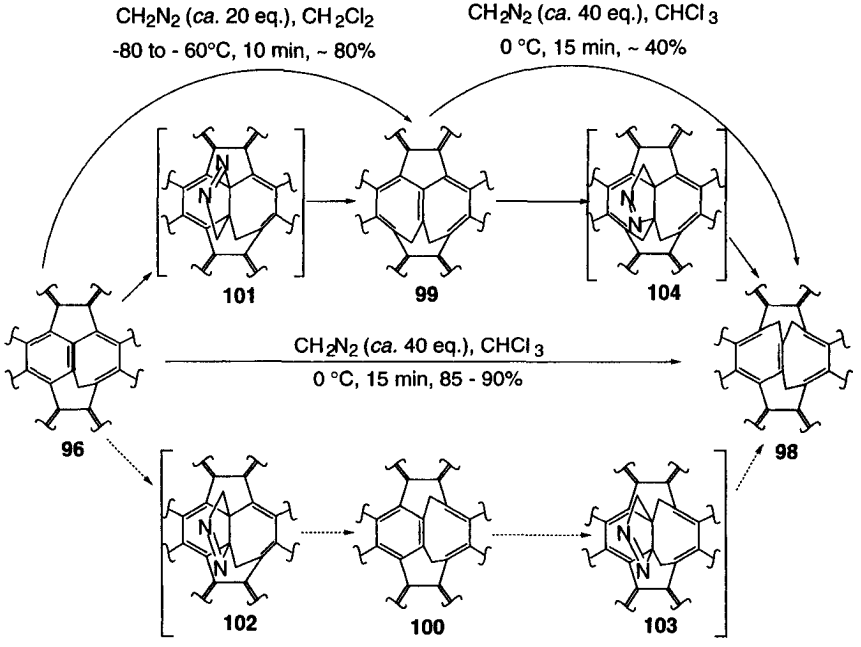

Scheme 38 Graphical summary of the experimental results aimed at elucidating the reaction pathway to **98** (for details see text above). At low temperatures (–80 to –60 °C), the heptakis-adduct **99** is formed. At 0 °C, the addition of CH_2N_2 to **96** leads directly to the octakis-adduct **98** in high yield, presumably *via* the 'vicinal' heptakis-adduct **100**. The reactive double bond of the C_1-symmetrical hexakis-adduct **96** is highlighted in bold. For clarity, the fullerene is shown only in part.

According to RHF-SCF-AM1 MO calculations [353] of the 'vicinal' heptakis-adduct **100**, the coefficients in the LUMO are by far the largest at the carbon atoms of

the vicinally bis-functionalized double bond[79]. Therefore the 1,3-dipolar addition of diazomethane should produce the pyrazoline **103**, from which upon dinitrogen extrusion the only C_1-symmetrical octakis-adduct which can be formed is **98a,b** (*vide supra*).

3.2.2.8 Attempted Synthesis of a C_{2v}-Symmetrical Tetrakis-Homofullerene Nonakis-Adduct of C_{60}.

A particularly attractive target molecule is the nonakis-adduct **105**, which would be formally obtained by inserting a methylene group into the remaining 6-5 bond of the double bond in pseudo octahedral position of octakis-adduct **98** (Scheme 39). In addition, the C_{2v}-symmetry of **105** would allow unambiguous structural assignment, and, since it can only be formed *via* the octakis-adduct **98**, it would also be an indirect proof of the molecular structure of **98**. However, even prolonged treatment (24 h) of octakis-adduct **98b** with a large excess (≥ 60 eq.) of diazomethane at 0 °C or at room temperature did not lead to a reaction and only unchanged starting material could be isolated.

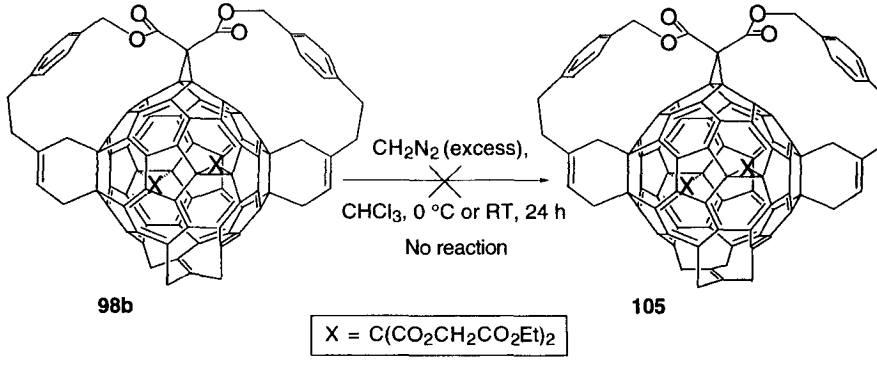

Scheme 39 Attempted synthesis of the C_{2v}-symmetrical nonakis-adduct **105**.

The low reactivity towards 1,3-dipolar cycloaddition of CH_2N_2 of the double bond which is partially lifted out of the fullerene sphere in the octakis-adduct **98b**, is likely the result of steric shielding by the methylene protons of the CH_2 groups bridging

[79]In contrast, RHF-SCF-AM1 MO calculations [353] of the LUMO of the 'geminal' heptakis-adduct **99** produce only very small coefficients at the carbon atoms of the geminally bis-functionalized double bond, and larger coefficients at the other carbon atoms of the double bonds of the corresponding doubly bridged pyracylene subunit of **99** depicted in Scheme 38. This is in agreement with the observed low regioselectivity of the reaction of **99** with diazomethane at 0 °C.

the 6-5 open junctions. In a SCF-RHF-PM3 optimized [347] space filling representation of **98** (Figure 34), in which for calculational ease the malonate addends and the tether have been replaced by hydrogen atoms, the steric crowding around the central double bond is clearly visible.

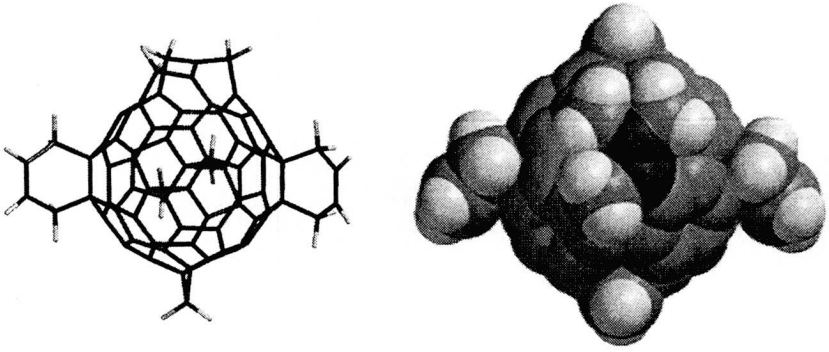

Figure 34. Depiction of a model of the octakis-adduct **98** as a tube model (on the left) showing the fullerene double bond which is partially lifted out of the fullerene sphere, and in a space filling representation (on the right) illustrating the steric shielding of the fullerene double bond (highlighted in dark gray).

3.2.2.9 Attempted Oxidative Opening of the Fullerene Sphere

The heptakis-adducts **99a,b** posses a double bond which is partially lifted out of the fullerene sphere (Scheme 36). Previously, *Wudl* and co-workers had shown in their synthesis of ketolactam (±)-**38b** (Scheme 14, section 2.3.3) that insertion of a nitrogen atom into a 6-5 bond allows to oxidatively cleave an adjacent 6-6 double bond of the fullerene[80]. It seems reasonable to assume that two factors are primarily responsible for facile oxidative cleavage of the double bonds which are adjacent to the bridging nitrogen atom of the azahomofullerene **36b**:

i) the nitrogen atom of azahomofullerene derivatives makes the adjacent bridgehead double bonds more susceptible towards oxidation by making them more electron rich (enamine type double bonds) and

ii) insertion of an atom into a 6-5 bond inflates the fullerene sphere and thus provides enough space to accommodate the carbonyl oxygens of the ketolactam (±)-**38b** (Scheme 14, section 2.3.3).

[80]Similarly *Taylor* and co-workers suggested that insertion of two oxygens into 6-5 bonds had preceded the oxidative cleavage of a double bond of C_{70} [354].

The necessity for enlarging the fullerene sphere by inserting atoms into 6-5 bonds in order to oxidatively cleave a double bond within the fullerene framework becomes apparent in the attempted opening of the fullerene reported by *Hirsch* and co-workers [274]. Treatment of the diol **106** with $Pb(OAc)_4$ did not produce the diketone **107**, but in almost quantitative yield the dioxetane **108** in which the fullerene cage structure is retained (Scheme 40). The experimental observation was rationalized by molecular modeling studies on **107**. These studies indicated that the rigidity of the fullerene cage forces the carbonyl groups of the diketone to align in an almost parallel fashion within *Van-der-Waals* contact, making **107** energetically very unfavorable [274].

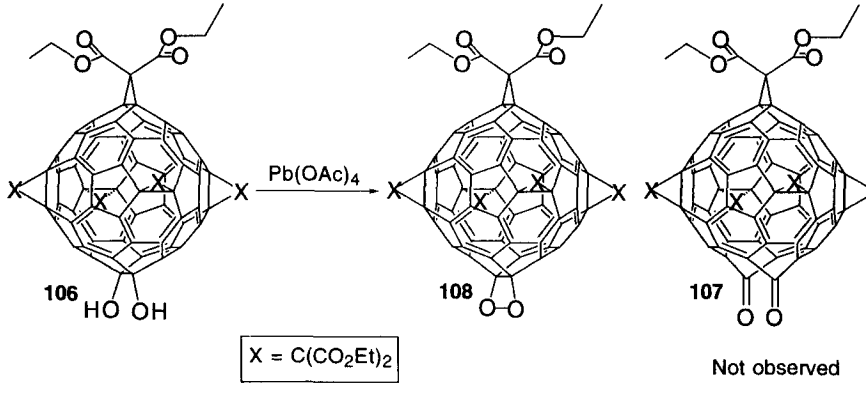

Scheme 40 Attempted opening of the fullerene sphere as reported by *Hirsch* and co-workers [274]. Oxidation of the diol produces only the dioxetane **108** and none of the diketone **107**.

In view of these results it was envisaged that oxidative cleavage of the geminally bis-functionalized double bond of **99a** could lead to the diketone **109** (Scheme 41) in which the fullerene framework has been opened up. It was believed that the two methylene groups bridging the 6-5 bonds of the heptakis-adduct **99a** would introduce enough space and flexibility into the fullerene framework to allow formation of the diketone **109**. An obvious side reaction in the oxidation of the fullerene double bond of **99a** could be the oxidation of the exohedral double bonds of the tether-cyclohexene moieties. However, inspection of frontier orbital calculations of **99a** at the semi empirical RHF-AM1 level [353] produced large coefficients in the HOMO–1 at the carbon atoms of the geminally bis-functionalized fullerene double bond and no coefficients (neither in the HOMO nor HOMO–1) at the sp^2-carbon atoms of the cyclohexene rings. We therefore expected that oxidation of **99a** would occur

preferentially at the fullerene double bond. Furthermore, preservation of the C_s symmetry of the heptakis-adduct **99a** in the intermediates and in diketone **109** would facilitate their structural elucidation.

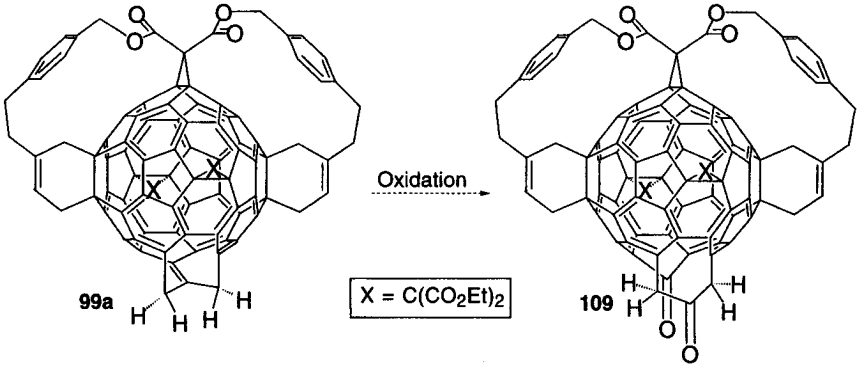

Scheme 41. Envisaged synthesis of the diketone **109** possessing a twelve membered ring orifice in the fullerene sphere.

3.2.2.10 Synthesis of a Bis-Homofullerenediol Heptakis-Adduct of C_{60}

It was decided to attempt the synthesis of **109** *via* the diol **110**, in analogy to the strategy used by *Hirsch* and co-workers in their attempted synthesis of diketone **107** (Scheme 41).

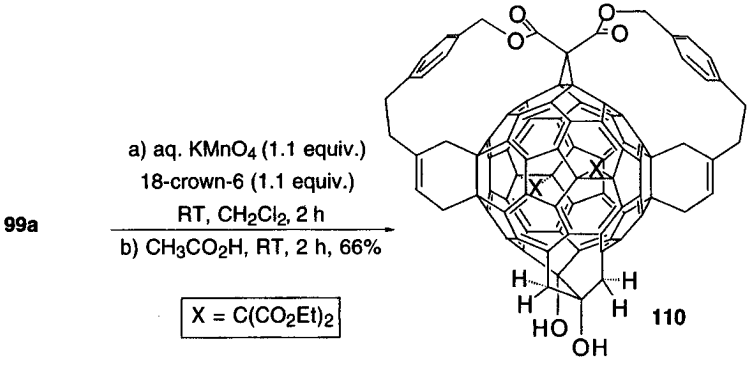

Scheme 42 Synthesis of diol **110**.

To this end, a solution of **99a** in CH_2Cl_2 was treated with 1.1 equiv. of an aqueous solution of $KMnO_4$ in the presence of 18-crown-6. After hydrolysis with

acetic acid and column chromatography (SiO_2-*H*, CH_2Cl_2/AcOEt 7:3), **110** was obtained as a bright yellow solid in 66% yield (Scheme 42). The high yield of diol **110** and the absence of products arising from the oxidation of the cyclohexene double bonds showed that the geminally bis-functionalized fullerene double bond is indeed more reactive towards oxidation than the exohedral double bonds of the cyclohexene rings in agreement with the frontier orbital calculations mentioned above.

The spectroscopic data of **110** are in agreement with the proposed C_s-symmetrical structure. ^{1}H NMR spectroscopy shows that the two pairs of enantiotopic protons of the methano bridges give rise to two doublets at 3.84 and 3.62 ppm, respectively. The alkene protons of the cyclohexene moieties appear as one triplet, further supporting the C_s symmetry of **110** (Figure 35). A sharp signal at 4.66 ppm was assigned to a OH group of **110**. This was confirmed by heating a solution of **110** in $CDCl_3$ with D_2O, which led to the disappearance of the signal due to exchange of the OH proton with a deuterium of D_2O. Furthermore, addition of D_2O also led to a decrease of the integral intensity of the signals of the CH_2 groups of the malonate addends between 4.40 and 4.15 ppm, indicating that these signals obscure the resonance of the second OH group of **110**.

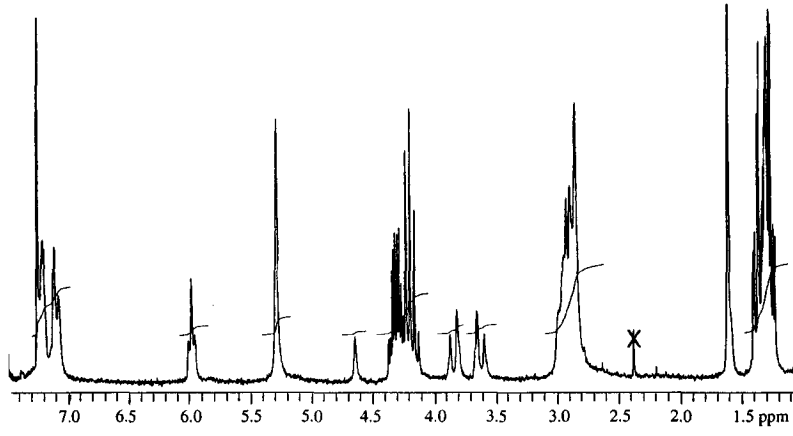

Figure 35. ^{1}H NMR spectrum (300 MHz, $CDCl_3$) of the C_s-symmetrical diol **110**. The peak at 2.4 ppm is due to acetone.

The C_s symmetry of **110** is also supported by the ^{13}C NMR spectrum which shows all expected 24 fullerene sp^2 carbon atoms. The FAB mass spectrum shows the expected molecular ion at m/z = 1541.6 as the base peak, the next most prominent signal

at m/z = 1523.1 being due to the loss of H_2O. The IR spectrum of **110** recorded in CCl_4 showed two signals for the OH groups at 3734 cm^{-1} and a broad signal at 3396 cm^{-1} for the free and associated OH stretch vibration, respectively.

3.2.2.11 Attempted Oxidative Cleavage of the Bis-Homofullerenediol Heptakis-Adduct

Oxidative cleavage of the diol was attempted with $Pb(OAc)_4$ which is known to be a versatile, reactive and yet very selective reagent for cleaving 1,2 diols [355] and, in contrast to $NaIO_4$, it can be used in organic solvents in which **110** is soluble. Furthermore, the high yield of the dioxetane **108** in the oxidation of the fullerene diol **106** (Scheme 41) as reported by *Hirsch* and co-workers [274] had demonstrated compatibility of the reagent with a highly functionalized fullerene derivative similar to **110**.

Within 1.25 h after the addition of 1.1 equiv. of $Pb(OAc)_4$ to a solution of **110** in CH_2Cl_2 no starting material could be detected by TLC. After extraction of the reaction mixture, column chromatography (SiO_2, CH_2Cl_2/AcOEt 9:1), and concentration of the product fraction, a yellow green solid was obtained in 62% yield.

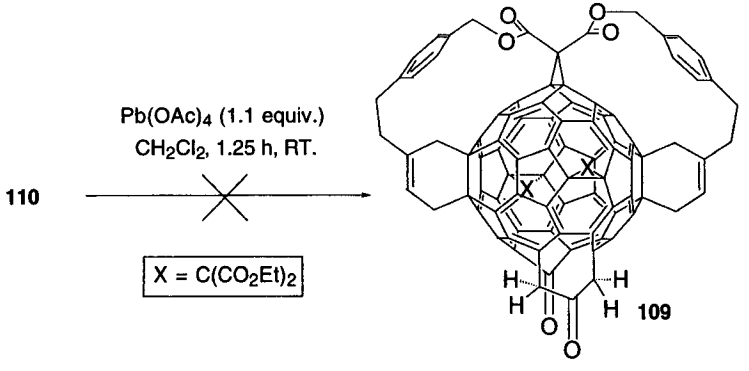

Scheme 41 Attempted synthesis of the fullerene diketone **109**.

The FAB mass spectrum of the product shows a relatively weak peak (18%) for the expected molecular ion of **109** at m/z = 1539.1. However, the structure of **109** could not be confirmed by other spectroscopic methods. The ^1H NMR spectrum (200, 300 and 500 MHz, $CDCl_3$) of the reaction product shows only very broad signals, which

makes it impossible to discern the coupling patterns of its protons. Furthermore, the signal corresponding to the alkene protons of the cyclohexene rings gives rise to a broad signal with two maxima around 6 ppm. This is not compatible with the expected C_s-symmetrical structure of **109**, for which the corresponding alkene protons should appear as one triplet. However, the spectral data could be compatible with two C_s-symmetrical conformers of **109**, which slowly interconvert on the NMR time scale. This would explain both the broadness of the signals in the ^{1}H NMR spectrum, as well as the splitting of the signal corresponding to the alkene protons. This hypothesis could not be confirmed by temperature dependent ^{1}H NMR studies. The spectra of the reaction product recorded at 25, 40, 60 and 80 °C in $C_2D_2Cl_4$ were virtually identical over the temperature range. The IR spectrum recorded in CCl_4 of the reaction product no longer shows the absorptions of the OH groups, but also no new C=O signals were observed **109**[81]. Attempts to get a clearer picture of the molecular structure of the reaction product by ^{13}C NMR failed as even after 30'000 scans (75 MHz, 9 mg in 0.5 ml $CDCl_3$) no peaks in the sp^2 region of the spectrum were visible. These results indicated that the oxidative cleavage of the diol produced a mixture of products, which are formed either through the side reactions during the oxidation with $Pb(OAc)_4$, or which are the result of secondary reactions occurring upon formation of diketone **109**. However, according to TLC analysis, the compound was pure and repeated column chromatography or taking multiple samples during elution of the product band had no influence on the ^{1}H NMR spectra. In view of these discouraging results, no further efforts to synthesize **109** were undertaken.

3.3 Investigation of the Influence of the Nature of the Addends on the Chemical Behavior of Highly Functionalized Fullerene Derivatives

3.3.1 Template Directed Synthesis of an All Cyclopropanated C_{2v}-Symmetrical Pentakis-Adduct of C_{60}

During the course of the work described above, a three step synthesis of the C_{2v}-symmetrical pentakis-adduct **47** (Scheme 44) was published by *Hirsch* and co-workers [274]. The pentakis-adduct **47** has the same addition pattern as the pentakis-adduct **90**, but in contrast to **90** in which two 6-6 bonds are functionalized by fusion of an cyclohexene rings, only has cyclopropane rings fused to 6-6 bonds of the fullerene core.

[81] However, the C=O stretch vibration of the ketone moieties of **109** could be masked by the C=O signals of the ester moieties of **109**.

It was decided to synthesize a series of all cyclopropanated multiple adducts with the same addition pattern as the hexakis-adducts **95**, **96** (Schemes 31 and 32) and the heptakis-adduct **99** (Scheme 36) to investigate the influence of the nature of the cyclopropane addends on the chemical and spectroscopic properties of the respective fullerene derivatives. Furthermore, the opening of the fullerene sphere on the all cyclopropanated heptakis-adduct was attempted.

Synthesis of the pentakis-adduct **47** was carried out according to the published procedure [274] and is shown in Schemes 43 and 44.

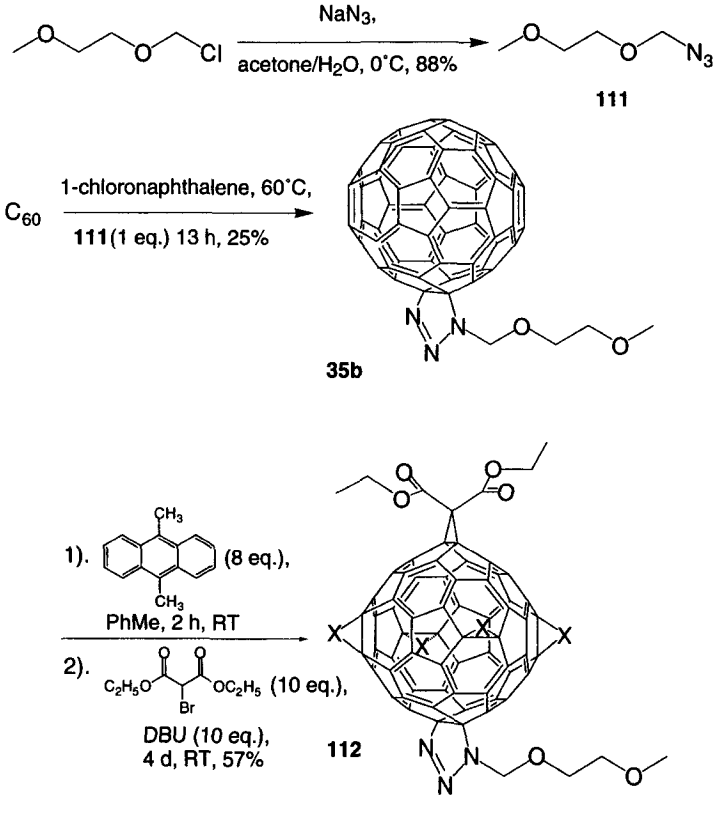

Scheme 43 Template mediated synthesis of hexakis-adduct **112** starting from the triazoline mono-adduct **35b**.

The synthesis is an extension of the reversible template-directed activation of C_{60} which was used for a one pot synthesis of the hexakis-adduct **48** reported previously by the same group [231] (see also section 2.4.4.2).

The key to the synthesis of **47** is the protection of one 6-6 double bond of C_{60} with an addend which can be removed once the four double bonds in an *e*- and the double bond in a *trans*-1 position to the protecting group have been functionalized. *Hirsch* and co-workers decided to use the 1,3 dipolar cycloaddition reaction of an azide derivative to mask one double bond of the fullerene sphere as a triazoline, since it had been previously shown that thermal treatment of such mono-adducts leads next to the formation of the corresponding aza-homofullerene and epiminofullerene derivatives also to a significant amount of free C_{60} through cycloreversion of the azide (see Section 2.3.3).

The triazoline **35b** [272] was synthesized by heating a solution of C_{60} in 1-chloronaphthalene with an equimolar amount of methoxyethoxymethylazide (MEMazide) **111** in the dark for 13 h at 60 °C[82]. After chromatographic purification, **35b** could be isolated in 25% yield.

The hexakis-adduct **112** was obtained by treating a degassed solution of the triazoline mono-adduct **35b** with an eight fold excess of 9,10-dimethylanthracene for 4 h and subsequent addition of 10 eq. of diethyl 2-bromomalonate and DBU. After stirring the reaction mixture for 4 d at RT, the hexakis-adduct **112** was isolated in 57% yield as a dark yellow solid after column chromatography (SiO_2, CH_2Cl_2/AcOEt 95:5) and concentration of the product fractions.

Subsequently, the protecting group (*i.e.* the triazoline) was removed by heating a solution of **112** in toluene to reflux for 18 h. After chromatographic removal of the azahomofullerene **113** and epiminofullerene **114**, the C_{2v}-symmetrical pentakis-adduct **47** was isolated in 41% yield (Lit. [274] 40%).

[82]The reaction was found to be highly temperature dependent. The yield of **35b** decreased to 18% at 65 °C compared to 25% when the reaction was carried out at 60 °C, under otherwise identical conditions.

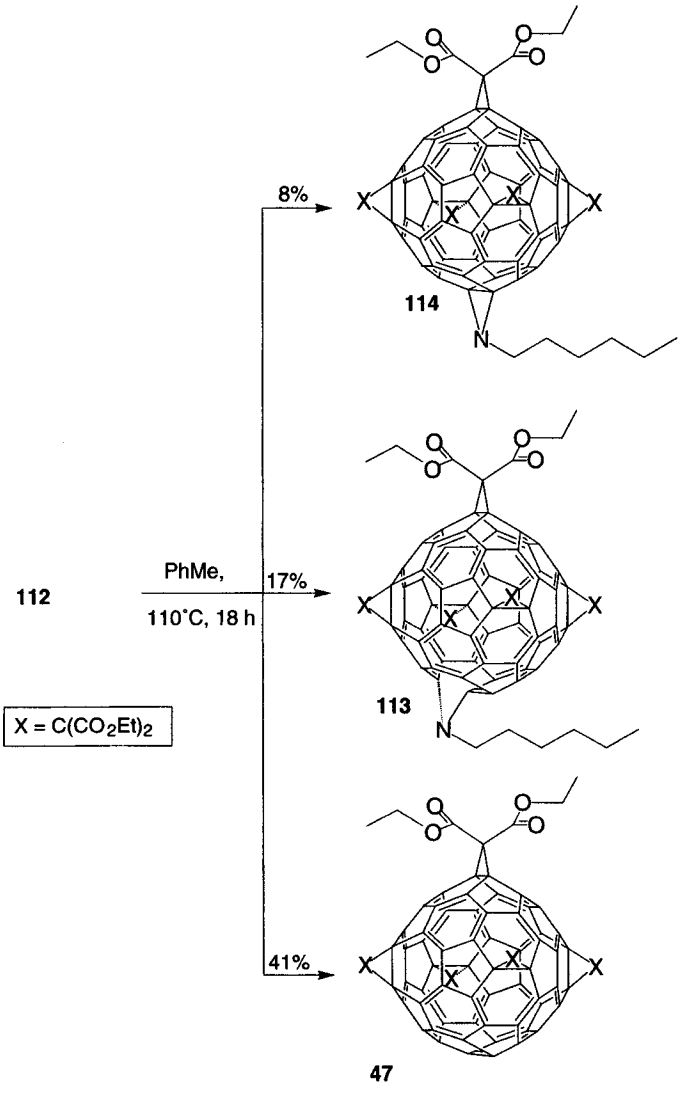

Scheme 44. Synthesis of the all cyclopropanated pentakis-adduct **47** by thermally induced 1,3-retro-cycloaddition of the MEMazide moiety of **112**.

3.3.2 Reaction of an All Cyclopropanated C_{2v}-Symmetrical Pentakis-Adduct with Diazomethane

In analogy to the synthesis of pyrazoline **95** (Scheme 31), **115** was synthesized by addition of a *ca.* 60-fold excess of etheral CH_2N_2 to a solution of **47** in $CHCl_3$ at 0 °C (Scheme 45). The reaction was completed within 20 min as indicated by the change in color of the solution from orange to yellow and TLC analysis. Column chromatography (SiO_2, CH_2Cl_2) followed by precipitation with pentane and drying of the product *in vacuo* allowed the isolation of **115** in 93% yield as a bright yellow solid. The shorter reaction time necessary for the synthesis of **115** compared to the synthesis of **95** (20 *vs.* 90 min), indicated that the pentakis-adduct **47** is a better dipolarophile than the corresponding pentakis-adduct **90**. This result was the first indication that the nature of the addends has a great influence on the chemical reactivity of the respective adducts.

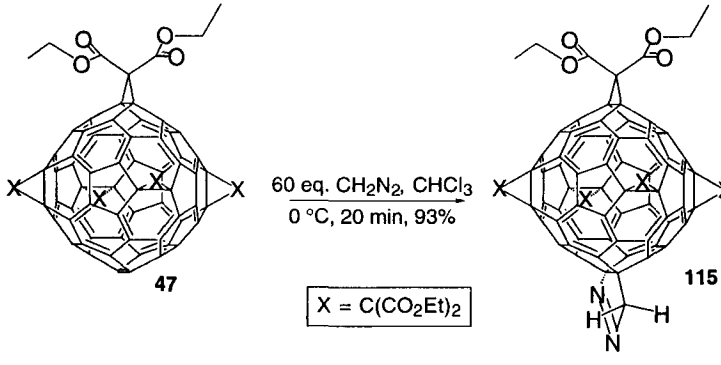

Scheme 45. Synthesis of pyrazoline **115**.

Spectroscopic analysis of **115** confirmed that the 1,3 dipolar cycloaddition of diazomethane had occurred as in the synthesis of **95** at the double bond in a pseudo octahedral position. The ^1H NMR spectrum of **115** shows no diastereotopic protons and a single resonance at 5.95 ppm for the enantiotopic pyrazoline-methylene protons supporting its C_s symmetry. The ^{13}C NMR spectrum shows 23 out of 24 sp^2 fullerene carbon resonances expected for the C_s-symmetry of the proposed structure. The expected N=N stretching vibration is weak but clearly visible in the IR spectrum at 1571 cm^{-1}. Under FAB-mass spectrometric conditions, **115** appears to be more stable than **95a,b** which show only a weak peak for the molecular ion (**95a**: 17%), or no signal

at all (**95b**). In contrast, the FAB-mass spectrum of **115** shows a strong signal for M^+ at m/z = 1553.3 (63%). Similar to **95a** and **95b** the base peak for **115** at m/z = 1539.3 arises from loss of dinitrogen.

3.3.3 Synthesis of a Five-Fold Cyclopropanated Homofullerene Hexakis-Adduct

The synthesis of the C_1-symmetrical hexakis-adduct **116** required heating a solution of **115** in $CHCl_3$ under reflux for 5 h. Similar to the thermal dinitrogen extrusion from **95a** and **95b**, the thermal treatment of **115** proceeded with high regioselectivity yielding exclusively the homofullerene **116** in 82% yield as a deep orange solid after column chromatography (SiO_2-*H*, CH_2Cl_2/AcOEt 90:10).

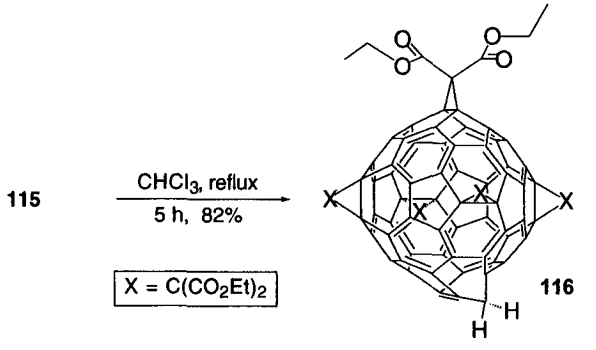

Scheme 46 Synthesis of the 6-5 open C_1-symmetrical hexakis-adduct **116** *via* regioselective dinitrogen extrusion from the respective pyrazoline precursor **115**.

The C_1 symmetry of **116** is apparent both in the ^1H NMR spectrum in which the two diagnostic doublets of the diastereotopic protons of the methano-group bridging the open 6-5 junction appear at 5.24 and 2.45 ppm as well as in the ^{13}C NMR spectrum which displays 48 out of the 50 fullerene sp^2-carbons as well as nine out of the ten bridgehead sp^3-carbons. The FAB-mass spectrum shows the expected molecular ion at m/z = 1525.1 as the base peak.

3.3.4 Synthesis of a Five-Fold Cyclopropanated Bis-Homofullerene Heptakis-Adduct

Synthesis of heptakis-adduct **117** was carried out in the same manner as the synthesis of **99a** and **99b** (Scheme 36) by addition of *ca.* 40 eq. diazomethane to a solution of **116** in CH_2Cl_2 at –80 °C and subsequent warming of the reaction mixture within 10 min to –60 °C. A change in color of the solution from orange to yellow indicated completion of the reaction, and the excess reagent was quenched with acetic acid. After column chromatography (SiO_2-*H*, CH_2Cl_2/AcOEt 10:1) and concentration of the product fraction, the heptakis-adduct **117** was obtained as a bright yellow solid in almost quantitative yield (98%) with the same addition pattern as observed in the heptakis-adducts **99a** and **99b** (Scheme 36).

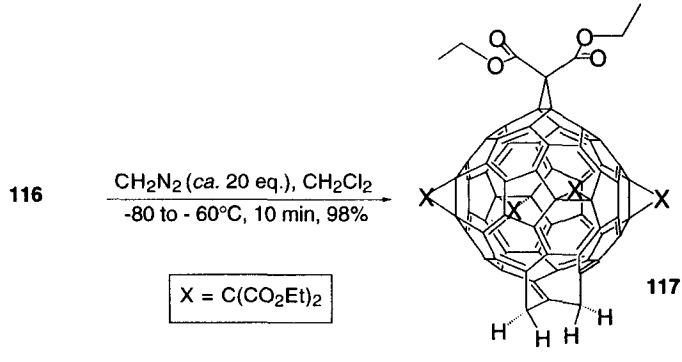

Scheme 47. Synthesis of the heptakis-adduct **117**.

The C_s symmetry as well as the geminal relationship of the two methano groups bridging 6-5 open junctions can be very nicely deduced from the ^1H and ^{13}C NMR spectra of **117**, respectively (Figures 36, and 37). The two pairs of enantiotopic protons of the methano bridges give rise to two doublets at 4.84 and 3.05 ppm, respectively, in agreement with the C_s symmetrical structure of **117**.

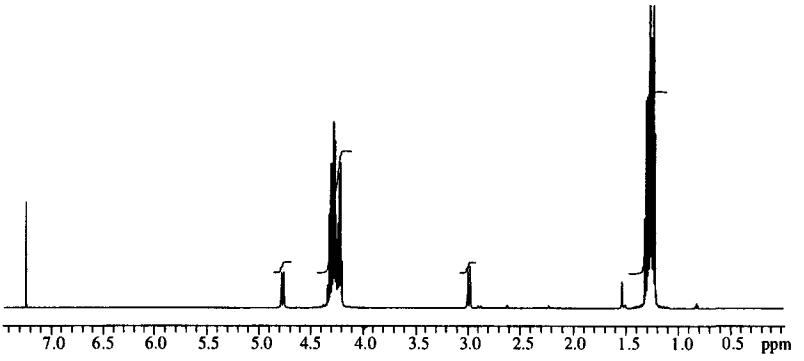

Figure 36. ^{1}H NMR spectrum (400 MHz, $CDCl_3$) of the C_s-symmetrical heptakis-adduct **117**.

The geminal relationship of the methano groups is apparent from the relative intensity and the number of the signals in the ^{13}C NMR spectrum. The ten carbonyl carbons are grouped into two sets of signals, namely, three signals of double intensity arising from the six enantiotopic carbonyl carbons and four signals of single intensity corresponding to the diastereotopic carbonyl carbons which lie in the plane of symmetry of **117**. For the corresponding heptakis-adduct in which the methylene groups are in a vicinal relation (such as **100** shown in Scheme 35) one would expect a total of six signals, four of double and two of single intensity, respectively. Further conformation of the molecular structure of **117** comes from inspection of the sp^2-region of the ^{13}C NMR, which shows all 26 expected signals, 24 of double and two of single intensity at 143.07 and 135.88 ppm arising from the diastereotopic carbons of the geminally bis-functionalized double bond. Again, this observation is only compatible with the structure of **117** as a vicinal relationship of the methylene groups would give rise to 25 signals, all of double intensity.

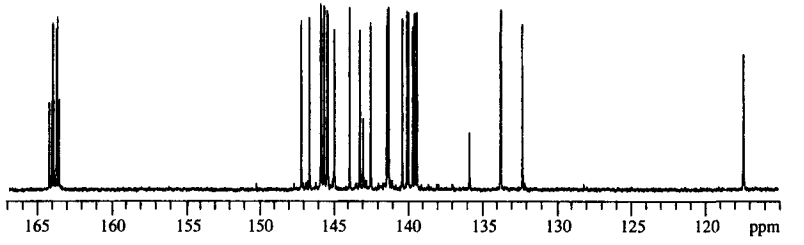

Figure 37. Expansion of the carbonyl- and fullerene sp^2-region of the ^{13}C NMR spectrum (100 MHz, $CDCl_3$) of the C_s-symmetrical heptakis-adduct **117**.

3.3.5 Synthesis of a Five-Fold Cyclopropanated Bis-Homofullerenediol Heptakis-Adduct

Having the heptakis-adduct **117** at hand, it was decided to re-attempt the oxidative cleavage of the reactive, geminally bis-functionalized fullerene double bond. The goal of these experiments was to see if the different nature of the addends of the heptakis-adduct **117** compared to heptakis-adduct **99a** containing two cyclohexene moieties would have an influence on the outcome of the oxidation of the diol **119** ultimately allowing the synthesis of diketone **120**.

In analogy to the synthesis of diol **110** (Scheme 42), a solution of **117** in CH_2Cl_2 was treated with 1.1 equiv. of an aqueous solution of $KMnO_4$ in the presence of 18-crown-6. After hydrolysis with acetic acid, column chromatography (SiO_2-*H*, CH_2Cl_2/AcOEt 1:1) and concentration of the solution, **119** was obtained as a bright yellow solid in 85% yield.

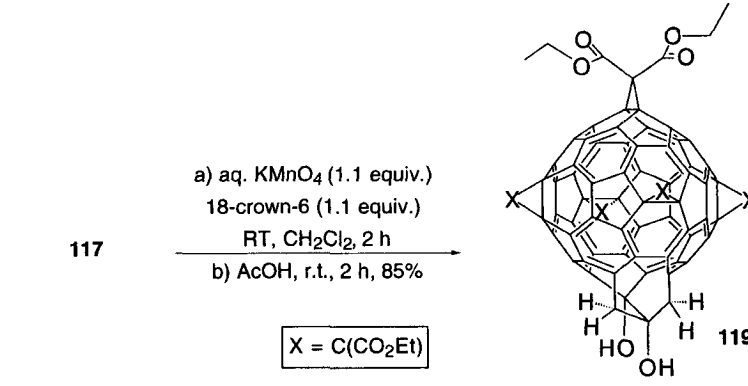

Scheme 48 Synthesis of diol **119**.

As previously observed in the synthesis of diol **110**, oxidation of the heptakis-adduct **117** takes place at the geminally bis-functionalized double bond. The ^1H NMR spectrum of **119** shows a broad signal for one OH group centered at 4.89 ppm. One doublet for the protons of the methano bridges is obscured by the signals of the CH_2 groups of the malonate addends, the other, integrating for two protons, is visible at 3.91 ppm, supporting the C_s symmetry of the compound[83]. The FAB mass spectrum of **119**

[83]Had the oxidation occurred at any other double bond of **117**, the corresponding diol would have C_1 symmetry, and one would expect the four diastereotopic protons of the methylene groups which bridge

shows the expected molecular ion at m/z = 1573.3. The IR spectrum of **119** recorded in $CHCl_3$ shows two signals for the OH groups at 3606 cm^{-1} and a broad signal at 3465 cm^{-1} for the free and associated OH stretch vibration, respectively.

3.3.6 Attempted Oxidative Cleavage of the Five-Fold Cyclopropanated Bis-Homofullerenediol Heptakis-Adduct

Disappointingly, the oxidation of diol **119** produced very similar results to those observed in the corresponding reaction with **110** (Scheme 41). Thus, treatment of **119** with 1.1 equiv. of $Pb(OAc)_4$ to a solution of **110** in CH_2Cl_2 led to the consumption of the starting material within 1.25 h and to the formation of two new products at higher R_f values (0.67 and *ca.* 0.9; CH_2Cl_2/AcOEt 98:2), as detected by TLC.

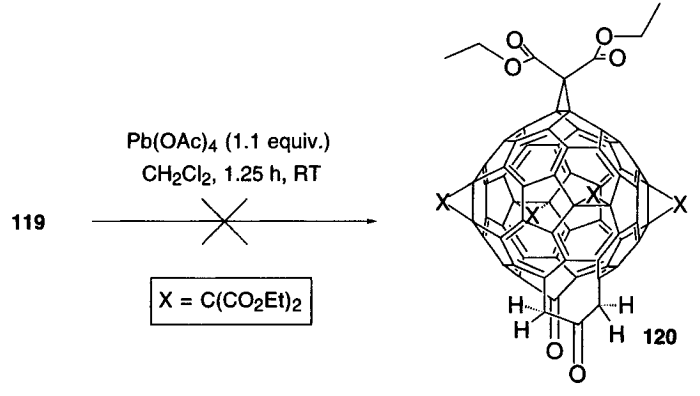

Scheme 49 Attempted synthesis of fullerene diketone **120**.

Again, the FAB mass spectrum of the crude reaction mixture shows a peak for the expected molecular ion of **120** at m/z = 1571.3. However, after chromatographic separation of the reaction mixture, the ^1H NMR spectra of both products were disappointingly similar, showing only very broad, unresolved peaks, indicating either the loss of the C_s symmetry of the precursor **119** or contamination of the product with many side products. The ^{13}C NMR spectra of either product show no interpretable signals. In view of these results and the results obtained in the attempted oxidative cleavage of diol **110**, it was decided to abandon the project.

the 6-5 junctions of **119** to appear as four doublets with their respective integral corresponding to one proton each.

3.4 Comparison of the Chemical Reactivity of the Two C_{2v}-Symmetrical Pentakis-Adducts 47 and 90

3.4.1 Theoretical and Experimental Considerations

In order to investigate the influence of the nature of the addends of multiple adducts with the same addition pattern on the reactivity, we decided to take a closer look at the kinetics of the 1,3-dipolar cycloaddition of diazomethane to the pentakis-adducts **47** and **90a**. Assuming that the reaction of diazomethane with **47** and **90a** proceeds *via* the same mechanism, the ratio of the rate constants of the respective reactions will give an indication of the difference of the transition state energies of the two reactions. This in turn allows to quantify the influence of the nature of the addends on the reactivity of the respective molecules.

For the sake of readability of the equations below, the pentakis-adduct **90a** shall be called Penta(I) and the pentakis-adduct **47** will be called Penta(II). Correspondingly, the pyrazolines **95a** will be Pyrazoline(I) and **115** will be Pyrazoline(II).

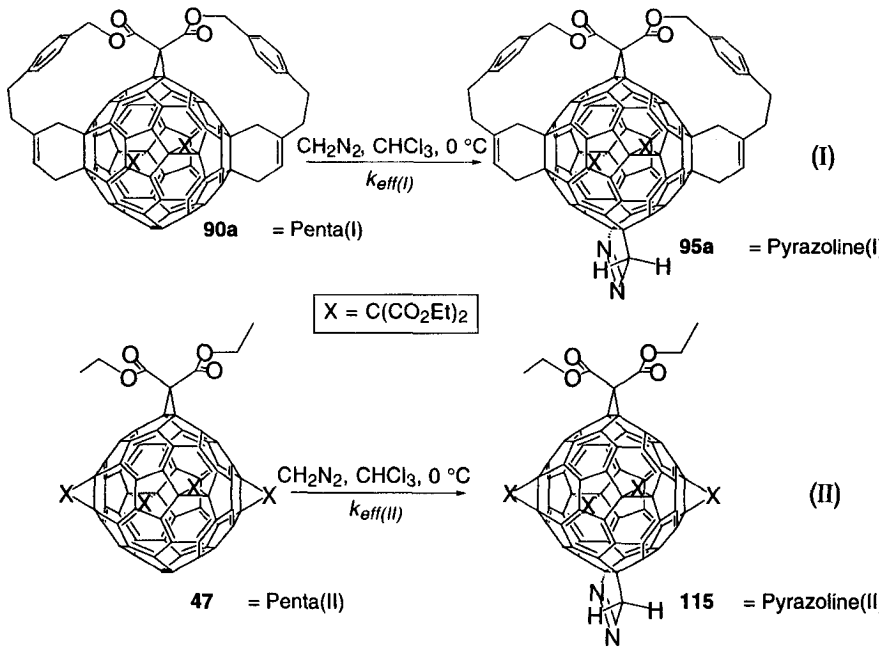

Figure 38. Illustration of the 1,3-dipolar cycloaddition reactions of diazomethane with the two pentakis-adducts **90a** and **47** used for the kinetic investigations.

The expression for the rate of the investigated reactions is:

$$v_I = -\frac{d[\text{Penta(I)}]}{dt} = \frac{d[\text{Pyrazoline(I)}]}{dt} = k_I\,[\text{Penta(I)}][CH_2N_2] \qquad (1)$$

and

$$v_{II} = -\frac{d[\text{Penta(II)}]}{dt} = \frac{d[\text{Pyrazoline(II)}]}{dt} = k_{II}[\text{Penta(II)}][CH_2N_2] \qquad (2)$$

By using large excess (*ca.* 100 eq.) of CH_2N_2 in reactions (I) and (II) the following approximation can be made

$$[CH_2N_2](t_0) \gg [\text{Penta}](t_0) \qquad (3)$$

therefore

$$[CH_2N_2](t_0) \approx [CH_2N_2](t) \approx \text{const.}$$

Thus, equations (1) and (2) can be simplified

$$v_I = -\frac{d[\text{Penta(I)}]}{dt} = k_{eff(I)}[\text{Penta(I)}] \qquad (4)$$

and

$$v_{II} = -\frac{d[\text{Penta(II)}]}{dt} = k_{eff(II)}\,[\text{Penta(II)}] \qquad (5)$$

with $k_{eff(I)} = k_I\,[CH_2N_2]$ and $k_{eff(II)} = k_2\,[CH_2N_2]$

Integration of (4) and (5), respectively, yields:

$$\ln\left(\frac{[\text{Penta(I)}](t_I)}{[\text{Penta(I)}](t_0)}\right) = k_{eff(I)}\,(t_I - t_0) \qquad (6)$$

$$\ln\left(\frac{[\text{Penta(II)}](t_{II})}{[\text{Penta(II)}](t_0)}\right) = k_{eff(II)}\,(t_{II} - t_0) \qquad (7)$$

Since we are interested in the *difference* in reactivity between the two pentakis-adducts, we are interested in the ratio of the rate constants of the reactions (I) and (II). Therefore we rearrange (6) and (7) to

$$\ln\left(\frac{[\text{Penta(I)}](t_I)}{[\text{Penta(I)}](t_0)}\right)(t_I - t_0)^{-1} = k_{eff(I)} \qquad (8)$$

$$\ln\left(\frac{[\text{Penta(II)}](t_{II})}{[\text{Penta(II)}](t_0)}\right)(t_{II}-t_0)^{-1} = k_{eff(II)} \qquad (9)$$

and divide (8) by (9)

$$\ln\left(\frac{[\text{Penta(I)}](t_I)}{[\text{Penta(I)}](t_0)} - \frac{[\text{Penta(II)}](t_{II})}{[\text{Penta(II)}](t_0)}\right)\frac{(t_{II}-t_0)}{(t_I-t_0)} = \frac{k_{eff(I)}}{k_{eff(II)}} \qquad (10)$$

with $\frac{[\text{Penta(I)}](t_I)}{[\text{Penta(I)}](t_0)} = \frac{[\text{Penta(II)}](t_{II})}{[\text{Penta(II)}](t_0)}$ the term in the brackets equals zero and we can simplify equation (10) to

$$\frac{k_{eff(I)}}{k_{eff(II)}} = \frac{(t_{II}-t_0)}{(t_I-t_0)} \qquad (11)$$

In order to be able to relate the ratio of the observed rate constants with the ratio of the actual rate constants of the respective reactions, we have to use equal concentrations of CH_2N_2 in the reaction (I) and (II)

$$\frac{k_{eff(I)}}{k_{eff(II)}} = \frac{k_I[CH_2N_2]}{k_{II}[CH_2N_2]} = \frac{k_I}{k_{II}} \qquad (12)$$

Equation (12) allows a comparison of the reactivity between the to pentakis-adducts Penta(I) (**90a**) and Penta(II) (**47**) with help of the *Eyring* equation $k(T) = \frac{kT}{h}\exp\left(\frac{-\Delta G^{\neq}}{RT}\right)$, and using (11) we obtain

$$\frac{k_{eff(I)}}{k_{eff(II)}} = \frac{(t_{II}-t_0)}{(t_I-t_0)} = \frac{k_I}{k_{II}} = \exp\left(\frac{\Delta G^{\neq}_{II}}{RT} - \frac{\Delta G^{\neq}_{I}}{RT}\right) \qquad (13)$$

which is equal to

$$RT\ln\left(\frac{k_I}{k_{II}}\right) = RT\ln\left(\frac{(t_{II}-t_0)}{(t_I-t_0)}\right) = \Delta G^{\neq}_{II} - \Delta G^{\neq}_{I} \qquad (14)$$

In order to satisfy the requirements necessary for using equation (14), we proceeded in the following manner.

A freshly prepared etheral solution of CH_2N_2 (0.5 ml, *ca.* 0.76 M, *ca.* 100 eq.) was added to a vigorously stirred solution of **90a** (0.00338 mmol) in $CHCl_3$ (10 ml) at 0 °C. The course of the reaction was monitored by taking samples of the reaction mixture every 15 min and analyzing the ratio of the reactant and product by HPLC. After 96 min, none of the starting pentakis-adduct **90a** could be detected by HPLC. The experiment was then repeated in an analogous manner with the all-cyclopropanated

pentakis-adduct **47**, taking samples of the reaction mixture every 7 to 8 min and analyzing them by HPLC.

3.4.2 Results and Discussion

As expected from the preceding experiments (sections 3.2.2.2 and 3.3.2), the 1,3-dipolar cycloaddition reaction of diazomethane with **47** proceeded much faster than with **90a** and, already after 22 min, none of the starting material (*i.e.* **47**) could be detected by HPLC. As a result of the rapid reaction in the case of the diazomethane addition to **47**, only analysis of the product distribution after 7 and 15 min, respectively, allowed determination of the ratio of product and reactant. It is therefore not possible to give an exact value for the difference of the free energy of the transition states in the reactions (I) and (II) using equations (10) and (13). However, it is possible to give an approximate value by using the times it took for the complete consumption of the starting material in the respective reactions. Thus, taking the ratio of $t_{II(end)}$= 22 min and $t_{I(end)}$= 96 min and using equation (14), we obtain $\Delta G_{II}^{\neq} - \Delta G_{I}^{\neq} \approx -3.3$ kJ mol^{-1} ≈ -0.8 kcal mol^{-1}.

The difference in the reactivity of the two pentakis-adducts **90a** and **47**, which have the same addition pattern, must be the result of the different nature of the addends (cyclohexene *vs.* cyclopropane).

An obvious explanation is that the cyclopropane addends of **47** reduce the σ-strain in the fullerene framework less efficiently than the cyclohexene addends of **90a** resulting in a higher pyramidalization at the sp^2-carbons of the central pyracylene subunit of **47**, and therefore a more pronounced dienophile character of the reactive double bond (for the correlation of pyramidalization and electrophilicity of double bonds, see section 1.4.3). Inspection of RHF-PM3 optimized [347] models of the structures of **121** and **122** (see Figure 39), however, does not support this hypothesis. The molecular models **121** and **122** correspond to **90a** and **47** in which the tether and the malonate addends have been replaced by hydrogens for calculational ease. The calculated pyramidalization *S* (expressed as the difference between 360° and the sum of the three bond angles at the atom) of the two sp^2-carbons of the central pyracylene subunit of the model structure **122** which corresponds to the more reactive pentakis-adduct **47**, is only slightly smaller (12.0°) than that of the corresponding atoms of **121** (12.1°). Therefore, the pyramidalization of the carbon atoms does not appear to be at the origin of the difference of the reactivity of the two pentakis-adducts.

An alternative explanation for the higher reactivity of **47**, compared to **90a** could lie in the electronic structures of the respective multiple adducts. According to frontier

orbital theory [262] one should expect the enhanced reactivity of **47** to be reflected in a lower energy of its LUMO compared to that of **90a**. Indeed, semi-empirical MO calculations of the model systems **121** and **122** using the SCF-RHF-AM1 [353] and the SCF-RHF-PM3 method [347], support this argument (Figure 39). In agreement with the higher dieneophile character of **122**, the energy of its LUMO is calculated to be lower than that of **121** by 0.14 eV (3.2 kcal mol^{-1}; RHF-SCF-PM3) and 0.17 eV (3.9 kcal mol^{-1}; RHF-SCF-AM1), respectively.

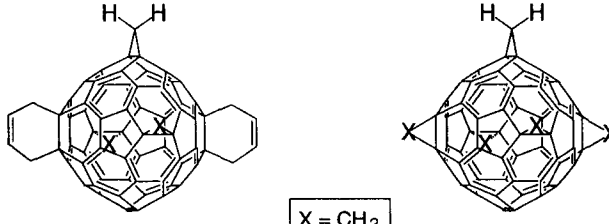

121 **122**

E_{LUMO} [eV]	**121**	**122**	ΔE_{LUMO}
RHF-PM3	−2.0118	−2.1528	−0.1410
RHF-AM1	−1.9115	−2.0813	−0.1698

Figure 39. Depiction of the model compounds used for the semi-empirical calculation of the energy of the respective LUMO.

These findings are in accordance with electrochemical studies on the C_{2v}-symmetrical *e,e,trans*-1-tris-adduct **85** (Scheme 29) and an all cyclopropanated *e,e,trans*-1-tris-adduct. It was found that the nature of the addend has a significant influence on the first reduction potential. The tris-adduct containing only cyclopropane addends (−1.12 V) is more readily reduced than **85** (−1.29 V) with one fused cyclopropane ring and two fused cyclohexene rings [352]. In the same study, it was found that the reduction potentials of the investigated fullerene derivatives correlated well with their calculated energies of the LUMO.

It may be concluded from the findings above, that the nature of the fused addends has a significant influence on the reactivity of the remaining fullerene chromophore. The dienophile character of the fullerene is less pronounced in pentakis-adduct **90a** which has three fused cyclopropane rings and two fused cyclohexene rings, compared to pentakis-adduct **47** which has the same addition pattern but only fused

cyclopropane rings. Furthermore, semi-empirical calculations indicate that the difference in the reactivity of the two pentakis-adducts is primarily reflected in the electronic properties of the respective fullerene derivatives (*i.e.* the energetic position of the LUMO) and not in their molecular structure (*i.e.* the pyramidalization of the reactive double bond).

3.5 Conclusions

The essence of the investigations of described in the main sections 3.2 to 3.6 can be summarized as follows:

i) Functionalization of the fullerene chromophore does not influence the regioselectivity of the thermal (sections 3.2.2.3 and 3.3.3) and photolytical (section 3.2.2.4) dinitrogen extrusion from fullerene pyrazolines. As previously observed for the parent fullerene pyrazoline $C_{61}H_2N_2$ (section 2.3.3), thermal dinitrogen extrusion proceeds highly regioselectively producing homofullerene derivatives, whereas photolysis of the pyrazoline produces mixtures of the 6-6 closed and 6-5 open regioisomers.

ii) The nature of the addends of multiple adducts of C_{60} with the same addition pattern does not have an influence on the regiochemistry of further chemical transformations. Thus, the C_1-symmetrical hexakis-adducts **96a,b** with two fused cyclohexene-rings and three fused cyclopropane-rings and of **116** with five fused cyclopropane-rings were transformed to heptakis-adducts with the same addition pattern upon treatment at low temperatures with CH_2N_2.

iii) C_{60} derivatives with the same addition pattern but only fused cyclopropane-rings have a more pronounced dipolarophile character than those with both fused cyclopropane- and cyclohexene-rings. According to semi-empirical RHF-SCF-AM1 [353] and RHF-SCF-PM3 [347] calculational studies, the origin of the difference of the reactivity appears to be of electronic nature and is not reflected in the molecular geometry of the respective derivatives.

4. Investigation of the Physical Properties of Highly Functionalized Buckminsterfullerenes

The emphasis of this Chapter is on the investigation of the physical changes which occur upon increasing functionalization of the fullerene sphere. The Chapter is divided into three Sections:

-Section 4.1 gives an account of the effect of multiple functionalization of the fullerene core on the magnetic properties of the respective $^3He@C_{60}$-derivatives as revealed by ^3He NMR spectroscopy and rationalization of the results in term of π-electron ring current effects.

-In Section 4.2, a closer look at some of the spectroscopic properties of the multiple adducts is taken.

-Section 4.3 gives a brief summary of the key findings of Sections 4.1 and 4.2

4.1 Investigation of π-Electron Ring Current Effects in Multiple Adducts of $^3He@C_{60}$ by ^3He NMR Spectroscopy

4.1.1 Prelude: ^1H NMR as a Probe of the Fullerene Chromophore

As discussed in Section 1.5.4, the resonances of protons near the fullerene surface are particularly affected by the paramagnetic ring currents associated with the pentagons of the fullerene [136-138]. These ring currents shift the resonances of the protons located atop or in close proximity to pentagons strongly downfield [29,131,139,140]. With each addition to central 6-6 bonds of pyracylene sub-units in C_{60}, the full π-electron delocalization becomes interrupted and, therefore, it was expected that higher functionalization would reduce the deshielding of the protons located above the five membered rings. Furthermore, as more addends are attached, the shielding influence of developing isolated benzenoid six-membered rings should become increasingly important.

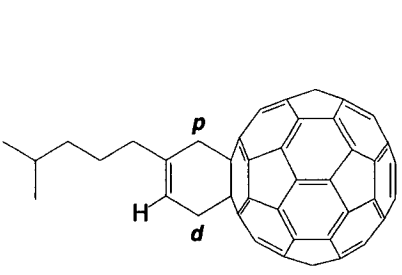

123

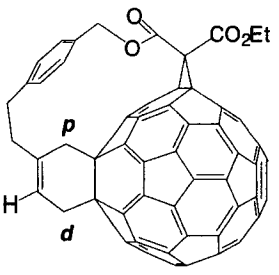

82b

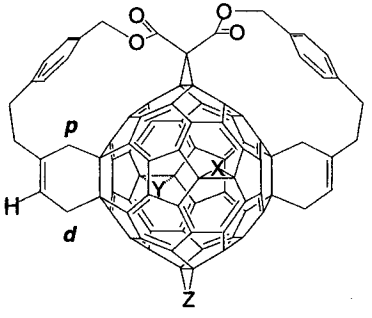

85 X = Y = Z = ——
89a X = $C(CO_2Et)_2$, Y = Z = ——
90b X = Y = $C(CO_2CH_2CO_2Et)_2$, Z = ——
91b X = Z = $C(CO_2CH_2CO_2Et)_2$, Y = ——
92a X = Y = Z = $C(CO_2Et)_2$

Figure 40. Depiction of the fullerene derivatives **123–92a** investigated in this Section.

Table 5. Selected ^1H NMR data (ppm) for a series of mono- through hexakis-adducts in $CDCl_3$. The cyclohexene CH_2 group near the anchor is labeled *p* (proximal), the one farther away *d* (distal).

	123[a]	**82a**[b]	**85**[c]	**89a**	**91b**	**90b**	**92a**
Benzyl CH_2O	—	5.25	5.18	5.19	5.30	5.12	5.22
=C–H	6.59	6.55	6.52	6.41	6.27	6.30	6.16
CH_2 (*p*)	3.98	3.48	3.42	3.28, 3.18	3.22, 3.12	3.07	2.95
CH_2 (*d*)	3.99	3.72	3.80	3.60, 3.56	3.45, 3.34	3.44	3.21

[a] Taken from [237a]. [b] Measured in $CDCl_3/CS_2$ 1:1. [c] Measured in $C_2D_2Cl_4$.

Comparison of the ^1H NMR spectra by *Isaacs et al.* [230,352] of *Diels-Alder* adduct **123** [237a] and **82a–92a** (Table 5) revealed significant changes in chemical shift, which can be rationalized by both effects. Whereas the benzylic CH_2O protons in **82a–92a** are not much affected by the degree of addition, the resonances of the proximal (*p*) and distal (*d*) CH_2 groups and the alkenyl protons of the cyclohexene

moieties shift upfield with increasing functionalization. The most substantial change was observed in the chemical shift of CH_2 (*p*), when passing from the mono- to hexakis-adduct ($\Delta\delta$ = 1.03 ppm). It is important to note that the largest change in chemical shift of the alkenyl protons ($\Delta\delta$ = 0.14 ppm) and of the CH_2 (*d*) protons ($\Delta\delta$ = 0.23 ppm) occurs on progressing from pentakis-adduct **90b** to the hexakis-adduct **92a**. This may be explained by the fact that transformation of the pentakis- to the hexakis-adduct results in the formation of four benzenoid rings as compared to earlier additions which only create either zero or two benzenoid rings.

4.1.2 Introduction

In contrast to the ^1H NMR study described above, which gives information about the *local* magnetic fields in the series **123–92a** generated by the ring currents in the fullerene chromophore (see also Section 1.4.5), ^3He NMR spectroscopy of endohedral ^3He fullerene complexes (in short ^3He@fullerene) yields information about the magnetic properties of the fullerene as a whole. The ^3He atoms at the center of the cage are exposed to the magnetic influence of the *entire* fullerene chromophore, *i.e.* to all π-electron currents, thus they represent a unique probe for investigating the influence of the degree of functionalization as well as the addition pattern on these currents.

The first ^3He NMR experiments on endohedral fullerene complexes were carried out by *Saunders et al.*, who incorporated ^3He into C_{60} and C_{70} under high pressure and temperature to an extent sufficient for NMR detection [141]. This work dramatically extended the initial mass spectrometric studies by *Schwarz et al.*, in which neutral He atoms were incorporated into the fullerenes by collision between noble gas atoms and fullerene ions in the gas phase, followed by neutralization [356]. And so, almost ten years after *Kroto et al.* suggested the experiment [6], the magnetic shielding environment inside the fullerene cavity could be probed experimentally. The measured ^3He NMR chemical shifts are δ = –6.36 (^3He@C_{60}) and –28.81 (^3He@C_{70}) relative to the resonance of free ^3He dissolved in 1-methylnaphthalene [141]. The significantly higher shielding of the ^3He nucleus in ^3He@C_{70} was expected on the basis of the measured magnetic susceptibilities [135a-b] as well as from ring current calculations [137]. The ^3He chemical shifts measured for ^3He@C_{60} and ^3He@C_{70} represent the extremes for neutral endohedral fullerenes isolated and measured so far. The ^3He atoms inside the higher fullerene compounds ^3He@C_{76}, ^3He@C_{78}, ^3He@C_{82}, and ^3He@C_{84}, display chemical shifts that lie between these two extremes [357]. Therefore, there is

no simple correlation between the ^{3}He shielding and the overall number of carbon atoms or the hexagon-to-pentagon ratio in the fullerene family.

As noted in Section 1.5.4, the chemical shift of ^{3}He@C_{60} results from both the magnetic fields generated by π-electron ring currents in the fullerene chromophore as well as from the shielding by the σ-electron framework of the fullerene cage [134,143]. For the following analysis of the ^{3}He chemical shift of the derivatives **124–129** (Figure 41), the contributions from σ-bond anisotropy are assumed to be roughly constant and therefore, changes in the ^{3}He NMR chemical shift should reflect mainly the different contributions of the various π-electron ring currents.

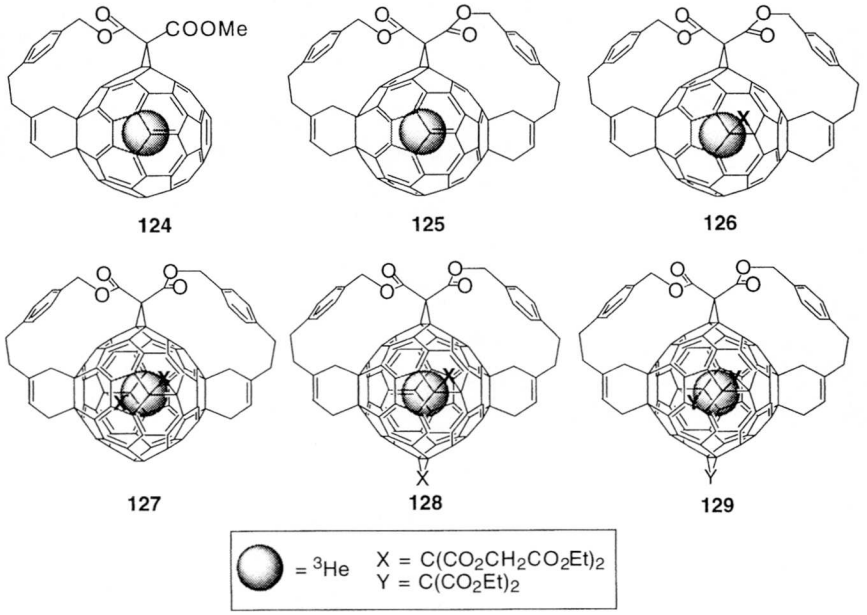

Figure 41. C_{60} multiple adducts **124–129** with ^{3}He atoms inside the cage.

Each covalent fullerene adduct with a ^{3}He atom inside measured so far gave a single sharp ^{3}He NMR resonance at a unique frequency [142,148,358]. The ^{3}He resonances of ^{3}He@C_{60} mono-adducts appear upfield of the resonance of ^{3}He@C_{60} [142]. In mono-adducts, in which the addend bridges a 6-6 bond, the ring size of the fused cycle has a pronounced influence on the ^{3}He NMR chemical shift of the

respective endohedral compound. Methanofullerene derivatives (*i.e.* cyclopropane fused derivatives) appear *ca.* 1.7 ppm upfield of $^3He@C_{60}$, whereas cyclohexene fused C_{60} derivatives shield the encapsulated ^3He atom more strongly and appear *ca.* 3.4 ppm upfield of the resonance of $^3He@C_{60}$ [142].

For the derivatives **124–129**, three influences of π-electron ring currents on the ^3He resonances were envisaged. Sequential addition to 6-6 bonds should reduce the strong paramagnetic ring currents in the pentagonal rings as well as the weaker diamagnetic ring currents that extend around the fullerene sphere [136,137]. Additionally, the development of localized benzenoid rings with diamagnetic ring currents should influence the ^3He resonances in the higher adducts **126–129**. Based on these considerations, a particularly strong shielding of the ^3He nucleus in hexakis-adduct **129** was expected since the X-ray analysis of corresponding helium-free hexakis-adducts had revealed a residual π-chromophore consisting of eight localized benzenoid rings [231,308,309,351].

4.1.3 Experimental Considerations

The endohedral compound $^3He@C_{60}$ was prepared at Yale University from pure C_{60} and according to the published procedures [359]. The incorporation level of ^3He was around 0.15%. Subsequently, compounds **124–129** (Figure 41) were synthesized at the ETH Zürich as described above for the corresponding derivatives lacking the helium atom [308,344,348]. The ^3He NMR measurements at 20 °C were again performed at Yale University by dissolving compounds **124–129** in a 1-methylnaphthalene/CD_2Cl_2 (3:1) mixture containing chromium(III) acetylacetonate as a relaxation agent.

Table 6 gives the chemical shifts of the ^3He in compounds **124–129** with respect to the signal of dissolved free ^3He set to 0.00 ppm. Also shown for comparison are the resonances of $^3He@C_{60}$ as well as of the known methanofullerene $^3He@C_{61}H_2$ [148]. The corresponding ^3He NMR spectra of compounds **124–129** are depicted in Figure 42. The minor impurities seen in the ^3He NMR spectra of the C_{60} bis- and tris-adducts **124** and **125** are attributed to oxidation products arising from $^1O_2$ ene reaction at their cyclohexene rings [348], with the formation of $^1O_2$ being efficiently sensitized by the fullerene derivatives (see also Section 2.3.2) [238]. In contrast, the C_{60} tetrakis- through hexakis-adducts **126–129** gave a single ^3He NMR resonance which is consistent with their reduced ability to photosensitize the formation of $^1O_2$ [348] (see also refs. [360-362]).

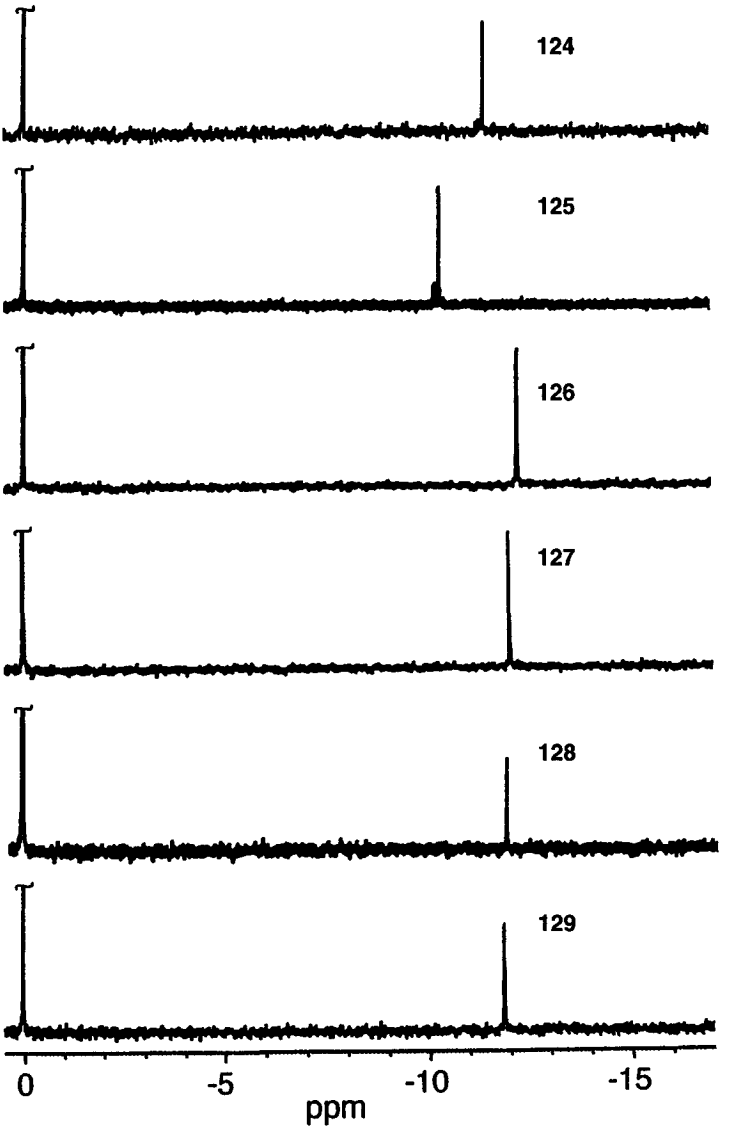

Figure 42. ^{3}He NMR spectra (1-methylnaphthalene/CD_2Cl_2 3:1) of C_{60} adducts **124–129**. The chemical shifts are relative to dissolved free ^{3}He.

4.1.4 ^{3}He NMR Results in the Series of the C_{60} Multiple Adducts 124–129.

The ^{3}He NMR resonances of multiple adducts **124–129** (Table 6) together with those of $^3He@C_{60}$ and $^3He@C_{61}H_2$ were plotted against the degree of functionalization (Fig. 42). The resonances of mono-adduct $^3He@C_{61}H_2$ (–8.11 ppm) and bis-adduct **124** (–11.45 ppm) showed strongly enhanced shielding with respect to the $^3He@C_{60}$ signal (–6.36 ppm) as was expected from previous literature data [142,148,358,363].

Table 6. ^{3}He NMR chemical shifts (1-methylnaphthalene/CD_2Cl_2 3:1) for the C_{60} adducts **124–129** in comparison to those of $^3He@C_{60}$ and $^3He@C_{61}H_2$. Chemical shifts given relative to dissolved free ^{3}He at 0 ppm.

Compound	Symmetry	Degree of functionalization	$\delta(^3He)$ [ppm]	$\Delta\delta(^3He)$ rel. to $^3He@C_{60}$ [ppm]	Lit.
$^3He@C_{60}$	I_h	—	–6.36	0.00	[148]
$^3He@C_{61}H_2$	C_{2v}	mono	–8.11	–1.75	[148]
124	C_s	bis	–11.45	–5.09	
125	C_{2v}	tris	–10.35	–3.99	
126	C_s	tetrakis	–12.26	–5.90	
127	C_{2v}	pentakis	–12.04	–5.68	
128	C_s	pentakis	–11.84	–5.48	
129	C_{2v}	hexakis	–11.89	–5.53	

However, the shielding of the ^{3}He resonances is not substantially enhanced by further functionalization. The resonance of tetrakis-adduct **126** (–12.26 ppm) displays the largest shielding, whereas those of the two pentakis-adducts **127** (–12.04 ppm) and **128** (–11.84 ppm) and of hexakis-adduct **129** (–11.89 ppm) appear at comparable chemical shifts, in the range of the ^{3}He resonance of bis-adduct **124**. This experimental result was initially quite surprising since we had expected a strong shielding of the ^{3}He atoms, particularly in the higher adducts, due to the vanishing of the paramagnetic ring currents of the pentagons [136-138] and the developing localized benzenoid rings with strong diamagnetic ring currents. As mentioned above, the π-chromophore in hexakis-

adduct **129** contains a total of eight localized benzenoid rings connected by biphenyl-type bonds [231,308,309,351].

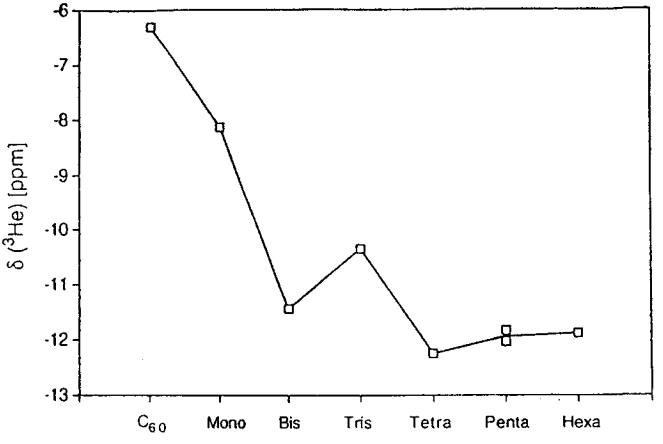

Figure 42. ^{3}He NMR chemical shifts of $^3He@C_{60}$ [141,148], $^3He@C_{61}H_2$ [148], and the $^3He@C_{60}$ multiple adducts **124–129** plotted against the degree of functionalization.

In order to rationalize these results it is proposed that the enhanced shielding upon changing from $^3He@C_{60}$ to bis-adduct **124**, in which full π-electron conjugation in four pentagons is destroyed, results mainly from the reduction of the paramagnetic ring currents in these rings. In the higher adducts **126–129**, however, the deshielding due to the functionalization-induced reduction in the diamagnetic ring currents that extend all around the fullerene sphere balances out the shielding due to the decrease in pentagon ring currents and the increase in localized benzenoid rings. As a result of this compensating effect, the ^{3}He resonances in **126–129** appear at very similar chemical shift.

These results differ with the ^{1}H NMR analysis of the helium free compounds **123** and **82a–92a** which shows a monotonic upfield shift of the cyclohexene CH_2 protons in the series (see Section 3.1.2) [352]. Compared to ^{3}He atoms at the center of the cage, protons located in a defined position atop the fullerene surface are more influenced by local changes in pentagon and (benzenoid) hexagon ring currents and less by changes in the diamagnetic ring currents extending around the entire C_{60} sphere. Although the latter have been calculated to be rather small in their local strength, they nevertheless have a significant effect on the resonance of ^{3}He atoms inside the cage due

to the large area they enclose. These extended ring currents have been conceptually correlated with three dimensional aromatic character [136,137,145], and, hence, higher functionalization can be viewed as a process which partially diminishes the aromaticity of the fullerene.

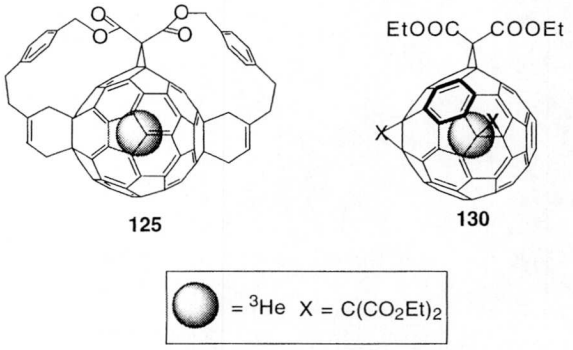

Figure 43. Depiction of the *e,e,trans-1*-tris-adduct **125** with no benzenoid substructure within the fullerene π-chromophore and of the *e,e,e*-tris-adduct **130** with one benzenoid substructure (highlighted in bold).

However, the importance of the contribution of benzenoid ring diamagnetic ring currents to the shielding of the ^{3}He atom becomes apparent in the comparison of the ^{3}He NMR resonances in the two different tris-adducts *e,e,trans*-1-**125** (-10.35 ppm) and *e,e,e*-**130** (-12.0 ppm) (Figure 43) [363]. Based on the higher shielding seen in cyclohexene-fused C_{60} mono-adducts as compared to cyclopropane-fused derivatives [142] (*vide supra*), a higher upfield shift of the resonance of doubly cyclohexene-fused **125** could be expected. However, **130** possesses a diamagnetically shielding benzenoid sub-structure which is absent in **2**, and this difference could well explain the upfield shift of the ^{3}He resonance in **130**. The large difference in ^{3}He NMR chemical shift ($\Delta\delta$ = 1.65 ppm) between the tris-adducts **125** and **130** nicely illustrates the influence of the nature of the addition pattern on the chemical shift of ^{3}He atoms inside C_{60} adducts.

4.1.5 Conclusions

This study reveals the large influence of functionalization on the diamagnetic ring currents that extend around the entire fullerene sphere. Despite an increasing degree of addition in the higher C_{60} adducts **124–129**, the ^{3}He NMR chemical shifts remain nearly constant due to the balancing out of the deshielding resulting from the

destruction of these ring currents and the shielding resulting from the vanishing paramagnetic pentagon ring currents and the increasing number of benzenoid rings with diamagnetic ring currents.

4.2 Spectroscopic Analysis of Highly Functionalized Homofullerene Derivatives

4.2.1 ^{1}H NMR Analysis of the Homofullerene and Methanofullerene Derivatives : Effect of the Addition Pattern on the Ring Currents of Highly Functionalized C_{60} Adducts

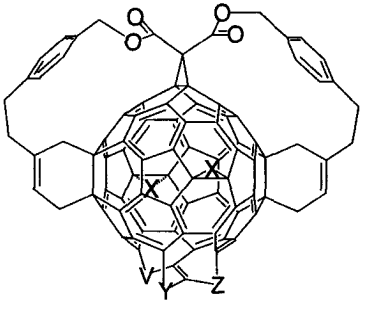

90 V = Y = Z = —
96 V = CH_2, Y = Z = —
99 V = —, Z = Y = CH_2
98 V = Y = Z = CH_2

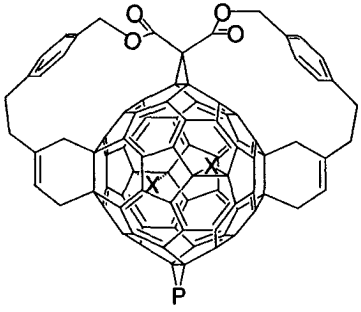

97 P = CH_2
95 P = —CH_2N_2—

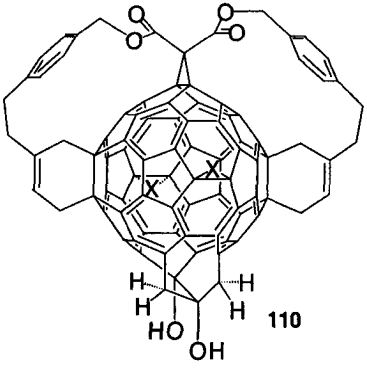

110

a X = $C(CO_2Et)_2$
b X = $C(CO_2CH_2CO_2Et)_2$

Figure 44. Depiction of the fullerene derivatives **90–110** investigated in this Section.

The analysis of the ^1H NMR spectra of the mono- to hexakis-adducts **123–92a** (Section 4.1.1) revealed a continuous upfield shift along the series for the protons located atop the five membered rings of the fullerene chromophore. These results were interpreted in terms of ring current effects, namely, the weakening of the paramagnetic ring currents in the pentagons of the fullerene as well as the developing of diamagnetic ring currents in the isolated benzenoid ring sub-structures. The chemical shift of the methylene tether-cyclohexene protons and, in particular, the methano-bridge protons (CH_2 *b*) of the higher adducts **90a,b–110** (Figure 44 and Table 7) allows to probe the influence of the addition pattern of these highly functionalized fullerene derivatives on their ring currents.

Inspection of Table 7 reveals a small upfield shift of the tether-cyclohexene alkene protons in C_1-symmetrical hexakis adducts **96a,b** by *ca.* 0.07 ppm for the insertion of one methylene group into a 6-5 bond of the remaining pyracylene subunit of the pentakis adducts **90a,b**. Subsequent insertion of one (**99a,b**) and two additional methylene groups (**98a,b**), respectively, results in a further upfield shift of the corresponding resonances by *ca.* 0.07 ppm per methylene unit. This trend may be rationalized by considering that, along the series **96a,b**, **99a,b**, **98a,b**, the central double bond of the pyracylene subunit of **90a,b** is increasingly lifted out of the fullerene sphere, resulting in a reduced conjugation of this double bond with the remaining chromophore. In other words, this double bond in the mono-, bis- and tris-homofullerenes **96a,b**, **99a,b**, and **98a,b** can be viewed as intermediate between a fully conjugated of the of the central double bond in the pyracylene subunit of the pentakis-adducts **90a,b** and completely removed the double bond such as in the hexakis adducts **95a,b**, **97**, and heptakis-diol **110**. Therefore, the upfield shift of the alkene protons of the tether-cyclohexene moiety can be rationalized by the gradual reduction of the paramagnetic ring currents in the bridged five membered rings, and concurrent development of isolated benzenoid ring substructures along the series **96a,b**, **99a,b**, **98a,b**, and **110**.

The chemical shift of the bridge CH_2 protons of the homofullerene derivatives **96a,b**, **99a,b**, and **110** shows trends which are compatible with the ring current picture discussed in Sections 1.5.4 and 4.1. The bridge methylene proton lying atop of the five membered ring in the C_1-symmetrical hexakis-adduct **96a** gives rise to a doublet at 4.71 ppm. Compared to the corresponding signal of the parent homofullerene $C_{61}H_2$ **28**, which appears at 6.35 ppm, it is shifted by 1.64 ppm upfield. Since the bridged five membered rings of the parent homofullerene **28** and hexakis-adduct **96a** are structurally identical, the difference of their respective magnetic properties must emanate from the

five addends bridging 6-6 bonds of the hexakis-adduct **96a**[84]. A further upfield shift of 0.27 ppm is observed for the methano bridge proton atop a former five membered ring in heptakis-adduct **99a**, as compared to the hexakis-adduct **96a**. This effect is consistent with the weakening of the paramagnetic ring current in the doubly bridged pentagon of **99a** (*vide supra*). Removal of the geminally bis-functionalized double bond of **99a** by oxidation leading to diol **110** produces a large upfield shift of 0.6 ppm of the protons lying above the former five membered ring in agreement with the ring current arguments discussed above.

In contrast to the protons located above the former five membered rings in the series **96a 99a**, and **110** the protons located atop former six membered rings are strongly deshielded ($\Delta\delta$ (**96a–110**) = 1.49 ppm). This opposite behavior may be the result of the pseudo benzylic position of the respective protons relative to the developing benzenoid ring substructures within the series[85].

Table 7. Selected ^{1}H NMR data (ppm) for the series of pentakis- through octakis-adducts in $CDCl_3$. The bridge CH_2 groups are labeled *b*.

	90a **90b**	**96a** **96b**	**99a** **99b**	**95a** **95b**	**97**	**98a** **98b**	**110**
=C–H	6.27;	6.21, 6.19;	6.13;	6.09;	6.10	6.07, 6.03;	6.01;
	6.30[a)]	6.23, 6.21	6.14	6.12	—	6.07, 6.02	—
CH_2 (*b*)	—	4.71, 2.13;	4.44, 2.76;	5.73[c)]	2.75	4.48, 4.41, 4.06, 3.39, 3.37, 2.04;	3.84, 3.62
	—	4.85-4.75[b)], 2.15	4.48, 2.75	5.70[c)]	—	4.53, 4.46, 4.10, 3.49, 3.38, 2.02	—

a) Taken from [230,352]. b) Resonance obscured by the signals of the CH_2-protons of the malonate addends. c) Pyrazoline CH_2-protons.

In the series of the all-cyclopropanated fullerene derivatives **116**, **117**, and **119**, the resonances of methylene bridge protons are shifted downfield by 0.29–0.53 ppm compared to the resonances of the corresponding protons in the series **96a 99a**, and **110**. This downfield shift is the result of the nature of the fused cyclopropane addends, which

[84]A similar upfield shift of 1.18 ppm is observed for the protons of the cyclopropane bridge of the hexakis-adduct **97** compared to the parent methanofullerene $C_{61}H_2$ [251a].

[85]The protons located atop the former five membered rings are also in a benzylic position to the developing benzenoid ring substructures within the series **96a 99a**, and **110**, however the upfield shift of the protons as a result of the weakening of the paramagnetic ring currents apparently outweighs the deshielding due to the formation of the benzenoid rings.

have a less pronounced effect on the π-system of the fullerene chromophore compared to the fused cyclohexene addends in the series **96a 99a**, and **110** (see Sections 1.5.3; 4.1 and 3.4.2).

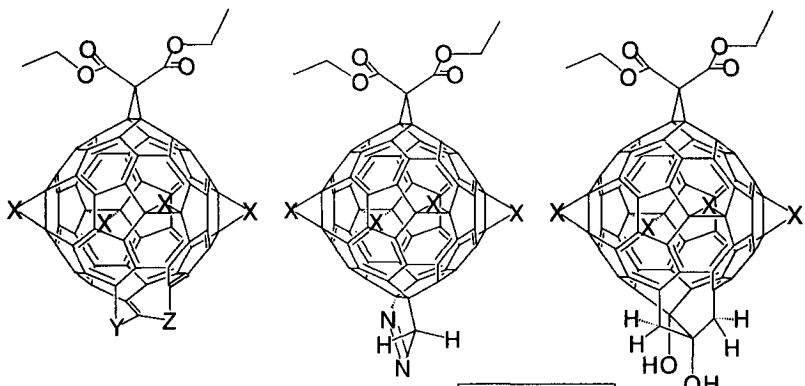

Figure 45. Depiction of the all-cyclopropanated fullerene derivatives **116–119** investigated in this Section.

This becomes apparent upon comparison of the chemical shift of the diastereotopic protons of hexakis-adducts **96a** (4.71 and 2.13 ppm) and **116** (5.24 and 2.45 ppm) to the corresponding resonances of the parent homofullerene $C_{61}H_2$ which appear at 6.35 and 2.78 ppm, respectively. Apparently the local magnetic properties of the parent homofullerene are less perturbed by fused cyclopropane rings than by fused cyclohexene rings. However, as can be seen in tables 7 and 8, respectively, the trends of the chemical shifts of the bridge protons are the same in both series.

Table 8. ^{1}H NMR data (ppm) of the methylene protons of the pyrazoline moiety of **115** and of the methylene protons of the CH_2 groups bridging 6-5 open junctions in the series **116–119** in $CDCl_3$. The bridge CH_2 groups are labeled *b*.

	115	**116**	**117**	**119**
CH_2 (*b*)	5.95	5.24, 2.45	4.80, 3.02	4.50-4.15[a], 3.91

[a] Resonance obscured by the signals of the CH_2-protons of the malonate addends.

It may be concluded that in both series the effect of increasing functionalization of the fullerene chromophore leads to changes in the chemical shifts of the protons

discussed above which can be rationalized by the ring current model introduced in Section 4.1. Furthermore, in agreement with the analysis of the chemical reactivity towards diazomethane of the two pentakis-adducts **90a** and **47**, (Section 3.4) the two fused cyclohexene moieties of the adducts have a greater influence on the electronic structure of the fullerene chromophore and therefore also on the magnetic properties of the respective adducts.

4.2.2 Electronic Absorption Spectroscopy

In previous UV/VIS studies of the bis- to hexakis-adducts **82a–92a** (see Scheme 28 and Figure 29) in which the addends exclusively bridge 6-6 bonds, it was found that changes in the extension of the conjugated π-chromophore of the fullerene have a pronounced effect on both the spectral shape as well as on the position of the end absorption of the UV/VIS spectra of the respective adducts [344,352]. In particular, the generation of isolated benzenoid ring substructures within the residual π-chromophore was found to lead to a large hypsochromic shift of the end absorption. This is particularly evident in the comparison of the UV/VIS spectra (Figure 46) of the pentakis-adduct **90a** which is orange in solution and the hexakis-adducts **97** and **95a** which are bright yellow.

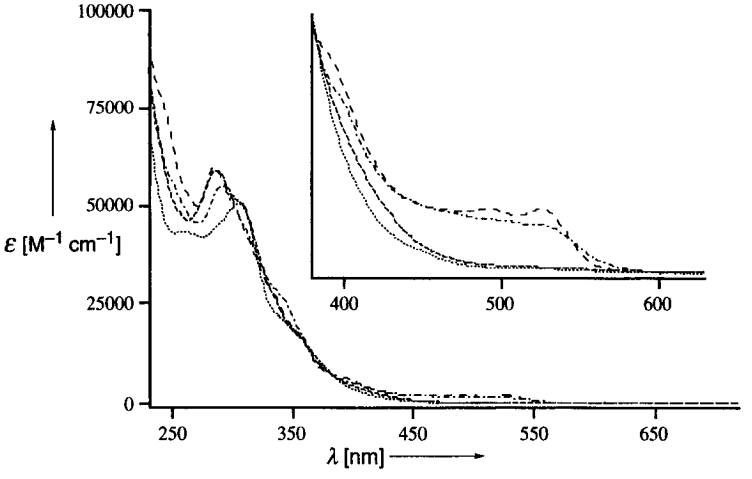

Figure 46. UV/VIS Spectra in CH_2Cl_2 of pentakis-adduct **90a**(– – –), C_1-symmetrical (6-5 open) hexakis-adduct **96a**(– · – · –), C_{2v}-symmetrical (6-6 closed) hexakis-adduct **97**(- - - -), and pyrazoline **95a**(·····).

The formation of four benzenoid rings in **97** and **95a** upon functionalization of the central double bond of the pyracylene subunit of **90a** leads to a large blue shift of *ca.* 100 nm of the end absorption (Figure 46). In contrast, the color and the UV/VIS spectrum of the hexakis-adduct **96a** in which a methylene moiety bridges an open 6-5 junction of the fullerene is practically identical to that of the pentakis adduct **90a**. This is in agreement with UV/VIS and electrochemical studies of the parent homofullerene $C_{61}H_2$ which revealed that its electronic structure is virtually identical to that of pristine C_{60} (see Section 1.5.3). The two hexakis-adducts **97** and **95a** are very similar in the visible region of the spectrum, however in the between 250 and 350 nm they exhibit distinct differences. The hexakis-adduct **97** has a maximum at 287 nm and a shoulder at 309 nm. In contrast the spectrum of the pyrazoline **95a** shows two maxima at 262 and 305 nm, respectively. As the addition pattern is identical in both cases the difference of their electronic absorption spectra should reflect the different nature of the sixth addend (cyclopropane *vs.* pyrazoline).

The influence of multiple bridging of 6-5 bonds on the UV/VIS spectra can be seen by comparing heptakis- **99b** and octakis-adduct **98b** (Figure 47).

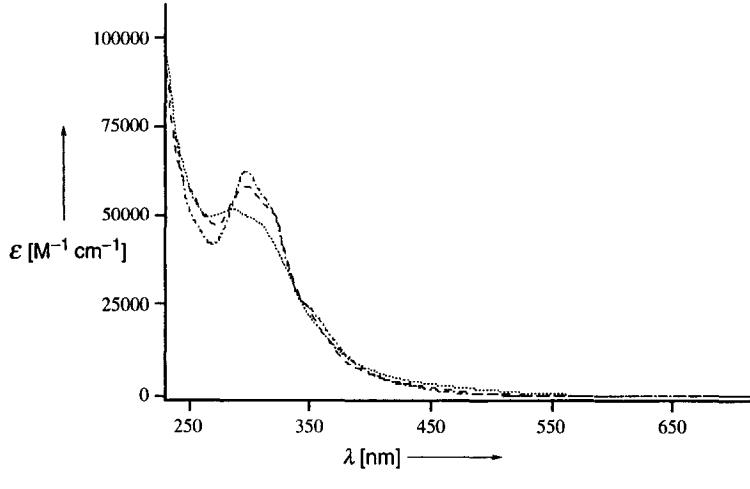

Figure 47. UV/VIS Spectra in CH_2Cl_2 of heptakis-adduct **99b**(– – –), diol **110**(– · – · –), and octakis-adduct **98b**(·····).

Both spectra show very little fine structure with only one maximum at 296 (**99b**) and 286 nm (**98b**), respectively. Contrary to what was expected, the end absorption of octakis-adduct **98b** (540 nm) is not hypsochromically shifted compared to that of

heptakis-adduct **99b** (510 nm). Furthermore, oxidation of the geminally bis-functionalized double bond of heptakis-adduct **99b** has little influence on the UV/VIS spectrum, as can be seen in the spectrum of diol **110** which is very similar to that of **99b**.

The influence of the nature of the addends on the electronic absorption spectra of multiple adducts with the same addition pattern is apparent upon inspection of figure 48. The UV/VIS spectrum of the C_1-symmetrical hexakis-adduct **96a** is rather unstructured and shows only one maximum at 291 nm and two absorption shoulders in the visible region at 498 and 527 nm, respectively. In comparison, the UV/VIS spectrum of **116** shows more fine structure and exhibits two distinct maxima in the UV region, one at 245 nm, which is not present in **96a**, and one at 287 nm. The visible region of the spectrum of **116** shows one maximum and a shoulder at 517 and 540 nm, respectively, corresponding to the two absorption shoulders in the same region of the spectrum of **96a**.

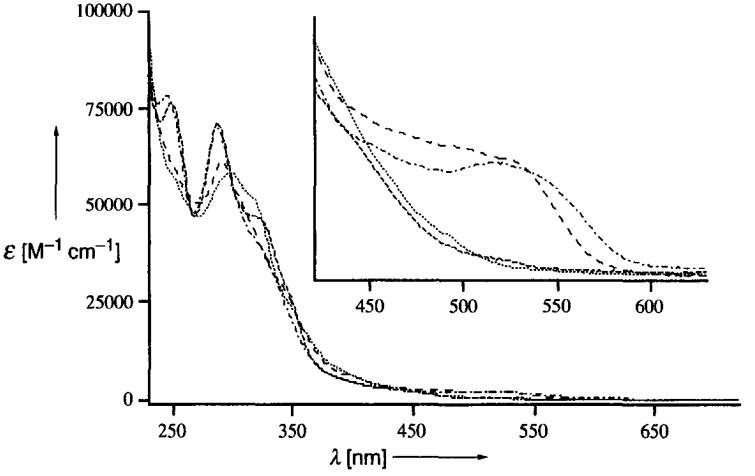

Figure 48. Comparison of the UV/VIS spectra in CH_2Cl_2 of the two C_1-symmetrical (6-5 open) hexakis-adducts **96a**(– – –) and **116**(– · – · –), and of the two heptakis-adducts **99b**(·····), and **117**(- - -).

Similar to the UV/VIS spectrum of **116**, the spectrum of heptakis-adduct **117** exhibits an absorption maximum at 249 nm, which is not present in the spectrum of the heptakis-adduct **99b**. The absorption maximum of **117** at 288 nm is slightly

hypsochromically shifted compared to the corresponding absorption maximum of **99b** which appears at 299 nm. Thus, the nature of the addends primarily influences the electronic absorption spectrum in the UV region, and only to a small extent in the visible region.

4.3 Conclusions

The essence of the investigations of described in Sections 4.1 to 4.3 can be summarized as follows:

i) ^{3}He NMR analysis of multiple adducts of C_{60}, on the one hand, provided further support for the importance of the contribution of benzenoid ring diamagnetic ring currents, apparent in the comparison of the ^{3}He NMR resonances in the two different tris-adducts *e,e,trans*-1-**125** (-10.35 ppm) and *e,e,e*-**130** (-12.0 ppm) (Figure 43). On the other hand, the study revealed the large influence of functionalization on the diamagnetic ring currents that extend around the entire fullerene sphere. As a consequence of the weakening of those extended diamagnetic ring currents by an increasing number of addends, the ^{3}He NMR chemical shifts remain nearly constant in the higher C_{60} adducts, despite the formation of an increasing number of benzenoid rings.

ii) ^{1}H NMR spectroscopic analysis of the highly functionalized homofullerene derivatives reveals trends which can be rationalized with the ring current model used for the interpretation of the ^{3}He NMR study in Section 4.2, further supporting the ring current arguments used throughout the thesis.

iii) UV/VIS study of the highly functionalized homofullerene derivatives showed that the nature of the addends bridging 6-6 bonds of the fullerene leads to distinct differences in the UV region of the respective adducts but only to small differences in the visible region of the spectra of the respective fullerene derivatives.

5. Investigation of the Origin of Regioselectivity in Homofullerene Formation by Addition of Diazo Compounds

In this chapter the origin of the regioselectivity for the thermal dinitrogen extrusion from diazoadducts of fullerenes is investigated. The chapter is divided into three sections:

-Section 5.1 gives a short introduction to the experimental work of *F.-G. Klärner* on the photolysis and thermolysis of diazopropane toluene- and xylene-adducts and its relevance to the photolytical and thermal dinitrogen extrusion from diazomethane adducts of fullerene derivatives.

-Section 5.2 describes the determination of the activation energy for the thermal dinitrogen extrusion from the highly functionalized fullerene-pyrazoline derivative.

-In section 5.3, the reaction mechanism of the thermal dinitrogen extrusion from the adduct of diazomethane with benzene is investigated by *ab initio* and density functional methods. The investigations described in this section were carried out in collaboration with *E.-U. Wallenborn*, who is responsible for all the calculations presented and who derived the equations necessary for the representation of the anisotropy of the ring-current (Figure 55).

5.1 Introduction: Thermal Dinitrogen Extrusion from a Diazopropane-Xylene- and a Diazopropane-Toluene-Adduct

In their ongoing research of the *Walk*-rearrangement [364] *Klärner et al.* investigated the thermal and photochemical behavior of the 2-diazopropane adduct of *m*-xylene **131** [365] (Table 9). The investigations showed that upon thermolysis at 60 °C in benzene, the pyrazoline **131** rearranges regiospecifically to the cycloheptatriene **132**. A small amount of the regioisomeric cycloheptatriene **133** could only be detected, when the thermolysis of **131** was carried out at 150 °C in the gas phase [365]. On the

other hand, photolysis of **131** in the presence of a triplet photosensitizer[86] provided a 1:1 mixture of the regioisomers **132** and **133**.

Table 9. Isomer distribution upon thermolysis and photolysis of the pyrazoline **131** as reported by *Klärner et al.* [365].

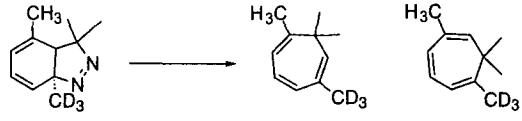

131 **132** **133**

Reaction Conditions	Product Distribution in %	
Δ (60 °C)	> 98	< 2
Δ (150 °C)	91	9
hv (350 nm, $Ph_2C{=}O$)	51	49

To account for the high regioselectivity of the thermal dinitrogen extrusion from **131**, the authors proposed an eight-electron orbital symmetry controlled [$2\pi_s + 2\pi_s + 2\sigma_a + 2\sigma_s$] concerted mechanism [365] (Scheme 50A). The mechanistic hypothesis was later on supported by the observation that the dinitrogen extrusion from the chiral diazopropane adduct (+)-**134** (Table 10) proceeds with inversion of configuration at the migrating carbon, producing (+)-**135**, and therefore fulfills the stereochemical requirements of such an orbital symmetry controlled process [366].

Table 10. Isomer distribution upon thermolysis of the chiral pyrazoline **134** as reported by *Klärner et al.* [366].

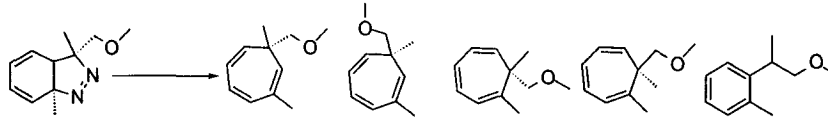

(+) -**134** (+) -**135** (−) -**135** (−) -**136** (+) -**136** **137**

Reaction Conditions	Product Distribution in %				
Δ (70 °C)	93	2	3	0	2

[86]Direct photolysis of **131** at 254 or 350 nm led predominantly to cycloreversion of the diazopropane moiety and the production of trideuteriomethyl-*m*-xylene.

Photolysis, in contrast, was proposed to proceed *via* the symmetrical diradical intermediate **138** (Scheme 50A), which upon radical recombination leads to the observed mixture of regioisomers **132** and **133**.

The regioselectivity for the thermal and photochemical dinitrogen extrusion from the diazopropane cycloadduct **131** is analogous to that of the diazomethane adduct of C_{60} (see Scheme 10, Section 2.3.3) as well as to that of highly functionalized fullerene pyrazoline derivatives (see Sections 3.2.2.3, 3.2.2.4, and 3.3.3) and of diazomethane adducts of C_{70} [139] (see Scheme 50B). Thermolysis of the respective pyrazoline cycloadducts (**139**), leads almost exclusively to the formation of 6-5 open homofullerene derivatives (**140**), whereas photolysis produces mixtures of the 6-5 open (**140**) and the 6-6 closed (**141**) regioisomers. Consequently, there exists a strong similarity between the thermal and photochemical reactivity of fullerene-fused pyrazolines, such as **139**, and the diazopropane-xylene adducts, such as **131**.

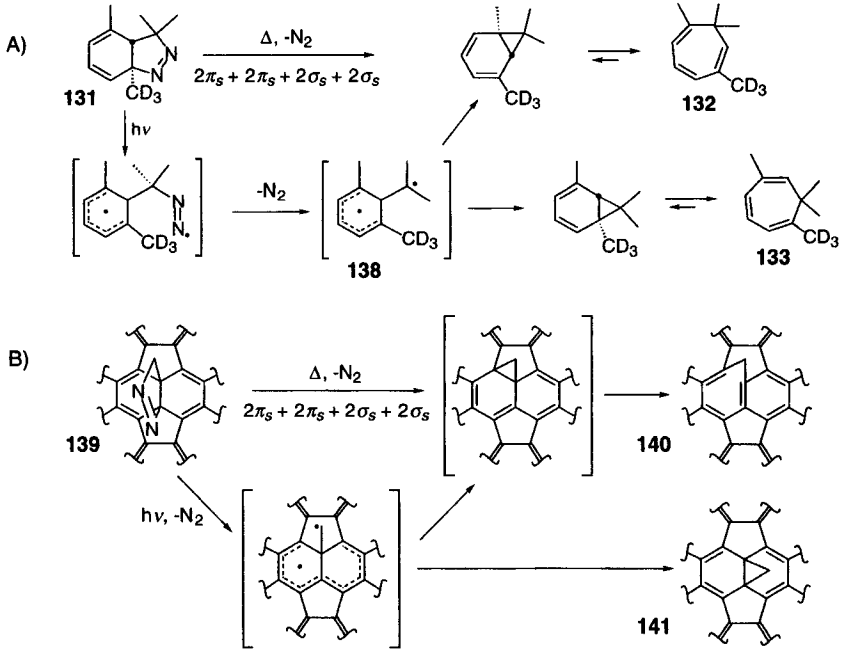

Scheme 50. Proposed mechanism for the thermal and photochemical dinitrogen extrusion from diazopropane adducts of xylene (A), and (B) from diazomethane adducts of fullerenes (shown only in part for clarity).

5.2 Determination of the Arrhenius Parameters for the Thermal Dinitrogen Extrusion from a Highly Functionalized Fullerene-Pyrazoline Derivative

In order to obtain a clearer picture of the mechanism of the formation of homofullerene derivatives *via* thermal dinitrogen extrusion, we decided to first investigate this process from **95a** and to compare the activation enthalpy of the reaction with that of the diazopropane-toluene adduct **142** investigated by *Klärner et al.* (Table 11 [365]).

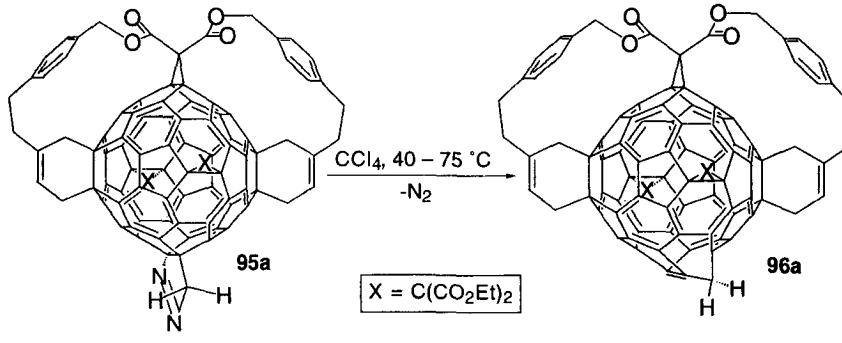

Scheme 51. Depiction of the thermal dinitrogen extrusion reaction investigated for determining the *Arrhenius* parameters.

Thermolysis of pyrazoline **95a** was carried out at 40, 50, 60, 67, and 75 °C and monitored by HPLC. Assuming a first order reaction kinetics for the thermal dinitrogen extrusion from **95a**, the rate constant of the reaction can be determined in the following manner (for the sake of readability, **95a** will be called Pyrazoline and **96a** will be called Hexa).

$$[\text{Pyrazoline}](t-t_0) = [\text{Pyrazoline}](t_0)\exp\{-k\,(t-t_0)\} \quad (15)$$

and

$$[\text{Hexa}](t-t_0) = [\text{Pyrazoline}](t_0) - [\text{Pyrazoline}](t-t_0) \quad (16)$$

The progression of the reaction was monitored by integration of the chromatogram peaks[87] (Figure 49) and taking the ratio of the product and the reactant at a given time. Therefore, we are interested in the ratio of equations (15) and (16).

[87]To account for the difference in the absorption of pyrazoline **95a** and of hexakis-adduct **96a** at the detection wavelength (310 nm) a correction factor has to be introduced: ε (**95a**) = 0.9653 ε (**96a**).

$$\frac{[\text{Pyrazoline}](t-t_0)}{[\text{Hexa}](t-t_0)} = \frac{[\text{Pyrazoline}](t_0)\,\exp\{-k\,(t-t_0)\}}{[\text{Pyrazoline}](t_0)\,(1-\exp\{-k\,(t-t_0)\})} = \frac{1}{\exp(-k\,(t-t_0)-1)} \quad (17)$$

and the expression for the rate constant k is therefore:

$$k\,(t-t_0) = \ln\left(\frac{[\text{Hexa}](t-t_0)}{[\text{Pyrazoline}](t-t_0)} + 1\right) \quad (18)$$

Equation (18) has the advantage that not the absolute concentration of the products, but only the ratio of starting pyrazoline **95a** to homofullerene **96a** is important for the evaluation of k, which eliminates systematic errors which could arise from inaccuracies of the absolute amount of the product analyzed by HPLC.

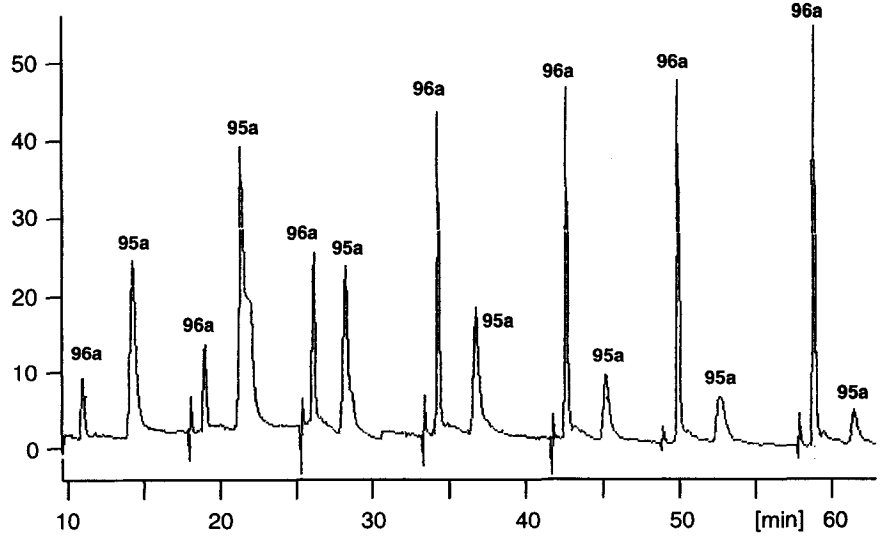

Figure 49. Depiction of the HPLC chromatogram of the thermal dinitrogen extrusion form the pyrazoline **95a** forming the C_1-symmetrical hexakis-adduct **96a** at 60 °C in CCl_4.

The rate constants of the thermal dinitrogen extrusion from **30** were thus determined and are listed in Table 12.

Table 12. Rate constants of the thermal dinitrogen extrusion from **95a** in CCl_4.

T [K]	313	323	333	340	348
$k\ 10^5$ [s^{-1}]	3.26 ± 0.06	12.5 ± 0.4	47.2 ± 2.3	134 ± 13	249 ± 52

According to the *Arrhenius* equations the temperature dependency of the rate constant is given by

$$k(T) = A\ (T)\exp\left(\frac{-E_A}{RT}\right) \tag{19}$$

which is equal to

$$\ln k(T) = \ln A\ (T) - \frac{E_A}{RT} \tag{20}$$

in which A (T) is the pre-exponential *Arrhenius* factor, and E_A is the activation energy according to *Arrhenius*.

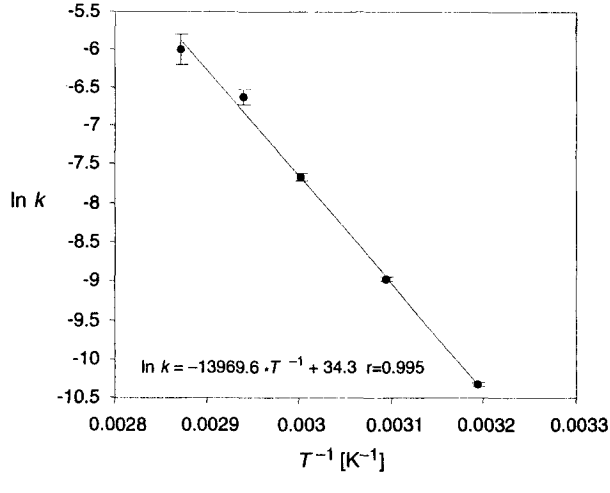

Figure 50. Depiction of the *Arrhenius* plot of the thermal dinitrogen extrusion from **95a** in CCl_4 between 40 and 75 °C.

Weighted linear regression of ln $k(T)$ *vs.* $1/T$ and upon consideration of the *Eyring* equation, $k(T) = \frac{kT}{h}\exp\left(\frac{-\Delta G^{\neq}}{RT}\right) = \frac{kT}{h}\exp\left(\frac{-\Delta S^{\neq}}{R}\right)\exp\left(\frac{-\Delta H^{\neq}}{RT}\right)$, we obtain:

57.5 °C: $\Delta H^{\neq} = 27.7 \pm 1.6$ kcal mol^{-1} (95%, Student-t)

$\Delta S^{\neq} \approx 9 \pm 55$ cal mol^{-1} K^{-1}, $\Delta G^{\neq} \approx 24.6$ kcal mol^{-1}.

The large error of the *Arrhenius* parameters determined in this investigation reflects the inaccuracies of the rate constants determined at 67 and 75 °C (see Table 12 and Figure 50). However, omitting those data does not have a significant influence on the values of $\Delta H^{\neq}$ and $\Delta S^{\neq}$.

The investigation allows to draw two important conclusions:

i) the thermal dinitrogen extrusion indeed proceeds with first order kinetics, analogous to the corresponding dinitrogen extrusion from **142** (Table 11),

and

ii) the activation enthalpy ($\Delta H^{\neq}$) for the thermal dinitrogen extrusion from the fullerene adduct **95a** is similar to that for the analogous reaction of the diazopropane-toluene adduct **142** (Table 11) ($\Delta H^{\neq}$ = 25.09(13) kcal mol^{-1}) [365]. Thus, not only the regioselectivity of the thermal dinitrogen extrusion from diazopropane adducts of xylene and toluene are analogous to that of fullerenes (Scheme 50), but also the activation energy of the reaction is comparable for the small system **142** and the fullerene derivative **95a**.

Table 11. Isomer distribution upon thermolysis of the diazopropane-adduct **142** as reported by *Klärner et al.* [365].

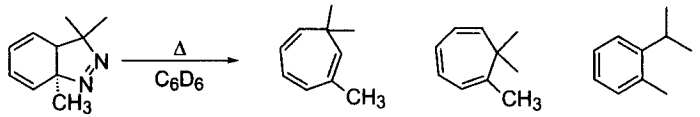

142 **143** **131** **144**

Reaction Conditions	Product Distribution in %		
Δ (28 – 50 °C)	94	3	3

5.3 Theoretical Investigation of the Thermal Dinitrogen Extrusion From a Diazomethane Benzene Adduct

In consideration of the fundamental importance of the regioselective dinitrogen extrusion reaction of diazoalkane-fullerene adducts for the formation of 6-5 open homofullerenes, we decided to investigate the reaction using theoretical methods. Thus, we investigated the thermal dinitrogen extrusion by high-level *ab initio* and density functional calculations. As a result of the prohibitive size of the fullerene for such an analysis, we chose the model system **145** (Scheme 52), which is similar to **131** (Scheme 50), investigated previously by *Klärner et al.* [365] (see Section 5.1).

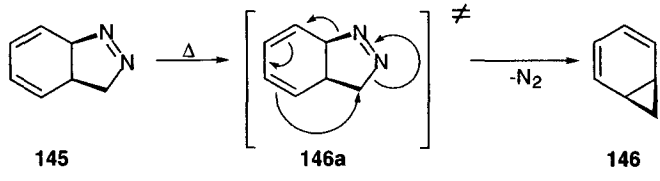

145 **146a** **146**

Scheme 52. Depiction of the thermal dinitrogen extrusion reaction investigated by *ab initio* and density functional methods.

Since eight electrons are involved in the orbital symmetry controlled $[2\pi_s + 2\pi_s + 2\sigma_a + 2\sigma_s]$ concerted dinitrogen extrusion reaction from the investigated pyrazolines, a pericyclic mechanism should proceed *via* a *Möbius* aromatic transition state [367,368]. Recent theoretical analyses of Diels-Alder reactions [369] and the 1,7-sigmatropic hydrogen shift [370] have demonstrated that the investigation of magnetic properties in the analysis of thermally allowed Woodward-Hoffmann type reactions is very useful. We have analyzed the reaction of **145** to **146** also in this respect. Finally, we enlarged and rigidified the model system to explore the sensitivity of the reaction mechanism towards changes of the model size.

5.3.1 Results and Discussion

5.3.1.1 Transition State Geometries and Energies

Following the work of *Barone* and *Arnaud* [371], who found that in general B3LYP/6-31G* calculations of Diels-Alder transition states reproduced the geometries of the reactants very well and resulted in accurate transition state geometries and energy barriers, we calculated geometries, their corresponding energies, and magnetic properties mainly using density functional methods. To support these calculations, we repeated most calculations on the MP2 level. In view of the fact that MP2 calculations of Woodward-Hoffmann-type reactions with heteroatoms are occasionally problematic [371,372] the MP2/6-31G* results were complemented by additional MP4/6-31G*//MP2/6-31G* calculations.

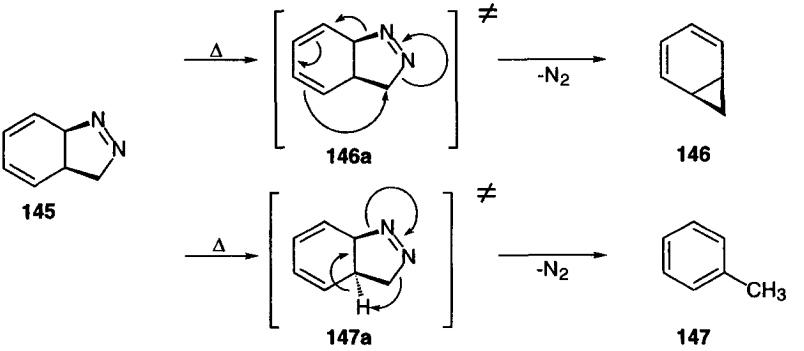

Scheme 53. Depiction of the reaction pathways found for the thermal dinitrogen extrusion reaction investigated by *ab initio* and density functional methods.

Transition state searches starting from **145** indicate two reaction pathways leading to norcaradiene (**146**) and toluene (**147**), respectively (Scheme 53). Since the formation of arene derivatives has been observed experimentally in the thermal degradation of **134** (Table 10) and of **142** (Table 11) [365,366], we decided to include this reaction pathway in the present analysis (cf. Scheme 53).

Figure 52 shows the calculated reactant **145** and the two transition state geometries **146a** and **147a**. The MP2 and B3LYP geometries of both reactant and transition states are quite similar. The equilibrium structure of pyrazoline **145** shows the expected bond length alternation in the cyclohexadiene fragment of the molecule. It should be noted that in **145**, the dihedral angle N(8)—C(9)—C(1)—C(6) is nonzero

(−16.4° on the B3LYP/6-31G* level and −28.3° on the LSDA/3-21G* level). This is, regarding the transferability of the results to larger systems such as fullerene derivatives, an interesting point and will be discussed in detail in Section 5.3.1.3. In the reaction towards norcaradiene **146**, a bond is formed between C(2) and C(9). The distance between these two atoms in the calculated reactant geometry is 2.528 Å (MP2/6-31G*) and 2.552 Å (B3LYP/6-31G*), respectively. In the transition state **146a** leading to norcaradiene, the distance between C(2) and C(9) has been reduced by *ca.* 0.3 Å to 2.278 Å (MP2/6-31G*) and 2.192 Å (B3LYP/6-31G*), respectively, which corresponds roughly to one third of the way towards the formation of the cyclopropane bond in **146**. Simultaneously, the C(2)—C(1)—C(9)—N(8) dihedral angle has been widened from 148.6° to 161.8° (MP2/6-31G*) or from 140.3° to 161.7° (B3LYP/6-31G*), respectively. This enhances the overlap between the σ^*-orbital of the C(9)—N(8) bond and a *p*-orbital on the C(2) atom.

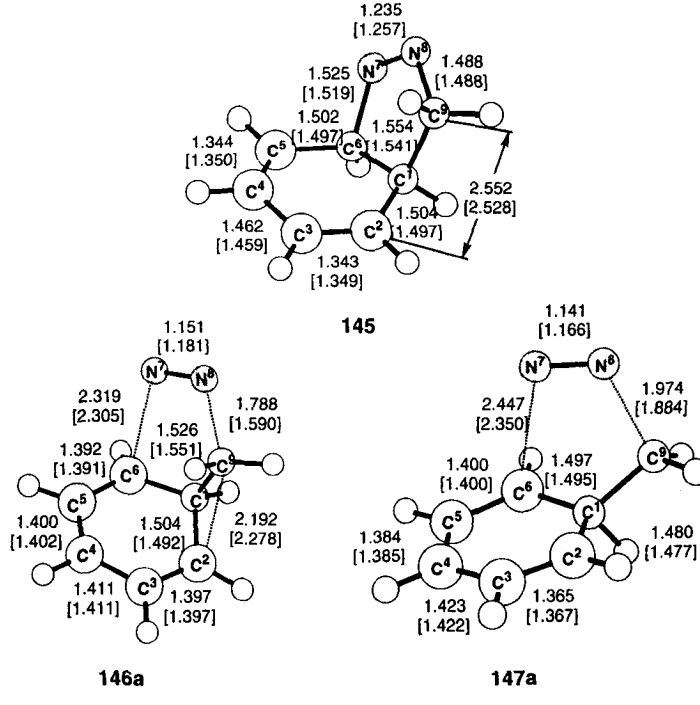

Figure 52. Depiction of 7,8-diazabicyclo[4.3.0]nona-2,4,7-triene (**145**), and the transition state geometries **146a** and **147a**. B3LYP/6-31G* and MP2/6-31G* (square brackets) distances are given in Å.

The dinitrogen extrusion from **145** to **146** then proceeds in a highly asynchronous fashion. Thus, in the transition state **146a** the C(6)—N(7) bond which connects the diazo moiety to the cyclohexadiene fragment of **146a** is significantly longer (2.305 Å in MP2/6-31G*, 2.319 Å in B3LYP/6-31G*) than the C(9)—N(8) bond (1.590 Å in MP2/6-31G*, 1.788 Å in B3LYP/6-31G*).

The bond lengths within the cyclohexadiene moiety (C(2)—C(6)) in **146a** show a markedly reduced alternation compared to **145** and **147a**. This bond length equalization can be interpreted as indicating aromaticity of **146a**, with the aromatic system extending over the six-membered ring. The high degree of asynchronicity in the extrusion of dinitrogen from **145** is quite surprising and will be discussed in further detail later in this section. The second reaction pathway going from the pyrazoline **145** to toluene (**147**) yields the transition state **147a**. The geometry of **147a** differs from **146a** mainly in the orientation of the C(9) methylene group. The dihedral angle C(2)—C(1)—C(9)—N(8) in this molecule is 85.5° (MP2/6-31G*) or 90.4° (B3LYP/6-31G*), respectively, which turns the methylene group into a position which enables the subsequent 1,2-hydrogen shift to take place producing toluene.

The loss of dinitrogen in **147a** proceeds in a slightly less asynchronous fashion than in **146a**. Again, the C(6)—N(7) distance (2.350 Å in MP2/6-31G*, 2.447 Å in B3LYP/6-31G*) is larger than the C(9)—N(8) distance (1.884 Å in MP2/6-31G*, 1.974 Å in B3LYP/6-31G*), however the difference is smaller than in **146a**. Comparing the results obtained by the MP2 and the B3LYP calculations, the bond lengths of the pyrazoline **145** and the two transition states **146a** and **147a** are generally the same within a few pm. The largest differences are observed for the carbon—nitrogen distances in the transition state geometries **146a** and **147a**.

As indicated before, the C(6)—N(7) distance in **146a** is substantially larger than the C(9)—N(8) distance, which could indicate that the C(6)—N(7) bond is cleaved first in the course of the reaction, generating the (hypothetical) diradical intermediate **148** (Figure 53), or that the transition state **146a** itself has significant diradicaloid character.

In order to check our analysis, we decided to characterize the electronic structure of **146a** in detail. Table 13 shows the relevant configuration state functions (absolute value of the CASSCF coefficient larger than 0.05) of the electronic ground states of CASSCF/6-31G* calculations employing an active space which consisted of the four highest occupied and the four lowest unoccupied molecular orbitals from a

single (closed shell) Hartree-Fock reference configuration on the B3LYP/6-31G* and MP2/6-31G* saddle points.

Table 13. CASSCF(8,8)/6-31G* ground state configuration of **146a**.

Geometry	Configuration	MCSCF coefficient
B3LYP/6-31G*	22220000	0.924755
	22202000	–0.270931
	22110101	0.125616
	22020002	–0.141899
	20220020	–0.051633
	11221010	0.058824
	22110101	0.072874
MP2/*6-31G*	22220000	0.898645
	22200002	–0.339899
	22110011	–0.162048
	22020020	–0.121100
	20220200	–0.050492
	11221100	0.062343
	02222000	–0.052071
	22110011	–0.086018
	22000022	0.056695

As can be seen from the Table, the electronic ground state configuration of **146a** is for both geometries dominated by the reference configuration (cf. the discussion in Refs. [373] and [374]). Additionally, the occupation numbers of the CASSCF pseudonatural orbitals were 1.8157 and 1.7181 for the highest occupied molecular orbital in the B3LYP/6-31G* and MP2/6-31G* geometries, respectively. The corresponding occupation numbers for the lowest unoccupied molecular orbital were 0.0176 and 0.0201, respectively. Therefore we argue that the electronic ground state of **146a** is in neither geometry a diradical.

The energy barriers for the dinitrogen extrusion from **145** were calculated for both reaction pathways leading to norcaradiene (**146**) and toluene (**147**) (Scheme 53). The difference in the transition state geometries of **146a** and **147a** is reflected in the energy profile shown in Table 14. Toluene is the thermodynamically favored product (it is more stable than norcaradiene by about 42 kcal mol^{-1}, in good agreement with the 'semi-experimental' value [375] of 38 kcal mol^{-1}). However, the transition state **147a** is approximately 5 kcal mol^{-1} higher in energy than **146a**, making norcaradiene (**146**)

the kinetically favored product. This is in agreement with experimental findings that the thermodynamically more stable arene derivatives produced in the degradation of analogs of **145** are minor side products (see Table 10, Table 11 and Refs. [365,366]). The overall activation energy of the reaction **145** to **146** is estimated to 15—20 kcal mol^{-1}.

Table 14 Energy profile. Values of **145** in atomic units, others in kcal mol^{-1} relative to **145**. The read window in the (rw) calculations contained orbitals 10 through 55.

	145	**146a**	**147a**	**146**+N_2	**147**+N_2
LSDA/3-21G*	-376.77515	21.44	35.45	7.88	-29.84
+ZPE	-376.63907	19.46	31.00	4.92	-32.84
HF/6-31G*	-378.55139	50.37	56.88	-41.11	-83.28
+ZPE	-378.39994	46.44	51.04	-45.49	-88.49
MP2(fc)/6-31G*	-379.76165	14.69	22.67	-36.85	-76.54
MP2(rw)/6-31G*//					
MP2(fc)/6-31G*	-378.80460	18.40	22.60		
MP4(rw)/6-31G*//					
MP2(fc)/6-31G*	-378.85388	17.94	21.45		
B3LYP/6-31G*	-380.89113	22.85	28.35	-26.52	-68.79
+ZPE	-380.84130	18.07	25.51	-26.63	-69.21
B3LYP/6-311+G(2d,2p)//					
B3LYP/6-31G*	-381.09510	21.12	24.13	-31.24	-73.81
+ZPE(B3LYP/6-31G*)	-380.95527	16.35	21.28	-31.35	-74.23

To locate the transition state geometries towards the possible diradical intermediates **148** and **149** (Figure 53), suitable initial guesses for **148** and **149** were optimized on the CAS(2,2)/STO-3G level, followed by series of constraint minimizations, during which the appropriate C–N distance was stepwise reduced from its equilibrium value, until an energy maximum was found. For both **148** and **149**, two conformations were found, which represent minima on the energy surface, with the N(7)—N(8) bond parallel to the C(9)—*endo*-H-C(9) and the C(9)—*exo*-H-C(9) bond, respectively, for **148** and parallel to the C(5)—C(6) bond and the C(6)—H-C(6) bond, respectively, for **149**. Consequently, the constraint minimizations located four saddle points. From these, ordinary transition state searches were performed on the CAS(2,2)/STO-3G level. On the transition state geometries obtained this way, high level *ab initio* calculations were performed to determine the relative energies of these diradicaloid transition states as well as their electronic structure. It was found that the lowest-energy diradicaloid transition state was 9.08 kcal mol^{-1} and 8.62 kcal mol^{-1}

higher in energy than that of **146a** on the CASPT2/6-31G* and the CCSD(T)/6-31G* level, respectively. For this transition state, the CASSCF pseudonatural occupation numbers of the frontier orbitals were 1.5172 (HOMO) and 0.4836 (LUMO). Based on the high energy barrier of the diradicaloid transition states, pathways involving **148** and **149** were neglected for the remainder of the investigation.

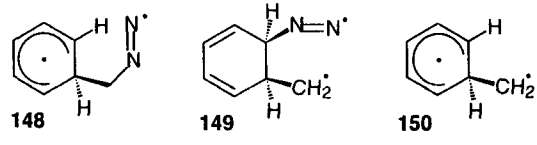

Figure 53. Possible diradical intermediates for the thermal dinitrogen extrusion from **146**.

5.3.1.2 Magnetic Properties

We also calculated the magnetic properties of the investigated species. Table 15 presents the isotropic magnetic susceptibility, $|\bar{\chi}|$ and its anisotropy, $\Delta\chi$, of **145**, both transition states, and both products (Table 15). Most notable is the very large magnetic anisotropy of transition state **146a**, which, in fact, even surpasses that of toluene, indicating a high degree of aromaticity. In comparison, transition state **147a** leading to toluene exhibits a magnetic anisotropy which is roughly half of that of **146a** and considerably weaker than that of toluene.

Table 15. Magnetic susceptibilities in cgs-ppm.

	145	**146a**	**147a**	**146**	**147**
B3LYP/6-31G* (CSGT)					
$\|\bar{\chi}\|$	47.50	70.86	59.87	51.51	53.75
$\Delta\chi$	36.97	89.41	50.35	31.44	66.05
B3LYP/6-311+G(2d,2p)//B3LYP/6-31G* (CSGT)					
$\|\bar{\chi}\|$	58.17	83.50	72.90	63.35	66.30
$\Delta\chi$	32.52	87.90	46.17	25.12	61.88

The calculated ^{1}H NMR chemical shifts confirm this picture. Table 16 presents the ^{1}H NMR chemical shifts of the species in question calculated with different methods and basis sets (note that at least for toluene, for which accurate experimental

values are available, the calculated shifts are in very good agreement with the measurements).

Table 16. ^{1}H NMR chemical shifts in ppm relative to TMS.

	145	**146a**	**147a**	**146**	**147**
B3LYP/6-31G* (CSGT)					
δ(H-C(1))	0.24	-0.99	3.09	0.30	1.26[a]
δ(H-C(2))	3.56	4.40	3.60	0.30	4.49
δ(*exo*-H-C(9))	3.43	5.89	4.56	0.30	1.26[a]
δ(*endo*-H-C(9))	2.39	0.37	5.49	-1.87	1.26[a]
B3LYP/6-311+G(2d,2p)//B3LYP/6-31G* (CSGT)					
δ(H-C(1))	2.26	0.59	6.23	1.97	2.33[a]
δ(H-C(2))	6.14	6.86	6.10	1.97	7.25
δ(*exo*-H-C(9))	5.31	7.76	6.22	1.50	2.33[a]
δ(*endo*-H-C(9))	4.00	1.76	7.26	-0.87	2.33[a]
B3LYP/6-311+G(2d,2p)//B3LYP/6-31G* (GIAO)					
δ(H-C(1))	2.41	0.65	6.32	2.00	2.42[a]
δ(H-C(2))	6.26	6.97	6.24	2.00	7.39
δ(*exo*-H-C(9))	5.45	7.82	6.33	1.61	2.42[a]
δ(*endo*-H-C(9))	4.15	1.92	7.32	-0.79	2.42[a]

[a]arithmetic mean of the chemical shifts of the H-C(1), *exo*-H-C(9), and *endo*-H-C(9) protons.

To evaluate the actual spatial extent of the aromatic system, we calculated maps of the current density tensor corresponding to a magnetic field of 1 au for the transition state **146a**. Figure 54 displays the induced current for a magnetic field perpendicular to the image plane. It also contains the same image for benzene to allow a comparison.

As can be seen, the 'ring current' extends over the entire transition state geometry and is not confined to the cyclohexadiene moiety. For benzene, the shape of the current density distribution as well as the magnitude of the current density is in agreement with earlier studies [376,377].

On the other hand, since the current density is large in regions where the electron density is large, it could be argued that Figure 54 simply maps the electron density. To counter this argument and to remove the arbitrariness in the choice of a particular magnetic field direction, we also mapped the anisotropy of the current density

tensor field. An isosurface of this (scalar) anisotropy field is displayed in Figure 55, again with the analogous map for benzene as comparison.

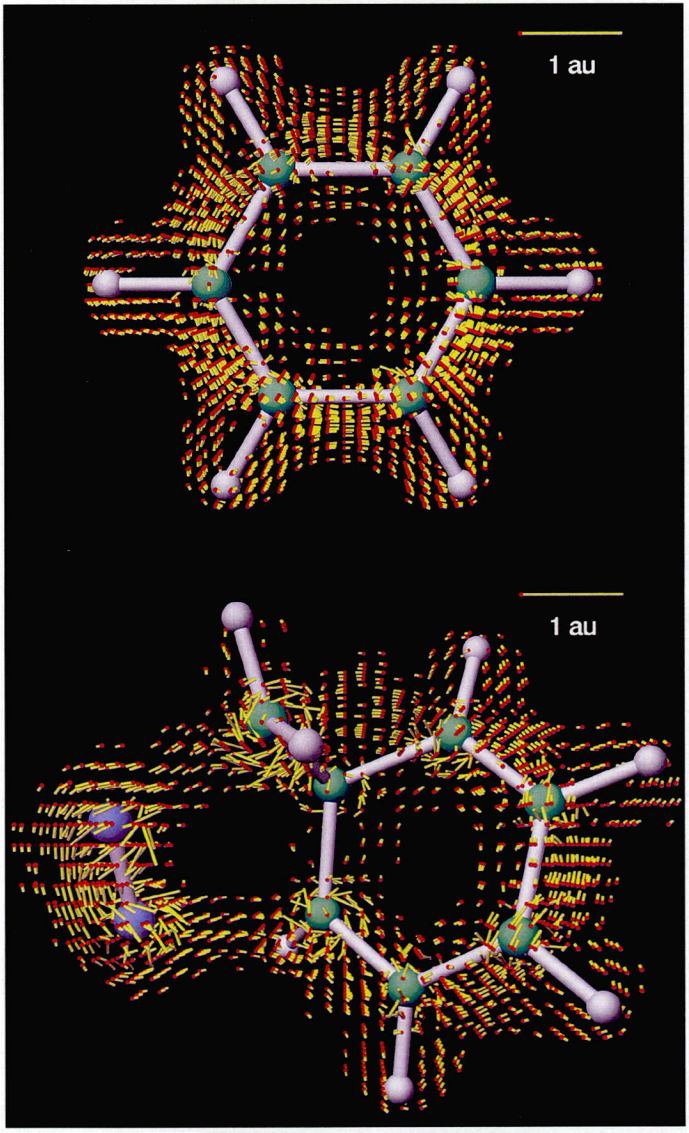

Figure 54. Current density vector field corresponding to a magnetic field of 1 au perpendicular to the image plane of benzene (top) and of **146a** (bottom).

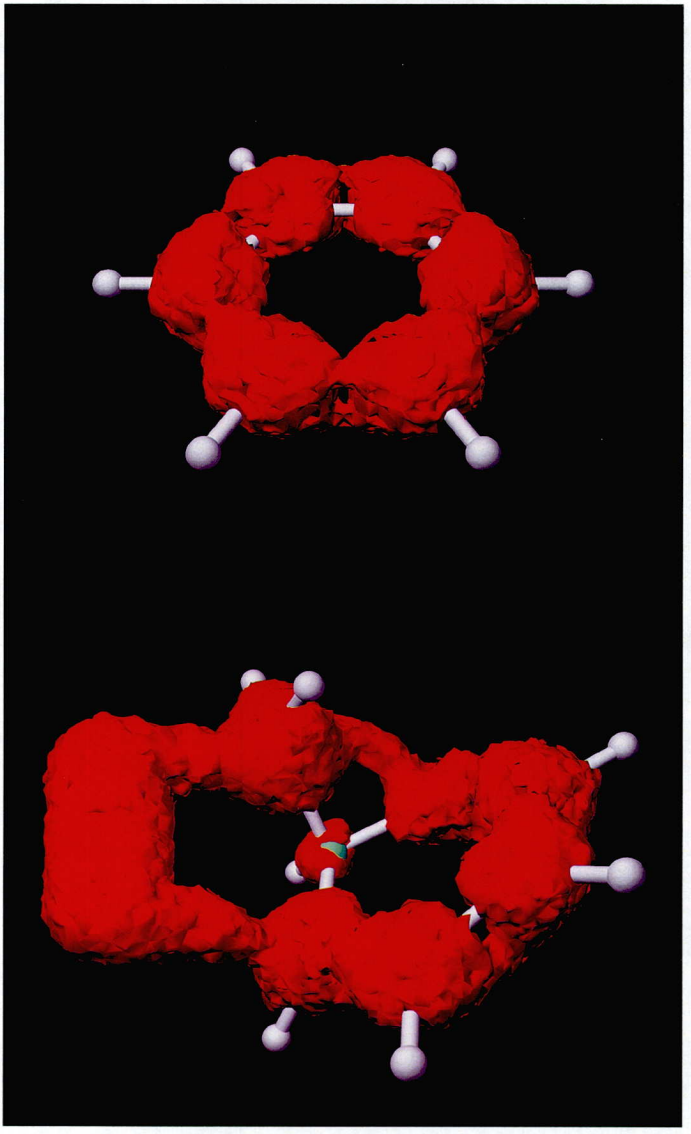

Figure 55. Anisotropy of the current density tensor field corresponding to a magnetic field of 1 au of benzene (top) and of **146a** (bottom). The images display the 0.075 au isosurface.

We also performed calculations along the Intrinsic Reaction Coordinate (IRC), to verify that the obtained transition states really connect the reactant and products of Scheme 53. These calculations were done on the B3LYP/6-31G* level and the results for the **145→146** path are presented below. Figure 56 displays the energy (top) and magnetic susceptibility along (bottom) the **145→146** path.

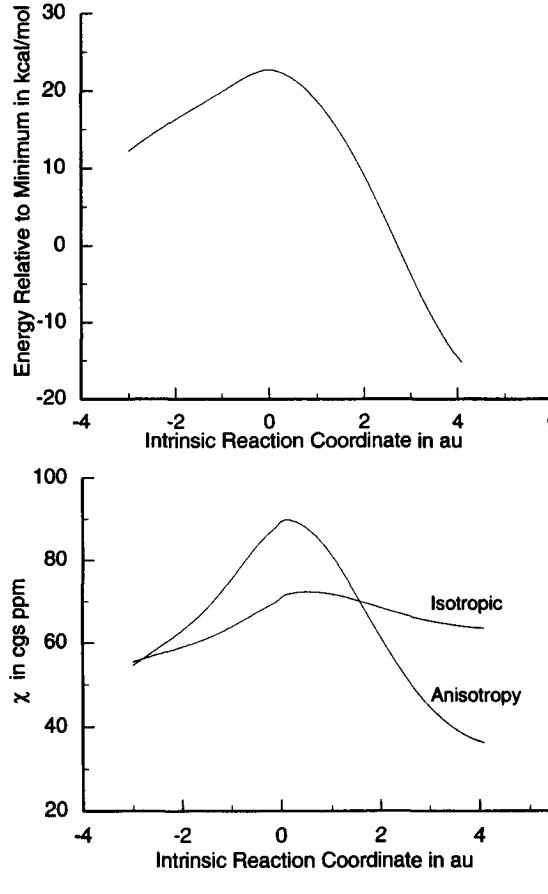

Figure 56. Intrinsic Reaction Coordinate connecting **145** to **146**. B3LYP/6-31G* energy in kcal mol^{-1} (top) and CSGT/B3LYP/6-31G* magnetic susceptibility isotropic part and anisotropy in cgs-ppm along the IRC.

The ^1H NMR chemical shifts along this IRC are shown in Figure 57. While four of the protons whose shifts are displayed in Figure 57, namely H-C(3)—H-C(6), basically remain olefinic during the reaction, the most interesting behavior is displayed

by the C(9)-methylene protons. The *endo*–H-C(9) proton moves in the course of the reaction into a position right above the plane of the cyclohexadiene moiety. The *exo*–H-C(9) on the other hand is rotated away from the ring system (cf. Figure 54). As a consequence, the proton chemical shifts of these two protons in the transition state **146a** differ by a remarkable 6 ppm (cf. Table 16). In norcaradiene (**146**), this difference is reduced to about 1 ppm. The shifts of the two protons connected to the bridgehead carbon atoms H-C(1) and H-C(2) must, for symmetry reasons, become equal, yet their behavior during the reaction differs greatly. Considering the nature and geometry of the transition state, this is hardly a surprise: given that the 'attack' is from C(2) towards C(9), the H-C(1) proton on the other side of the C(1) atom is always below the plane of the aromatic system and therefore is expected to be shielded, whereas the H-C(2) proton should at the transition state exhibit the chemical shift of an ordinary aromatic proton.

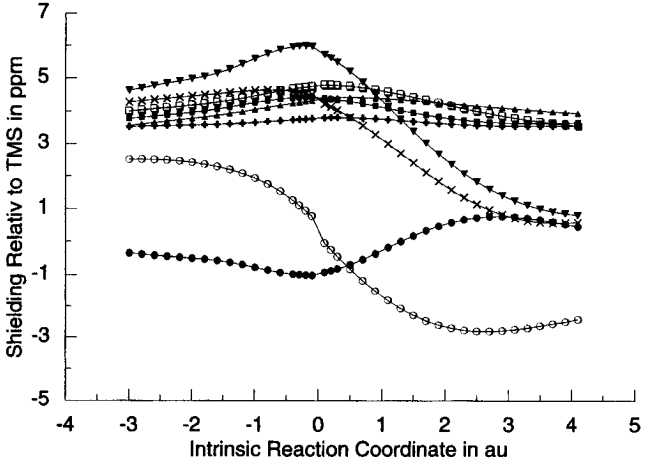

Figure 57. Intrinsic Reaction Coordinate connecting **145** and **146**. ^{1}H NMR CSGT/B3LYP/6-31G* chemical shift in ppm relative to TMS. ●: H-C(1), ×: H-C(2), ▲: H-C(3), ✚: H-C(4), ❑: H-C(5), ■: H-C(6), ▼: *exo*-H-C(9), ○: *endo*-H-C(9).

5.3.1.3 Larger Model System

To investigate model size effects we repeated the transition state search using an enlarged pyracene (1,2,5,6-tetrahydro-cyclopenta<*fg*>-acenaphtylene) model, **152**, which corresponds to the excerpt of the fullerene shown in Scheme 1 and was chosen because it resembles C_{60} more closely in its geometry and rigidity than the smaller system **145**. Figure 9 shows the calculated transition state **151a** on the way from **152** to

the 6-5-open methano-bridged structure **151** (we did not calculate IRC paths, but minimizations starting from a slightly distorted **151a** did neither on the LSDA/3-21G* nor on the B3LYP/6-31G* level converge to norcaradiene-analog 6-5-closed structures but proceeded directly to **151**. Vibrational analysis verified that the geometry in Figure 9 is the first order saddle point of the concerted dinitrogen extrusion. Correspondingly, the calculated transition state geometry differs little from **146a**. The C—N distances in **151a** differ from their counterparts in **146a** by less than 0.1 Å.

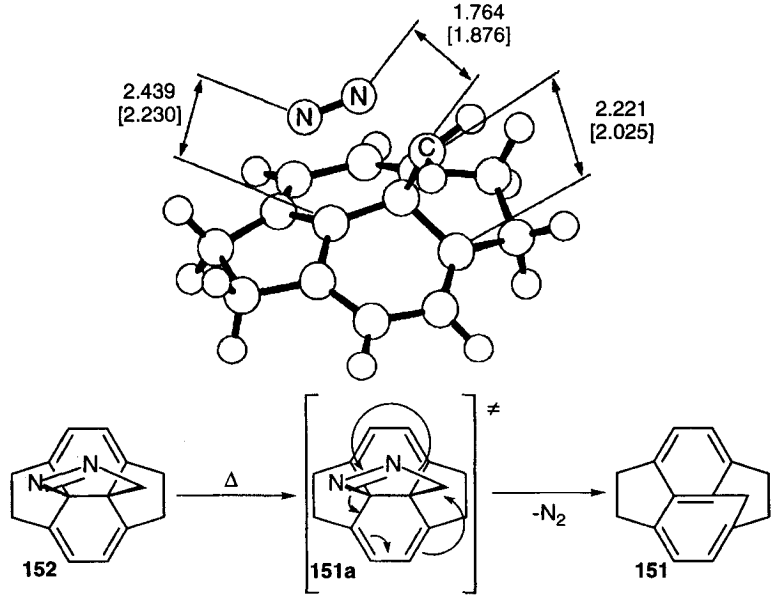

Figure 58. Transition state **151a**, analog to **146a**. B3LYP/6-31G* and LSDA/3-21G* (square brackets) distances in Å.

The computed activation energies for this model system were slightly smaller than those for the reaction **145→146**, namely 17.96 kcal mol^{-1} on the LSDA/3-21G* and 15.17 kcal mol^{-1} on the B3LYP/6-31G* level, respectively (without ZPE). The Zero-Point correction to these values was calculated exclusively on the LSDA/3-21G* level and amounts to −1.68 kcal mol^{-1}. The reason for the smaller activation energy of **152** compared to **145** is not entirely clear. It could be argued that, since the equilibrium geometry of **152** has C_s-symmetry, **152** is more strained than **145**, whose minimum, as pointed out above, has a nonvanishing N(8)—C(9)—C(1)—C(6) dihedral angle. To

investigate this, we performed two series of constrained minimizations on **145**, varying the N(8)—C(9)—C(1)—C(6) dihedral angle in steps of 3° from 33° to 45° on the LSDA/3-21G* level and from 33° to –27° on the B3LYP/6-31G* level, respectively. On the LSDA/3-21G* level the global minimum, at a N(8)—C(9)—C(1)—C(6) dihedral angle of –28.3°, is 1.96 kcal mol^{-1} lower in energy than the corresponding constrained minimum with vanishing N(8)—C(9)—C(1)—C(6) dihedral angle. On the other hand, on the B3LYP/6-31G* level, this stabilization amounts only to 0.28 kcal mol^{-1}. Despite the difference in activation energies, **146a** and **151a** show very similar transition state geometries. Therefore we conclude that the dinitrogen extrusion from **145** and **152** proceeds *via* the same reaction mechanism.

5.3.2 Conclusions

The calculations show that the dinitrogen extrusion from 7,8-diaza-bicyclo[4.3.0]nona-2,4,7-triene (**145**) to form bicyclo[4.1.0]hepta-2,4-diene (norcaradiene, **146**) proceeds *via* the aromatic transition state **146a** rather than a diradical intermediate. The reaction towards norcaradiene is the kinetically favored one (as compared to the reaction towards the thermodynamically more stable product toluene). These findings are in good agreement with the experimental data, reproducing both the energetical aspects of the reaction as well as the experimentally determined product distribution and fully support the proposed eight electron $[2\pi_s + 2\pi_s + 2\sigma_a + 2\sigma_s]$ *Woodward-Hoffmann* allowed mechanism, despite the high asynchronicity of the reaction indicated by the transition state geometry **146a**.

Further calculations on a larger, more rigid system indicated that these results are transferable to the mechanism of the dinitrogen extrusion from **152** *via* transition state **151a**.

Considering the fact that experimental results on the model system were essentially identical to those reported for the fullerene-pyrazoline adducts such as **95a**, we think that it is safe to assume that the same mechanism is responsible for the high regioselectivity observed in the dinitrogen extrusion from **95a** (cf. Scheme 51), leading to the 6-5-open homofullerene **96a**, and also for as well as for the parent fullerene pyrazoline $C_{61}H_2N_2$ **27** (see Scheme 10, Section 2.3.3) as well as for the general case of the dinitrogen extrusion from substituted pyrazoline-fullerene adducts **30** (Scheme 11 Table 3, Section 2.3.3). There, however, sterical effects and the influence of the substituents on the electronic structure of the pyrazoline moiety are assumed to play an important role. These effects, not investigated in the present work, are likely to be

responsible for the observed diastereoselectivity in the thermal decomposition of unsymmetrically substituted pyrazoline-fullerene adducts (see Table 3, Section 2.3.3).

Finally, we note that the presented mechanism may well also apply to the thermal dinitrogen extrusion from azide adducts to C_{60}, generating 6-5-open azahomofullerenes, which represents the only other general reaction currently providing access to 6-5-open bridged fullerene derivatives (see Scheme 14, Section 2.3.3).

6. Experimental Part

6.1 Instrumentation

Column chromatography (CC): silica gel 60 (70 - 270 mesh, 0.05 - 0.2 mm) from *Macherey-Nagel*; silica gel 60 (70 - 230 mesh, 0.063 - 0.2 mm) from *Merck*; silica gel 60 (230 - 400 mesh, 0.04 - 0.063 mm) from *Macherey-Nagel*; silica gel 60 (230 - 400 mesh, 0.04 - 0.063 mm) from *Fluka*. CC with a head pressure of ≈ 0.3 bar. Silica gel *H* (5 - 40 μm) from *Fluka*, with a head pressure of ≈ 0.5 bar [378].

Thin layer chromatography (TLC): *Polygram SIL G/UV$_{254}$* from *Macherey-Nagel* and glass backed SiO_2-*60* F_{254} from *Merck*, visualization by UV-light (254 or 366 nm).

High performance liquid chromatography (HPLC). For kinetic measurements: Column: *250/8/4 Nucleosil 100-7* from *Macherey-Nagel*. Instrumentation: *Knauer* HPLC pump *64* (anal.); *Knauer* UV-detector *A0293* ; Wavelength fixed at λ = 310 nm; flow rate fixed at 2 ml min^{-1}.

Melting points: *Büchi* 510 apparatus. All melting points were measured in open capillaries and are uncorrected.

IR spectra: *Perkin-Elmer-FT1600* spectrometer. The spectra were measured as KBr pellets, as solutions in $CHCl_3$ or CCl_4, or as thin films of neat compound. The absorptions are given in wavenumbers (cm^{-1}). The intensity of the bands is described as *s* (strong), *m* (medium), or *w* (weak).

UV/VIS spectra: *Varian-CARY-5* spectrophotometer. All spectra were measured as solutions in the indicated solvents. Absorption maxima (λ_{max}) are reported in nm and extinction coefficients (ε) in M^{-1} cm^{-1}. Shoulders are indicated (sh).

NMR spectra: ^{1}H and ^{13}C NMR spectra: *Bruker AMX-500, Bruker AMX-400, Varian GEMINI-200* and *-300* spectrometers. All spectra were measured at 293 K in the indicated solvents. For ^{1}H- and ^{13}C-NMR spectra the chemical shift values are given in ppm relative to the solvent resonances ($CHCl_3$ at 7.26 (^{1}H) and 77.0 (^{13}C),

$CHCl_2CDCl_2$ at 5.91 (^1H) and 74.2 (^{13}C) ppm). The resonance multiplicity is described as *s* (singlet), *d* (doublet), *t* (triplet), *q* (quartet), and *m* (multiplet). Broad resonances are indicated (br.). Coupling constants *J* are given in Hz.

Mass spectra: FAB mass spectra were performed by the MS service at the ETH Zürich. FAB-MS (*m/z* (%)): *VG-ZAB2-SEQ* spectrometer; spectra were determined in *m*-nitrobenzyl alcohol (3-NOBA) as the matrix. For FAB mass spectra of all fullerene derivatives, the experimentally observed highest peak in the molecular ion cluster is reported followed in parenthesis by the isotopic molecular formula corresponding to the calculated most intense peak in the cluster.

Photolysis experiments: Tap water cooled *Pyrex* photochemical reactor, with a 250 W medium-pressure mercury lamp.

6.2 Materials and General Techniques

Reagents and solvents were reagent-grade and were used without further purification. THF and Et_2O were distilled from Na/benzophenone, PhMe from Na immediately before use, CH_2Cl_2 from CaH_2. Anh. PhCl was dried over molecular sieves (4 Å) for several days before use. HPLC solvents were purchased from *Biosolve*. Molecular sieves (4 Å) were activated by heating in a drying pistol to 300 °C for 6 h and stored in a dessicator over NaOH. All reactions were performed in standard glassware under an atmosphere of N_2 or Ar. Reactions involving the multiply functionalized fullerenes were conducted under strict exclusion of light and air. Degassing of solvents was performed by repetitive freeze-pump-thaw cycles or by purging with Ar before use. Evaporation and concentration was done at water-aspirator pressure, and isolated solid products were dried at 10^{-1} or 10^{-7} Torr. CC was performed using distilled technical grade solvents.

Fullerene soot extract and crude fullerene-enriched soot were purchased from *MER Corporation*, Tuscon, Arizona (AZ) 85706, USA. C_{60} was purified according to literature procedure [29,233].

6.3 Nomenclature

All fullerene derivatives were named by the CAS recommendations or generated according to the CAS recommendations for nomenclature [379]. The AUTONOM (*Beilstein* © 1991) program was used for naming the other compounds.

6.4 General Procedures for Kinetic Measurements (Sections 3.4 and 5.2)

Addition of CH_2N_2 to **90a**: To a vigorously stirred solution of **90a** (5.0 mg, 0.00338 mmol) in CH_2Cl_2 (10 ml) at 0 °C was added an etheral solution of CH_2N_2 (0.5 ml, *ca.* 0.76 M, *ca.* 0.38 mmol). Every 15 min, 20 µl of the mixture was analyzed by HPLC (CH_2Cl_2/AcOEt 99:1, 2 ml min^{-1}, retention times: **90a** 3.3 min, **95a** 6.0 min). After 96 min, no more **90a** was detected by HPLC.

Addition of CH_2N_2 to **47**: To a vigorously stirred solution of **47** (5.1 mg, 0.00338 mmol) in CH_2Cl_2 (10 ml) at 0 °C was added an etheral solution of CH_2N_2 (0.5 ml, *ca.* 0.76 M, *ca.* 0.38 mmol). Every 8 min, 20 µl of the mixture was analyzed by HPLC (CH_2Cl_2/AcOEt 98:2, 2 ml min^{-1}, retention times: **47**: 2.7 min, **115**: 5.5 min). After 22 min, no more **47** was detected by HPLC.

Thermal dinitrogen extrusion from **95a**: Vigorously stirred solutions of **95a** (5.6 mg,) in CCl_4 (10 ml) were heated to 40, 50, 60, 67, and 75 °C. Every 5–10 min, 20 µl of the mixture were analyzed by HPLC (CH_2Cl_2/AcOEt 99:1, 2 ml min^{-1}, retention times: **96a** 3.0 min, **95a** 6.0 min). In an independent experiment, the times it took for the solution to reach the indicated temperatures were determined. Only product distributions from that point on where included in determining the *Arrhenius* parameters. At the detection wavelength (310 nm) a correction factor has to be introduced to account for the difference of the extinction coefficients of the respective adducts: ε (**96a**) = 0.9653 ε (**96a**).

6.5 Experimental Details

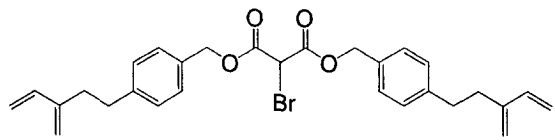

Methyl 4-(3-Methylidenpent-4-enyl)benzyl 2-Bromopropanedioate **(86)** [348]:

To a soln. of **87** ([348]) (2.000g, 4.499 mmol) in THF (90 ml), was added DBU (0.822 g, 5.399 mmol) at RT. After 5 min, the mixure was cooled to –78 °C, and, after 5 min at –78 °C, a soln. of CBr_4 (1.791 g, 5.399 mmol) in THF (25 ml) was added. The yellow mixture was quenched after 1.25 h with 0.1 M HCl, diluted with Et_2O (50 ml), washed with 0.1 M HCl, sat. aq. NaCl, and dried ($MgSO_4$). After evaporation, CC (SiO_2, CH_2Cl_2/hexane 1:1) provided **86** (1.52 g, 2.904 mmol) as a colorless oil in 65% yield.

TLC (SiO_2, CH_2Cl_2/hexane 1:1) R_f 0.45. IR (neat): 3087*w*, 2939*m*, 1763*s*, 1744*s*, 1594*m*, 1515*w*, 1459*w*, 1421*w*, 1374*w*, 1281*m*, 1231*m*, 1142*m*, 992*m*, 899*m*, 814*m*. ^{1}H-NMR (200 MHz, $CDCl_3$): 7.29 (*d*, *J* = 7.3, 4 H); 7.24 (*d*, *J* = 7.3, 4 H); 6.45 (*dd*, *J* = 17.4, 10.8, 2 H); 5.35-5.00 (*m*, 8 H); 5.23 (*s*, 4 H); 4.94 (*s*, 1 H); 2.90-2.80 (*m*, 4 H); 2.60-2.50 (*m*, 4 H). ^{13}C-NMR (50 MHz, $CDCl_3$): 162.1; 143.2; 140.6; 136.4; 129.8; 126.4; 126.2; 113.9; 111.0; 66.3; 39.9; 31.8; 30.7.

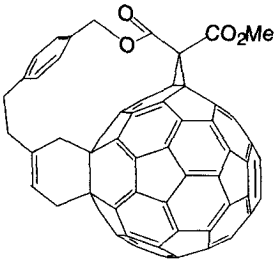

Methyl 3',6-Dihydro-17'-oxo-5',3''-(ethano[1,4]benzenomethanoxymethano)-3''H-benzo[1,9]cyclopropa-[16,17][5,6]fullerene-C_{60}-I_h-3''-carboxylate **82b** [348].

To a soln. of C_{60} (133 mg, 0.184 mmol) and **83** (40 mg, 0.110 mmol) in PhMe (100 ml) was added DBU (16 mg, 0.110 mmol) in PhMe (1 ml) by syringe. After 1 h, the mixture was concentrated to 30 ml and diluted with hexane (30 ml). The resulting soln. was chromatographed (SiO_2, PhMe/hexane 1:1 then 2:1) to give a wine-red soln. of the methanofullerene mono-adduct. After evaporation of hexane, the remaining soln. was diluted with PhMe (to 200 ml), deoxygenated by purging with Ar for 10 min, and heated at reflux for 36 h. Concentration and CC (SiO_2, PhMe) evaporation and re-dissolution in a minimum amount of CS_2, followed by precipitation with pentane, afforded **82b** (23 mg, 0.023 mmol) in 21% yield as a dark brown powder.

TLC (SiO_2, PhMe) R_f 0.70. M.p. : >270 °C. ^{1}H-NMR (200 MHz, $CDCl_3$): 7.30 - 7.10 (br. *m*, 4 H); 6.55 (*t*, *J* = 5.5, 1 H); 5.40 - 5.10 (br. *s*, 2 H); 4.03 (*s*, 3 H); 3.72 (*d*, *J* = 5.5, 2 H); 3.48 (br. *s*, 2 H); 3.11 (br. *s*, 4 H).

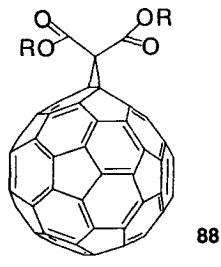

88

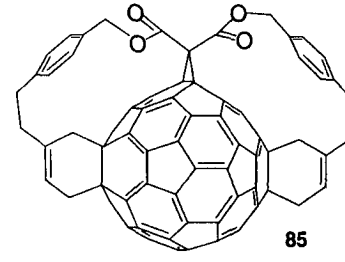

85

R =

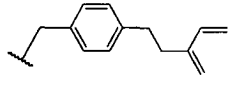

Bis[4-(3-methylidenepent-4-enyl)phenyl]methyl 3 'H-cyclopropa[1,9][5,6]fullerene-C_{60}-I_h-3',3'-dicarboxylate **(88) and** ***3',3'',6',6''-Tetrahydro-5',3''':5'',3'''-bis(ethano[1,4]benzenomethanoxymethano)-3'''H-dibenzo-[1,9:52,60]-cyclopropa[16,17][5,6]fullerene-C_{60}-I_h-17',17''-dione*** **(85)** [348]:

To a degassed soln. of C_{60} (3.097 g, 4.298 mmol) and **86** (1.500 g, 2.866 mmol) in PhMe (1300 ml), DBU (0.480 g, 3.152 mmol) in PhMe (10 ml) was added over 5 min. After 16 h, the mixture was concentrated to 700 ml, diluted with hexane (700 ml), and chromatographed (SiO_2, PhMe/hexane 1:1 then PhMe) yielding a wine red soln. of **88** (TLC, SiO_2, PhMe/hexane 1:1; R_f 0.34). After evaporation of hexane, PhMe was added to give a total volume of 3.5 l, then the soln. was deoxygenated by purging with Ar for 20 min and heated to reflux for 30 h. Concentration and CC (SiO_2, PhMe), evaporation and re-dissolution in a minimum amount of CS_2, followed by precipitation with pentane, afforded **85** (1.750 g, 1.519 mmol) in 53% as a dark brown powder.

TLC (SiO_2, PhMe) R_f 0.45. M.p. : >270 °C. ^{1}H-NMR (200 MHz, $CDCl_3$): 7.22 (br. *s*, 8 H); 6.60 (*t*, *J* = 5.4, 2 H); 5.28 (*s*, 4 H); 3.89 (*d*, *J* = 5.4, 4 H); 3.54 (*s*, 4 H); 3.16 (*s*, 8 H). FAB-MS: 1162.3 (24, M^+; calc. for $^{12}C_{89}H_{30}O_4$: 1162.2), 719.9 (32, C_{60}^+).

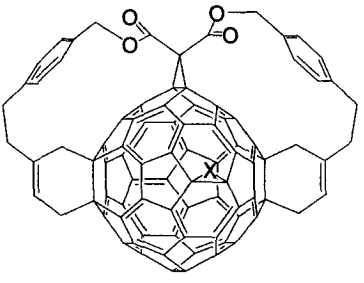

X = $C(CO_2Et)_2$

Diethyl 3',3'',6',6''-tetrahydro-17',17''-dioxo-5',3''':5'',3'''-bis(ethano[1,4]benzenomethanoxymethano)-3'''H,3''''H-dibenzo-[[1,9:52,60]-bis(cyclopropa)[16,17:21,40][5,6]fullerene-C_{60}-I_h-3''',3''''-dicarboxylate (**89a**) [348]:

To a degassed suspension of **85** (1016 mg, 0.873 mmol) and diethyl 2-bromopropanedioate (1043 mg, 4.364 mmol) in dry PhCl (550 ml), DBU (664 mg, 4.364 mmol) in PhCl (10 ml) was added. After 1.75 h, the reaction was quenched with 0.1 M HCl and the mixture was washed with 0.1 M HCl, H_2O and sat. aq. NaCl soln. and dried ($MgSO_4$). CC (SiO_2, CH_2Cl_2) evaporation, and re-dissolution in a minimum amount of CH_2Cl_2, followed by precipitation with hexane, afforded 20% unreacted **85** (205 mg, 0.175 mmol), and 54% of **89a** (626 mg, 0.471 mmol) as a bright red solid.

TLC (SiO_2, CH_2Cl_2) R_f 0.75. M.p. : 250–270 °C (decomp.). IR (KBr): 3053*w*, 1741*s*, 1602*m*, 1558*w*, 1540*w*, 1507*w*, 1457*w*, 1370*m*, 1303*m*, 1248*m*, 1145*m*, 1029*m*, 931*w*, 908*w*. ^{1}H-NMR (200MHz, $CDCl_3$): 7.22 (br. *s*, 4 H); 7.14 (br. *s*, 4 H); 6.42 (*t*, *J* = 5.3, 2 H); 5.21 (br. *s*, 4 H); 4.40-4.25 (*m*, 4 H); 3.70-3.50 (*m*, 4 H); 3.31 (*d*, *J* = 14.1, 2 H); 3.19 (*d*, *J* = 14.1, 2 H); 3.08 (*s*, 8 H); 1.40-1.20 (*m*, 6 H). FAB-MS: 1321.5 (44, [M^++H]), 1320.4 (36, M^+ ; calc. for $^{12}C_{96}H_{40}O_8$: 1320.3), 720.1 (100, C_{60}^+).

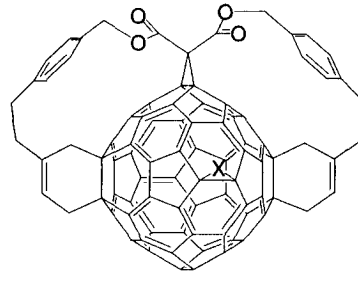

X = $C(CO_2CH_2CO_2Et)_2$

Bis(2-ethoxy-2-oxoethyl) 3',3'',6',6''-Tetrahydro-17',17''-dioxo-5',3''':5'',3'''-bis(ethano[1,4]benzenomethanoxymethano)-3'''H,3''''H-dibenzo-[1,9:52,60]-bis(cyclopropa)[16,17:21,40][5,6]fullerene-C_{60}-I_h-3''',3''''-dicarboxylate **(89b)** [348]:

To a degassed suspension of **85** (385 mg, 0.331 mmol) in PhCl (290 ml) was added bis(2-ethoxy-2-oxoethyl) 2-bromopropanedioate (880 mg, 2.482 mmol) and DBU (380 mg, 2.482 mmol) in PhCl (1 ml). After 2 h, the reaction was quenched with 0.1 M HCl and the mixture was washed with 0.1 M HCl, H_2O and sat. aq. NaCl soln. and dried ($MgSO_4$). CC (SiO_2-*H*, CH_2Cl_2) evaporation, and re-dissolution in a minimum amount of CH_2Cl_2, followed by precipitation with hexane, afforded 16% unreacted **85** (61 mg, 0.052 mmol), and 69% of the title compound **89b** (328 mg, 0.228 mmol) as a bright red solid.

TLC (SiO_2, CH_2Cl_2) R_f 0.48. M.p. : 225–235 °C (decomp.). ^{1}H-NMR (200 MHz, $CDCl_3$): 7.19 (*s*, 4 H); 7.13 (*s*, 4 H); 6.40 (*t*, *J* = 5.4, 2 H); 5.18 (br. *m*, 4 H); 4.76 (*s*, 2 H); 4.73 (*s*, 2 H); 4.22 (*q*, *J* = 7.1, 3 H); 4.19 (*q*, *J* = 7.1, 3 H); 3.64 (*dd*, *J* = 5.4, 14.4, 4 H); 3.55 (*dd*, *J* = 5.4, 14.4, 4 H); 3.28 (*d*, *J* = 14.2, 2 H); 3.18 (*d*, *J* = 14.2, 2 H); 3.05 (br. *s*, 8 H); 1.35 - 1.15 (*m*, 6 H).

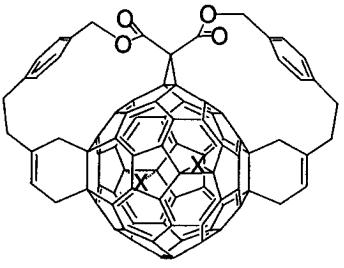

X = $C(CO_2Et)_2$

Tetraethyl 3',3'',6',6''-Tetrahydro-17',17''-dioxo-5',3''':5'',3'''-bis(ethano[1,4]benzenomethanoxymethano)-3'''H,3''''H,3'''''H-dibenzo-[1,9:52,60]-tris(cyclopropa)[16,17:21,40:30,31][5,6]fullerene-C_{60}-Ih-3'''',3''''',3''''',3'''''''-tetracarboxylate **90a**:

To a soln. of **85** (764 mg, 0.578 mmol) in PhCl (50 ml) was added at 0 °C diethyl 2-bromopropanedioate (1.04 g, 4.34 mmol) and DBU (0.660 g, 4.337 mmol). The resulting mixture was stirred for 90 min, then washed with sat. aq. NH_4Cl and sat. aq. NaCl solution, and dried ($MgSO_4$). Evaporation and re-dissolution of the red viscous residue in a minimum amount of CH_2Cl_2, followed by precipitation with pentane, afforded an orange powder which was chromatographed (SiO_2-*H*, CH_2Cl_2/hexane: 9:1) to yield the hexakis-adduct **92a** (412 mg, 0.252 mmol, 44%) and **90a** (280 mg, 0.189 mmol, 33%) as well as mixed fractions containing **90a** and **91a**.

TLC (SiO_2, CH_2Cl_2): R_f 0.25. M.p. : 235–245 °C (decomp.). UV/VIS (λ_{max} (ε) in CH_2Cl_2): 526 (1960), 492 (1970), 387 (sh, 7020), 356 (sh, 17100), 285 (59900). IR (KBr): 2978*w*, 2922*w*, 2833*w*, 1747*s*, 1444*m*, 1367*m*, 1290*m*, 1250*s*, 1206*s*, 1077*m*, 1063*m*, 1031*m*, 1011*m*, 854*w*, 753*m*, 707*m*, 661*w*, 590*w*, 538*m*, 528*m*. ^{1}H-NMR (400 MHz, $CDCl_3$): 7.07 (br. *s*, 8 H); 6.27 (*t*, *J* = 5.3, 2 H); 5.11 (br. *s*, 4 H); 4.36 (*q*, *J* = 7.1, 4 H); 4.33 (*q*, *J* = 7.1, 4 H); 3.42 (*d*, *J* = 5.3, 4 H); 3.05-2.90 (*m*, 12 H); 1.34 (*t*, *J* = 7.1, 6 H); 1.33 (*t*, *J* = 7.1, 6 H). ^{13}C-NMR (100 MHz, $CDCl_3$): 163.89, 163.64, 162.39, 157.96, 153.47, 147.56, 145.90, 145.68, 145.37, 145.24, 143.34, 142.50, 142.43, 141.95 (br.), 141.78, 141.57, 141.48, 138.29, 131.80, 130.20 (br.), 128.19 (br.), 125.30, 70.99, 68.47, 66.73, 62.78, 62.67, 62.36, 61.90, 53.61, 45.47, 42.43, 38.98, 34.89, 34.27, 14.16. FAB-MS: 1528.3 (12, [*M* + 2 O]$^+$), 1512.0 (49, [*M* + O]$^+$), 1480.6 (100, [*M* + H]$^+$), 1479.6 (82, *M*$^+$; calc. for $^{13}C^{12}C_{102}H_{50}O_{12}$: 1479.3), 720.2 (5, C_{60}^+).

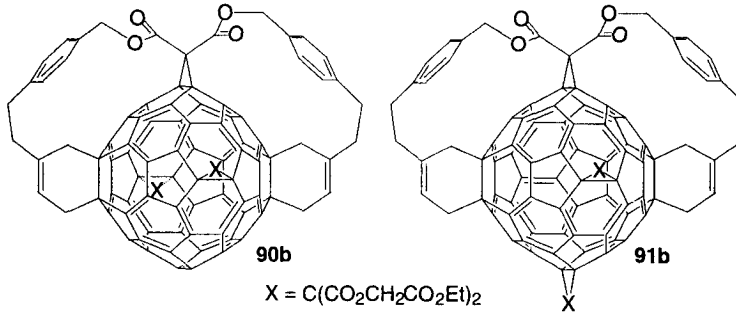

Tetrakis(2-ethoxy-2-oxoethyl) 3',3'',6',6''-tetrahydro-17',17''-dioxo-5',3''':5'',3''''-bis(ethano[1,4]benzenomethanoxymethano)-3'''H,3''''H,3'''''H-dibenzo-[1,9:52,60]-tris(cyclopropa)[16,17:21,40:30,31][5,6]fullerene-C_{60}-I_h-3''''',3''''',3''''''',3'''''''-tetracarboxylate **(90b)** **and** ***Tetrakis(2-ethoxy-2-oxoethyl) 3',3'',6',6''-tetrahydro-17',17''-dioxo-5',3''':5'',3''''-bis(ethano[1,4]benzenomethanoxymethano)-3'''H,3''''H,3'''''H-dibenzo-[1,9:52,60]-tris(cyclopropa)[16,17:21,40:44,45][5,6]fullerene-C_{60}-I_h-3''''',3''''',3''''''',3'''''''-tetracarboxylate*** **(91b)** [348]:

To a soln. of **89b** (89.9 mg, 0.063 mmol) in PhCl (0.5 ml) was added DBU (9.5 mg, 0.063 mmol) and bis(2-ethoxy-2-oxoethyl) 2-bromopropanedioate (22.2 mg, 0.063 mmol), each in PhCl (0.1 ml). The resulting soln. was stirred for 22 h at RT and then chromatographed (SiO_2-*H*, CH_2Cl_2/EtOAc 100:1.5) to elute first unreacted **89b** (28.1 mg) followed by **90b** and **91b**. Trace quantities of a third compound running slightly faster than **90b** were removed. The product fractions were diluted with cyclohexane and concentrated giving **90b** (30.0 mg, 28%) and **91b** (12.3 mg, 11%).

90b: TLC (CH_2Cl_2) R_f 0.18. M.p. : 195–205 °C (decomp.). ^{1}H-NMR (300 MHz, $CDCl_3$): 7.12 (*s*, 8 H); 6.30 (*t*, *J* = 5.1, 2 H); 5.13 (br.*s*, 4 H); 4.84 (*s*, 2 H); 4.80 (*s*, 2 H); 4.30 - 4.10 (*m*, 4 H); 3.44 (*d*, *J* = 5.1, 4 H); 3.07 (*s*, 4 H); 3.10 - 2.90 (br. *m*, 8 H); 1.28 (*t*, *J* = 7.2, 6 H); 1.25 (*t*, *J* = 7.1, 6 H).

91b: TLC (CH_2Cl_2) R_f 0.13. M.p. : 195–205 °C (decomp.). ^{1}H-NMR (300 MHz, $CDCl_3$): 7.30 - 7.10 (br. *m*, 8 H); 6.27 (*t*, *J* = 5.1, 2 H); 5.40 - 5.20 (br. *m*, 4 H); 4.75 (*s*, 4 H); 4.71 (*s*, 2 H); 4.66 (*s*, 2 H); 4.30 - 4.10 (*m*, 8 H); 3.45 (*dd*, *J* = 5.1, 14.0, 2 H); 3.34 (*dd*, *J* = 5.1, 14.0, 2 H); 3.22 (*d*, *J* = 14.2, 4 H); 3.12 (*d*, *J* = 14.2, 2 H); 3.10 - 2.90 (br. *m*, 8 H); 1.30 - 1.15 (*m*, 12 H).

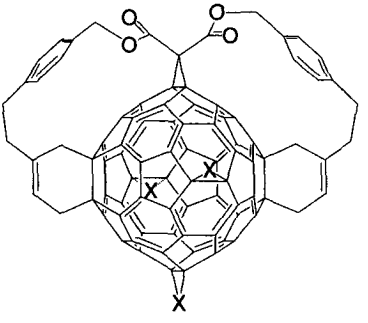

X = $C(CO_2Et)_2$

Hexaethyl 3',3'',6',6''-Tetrahydro-17',17''-dioxo-5',3''':5'',3'''-bis(ethano[1,4]benzenomethanoxymethano)-3'''H,3''''H,3'''''H,3''''''H-dibenzo-[1,9:52,60]-tetrakis(cyclopropa)[16,17:21,40:30,31,44,45][5,6]fullerene-C_{60}-I_h-3'''',3''''',3''''',3'''''3''''''',3''''''-hexaacarboxylate (**92a**) [348]:

To a soln.of **85** (22 mg, 0.019 mmol) in PhCl (0.5 ml), diethyl 2-bromopropanedioate (45 mg, 0.188 mmol) in PhCl (0.5 ml) and DBU (28 mg, 0.188 mmol) in PhCl (0.5 ml) were added. After 3 h, the mixture was directly chromatographed (SiO_2, CH_2Cl_2); the bright yellow product fraction was diluted with cyclohexane, and concentration afforded a precipitate which was dried to give **92a** (26 mg, 0.013 mmol) as a bright yellow powder in 70 % yield.

TLC (CH_2Cl_2) R_f 0.41. ^{1}H-NMR (300 MHz, $CDCl_3$): 7.25 - 7.05 (br. *m*, 8 H); 6.16 (*t*, *J* = 5.5, 2 H); 5.22 (*s*, 4 H), 4.34 (*q*, *J* = 7.1, 4 H); 4.28 (*q*, *J* = 7.1, 4 H); 4.24 (*q*, *J* = 7.1, 4 H); 3.21 (*d*, *J* = 5.5, 4 H); 3.05 - 2.85 (*m*, 8 H); 1.35 (*t*, *J* = 7.1, 6 H); 1.29 (*t*, *J* = 7.1, 6 H); 1.26 (*t*, *J* = 7.1, 6 H).

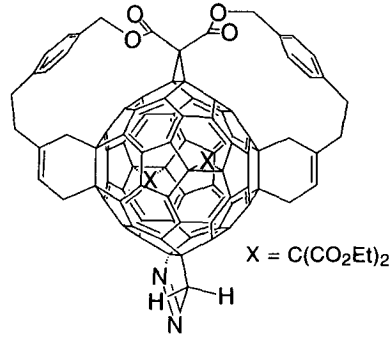

Tetraethyl 3',3'',6',6''-tetrahydro-17',17''-dioxo-5',3''':5'',3'''-bis(ethano[1,4]benzenomethanoxymethano)-3'''H,3''''H,3'''''H-3''''''H-dibenzo[21,40:30,31]tris(cyclopropa)[1,9:16,17:44,45] [5,6]fullereno-C_{60}-I_h-[52,60-d]pyrazole-3'''',3'''',3''''',3''''''-tetracarboxylate **95a**:

To a soln. of **90a** (30 mg, 0.020 mmol) in $CHCl_3$ (5 ml) was added under Ar at 0 °C diazomethane (2 ml; conc. ≤ 0.64M in Et_2O, *ca.* 60 eq.). After 90 min, the color of the soln. had changed from orange to bright yellow. Subsequent evaporation at RT, CC (SiO_2-*H*, CH_2Cl_2), and re-dissolution in a minimum amount of CH_2Cl_2, followed by precipitation with pentane, afforded the pyrazoline **95b** as a yellow powder in 71% yield (22 mg, 0.015 mmol).

TLC (SiO_2, CH_2Cl_2): R_f 0.20. M.p. 80–90 °C (decomp.). UV/VIS (λ_{max} (ε) in CH_2Cl_2): 349 (sh, 19700), 305 (52000), 262 (44300). IR (KBr): 2978*w*, 2924*w*, 2833*w*, 1745*s*, 1615*w*, 1569*w*, 1513*w*, 1447*m*, 1367*m*, 1292*m*, 1251*s*, 1217*s*, 1095*m*, 1066*m*, 1022*m*, 967*w*, 903*w*, 852*w*, 789*m*, 764*m*, 753*m*, 708*m*, 667*w*, 588*w*, 531*m*. ^{1}H-NMR (200 MHz, $CDCl_3$): 7.30-7.05 (*m*, 8 H); 6.12 (*t*, *J* = 5.3, 2 H); 5.73 (*s*, 2 H); 5.28 (*s*, 4 H); 4.45-4.20 (*m*, 8 H); 3.15-2.80 (*m*, 16 H); 1.40-1.20 (*m*, 12 H). ^{13}C-NMR (50 MHz, $CDCl_3$): 164.21; 163.98; 163.90; 163.38; 156.67; 156.37; 155.04; 153.79; 150.15; 147.72; 146.32; 145.82; 145.40; 145.35; 145.04; 144.65; 143.63; 143.50; 143.37; 142.79; 142.74; 141.77; 140.99; 140.77; 140.70; 138.55; 137.84; 131.98; 130.58; 130.53; 128.54; 125.11; 113.93; 92.02; 70.73; 69.73; 69.50; 68.84; 62.92; 62.79; 62.76; 62.06; 61.48; 57.95; 45.77; 42.26; 39.15; 34.93; 34.24; 14.21; 14.11; 14.05. FAB-MS: 1521.5 (17, M^+; calc. for $^{13}C^{12}C_{103}H_{52}O_{12}N_2$: 1521.5), 1493.6 (100, [M - N_2]$^+$), 1479.5 (14, [M - CH_2N_2]$^+$), 720.1 (13, C_{60}^+).

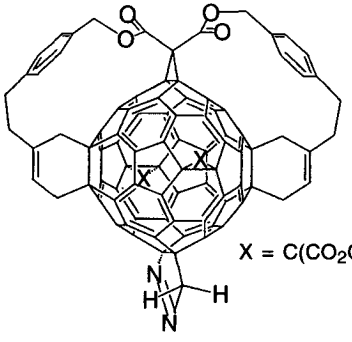

***Tetrakis(2-ethoxy-2-oxoethyl) 3',3'',6',6''-tetrahydro-17',17''-dioxo-5',3''':5'',3'''-bis(ethano[1,4]benzenomethanoxymethano)-3'''H,3''''H,3'''''H-3''''''H-dibenzo[21,40:30,31]tris(cyclopropa)[1,9:16,17:44,45] [5,6]fullereno-C_{60}-I_h-[52,60-d]pyrazole-3'''',3''''',3''''''-tetracarboxylate* 95b**:

To a soln. of **90b** (98 mg, 0.057 mmol) in $CHCl_3$ (10 ml) was added under Ar at 0 °C diazomethane (3 ml; conc. ≤ 0.64M in Et_2O, *ca.* 35 eq.). After 90, min the color of the soln. had changed from orange to bright yellow. Subsequent evaporation at RT, CC (SiO_2-*H*, CH_2Cl_2/AcOEt: 50:1) and re-dissolution in a minimum amount of CH_2Cl_2, followed by precipitation with pentane, afforded the pyrazoline **95b** as a yellow powder in 93% yield (93 mg, 0.053 mmol).

TLC (SiO_2, CH_2Cl_2/AcOEt 95:5): R_f 0.48. M.p. 80–90 °C (decomp.). UV/VIS (λ_{max} (ε) in CH_2Cl_2): 342 (sh, 24300), 305 (57300), 256 (51100). IR ($CHCl_3$): 3022*w*, 2933*w*, 2844*w*, 1750*s*, 1567*w*, 1450*w*, 1422*w*, 1377*m*, 1294*m*, 1189*s*, 1094*m*, 1061*m*, 1028*w*, 906*w*, 850*w*. ^{1}H-NMR (300 MHz, $CDCl_3$): 7.25-7.10 (*m*, 8 H); 6.09 (*t*, *J* = 5.0, 2 H); 5.70 (*s*, 2 H); 5.26 (br. *s*, 4 H); 4.78 (*s*, 2 H); 4.77 (*s*, 2 H); 4.72 (*s*, 2 H); 4.70 (*s*, 2 H); 4.30-4.10 (*m*, 8 H); 3.10-2.80 (br. *m*, 16 H); 1.45-1.15 (*m*, 12 H). ^{13}C-NMR (50 MHz, $CDCl_3$): 166.97; 166.88; 166.83; 163.35; 163.25; 163.07; 162.98; 156.78; 156.46; 155.11; 153.92; 150.27; 147.75; 146.39; 145.93; 145.73; 145.57; 145.49; 144.79; 143.86; 143.80; 143.73; 143.60; 142.98; 142.89; 141.95; 140.91; 140.56; 140.31; 139.08 (br.); 138.83 (br.); 138.32; 137.66; 132.04; 130.66 (br.); 128.72 (br.); 125.17; 114.03; 92.17; 69.36; 69.13; 69.00; 66.58; 62.60; 62.51; 62.22; 61.90; 61.79; 61.63; 60.63; 58.09; 44.61; 45.04; 42.96; 42.41; 39.27; 35.05; 34.34; 14.34; 14.29;

14.25. FAB-MS : 1741.7 (39, $[M - N_2 + O]^+$), 1725.1 (100, $[M - N_2]^+$), 1711.4 (82, $[M - CH_2N_2]^+$).

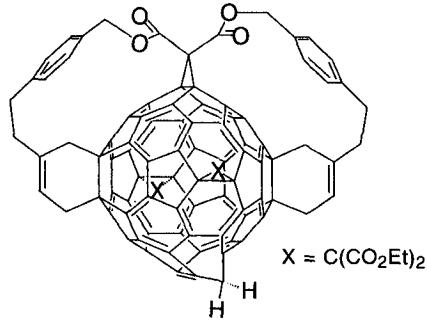

Tetraethyl 3',3'',6',6''-tetrahydro-17',17''-dioxo-5',3''':5'',3''''-bis(ethano[1,4]benzenomethanoxymethano)-3'''H,3''''H,3'''''H-dibenzo-[21,40:30,31]-tris(cyclopropa)[16,17:44,45:52,60] 1,2(2a)-homo[5,6]fullerene-C_{60}-I_h-3'''',3''''',3''''',3'''''-tetracarboxylate **96a**:

A soln. of **95a** (22 mg, 0.0145 mmol) in CCl_4 (30 ml) was heated to reflux for 15 min, leading to a color change of the soln. from yellow to orange. Subsequent CC (SiO_2-*H*, CH_2Cl_2), evaporation, and re-dissolution in a minimum amount of CH_2Cl_2, followed by precipitation with pentane, afforded **96a** (20 mg, 0.0134 mmol) as an orange powder in 93% yield.

TLC (SiO_2, CH_2Cl_2): R_f 0.27. M.p. : 250–260 °C (decomp.). UV/VIS (λ_{max} (ε) in CH_2Cl_2): 527 (sh, 1460), 498 (sh, 1620), 397 (sh, 5780), 341 (sh, 27500), 291 (56600). IR (KBr): 2979*w*, 2925*w*, 2835*w*, 1745*s*, 1616*w*, 1513*w*, 1449*m*, 1367*m*, 1290*m*, 1253*s*, 1209*s*, 1094*m*, 1064*m*, 1022*m*, 961*w*, 857*w*, 800*m*, 753*m*, 710*m*, 667*m*, 589*w*, 531*m*. ^{1}H-NMR (400 MHz, $CDCl_3$): 7.25-7.10 (br. *s*, 8 H); 6.21 (*t*, *J* = 5.2, 1 H); 6.19 (*t*, *J* = 5.2, 1 H); 5.14 (br. *s*, 4 H); 4.71 (*d*, *J* = 9.9, 1 H); 4.40-4.25 (*m*, 8 H); 3.35-3.25 (*m*, 4 H); 3.05-2.90 (*m*, 12 H); 2.13 (*d*, *J* = 9.9, 1 H); 1.40-1.30 (*m*, 12 H). ^{13}C-NMR (100 MHz, $CDCl_3$): 164.05; 163.98; 163.84; 163.67; 162.67; 162.62; 156.64; 155.09; 154.81; 154.49; 154.22; 153.09; 152.69; 148.35; 147.28; 146.68; 146.59; 145.64; 145.58; 145.51; 145.44; 145.36; 143.97; 143.90; 143.62; 143.46; 143.01; 142.92; 142.74; 142.66; 142.48; 142.43; 142.26; 142.22; 141.93; 141.29; 141.05; 140.93; 140.70; 139.66; 139.39; 139.05; 138.53; 138.39; 138.36; 138.28; 137.19; 136.83;

136.72; 131.88; 131.84; 130.94; 130.26; 130.22; 128.36; 128.14; 128.03; 125.24; 124.42; 118.61; 72.40; 68.93; 68.46; 66.90; 66.47; 65.70; 64.76; 62.66; 62.61; 62.55; 62.50; 62.11; 61.96; 61.25; 51.88; 45.06; 44.13; 42.40; 42.03; 41.11; 38.96; 35.53; 34.90; 34.86; 34.33; 34.24; 14.19; 14.15; 14.14. FAB-MS: 1510.1 (26, $[M + O]^+$), 1493.7 (100, M^+; calc. for $^{13}C^{12}C_{103}H_{52}O_{12}$: 1493.3), 1479.6 (2, $[M - CH_2]^+$), 720.1 (2, C_{60}^+).

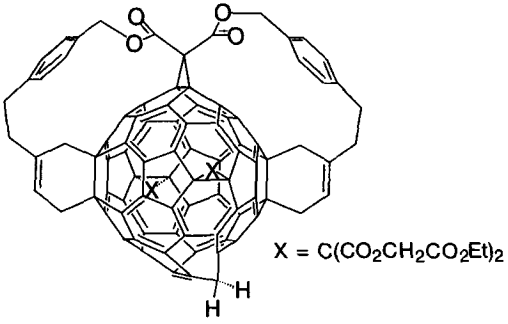

***Tetrakis(2-ethoxy-2-oxoethyl) 3',3'',6',6''-Tetrahydro-17',17''-dioxo-5',3''':5'',3'''-bis(ethano[1,4]benzenomethanoxymethano)-3'''H,3''''H,3'''''H-dibenzo-[21,40:30,31]-tris(cyclopropa)[16,17:44,45:52,60] 1,2(2a)-homo[5,6]fullerene-C_{60}-I_h-3'''',3''''',3''''',3'''''-tetracarboxylate* 96b**:

A soln. of **95b** (55 mg, 0.032 mmol) in CCl_4 (50 ml) was heated to reflux for 15 min, leading to a color change of the soln. from yellow to orange. Subsequent CC (SiO_2-*H*, CH_2Cl_2/AcOEt 95:5), evaporation, and re-dissolution in a minimum amount of CH_2Cl_2, followed by precipitation with pentane, afforded **96b** (51 mg, 0.030 mmol) as an orange powder in 93% yield.

TLC (SiO_2, CH_2Cl_2/AcOEt 95:5): R_f 0.55. M.p. : 230–245 °C (decomp.). UV/VIS (λ_{max} (ε) in CH_2Cl_2): 525 (sh, 1530), 497 (sh, 1650), 399 (sh, 1820), 359 (sh, 6670), 342 (sh, 23200), 291 (49300), 257 (sh, 51300). IR ($CHCl_3$): 2922*w*, 2855*w*, 1757*s*, 1450*w*, 1421*w*, 1379*m*, 1360*w*, 1290*m*, 1243*m*, 1185*s*, 1095*m*, 1061*m*, 1033*w*, 963*w*, 852*w*. ^{1}H-NMR (300 MHz, $CDCl_3$): 7.25-7.10 (br. *s*, 8 H); 6.23 (*t*, *J* = 4.9, 1 H); 6.21 (*t*, *J* = 4.9, 1 H); 5.16 (br.*s*, 4 H); 4.85-4.75 (br. *m*, 9 H); 4.30-4.10 (*m*, 8 H); 3.40-3.30 (*m*, 4 H); 3.10-2.90 (*m*, 12 H); 2.15 (*d*, *J* = 9.8, 1 H); 1.35-1.20 (*m*, 12 H). ^{13}C-NMR (75 MHz, $CDCl_3$): 166.69; 166.56; 166.51; 163.02; 162.87; 162.71; 162.58; 162.52;

156.68; 155.06; 154.85; 154.51; 154.28; 153.12; 152.73; 148.30; 147.35; 146.84; 146.73; 145.67; 145.62; 145.54; 145.40; 144.07; 143.75; 143.58; 143.52; 143.06; 142.78; 142.60; 142.50; 142.42; 142.26; 141.98; 141.73; 141.48; 141.39; 141.15; 141.01; 140.74; 140.66; 140.44; 139.68; 139.50; 139.10; 138.95; 138.44; 138.14; 137.88; 137.22; 137.07; 136.25; 131.90; 131.81; 131.77; 130.97; 130.26; 128.43; 128.27; 128.19; 125.22; 124.59; 118.80; 71.89; 68.68; 68.52; 68.43; 66.86; 66.44; 65.27; 64.35; 62.54; 62.36; 62.27; 62.16; 62.12; 61.99; 61.65; 61.55; 61.51; 61.28; 51.93; 43.81; 42.96; 42.43; 42.05; 41.08; 38.94; 35.41; 34.92; 34.88; 34.28; 34.20; 14.14; 13.96. FAB-MS: 1757.1 (9, $[M + 2\ O]^+$), 1741.6 (12, $[M + O]^+$), 1725.1 (100, M^+; calc. for $^{13}C^{12}C_{111}H_{60}O_{20}$: 1725.4), 719.8 (62, C_{60}^+).

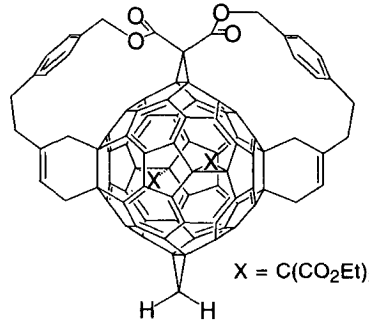

***Tetraethyl 3',3'',6',6''-tetrahydro-17',17''-dioxo-5',3''':5'',3'''-bis(ethano[1,4]benzenomethanoxymethano)-3'''H,3''''H,3'''''H-dibenzo-[1,9:52,60]-tetrakis(cyclopropa)[16,17:21,40:30,31:44,45][5,6]fullerene-C_{60}-I_h-3'''',3'''',3''''',3'''''-tetracarboxylate* 97**:

Solutions of **95a** in C_6D_6 (9.6 mM) in an NMR tube were held adjacent to a photolysis apparatus (medium pressure Hg-lamp) and were photolyzed for ca. 8 min. During the photolysis, the mixture was repeatedly cooled (ca. every 1.5 min) by holding the NMR tube into ice water for ca. 15 s. After CC (SiO_2-*H*, CH_2Cl_2), **97** and the C_1-symmetrical regioisomer **96a** were obtained in a combined yield between 9 and 21%. Subsequent addition of CH_2N_2 at 0 °C to the product mixture in CH_2Cl_2 (25 ml) led to an immediate color change of the soln. from orange to yellow. CC (SiO_2-*H*, CH_2Cl_2) evaporation, and re-dissolution in a minimum amount of CH_2Cl_2, followed by precipitation with pentane, afforded **97** as a bright yellow solid.

TLC (SiO_2, CH_2Cl_2): R_f 0.27. M.p. : >260 °C. UV/VIS (λ_{max} (ε) in CH_2Cl_2): 357 (sh, 16300), 309 (sh, 49900), 287 (58600). IR (CH_2Cl_2): 2961*w*, 2928*w*, 2853*w*, 1740*s*, 1465*w*, 1450*w*, 1368*m*, 1294*m*, 1256*s*, 1096*m*, 1078*m*, 1065*m*, 1020*m*, 859*w*. ^{1}H-NMR (400 MHz, $CDCl_3$): 7.10-7.10 (br. *m*, 8 H); 6.10 (*t*, *J* = 5.3, 2 H); 5.14 (br. *s*, 4 H); 4.26 (*q*, *J* = 7.1, 4 H); 4.20 (*q*, *J* = 7.1, 4 H); 3.14 (*d*, *J* = 5.3, 4 H); 2.95-2.80 (*m*, 12 H); 2.57 (*s*, 2 H) 1.27 (*t*, *J* = 7.1, 6 H); 1.21 (*t*, *J* = 7.1, 6 H). ^{13}C-NMR (100 MHz, $CDCl_3$): 163.99; 163.74; 163.11; 156.20; 154.87; 145.51; 145.41; 143.50; 143.15; 142.78; 142.53; 140.33; 139.82; 138.91; 131.81; 130.25; 128.28; 125.15; 71.12; 68.54; 63.57; 62.54; 62.51; 61.98; 61.73; 46.10; 42.28; 39.66; 34.87; 34.32; 14.16; 14.08. FAB-MS: 1510.2 (23, $[M + O]^+$), 1493.7 (100, M^+; calc. for $^{13}C^{12}C_{103}H_{52}O_{12}$: 1493.3), 720.1 (3, C_{60}^+).

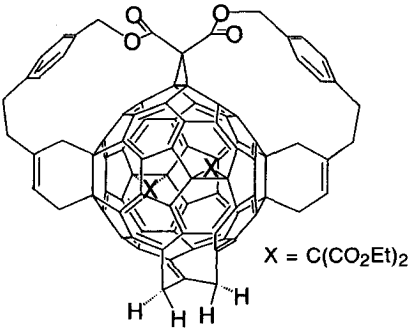

Tetraethyl 3',3'',6',6''-tetrahydro-17',17''-dioxo-5',3''':5'',3'''-bis(ethano[1,4]benzenomethanoxymethano)-3''''H,3'''''H,3''''''H-dibenzo-[21,40:30,31]-tris(cyclopropa)[16,17:44,45:52,60] [1,2(2a):1,5(5a)]-dihomo[5,6]fullerene-C_{60}-I_h-3''''',3''''',3''''''',3'''''''-tetracarboxylate **99a**:

To a soln. of **96a** (81 mg, 0.054 mmol) in CH_2Cl_2 (20 ml) was added at –80 °C CH_2N_2 (3 ml, conc. < 0.64 M in Et_2O ca. 40 eq.). The cooling bath was subsequently removed and, once the temperature of the mixture reached –55 °C, the reaction was quenched immediately with 3 ml of glacial acetic acid. Concentration in vacuo, CC (SiO_2-*H*, CH_2Cl_2/AcOEt 98:2) evaporation, and re-dissolution in a minimum amount of CH_2Cl_2, followed by precipitation with hexane, afforded **99a** as a yellow powder in 82% yield (67 mg, 0.044 mmol).

M.p. 230–240 °C (decomp.). UV/VIS (λ_{max} (ε) in CH_2Cl_2): 395 (sh, 14900), 365 (sh, 26100), 349 (sh, 36200), 315 (sh, 67000), 296 (80000), 252 (sh, 80700). IR (KBr): 2923*m*, 1746*s*, 1634*m*, 1445*m*, 1367*m*, 1249*s*, 1216*m*, 1062*m*, 798*w*, 536*m*, 457*w*. ^{1}H-NMR (400 MHz, $CDCl_3$): 7.20-7.10 (br. *m*, 8 H); 6.13 (*t*, *J* = 5.3, 2 H); 5.22 (br. *s*, 4 H); 4.44 (*d*, *J* = 10.9, 2 H); 4.37 (*q*, *J* = 7.1, 2 H); 4.35-4.20 (*m*, 6 H); 3.22 (*dd*, *J* = 14.2, 5.4, 2 H); 3.16 (*dd*, *J* = 14.2, 5.4, 2 H); 3.05-2.85 (*m*, 12 H); 2.76 (*d*, *J* = 10.9, 2 H); 1.38 (*t*, *J* = 7.1, 3 H); 1.32 (*t*, *J* = 7.1, 3 H); 1.26 (*t*, *J* = 7.1, 6 H). ^{13}C-NMR (100 MHz, $CDCl_3$): 164.26; 164.14; 163.78; 162.90; 156.57; 153.94; 153.30; 146.76; 146.53; 146.30; 145.72; 145.53; 145.41; 144.36; 144.21; 143.62; 142.68; 142.47; 141.63; 141.18; 140.45; 140.12; 138.61; 138.37; 136.92; 134.51; 133.76; 131.90; 131.00; 130.34; 130.30; 128.24; 125.11; 116.45; 68.52; 67.26; 66.13; 62.53; 62.50; 62.41; 62.25; 61.63; 61.54; 61.33; 47.92; 45.04; 44.70; 42.19; 40.69; 34.89; 34.24; 14.23; 14.16; 14.12; 14.09. FAB-MS: 1507.5 (100, M^+; calc. for $^{13}C^{12}C_{104}H_{54}O_{12}$ 1507.6), 1493.5 (16, M -$CH_2]^+$), 1479.2 (8, [M - 2 $CH_2]^+$), 1462.4 (10, [M - $C_2H_5O]^+$), 720.0 (C_{60}^+)

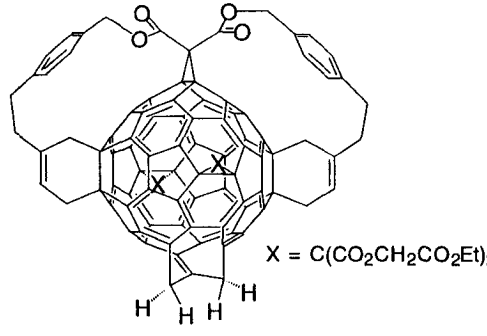

Tetrakis(2-ethoxy-2-oxoethyl) 3',3'',6',6''-tetrahydro-17',17''-dioxo-5',3''':5'',3'''-bis(ethano[1,4]benzenomethanoxymethano)-3'''H,3''''H,3'''''H-dibenzo-[21,40:30,31]-tris(cyclopropa)[16,17:44,45:52,60][1,2(2a):1,5(5a)]-dihomo[5,6]fullerene-C_{60}-I_h-3'''',3''''',3'''''',3''''''-tetracarboxylate **99b**:

To a soln. of **96b** (150 mg, 0.087 mmol) in CH_2Cl_2 (10 ml) was added at –80 °C CH_2N_2 (3 ml, conc. < 0.64 M in Et_2O; ca. 20 eq.). The cooling bath was subsequently removed and, once the temperature of the mixture reached –60 °C, the reaction was quenched immediately with glacial acetic acid (3 ml). Concentration in vacuo, CC

(SiO_2-*H*, CH_2Cl_2/AcOEt 95:5) evaporation, and re-dissolution in a minimum amount of CH_2Cl_2, followed by precipitation with pentane, afforded **99b** as a yellow powder in 79 % yield (119 mg, 0.069 mmol).

TLC (SiO_2, CH_2Cl_2): R_f 0.21. M.p. 195–210 °C (decomp.). UV/VIS (λ_{max} (ε) in CH_2Cl_2): 393 (sh, 7040), 348 (sh, 24400), 317 (sh, 51500), 299 (58100), 250 (sh, 52600). IR (KBr): 2923*w*, 1750*s*, 1450*w*, 1422*w*, 1396*w*, 1379*m*, 1285*m*, 1251*m*, 1193*s*, 1092*m*, 1060*m*, 1033*m*, 964*w*, 852*w*, 797*w*, 769*w*, 754*w*, 716*w*, 589*w*, 571*w*, 546*w*, 535*w*. ^{1}H-NMR (400 MHz, $CDCl_3$): 7.20-7.05 (*m*, 8 H), 6.14 (*t*, *J* = 5.4, 2 H), 5.21 (br. *s*, 4 H), 4.81 (*s*, 2 H), 4.75 (*s*, 2 H), 4.73 (*s*, 2 H), 4.71 (*s*, 2 H), 4.48 (*d*, *J* = 10.9, 2 H), 4.26 (*q*, *J* = 7.1, 2 H), 4.22 (*q*, *J* = 7.1, 2 H), 4.21 (*q*, *J* = 7.1, 2 H), 4.15 (*q*, *J* = 7.1, 2 H), 3.21 (*dd*, *J* = 14.2, 5.4, 2 H), 3.15 (*dd*, *J* = 14.2, 5.4, 2 H), 3.05-2.85 (*m*, 12 H), 2.75 (*d*, *J* = 10.9, 2 H), 1.30 (*t*, *J* = 7.1, 3 H), 1.27 (*t*, *J* = 7.1, 3 H), 1.26 (*t*, *J* = 7.1, 3 H), 1.20 (*t*, *J* = 7.1, 3 H). ^{13}C-NMR (100 MHz, $CDCl_3$): 166.74; 166.67; 166.62; 166.57; 163.29; 163.12; 163.04; 163.00; 162.81; 162.78; 156.58; 153.94; 153.34; 146.86; 146.47; 146.39; 145.76; 145.61; 145.54; 144.37; 144.29; 143.73; 142.76; 142.70; 142.46; 141.19; 141.14; 140.48; 139.62; 139.50 (br.); 138.39 (br.); 138.05; 137.96; 136.95; 134.75; 133.77; 131.81; 131.46; 130.33 (br.); 130.30 (br.); 128.35 (br.); 125.07; 116.63; 68.55; 68.09; 67.17; 66.05; 62.24; 62.18; 62.05; 61.63; 61.60; 61.57; 61.49; 61.41; 61.33; 61.16; 47.94; 44.96; 43.55; 42.87; 42.18; 40.64; 34.89; 34.75; 14.18; 14.13; 14.10; 14.04. FAB-MS: 1771.1 (10, $[M + 2\ O]^+$), 1755.2 (14, $[M + O]^+$), 1739.1 (100, M^+; calc. for $^{13}C^{12}C_{112}H_{62}O_{20}$: 1739.4), 1725.1 (7, $[M - CH_2]^+$), 1711.3 (3, $[M - 2\ CH_2]^+$), 719.8 (7, C_{60}^+).

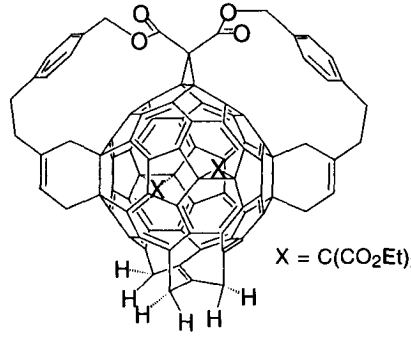

Tetraethyl 3',3'',6',6''-tetrahydro-17',17''-dioxo-5',3''':5'',3'''-bis(ethano[1,4]benzenomethanoxymethano)-3'''H,3''''H,3'''''H-dibenzo-[21,40:30,31]-tris(cyclopropa)[16,17:44,45:52,60] [1,2(2a):1,5(5a):8,9(9a)]-trihomo[5,6]fullerene-C_{60}-I_h-3''',3'''',3''''',3'''''-tetracarboxylate **98a**:

To a soln. of **96a** (25 mg, 0.0167 mmol) in $CHCl_3$ (5 ml) was added under Ar at 0 °C diazomethane (2 ml; conc. ≤ 0.64M in Et_2O, *ca.* 75 eq.). The mixture was stirred at 0 °C for 10 min. Within 1 min the color of the soln. had changed from orange to orange-yellow. Subsequent evaporation, CC (SiO_2-*H*, CH_2Cl_2), and re-dissolution in a minimum amount of CH_2Cl_2, followed by precipitation with pentane, afforded the octakis-adduct **98a** in 85 % yield (22 mg, 0.0142 mmol).

TLC (SiO_2, CH_2Cl_2): R_f 0.35. M.p. : 215–235 °C (decomp.). UV/VIS (λ_{max} CH_2Cl_2): 303 (sh), 286. ^{1}H-NMR (500 MHz, $CDCl_3$): ^{1}H-NMR (500 MHz, $CDCl_3$): 7.30-7.10 (*m*, 8 H), 6.07 (*t*, *J* = 5.3, 1 H); 6.03 (*t*, *J* = 5.3, 1 H); 5.30-5.20 (br. *m*, 4 H); 4.48 (*d*, *J* = 15.3, 1 H); 4.41 (*d*, *J* = 15.1, 1 H); 4.42-4.37 (*m*, 2 H); 4.30-4.15 (*m*, 6 H);4.06 (*d*, *J* = 10.0, 1 H); 3.39 (*d*, *J* = 15.3, 1 H); 3.37 (*d*, *J* = 15.1, 1 H); 3.15-2.85 (*m*, 12 H); 2.80 (*d*, *J* = 14.1, 2 H); 2.71 (*d*, *J* = 14.1, 2 H); 2.04 (*d*, *J* = 10.0, 1 H); 1.40 (*t*, *J* = 7.1, 3 H); 1.30-1.20 (*m*, 9 H). ^{13}C-NMR (125 MHz, $CDCl_3$): 164.16; 164.08; 163.98; 163.70; 163.36; 162.90; 157.93; 154.96; 154.70; 154.36; 153.19; 151.93; 147.76; 145.77; 145.66; 145.49; 145.38; 145.16; 144.91; 144.71; 144.49; 144.06; 143.56; 143.35; 143.09; 142.75; 142.58; 142.50; 142.22; 141.51; 140.84; 140.78; 140.73; 139.90; 139.30; 139.24; 139.13; 138.69; 137.94; 137.69; 137.31; 136.17; 135.67; 134.61; 134.30; 132.76; 131.90; 131.87; 131.58; 131.42; 130.36; 130.29; 129.61; 128.64; 128.10; 126.02; 125.12; 124.76; 115.77; 70.98; 68.61; 68.49; 66.20; 66.04; 62.58; 62.53; 62.44; 62.34; 62.01; 61.11; 60.90; 60.84; 58.32; 47.25; 46.23; 45.50; 43.85;

42.47; 41.97; 40.91; 40.58; 37.80; 37.63; 34.86; 34.75; 34.70; 34.23; 14.24; 14.13; 14.06. FAB-MS: 1537.2 (15, $[M + O]^+$), 1521.2 (100, M^+; calc. for $^{13}C^{12}C_{105}H_{56}O_{12}$: 1521.4), 1507.5 (13, $[M - CH_2]^+$), 1493.3 (15, $[M - 2\ CH_2]^+$).

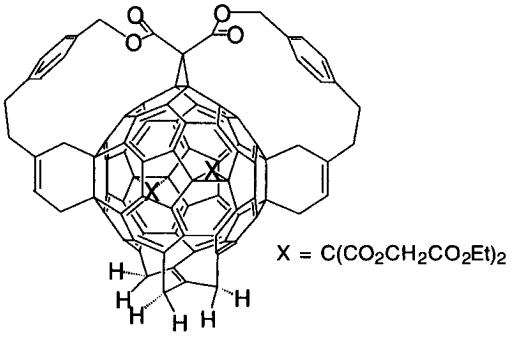

Tetrakis(2-ethoxy-2-oxoethyl) 3',3'',6',6''-tetrahydro-17',17''-dioxo-5',3''':5'',3'''-bis(ethano[1,4]benzenomethanoxymethano)-3'''H,3''''H,3'''''H-dibenzo-[21,40:30,31]-tris(cyclopropa)[16,17:44,45:52,60] [1,2(2a):1,5(5a):8,9(9a)]-trihomo[5,6]fullerene-C_{60}-I_h-3'''',3''''',3'''''',3'''''''-tetracarboxylate **98a**:

To a soln.of **96b** (75 mg, 0.044 mmol) in $CHCl_3$ (10 ml) was added under Ar at 0 °C diazomethane (3 ml; conc. ≤ 0.64M in Et_2O, *ca.* 40 eq.). The mixture was stirred at 0 °C for 10 min. Within 1 min, the color of the soln. had changed from orange to yellow. Subsequent evaporation, CC (SiO_2-*H*, CH_2Cl_2 to CH_2Cl_2/AcOEt 98:2), and re-dissolution in a minimum amount of $CHCl_3$, followed by precipitation with cyclohexane, afforded the octakis-adduct **98b** in 90 % yield (69 mg, 0.039 mmol).

M.p. 200–215 °C (decomp.). UV/VIS (λ_{max} (ε) in CH_2Cl_2): 303 (sh, 48700), 286 (51500). IR ($CHCl_3$): 2958*w*, 2925*w*, 2856*w*, 1750*s*, 1602*w*, 1451*w*, 1422*w*, 1381*m*, 1360*w*, 1293*m*, 1275*m*, 1257*m*, 1190*s*, 1096*m*, 1061*w*, 1021*w*, 919*w*, 853*w*. ^{1}H-NMR (500 MHz, $CDCl_3$): 7.30-7.10 (*m*, 8 H), 6.07 (*t*, *J* = 5.3, 1 H); 6.02 (*t*, *J* = 5.3, 1 H); 5.30-5.20 (br. *m*, 4 H); 4.84 (*s*, 2 H); 4.75-4.55 (*m*, 6 H); 4.53 (*d*, *J* = 15.6, 1 H); 4.46 (*d*, *J* = 15.2, 1 H); 4.30-4.20 (*m*, 2 H); 4.28 (*q*, *J* = 7.1, 2 H); 4.20 (*q*, *J* = 7.1, 2 H); 4.13 (*q*, *J* = 7.1, 2 H); 4.10 (*d*, *J* = 10.5, 1 H); 3.49 (*d*, *J* = 15.6, 1 H); 3.38 (*d*, *J* = 15.2, 1 H); 3.15-2.85 (*m*, 12 H); 2.81 (*d*, *J* = 14.1, 2 H); 2.71 (*d*, *J* = 14.1, 2 H); 2.02 (*d*, *J* = 10.2, 1 H); 1.31 (*t*, *J* = 7.1, 3 H); 1.30 (*t*, *J* = 7.1, 3 H); 1.25 (*t*, *J* = 7.1, 3 H); 1.18 (*t*, *J* = 7.1, 3

H). ^{13}C-NMR (125 MHz, $CDCl_3$): 166.76; 166.69; 166.66; 166.56; 163.61; 163.27; 163.22; 163.06; 163.01; 162.05; 157.93; 154.93; 154.73; 154.41; 153.21; 151.97; 147.81; 146.42; 146.17; 145.86; 145.77; 145.70; 145.43; 145.40; 144.93; 144.71; 144.66; 144.30; 144.09; 143.71; 143.46; 143.22; 143.16; 143.00; 142.78; 142.71; 142.50; 142.43; 140.97; 140.86; 140.82; 140.47; 139.75; 139.48; 139.33; 138.79; 138.72; 138.20; 138.05; 137.30; 136.90; 136.27; 135.64; 134.70; 134.55; 132.66; 132.45; 131.97; 131.84; 131.79; 130.40; 130.28; 129.47; 128.74; 128.15; 126.34; 125.09; 124.80; 116.88; 70.52; 68.66; 68.54; 68.03; 66.75; 66.14; 65.46; 62.60; 62.26; 62.20; 62.02; 61.89; 61.64; 61.56; 61.46; 61.42; 61.12; 60.88; 60.63; 58.35; 47.37; 46.28; 44.16; 42.61; 42.47; 41.97; 40.89; 40.53; 37.76; 34.90; 34.74; 34.64; 34.18; 14.20; 14.17; 14.12; 14.01. FAB-MS: 1770.0 (13, $[M + O]^+$), 1753.3 (100, M^+; calc. for $^{13}C^{12}C_{113}H_{64}O_{20}$: 1753.4), 1739.1 (12, $[M - CH_2]^+$), 719.9 (31, C_{60}^+).

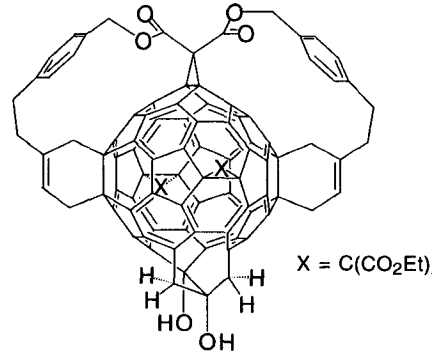

Tetraethyl 1,3',3'',6',6'',9-hexahydro-1,9-dihydroxy-17',17''-dioxo-5',3''':5'',3'''-bis(ethano[1,4]benzenomethanoxymethano)-3'''H,3''''H,3'''''H-dibenzo-[21,40:30,31]-tris(cyclopropa)[16,17:44,45:52,60][1,2(2a):1,5(5a)]-dihomo[5,6]fullerene-C_{60}-I_h-3'''',3''''',3''''',3'''''-tetracarboxylate **119**:

To a degassed soln. of **99a** (52 mg, 0.035 mmol) in CH_2Cl_2 (50 ml) was added at RT an aq. soln. of $KMnO_4$ and [18]crown-6 (3.8 ml, 0.01 M $KMnO_4$; 0.01 M [18]crown-6). The intermediate manganate complex was hydrolyzed after 2 h by addition of 5 ml of glacial acetic acid and stirring for an additional 2 h at RT. The reaction was subsequently quenched with aq. $NaHCO_3$, the solutions filtered and washed with sat. aq. $NaHCO_3$, sat. aq. NaCl soln., and twice with H_2O. The aqueous phase was re-extracted with CH_2Cl_2, and the combined organic phases were dried (Na_2SO_4). CC

(SiO_2-*H*, CH_2Cl_2/AcOEt 7:3), evaporation, and re-dissolution in a minimum amount of CH_2Cl_2, followed by precipitation with pentane, afforded **119** in 66% yield (35 mg, 0.023 mmol) as a bright yellow solid.

TLC (SiO_2, CH_2Cl_2/AcOEt 90:10): R_f 0.32. M.p. : 186–192 °C (decomp.). UV/VIS (λ_{max} (ε) in CH_2Cl_2): 425 (sh, 3290), 348 (sh, 24500), 313 (sh, 55100), 297 (62900), 259 (sh, 46300). IR (KBr): 3734*w*, 3396*w*, 2921*w*, 2851*w*, 1746*s*, 1636*m*, 1560*w*, 1541*w*, 1508*w*, 1457*w*, 1396*w*, 1368*w*, 1251*s* , 1094*m* , 1066*m*, 1025*m*, 802*w*, 769*w*, 720*w*, 668*w*, 584*w*, 530*w*, 453*w*. (CCl_4): 3734*w*, 3396*w*, 2981*w*, 2960*w*, 2929*w*, 2872*w*, 2851*w*, 1746*s*, 1652*w*, 1615*w*, 1514*w*, 1450*m*, 1367*w*, 1244*s*, 1095*m*, 1065*m*, 1024*m*, 976*w*, 911*w*, 858*w*. ^{1}H-NMR (200 MHz, $CDCl_3$): 7.25-7.09 (br. *m*, 8 H); 6.01 (*t*, *J* = 5.3, 2 H); 5.31 (*s*, 4 H); 4.66 (br. *s*, 1 H); 4.40-4.20 (br. *s*, 1 H); 4.33 (*q*, *J* = 7.1, 2 H); 4.31 (*q*, *J* = 7.1, 2 H); 4.19 (*q*, *J* = 7.1, 4 H); 3.84 (br. *d*, *J* = 11.6, 2 H); 3.62 (br. *d*, *J* = 11.6, 2 H); 2.91-2.84 (br. *m*, 14 H); 1.34 (*t*, *J* = 7.1, 3 H); 1.33 (*t*, *J* = 7.1, 3 H); 1.25 (*t*, *J* = 7.1, 6 H). ^{13}C-NMR (75 MHz, $CDCl_3$): 164.68; 164.23; 164.22; 163.56; 163.30; 158.05; 156.77; 151.48; 149.88; 148.49 ; 147.82; 146.43; 145.73 ; 145.17; 144.86; 144.68; 144.02; 143.53; 143.21; 142.79; 142.55; 141.64; 141.59; 140.99; 138.91; 138.33; 136.93; 135.06; 134.43; 133.08; 132.03; 130.64; 130.56; 128.52; 124.93; 84.40; 68.81; 69.94; 62.63; 62.59; 62.37; 61.63; 61.11; 60.99; 60.33; 49.85; 42.15; 40.34; 34.88; 34.17; 14.18; 14.08. FAB-MS: 1541.6 (100, M^+; calc. for $^{13}C^{12}C_{104}H_{56}O_{14}$: 1541.6), 1525.3 (26, [*M* - OH]$^+$), 1523.1 (45, [*M* - H_2O]$^+$), 1495.1 (16, [*M* - C_2H_5O]$^+$), 1382.7 (9, [*M* - $C(CO_2CH_2CH_3)_2$]$^+$), 1225.0 (5, [*M* - 2 $C(CO_2CH_2CH_3)_2$]$^+$), 719.8 (7, C_{60}^+).

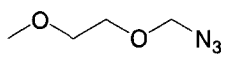

***2-Methoxyethoxymethyl azide* 153**: To a suspension of sodium azide (0.69 g, 8.9 mmol) and [18]crown-6 (*ca.* 5 mg 0.012 mmol) in acetone (11 ml) and H_2O (0.5 ml), was added at 0 °C 2-methoxyethoxymethyl chloride (MEMCl; 1.11 g, 8.9 mmol) over a period of 5 min. After stirring at 0 °C for 15 min, the mixture was allowed to warm to RT. After 2 h, the reaction was quenched with 5 ml of H_2O and extracted with Et_2O. The organic phase was washed with sat. aq. NaCl and dried (Na_2SO_4). Evaporation of Et_2O afforded **153** (1.024 g, 7.8 mmol) as a colorless liquid in 88% yield.

IR (neat): 3333*w* , 2981*s* , 2442*w*, 2360*m*, 2120*s* (N_3 st as), 1457*s* , 1387*m* , 1365*m*, 1228*s* , 1103*s* (N_3 st. sy.), 1025*m*, 876*m*, 699*m*.. ^{1}H-NMR (200 MHz, $CDCl_3$): 4.71 (br. *s*, 2 H); 3.79-3.75 (*m*, AA'BB', 2 H); 3.61-3.57 (*m*, 2 H); 3.40 (*s*, 3 H). ^{13}C-NMR (50 MHz, $CDCl_3$): 82.76; 71.11; 68.28; 58.63.

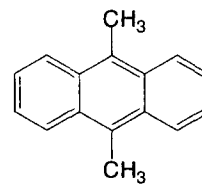

9,10-Dimethylanthracene [380]: To a suspension of 9,10-dibromoanthracene (8.519 g, 39.44 mmol) in 130 ml dry Et_2O was added at RT *n*-BuLi (1.67 ml, 1.6 M in hexanes, 106.5 mmol) over a period of 30 min (careful!). The color of the suspension changed during the course of the strongly exothermic reaction from red-orange to light orange. The mixture was subsequently allowed to cool to RT by stirring for an additional 10 min. Subsequently, methyl iodide (15.11 g, 106.5 mmol) was added carefully at RT and the mixture was heated to reflux for 4 h. After cooling to RT, the crude mixture was washed 4 times with H_2O and dried ($MgSO_4$). The title compound precipitated from the soln. upon concentration *in vacuo*, yielding 61 % (4.99 g, 24.06 mmol) of **154** as light yellow, crystalline solid after recrystallization from EtOH (200 ml).

TLC (SiO_2, hexane) R_f 0.28. M.p.: 182° C (Lit. 182.5-184 [380]). IR ($CHCl_3$): 3087*w* , 3008*w*, 2934*w*, 1620*m*, 1527*m*, 1443*m*, 1388*s*, 1364*s*, 1179*w*, 990*m*. ^{1}H-NMR (200 MHz, $CDCl_3$): 8.35-7.35 (*m*, 8 H); 3.12 (*s*, 6 H, CH_3). ^{13}C-NMR (50 MHz, $CDCl_3$): 127.93; 124.91; 124.31; 110.88; 13.65.

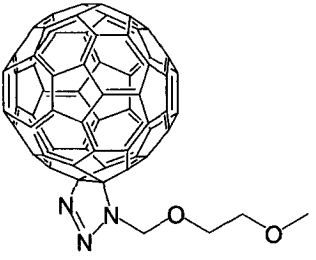

3'-Methoxyethoxymethyl-[5,6]fullereno-C_{60}-I_h-[1,9]triazol [272]. To a soln. of C_{60} (1616 mg, 2.24 mmol) in 1-chloronaphthalene (20 ml) was added at RT **111** (294 mg, 2.24 mmol) in 1-chloronaphthalene (3 ml). The resulting mixture was stirred for 13 h at 60 °C. Subsequent CC (SiO_2, PhMe, then CH_2Cl_2) and evapoaration afforded **35b** in 25% yield (472 mg, 0.55 mmol) as a dark brown microcrystalline solid.

TLC (SiO_2, PhMe): R_f 0.08. IR ($CHCl_3$): 3026*s*, 2976*s*, 1522*m* (N=N), 1477*m*, 1423*m*, 1046*s*, 929*s*, 877*m*, 627*s*. ^{1}H-NMR (200 MHz, $CDCl_3$): 6.03 (*s*, 2 H); 4.10-4.05 (*m*, 2 H), 3.67-3.62 (*m*, 2 H); 3.4 (*s*, 3 H).

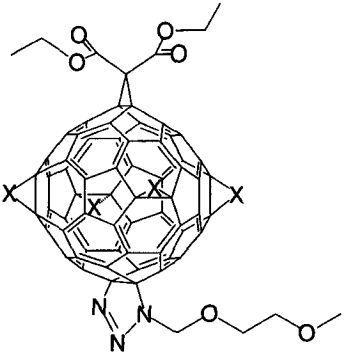

X = $C(CO_2Et)_2$

Decaethyl 3'-methoxyethoxymethyl-3''H,3'''H,3''''H,3'''''H,3''''''H-pentakis(cyclopropa)[1,9:16,17:21,40:30,31:44,45] [52,60][5,6]fullereno-C_{60}-I_h-[52,60]triazole3',3',3'',3'',3''',3''',3'''',3'''',3''''',3''''',3''''''-decacarboxylate **112** [274].

To a degassed soln. of **35b** (694 mg, 0.815 mmol) in PhMe (500 ml) was added 9,10-dimethylanthracene (1345 mg, 6.520 mmol). The resulting mixture was protected from

light and stirred for 2 h at RT. Subsequently, DBU (1241 mg, 8.153 mmol) and diethyl 2-bromopropanedioate (1949 mg, 8.153 mmol) were added and the mixture was stirred in an Ar atmosphere for 2 d, then washed with sat. aq. NH_4Cl and sat. aq. NaCl solution, and dried (Na_2SO_4). CC (SiO_2, PhMe to remove DMA then AcOEt), evaporation, and re-dissolution of the red viscous residue in a minimum amount of CH_2Cl_2, followed by precipitation with pentane, afforded an orange powder which was chromatographed (SiO_2-*H*, CH_2Cl_2/AcOEt 95:5) providing the yellow hexakis-adduct **112** in 57% yield (767 mg, 0.473 mmol).

TLC (SiO_2, AcOEt): R_f 0.28. M.p. : 105–112 °C (decomp.). UV/VIS (λ_{max} (ε) in CH_2Cl_2): 332 (sh, 33400), 312 (49000), 279 (sh, 6250), 268 (68900). IR (KBr): 3035*w*, 2986*m*, 2939*w*, 2873*w*, 1741*s*, 1466*m*, 1446*m*, 1394*m*, 1369*m*, 1299*s*, 1256*s*, 1096*s*, 1069*s*, 1019*m*, 909*m*, 859*m*, 825*w*, 652*w*. ^{1}H-NMR (200 MHz, $CDCl_3$): 5.58 (br. *s*, 2 H); 4.44-4.22 (*m*, 20 H); 3.80-3.45 (*m*, 4 H); 3.34 (*s*, 3 H); 1.40-1.20 (*m*, 30 H). ^{13}C-NMR (50 MHz, $CDCl_3$): 161.7; 161.5; 161.3; 161.2; 161.2; 144.6; 144.3; 143.7; 143. 6; 143.2; 143.1; 143.0; 142.9; 141.5; 141.2; 141.1; 139.8; 139.3; 138.3; 138.6; 138.5; 137.7; 137.6; 137.2; 137.1; 73.8; 69.1; 67.4; 65.6; 65.3; 60.6; 60.5; 60.4; 59.6; 56.6; 54.0; 43.1; 42.8; 11.6; 11.5; 11.4. FAB-MS: 1643.0 (21, $[M + H]^+$; calc. for $^{13}C^{12}C_{98}H_{59}N_3O_{22}$: 1641.4); 1614.0 (13, $[M - N_2]^+$); 1527.3 (8, $[M - C_4H_9O_2N + H]^+$); 1510.8 (100, $[M - C_4H_9O_2N_3]^+$); 1465.4 (15, $[M - N_2 - C(CO_2CH_2CH_3)_2]^+$); 1353.0 (7, $[M - C_4H_9O_2N_3 - C(CO_2CH_2CH_3)_2]^+$); 1195.0 (2, $M - C_4H_9O_2N_3 - 2\ C(CO_2CH_2CH_3)_2]^+$); 1035.9 (1, $[M^+ - C_4H_9O_2N_3 - 3\ C(CO_2CH_2CH_3)_2]^+$); 878 (1, $[M - C_4H_9O_2N_3 - 4\ C(CO_2CH_2CH_3)_2]^+$); 719.7 (14, C_{60}^+).

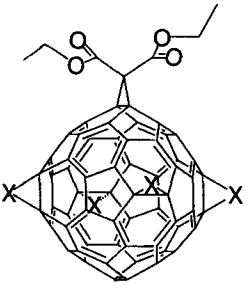

X = $C(CO_2Et)_2$

Decaethyl 3'H,3''H,3'''H,3''''H,3'''''H-pentakis(cyclopropa)[1,9:16,17:21,40:30,31:44,45] [5,6]fullerene-C_{60}-I_h-3',3',3'',3'',3''',3''',3'''',3'''',3''''',3'''''-decacarboxylate **47** [274]: A degassed soln. of **112** (653 mg, 0.398 mmol) in PhMe (130 ml) was heated to reflux for 18 h. CC (SiO_2, CH_2Cl_2/AcOEt 95:5), evaporation, and re-dissolution in a minimum amount of CH_2Cl_2, followed by precipitation with pentane, afforded **47** as an orange powder in 41% yield (239 mg, 0.163 mmol) as a red orange powder.

TLC (SiO_2, CH_2Cl_2): R_f 0.25. M.p. : 243–255 °C (decomp.). IR (KBr): 2979*m* , 1744*s*, 1654*w*, 1465*m*, 1444*m*, 1389*m*, 1367*m*, 1296*m*, 1257*s* , 1218*s* , 1077*m*, 1018*m*, 856*m*, 712*m*, 669*w*, 526*m* . ^{1}H-NMR (200 MHz, $CDCl_3$): 4.50-4.35 (*m*, 12 H); 4.28 (*q*, *J* = 7.5, 8 H); 1.50-1.35 (*m*, 24 H); 1.28 (*t*, *J* = 7.5, 6 H). ^{13}C-NMR (50 MHz, $CDCl_3$): 163.52; 163.39; 162.88; 148.12; 146.50; 145.67; 145.33; 144.69; 144.18; 143.83; 143.64; 142.72; 141.93; 139.45; 139.33; 69.52; 68.74; 68.79; 62.56; 62.31; 13.65; 13.55. FAB-MS: 1511.1 (100, M^+; calc. for $^{12}C_{95}H_{50}O_{20}$: 1511.4), 1466.0 (14, [*M* - $C_2H_5O]^+$), 1353.1 (4, [*M* - $C(CO_2CH_2CH_3)_2]^+$), 1195.2 (1, [*M* - 2 $C(CO_2CH_2CH_3)_2]^+$), 1037 (1, [*M* - 3 $C(CO_2CH_2CH_3)_2]^+$), 879.1 (1, [*M* - 4 $C(CO_2CH_2CH_3)_2]^+$), 720.0 (27, C_{60}^+).

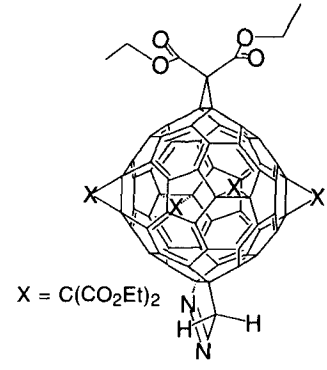

D e c a e t h y l 3 'H,3''H,3'''H,3''''H,3'''''H-pentakis(cyclopropa)[1,9:16,17:21,40:30,31:44,45] [5,6]fullerene-C_{60}-I_h-[52,60-d]pyrazole-3',3',3'',3'',3''',3''',3'''',3'''',3''''',3'''''-decacarboxylate **115:**

To a soln. of **47** (130 mg, 0.086 mmol) in CH_2Cl_2 (20 ml) was added under Ar at 0 °C diazomethane (3 ml; conc. ≤ 0.64M in Et_2O, ca. 20 eq.). After 20 min the color of the soln. had changed from orange to bright yellow. Subsequent evaporation under reduced pressure at RT, evaporation, and re-dissolution in a minimum amount of CH_2Cl_2, followed by precipitation with pentane, afforded **115** as a yellow powder in 94% yield (125 mg, 0.015 mmol).

TLC (SiO_2, CH_2Cl_2): R_f 0.20. M.p. : 96–103 °C (decomp.). UV/VIS (CH_2Cl_2): 579 (sh), 544, 508 (sh), 459, 415, 385, 297, 277. IR (KBr): 2981*m*, 2932*m*, 1743*s*, 1636*w*, 1571*w* (N=N), 1464*w*, 1368*w*, 1239*s*, 1095*m*, 1022*m*, 859*w*, 800*m*, 713*w*, 539*w*. ^{1}H-NMR (200 MHz, $CDCl_3$): 5.95 (*s*, 2 H); 4.45-4.20 (*m*, 20 H); 1.43-1.27 (*m*, 30 H). ^{13}C-NMR (50 MHz, $CDCl_3$): 163.21; 163.02; 162.93; 162.83; 150.86; 146.45; 145.85; 145.25; 145.12; 145.06; 144.90; 144.80; 144.74; 144.61; 144.30; 143.06; 142.61; 141.44; 141.22; 141.12; 140.90; 140.74; 139.98; 139.63; 139.53; 139.19; 138.39; 114.84; 91.03; 68.97; 68.40; 67.20; 67.01; 61.99; 58.82; 44.69; 44.54; 44.21; 41.20; 13.04. FAB-MS: 1553.3 (63, M^+; calc for $^{12}C_{95}{}^{13}CH_{52}O_{20}N_2$: 1553.3), 1539.3 (100, [*M* - N]$^+$), 1525.4 (29, [*M* - N_2]$^+$), 1508.3 (19, [*M* - C_2H_5O]$^+$), 1495.3 (29, [*M* - N_2 - C_2H_5O]$^+$), 1395.4 (30, [*M* - $C(CO_2CH_2CH_3)_2$]$^+$), 720.1 (28, C_{60}^+).

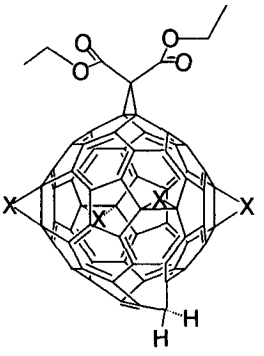

X = $C(CO_2Et)_2$

Decaethyl 3'H,3''H,3'''H,3''''H,3'''''H-pentacyclopropa[16,17:21,40:30,31:44,45:52,60] 1,2(2a)-homo[5,6]fullerene-C_{60}-I_h-3',3',3'',3'',3''',3''',3'''',3'''',3''''',3'''''-decacarboxylate **116**.

A soln. of **115** (59 mg, 0.038 mmol) in $CHCl_3$ (5 ml) was heated to reflux for 5 h, leading to a color change of the soln. from yellow to orange. CC (SiO_2-*H*, CH_2Cl_2/AcOEt 9:1), evaporation, and re-dissolution in a minimum amount of CH_2Cl_2, followed by precipitation with pentane, afforded **116** as an orange powder in 82% yield (40 mg, 0.031 mmol) as a red orange powder.

TLC (SiO_2, CH_2Cl_2): R_f 0.32. M.p. : >250 °C (decomp.). UV/VIS (λ_{max} (ε) in CH_2Cl_2): 540 (sh, 1500), 517 (1720), 414 (sh, 3340), 348 (sh, 20700), 322 (sh, 39700), 287 (69800), 245 (77900). IR (KBr): 2980*w*, 2931*w*, 1744*s*, 1465*w*, 1446*w*, 1390*w*, 1389*w*, 1367*m*, 1257*s*, 1219*s*, 1095*m*, 1079*m*, 1020*m*, 858*w*, 814*w*, 717*m*, 544*m*, 529*m*, 519*w*. ^{1}H-NMR (400 MHz, $CDCl_3$): 5.24 (*d*, *J* = 9.9, 1 H); 4.45-4.25 (*m*, 20 H); 2.45 (*d*, *J* = 9.9, 1 H), 1.45-1.29 (*m*, 30 H). ^{13}C-NMR (100 MHz, $CDCl_3$): 164.08; 164.05; 163.96; 163.93; 163.87; 163.85; 163.57; 163.49; 163.40; 147.61; 147.29; 146.67; 146.54; 146.24; 146.11; 145.99; 145.73; 145.69; 145.00; 144.66; 144.41; 144.38; 143.34; 142.99; 142.75; 142.69; 142.47; 141.93; 141.51; 141.41; 141.36; 141.26; 141.23; 140.92; 140.58; 140.08; 139.96; 139.78; 139.67; 139.55; 139.25; 139.00; 137.56; 135.08; 134.66; 132.93; 131.43; 124.95; 119.29; 70.62; 70.01; 69.64; 69.47; 69.02; 68.57; 67.26; 64.48; 63.17; 62.85; 62.82; 62.68; 62.64; 52.19; 46.16; 45.78; 44.56; 43.87; 35.6; 14.15; 14.02; 14.07; 14.05; 13.99. FAB-MS: 1525.1 (100, M^+; calc.

for $^{13}C^{12}C_{95}H_{52}O_{20}$: 1525.3), 1480.1 (23, [*M* - C_2H_5O]$^+$), 1366.0 (5, [*M* - $C(CO_2CH_2CH_3)_2$]$^+$), 719.8 (26, C_{60}^+).

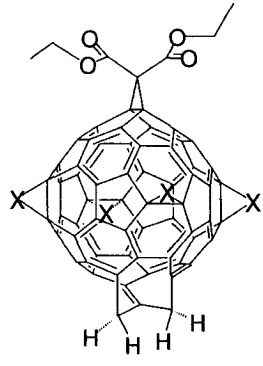

X = $C(CO_2Et)_2$

Decaethyl 3'H,3''H,3'''H,3''''H,3'''''H-pentakis(cyclopropa)[16,17:21,40:30,31:44,45:52,60] [1,2(2a):1,5(5a)]-dihomo[5,6]fullerene-C_{60}-I_h-3',3',3'',3'',3''',3''',3'''',3'''',3''''',3'''''-decacarboxylate **117**:

To a soln. of **116** (108 mg, 0.071 mmol) in CH_2Cl_2 (10 ml) was added at –80 °C CH_2N_2 (3 ml, conc. ≤ 0.64 M in Et_2O; ca. 25 eq.). The cooling bath was subsequently removed and once the temperature of the mixture reached –60 °C, the reaction was quenched immediately with glacial acetic acid (4 ml). Evaporation and re-dissolution in a minimum amount of CH_2Cl_2, followed by precipitation with hexane, afforded **117** as a yellow powder in 98 % yield (107 mg, 0.070 mmol).

TLC (SiO_2, CH_2Cl_2): R_f 0.28. M.p. : 210–220 °C (decomp.). UV/VIS (λ_{max} (ε) in CH_2Cl_2): 346 (sh, 28300), 318 (sh, 46700), 288 (71100), 249 (76000). IR (KBr): 2980*w*, 2934*w*, 1744*s*, 1558*w*, 1465*m*, 1445*m*, 1390*m*, 1368*m*, 1296*m*, 1256*s*, 1220*s*, 1095*m*, 1078*m*, 1034*m*, 860*w*, 720*w*, 544*w*. ^{1}H-NMR (500 MHz, $CDCl_3$): 4.80 (*d*, *J* = 10.9, 2 H); 4.40-4.20 (*m*, 20 H); 3.02 (*d*, *J* = 10.9, 2 H); 1.35-1.25 (*m*, 30 H). ^{13}C-NMR (125 MHz, $CDCl_3$): 164.31; 164.13; 164.06; 164.01; 163.81; 163.74; 163.63; 147.26; 146.70; 145.93; 145.89; 145.72; 145.52; 145.45; 145.02; 143.98; 143.29; 143.07; 142.58; 141.49; 141.43 ; 141.36; 140.43; 140.13; 140.03; 139.72; 139.58; 139.43;

135.88; 133.79; 133.75; 132.31; 117.34 ; 70.19; 69.26; 69.02; 68.19; 66.98; 62.76; 62.71; 62.69; 62.62; 62.34; 60.32; 45.63; 45.30; 44.45; 43.52; 14.09; 14.04; 14.01; 13.97. FAB-MS: 1539.1 (100, M^+; calc. for $^{13}C^{12}C_{96}H_{54}O_{20}$: 1539.3), 1525.1 (7, [$M$ - CH_2]$^+$), 1511.1 (4, [M - 2 CH_2]$^+$), 1494.1 (29, [M - C_2H_5O]$^+$), 1380.0 (5, [M - $C(CO_2CH_2CH_3)_2$]$^+$), 719.8 (16, C_{60}^+).

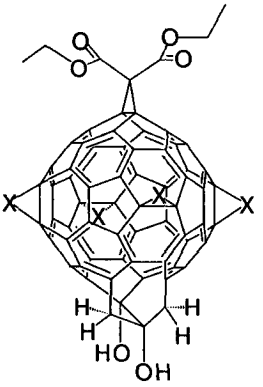

X = $C(CO_2Et)$

Decaethyl 1,9-dihydro-3'H,3''H,3'''H,3''''H,3'''''H-pentakis(cyclopropa)[16,17:21,40:30,31:44,45:52,60] 1,9-dihydroxy-[1,2(2a):1,5(5a)]-bishomo[5,6]fullerene-C_{60}-I_h-3',3',3'',3'',3''',3''',3'''',3'''',3''''',3'''''-decacarboxylate **119**:

To a soln. of **117** (30 mg, 0.019 mmol) in CH_2Cl_2 (30 ml), was added at RT an aq. soln. of $KMnO_4$ and [18]crown-6 (2.5 ml, 0.01 M $KMnO_4$; 0.01 M [18]crown-6). The intermediate manganate complex was hydrolyzed after 3 h by addition of 3 ml of glacial acetic acid and stirring for an additional 2 h at RT. The reaction was subsequently quenched with aq. $NaHCO_3$, and the soln. were filtered and washed with sat. aq. $NaHCO_3$, sat. aq. NaCl solution, and twice with H_2O. The aqueous phase was re-extracted with CH_2Cl_2, and the combined organic phases were dried (Na_2SO_4). CC (SiO_2-*H*, CH_2Cl_2/AcOEt 1:1), evaporation, and re-dissolution in a minimum amount of CH_2Cl_2, followed by precipitation with pentane, afforded **119** (26 mg, 0.017 mmol) in 85% yield as a bright yellow solid.

TLC (SiO_2, AcOEt) R_f 0.8. IR ($CHCl_3$): 3605*m* (O-H, free), 3464*w* , 3008*m*, 1739*s*, 1602*s*, 1256*s*. ^{1}H-NMR (200 MHz, $CDCl_3$): 4.89 (br., 2 H); 4.50-4.15 (*m*, 22 H); 3.91 (*d*, *J* = 11.6, 2 H). FAB-MS: 1573.2 (84, M^+; calc. for $^{13}C^{12}C_{96}H_{56}O_{22}$: 1573.3), 1556.4 (50, $[M - H_2O]^+$), 1539.3 (10, $[M - 2\ OH]^+$), 1528.4 (24, $[M + H - C_2H_5O]^+$), 1527.3 (28, $[M - C_2H_5O]^+$), 1510.5 (10, $[M - H_2O - C_2H_5O]^+$), 1417.1 (7, $[M - C(CO_2CH_2CH_3)_2]^+$), 719.9 (40, C_{60}^+).

6.6 Kinetic Data for the Dinitrogen Extrusion from 95a

Rate Constants

T [°C]	**96a**(t)	**96a**(t) corrected	**95a**(t)	t [min]	t [s]	ln([**96a**](t)/[**95a**(t)+1)
40	785.9	758.6293	6317.9	0	0	
	911.2	879.5814	6537.2	10	600	
	988.4	954.1025	6827.2	20	1200	0.130809107
	1177.4	1136.544	7121.9	30	1800	0.148061648
	1334.9	1288.579	7113.1	40	2400	0.166493412
	1408	1359.142	7055.7	50	3000	0.176161251
	1564.5	1510.212	7066.9	60	3600	0.193675349
	1632.8	1576.142	6644.5	70	4200	0.212858863
	1812.6	1749.703	6955.2	80	4800	0.224396849
	1947	1879.439	6869.3	90	5400	0.241847367
	2059.7	1988.228	6745.2	100	6000	0.258326821
	1104.6	1066.27	3361	110	6600	0.275544593
	2026.6	1956.277	4569.3	135	8100	0.356369358
	3483.3	3362.429	5333.9	195	11700	0.488818305
	3200.2	3089.15	4244.8	225	13500	0.546819548
	3732.2	3602.69	4487.3	255	15300	0.58937631
	3719.2	3590.14	3978.5	285	17100	0.643108531
	4067.4	3926.26	3991.6	315	18900	0.684928814
	4008.1	3869.02	3527.4	345	20700	0.740435044
(not used)	(3677.1)	(3549.505)	(2937.5)	420	25200	(0.792242066)
						k=3.269± 0.059E-5
50	1286.1	1241.472	6952.2	0	0	
	1251.6	1208.169	7238	8	480	
	1096.1	1058.065	3812.4	17	1020	
	2347.7	2266.235	5930.2	30	1800	0.323641364
	3049.9	2944.068	5256.4	45	2700	0.444744844
	3552.3	3429.035	4597.4	60	3600	0.557249543
	3961.9	3824.422	3624.5	100	6000	0.720352976
	4368.9	4217.3	2368.2	121	7260	1.02274009
	4549	4391.15	2154.1	134	8040	1.111366593
	4706.1	4542.8	1781.1	149	8940	1.267104955

	4743.1	4578.51	1313.8	199	11940	1.500724409
	4896.5	4726.59	722.7	241	14460	2.020246406
	4918.2	4747.54	604.6	269	16140	2.180684678
	4887.6	4718	303.3	369	22140	2.806721729
						k=1.257± 0.037E-4
60	1080.2	1042.717	7042.4	0	0	
	1753	1692.171	6852.2	9	540	
	2594.7	2504.664	5089.8	16	960	
	3703.9	3575.37	4106.1	25	1500	0.626337262
	4248.8	4101.37	3450.4	33	1980	0.783291807
	4438.3	4284.29	2749.5	40	2400	0.939306602
	4655.5	4493.95	1578.1	50	3000	1.347474683
	4767	4601.59	1480.7	58	3480	1.412866321
	4856.1	4687.59	837.9	67	4020	1.886228449
	4930.1	4759.03	539.9	80	4800	2.283876255
	4986.9	4813.855	296.7	108	6480	2.846341761
						k=4.71±0.24E-4
67	883.8	853.132	6943.2	0	0	
	1035.8	999.858	2382.7	6	360	0.35039793
	2089.2	2016.7	3573.9	13	780	0.447429179
	4777.6	4611.82	1695.1	20	1200	1.313905707
	4950.8	4779.01	1027	28	1680	1.732251657
	5030.4	4855.85	497.3	37	2220	2.376246986
	5129.9	4951.89	150.4	45	2700	3.524146326
						k=1.34±0.13E-3
75	981.5	947.442	7462.1	0	0	
	1011.2	976.111	7769	6	360	0.118353345
	4583.5	4424.45	3063.5	12	720	0.893737009
	4797.7	4631.22	1016.5	18	1080	1.71488657
	5272.8	5089.83	125.6	24	1440	3.726274564
	5712.5	5514.276	196.6	31	1860	3.368956498
						k=2.49±0.52E-3

Arrheniusplot

T [°C]	T [K]	1/T [K^{-1}]	ln k	s (ln k)
40	313.15	0.00319336	−10.2383	0.01809
50	323.15	0.00309454	−8.9814	0.02932
60	333.15	0.00300165	−7.6595	0.04994
67	340.15	0.00293988	−6.6132	0.09709
75	348.15	0.00287233	−5.9969	0.20963

Weighted linear Regression

Coefficient estimates

	Estimate	Std. Error
Variable	−13969.6	258.778
Constant	34.2965	0.814649

r^2	Sigma hat	Number of cases	Degrees of freedom
0.9989	1.2819	5	3

$\Delta H^{\neq}$ =27.7±1.6 kcal mol^{-1} (with t_s (df=3, 95%) = 3.18244...)

$\Delta S^{\neq}$ =9.22cal $mol^{-1}K^{-1}$; s ($\Delta S^{\neq}$) =55.50 cal $mol^{-1}K^{-1}$

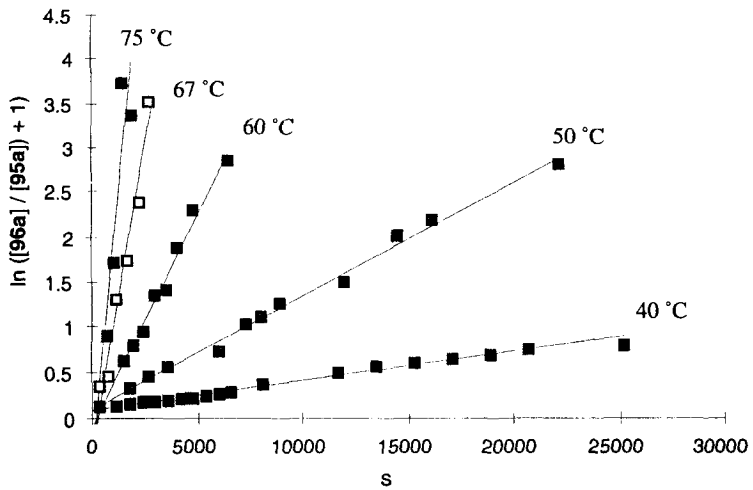

Figure 59 Depiction of linear the regressions of $\ln\left(\frac{[96a](t)}{[95a](t)}+1\right)$ at 40, 50, 60, 67, and 75 °C *vs.* t-t_0 used for determining k (T).

7. Literature

[1] P. E. Eaton, T. W. Cole Jr., *J. Am. Chem. Soc.* **1964**, *86*, 3157-3158. Cubane.

[2] L. A. Paquette, R. J. Ternansky, D. W. Balogh, G. Kentgen, *J. Am. Chem. Soc.* **1983**, *105*, 5446-5450. Total Synthesis of Dodecahedrane.

[3] a) R. C. Haddon, *Acc. Chem. Res.* **1992**, *25*, 127-133. Electronic Structure, Conductivity, and Superconductivity of Alkali Metal Doped C_{60}. b) A. F. Hebard, *PHYSICS TODAY* **1992**, 26-32. Superconductivity in Doped Fullerenes.

[4] A. F. Hebard, M. J. Rosseinsky, R. C. Haddon, D. W. Murphy, S. H. Glarum, T. T. M. Palstra, A. P. Ramirez, A. R. Kortan, *Nature (London)* **1991**, *350*, 600-601. Superconductivity at 18 K in Potassium-doped C_{60}.

[5] E. A. Rohlfing, D. M. Cox, A. Kaldor, *J. Chem. Phys.* **1984**, *81*, 3322-3330. Production and Characterization of Supersonic Carbon Cluster Beams.

[6] H. W. Kroto, J. R. Heath, S. C. O'Brien, R. F. Curl, R. E. Smalley, *Nature (London)* **1985**, *318*, 162-163. C_{60}: Buckminsterfullerene.

[7] W. Krätschmer, L. D. Lamb, K. Fostiropoulos, D. R. Huffman, *Nature (London)* **1990**, *347*, 354-358. Solid C_{60}: A New Form of Carbon.

[8] W. Krätschmer, K. Fostiropoulos, D. R. Huffman, *Chem. Phys. Lett.* **1990**, *170*, 167-170. The Infrared and Ultraviolet Absorption Spectra of Laboratory-Produced Carbon Dust: Evidence for the Presence of the C_{60} Molecule.

[9] Z. C. Wu, D. A. Jelski, T. F. George, *Chem. Phys. Lett.* **1987**, *137*, 291-294. Vibrational Motions of Buckminsterfullerene.

[10] S. J. Cyvin, E. Brendsdal, B. N. Cyvin, J. Brunvoll, *Chem. Phys. Lett.* **1988**, *143*, 377-380. Molecular Vibrations of Footballene.

[11] R. E. Stanton, M. D. Newton, *J. Phys. Chem.* **1988**, *92*, 2141-2145. Normal Vibrational Modes of Buckminsterfullerene.

[12] D. E. Weeks, W. G. Harter, *J. Chem. Phys.* **1989**, *90*, 4744-4771. Rotation-Vibration Spectra of Icosahedral Molecules. II. Icosahedral Symmetry, Vibrational Eigenfrequencies, and Normal Modes of Buckminsterfullerene.

[13] R. L. Whetten, M. M. Alvarez, S. J. Anz, K. E. Schriver, R. D. Beck, F. N. Diederich, Y. Rubin, R. Ettl, C. S. Foote, A. P. Darmanyan, J. W. Arbogast, *Mat. Res. Soc. Symp. Proc.* **1991**, *206*, 639-651. Spectroscopic and Photophysical Properties of the Soluble C_n Molecules, n=60, 70, 76/78, 84.

[14] H. Ajie, M. M. Alvarez, S. J. Anz, R. D. Beck, F. Diederich, K. Fostiropoulos, D. R. Huffman, W. Krätschmer, Y. Rubin, K. E. Schriver, D. Sensharma, R. L. Whetten, *J. Phys. Chem.* **1990**, *94*, 8630-8633. Characterization of the Soluble All-Carbon Molecules C_{60} and C_{70}.

[15] R. Taylor, J. P. Hare, A. K. Abdul-Sada, H. W. Kroto, *J. Chem. Soc., Chem. Commun.* **1990**, 1423-1425. Isolation, Separation and Characterisation of the Fullerenes C_{60} and C_{70}: The Third Form of Carbon.

[16] J. R. Heath, S. C. O'Brien, Q. Zhang, Y. Liu, R. F. Curl, H. W. Kroto, F. K. Tittel, R. E. Smalley, *J. Am. Chem. Soc.* **1985**, *107*, 7779-7780. Lanthanum Complexes of Spheroidal Carbon Shells.

[17] H. W. Kroto, *Nature (London)* **1987**, *329*, 529-531. The Stability of the Fullerenes Cn, with n=24, 28, 32, 36, 50, 60 and 70.

[18] F. Diederich, R. Ettl, Y. Rubin, R. L. Whetten, R. Beck, M. Alvarez, S. Anz, D. Sensharma, F. Wudl, K. C. Khemani, A. Koch, *Science (Washington D.C.)* **1991**, *252*, 548-551. The Higher Fullerenes: Isolation and Characterization of C_{76}, C_{84}, C_{90}, C_{94}, and $C_{70}O$, an Oxide of D_{5h}-C_{70}.

[19] R. Ettl, I. Chao, F. Diederich, R. L. Whetten, *Nature (London)* **1991**, *353*, 149-153. Isolation of C_{76}, a Chiral (D_2) Allotrope of Carbon.

[20] F. Diederich, R. L. Whetten, C. Thilgen, R. Ettl, I. Chao, M. M. Alvarez, *Science (Washington D.C.)* **1991**, *254*, 1768-1770. Fullerene Isomerism: Isolation of C_{2v}-C_{78} and D_3-C_{78}.

[21] K. Kikuchi, N. Nakahara, T. Wakabayashi, S. Suzuki, H. Shiromaru, Y. Miyake, K. Saito, I. Ikemoto, M. Kainosho, Y. Achiba, *Nature (London)* **1992**, *357*, 142-145. NMR Characterizations of Isomers of C_{78}, C_{82} and C_{84} Fullerenes.

[22] F. H. Hennrich, R. H. Michel, A. Fischer, S. Richard-Schneider, S. Gilb, M. M. Kappes, D. Fuchs, M. Bürk, K. Kobayashi, S. Nagase, *Angew. Chem.* **1996**, *108*, 1839-1841; *Angew. Chem. Int. Ed.* **1996**, *35*, 1732-1734. Isolation and Characterization of C_{80}.

[23] R. F. Curl, R. E. Smalley, *Science (Washington D.C.)* **1988**, *242*, 1017-1022. Probing C_{60}.

[24] R. E. Haufler, J. Conceicao, L. P. F. Chibante, Y. Chai, N. E. Byrne, S. Flanagan, M. M. Haley, S. C. O'Brien, C. Pan, Z. Xiao, W. E. Billups, M. A. Ciufolini, R. H. Hauge, J. L. Margrave, L. J. Wilson, R. F. Curl, R. E. Smalley, *J. Phys. Chem.* **1990**, *94*, 8634-8636. Efficient Production of C_{60} (Buckminsterfullerene), $C_{60}H_{36}$, and the Solvated Bucky Ion.

[25] W. A. Scrivens, J. M. Tour, *J. Org. Chem.* **1992**, *57*, 6932-6936. Synthesis of Gram Quantities of C_{60} by Plasma Discharge in a Modified Round-Bottomed Flask - Key Parameters for Yield Optimization and Purification.

[26] T. J. S. Dennis, T. Kai, T. Tomiyama, H. Shinohara, *Chem. Commun.* **1998**, 619-620. Isolation and Characterization of the Two Major Isomers of [84]Fullerene (C_{84}).

[27] A. L. Balch, A. S. Ginwalla, J. W. Lee, B. C. Noll, M. M. Olmstead, *J. Am. Chem. Soc.* **1994**, *116*, 2227-2228. Partial Separation and Structural Characterization of C_{84} Isomers by Crystallization of $(\eta^2$-$C_{84})Ir(Co)Cl(P(C_6H_5)_3)_2$.

[28] M. S. Meier, J. P. Selegue, *J. Org. Chem.* **1992**, *57*, 1924-1926. Efficient Preparative Separation of C_{60} and C_{70} - Gel Permeation Chromatography of Fullerenes Using 100-Percent Toluene as Mobile Phase.

[29] L. Isaacs, A. Wehrsig, F. Diederich, *Helv. Chim. Acta* **1993**, *76*, 1231-1250. Improved Purification of C_{60} and Formation of σ-Homoaromatic and π-Homoaromatic Methano-Bridged Fullerenes by Reaction with Alkyl Diazoacetates.

[30] W. A. Scrivens, P. V. Bedworth, J. M. Tour, *J. Am. Chem. Soc.* **1992**, *114*, 7917-7919. Purification of Gram Quantities of C_{60}. A New Inexpensive and Facile Method.

[31] X. Zhou, Z. Gu, Y. Wu, Y. Sun, Z. Jin, Y. Xiong, B. Sun, Y. Wu, H. Fu, J. Wang, *Carbon* **1994**, *32*, 935-937. Separation of C_{60} and C_{70} Fullerenes in Gram Quantities by Fractional Crystallization.

[32] A. S. Koch, K. C. Khemani, F. Wudl, *J. Org. Chem.* **1991**, *56*, 4543-4545. Preparation of Fullerenes with a Simple Benchtop Reactor.

[33] D. E. Manolopoulos, *Chem. Phys. Lett.* **1992**, *192*, 330. Comment on "Favourable Structures for Higher Fullerenes".

[34] P. W. Fowler, *Contemp. Phys.* **1996**, *37*, 235-247. Fullerene Stability and Structure.

[35] C. Piskoti, J. Yarger, A. Zettl, *Nature (London)* **1998**, *393*, 771-774. C_{36}, a New Carbon Solid.

[36] T. G. Schmalz, W. A. Seitz, D. J. Klein, G. E. Hite, *Chem. Phys. Lett.* **1986**, *130*, 203-207. C_{60} Carbon Cages.

[37] T. G. Schmalz, W. A. Seitz, D. J. Klein, G. E. Hite, *J. Am. Chem. Soc.* **1988**, *110*, 1113-1127. Elemental Carbon Cages.

[38] P. W. Fowler, D. E. Manolopoulos, 'An Atlas of Fullerenes', Clarendon Press, Oxford, 1995.

[39] a) N. L. Allinger, *J. Am. Chem. Soc.* **1977**, 8127-8134. Conformational Analysis. 130. MM2. A Hydrocarbon Force Field Utilizing V_1 and V_2 Torsional Terms. b) U. Burkert, N. L. Allinger, 'Molecular Mechanics', American Chemical Society, Washington D.C., 1982.

[40] S. J. Austin, P. W. Fowler, D. E. Manolopoulos, G. Orlandi, F. Zerbetto, *J. Phys. Chem.* **1995**, *99*, 8076-8081. Structural Motifs and the Stability of Fullerenes.

[41] B. A. Hess Jr., L. J. Schaad, *J. Org. Chem.* **1986**, *51*, 3902-3903. The Stability of Footballene.

[42] A. D. J. Haymet, *J. Am. Chem. Soc.* **1986**, *108*, 319-321. Footballene: A Theoretical Prediction for the Stable, Truncated Icosahedral Molecule C_{60}.

[43] D. J. Klein, T. G. Schmalz, G. E. Hite, W. A. Seitz, *J. Am. Chem. Soc.* **1986**, *108*, 1301-1302. Resonance in C_{60}, Buckminsterfullerene.

[44] D. J. Klein, W. A. Seitz, T. G. Schmalz, *Nature (London)* **1986**, *323*, 703-706. Icosahedral Symmetry Carbon Cage Molecules.

[45] R. Taylor, *Tetrahedron Lett.* **1991**, *32*, 3731-3734. A Valence Bond Approach to Explaining Fullerene Stabilities.

[46] J.-I. Aihara, S. Oe, M. Yoshida, E. Osawa, *J. Comput. Chem.* **1996**, *17*, 1387-1394. Further Test of the Isolated Pentagon Rule: Thermodynamic and Kinetic Stabilities of C_{84} Fullerene Isomers.

[47] J.-I. Aihara, *J. Am. Chem. Soc.* **1995**, *117*, 4130-4136. Bond Resonance Energy and Verification of the Isolated Pentagon Rule.

[48] E. E. B. Campbell, P. W. Fowler, D. Mitchell, F. Zerbetto, *Chem. Phys. Lett.* **1996**, *250*, 544-548. Increasing Cost of Pentagon Adjacency for Larger Fullerenes.

[49] C. S. Yannoni, R. D. Johnson, G. Meijer, D. S. Bethune, J. R. Salem, *J. Phys. Chem.* **1991**, *95*, 9-10. ^{13}C NMR Study of the C_{60} Cluster in the Solid State: Molecular Motion and Carbon Chemical Shift Anisotropy.

[50] R. Tycko, R. C. Haddon, G. Dabbagh, S. H. Glarum, D. C. Douglass, A. M. Mujsce, *J. Phys. Chem.* **1991**, *95*, 518-520. Solid-State Magnetic Resonance Spectroscopy of Fullerenes.

[51] J. M. Hawkins, A. Meyer, T. A. Lewis, S. Loren, F. J. Hollander, *Science (Washington D.C.)* **1991**, *252*, 312-313. Crystal Structure of Osmylated C_{60}: Confirmation of the Soccer Ball Framework.

[52] P. J. Fagan, J. C. Calabrese, B. Malone, *Science (Washington D.C.)* **1991**, *252*, 1160-1161. The Chemical Nature of Buckminsterfullerene (C_{60}) and the Characterization of a Platinum Derivative.

[53] S. Liu, Y. Lu, M. M. Kappes, J. A. Ibers, *Science (Washington D.C.)* **1991**, *254*, 408-410. The Structure of the C_{60} Molecule: X-Ray Crystal Structure Determination of a Twin at 110 K.

[54] W. I. F. David, R. M. Ibberson, J. C. Matthewman, K. Prassides, T. J. S. Dennis, J. P. Hare, H. W. Kroto, R. Taylor, D. R. M. Walton, *Nature (London)* **1991**, *353*, 147-149. Crystal Structure and Bonding of Ordered C_{60}.

[55] H.-B. Bürgi, E. Blanc, D. Schwarzenbach, S. Liu, Y. Lu, M. M. Kappes, J. A. Ibers, *Angew. Chem.* **1992**, *104*, 667-669; *Angew. Chem. Int. Ed.* **1992**, *31*, 640-643. The Structure of C_{60}: Orientational Disorder in the Low-Temperature Modification of C_{60}.

[56] K. Hedberg, L. Hedberg, D. S. Bethune, C. A. Brown, H. C. Dorn, R. D. Johnson, M. De Vries, *Science (Washington D.C.)* **1991**, *254*, 410-412. Bond Lengths in Free Molecules of Buckminsterfullerene, C_{60}, from Gas-Phase Electron Diffraction.

[57] C. S. Yannoni, P. P. Bernier, D. S. Bethune, G. Meijer, J. R. Salem, *J. Am. Chem. Soc.* **1991**, *113*, 3190-3192. NMR Determination of the Bond Lengths in C_{60}.

[58] J. D. Crane, P. B. Hitchcock, H. W. Kroto, R. Taylor, D. R. M. Walton, *J. Chem. Soc., Chem. Commun.* **1992**, 1764-1765. Preparation and Characterisation of C_{60}(Ferrocene)$_2$.

[59] Q. Zhu, D. E. Cox, J. E. Fischer, K. Kniaz, A. R. McGhie, O. Zhou, *Nature (London)* **1992**, *355*, 712-714. Intercalation of Solid C_{60} with Iodine.

[60] A. L. Balch, J. W. Lee, B. C. Noll, M. M. Olmstead, *J. Chem. Soc., Chem. Commun.* **1993**, 56-58. Disorder in a Crystalline Form of Buckminsterfullerene C_{60}·4C_6H_6.

[61] a) A. Streitwieser Jr., 'Molecular Orbital Theory for Organic Chemists', Wiley & Sons, New York, 1661. b) E. Heilbronner, H. Bock, 'Das HMO-Modell und seine Anwendung', Verlag Chemie, GmbH, Weinheim, 1970.

[62] R. C. Haddon, L. T. Scott, *Pure Appl. Chem.* **1986**, *58*, 137-142. π-Orbital Conjugation and Rehybridization in Bridged Annulenes and Deformed Molecules in General: π-Orbital Axis Vector Analysis.

[63] R. C. Haddon, L. E. Brus, K. Raghavachari, *Chem. Phys. Lett.* **1986**, *125*, 459-464. Electronic Structure and Bonding in Icosahedral C_{60}.

[64] R. C. Haddon, *Science (Washington D.C.)* **1993**, *261*, 1545-1550. Chemistry of the Fullerenes: The Manifestation of Strain in a Class of Continuous Aromatic Molecules.

[65] V. Elser, R. C. Haddon, *Nature (London)* **1987**, *325*, 792-794. Icosahedral C_{60}: an Aromatic Molecule with a Vanishingly Small Ring Current Magnetic Susceptibility.

[66] K. Balasubramanian, *Chem. Phys. Lett.* **1994**, *224*, 325-332. Laplacian Polynomials of Fullerenes (C_{20}-C_{40}).

[67] M. Solà, J. Mestres, M. Duran, *J. Phys. Chem.* **1995**, *99*, 10752-10758. Molecular Size and Pyramidalization: Two Keys for Understanding the Reactivity of Fullerenes.

[68] a) N. G. Rondan, M. N. Paddon-Row, P. Caramella, K. N. Houk, *J. Am. Chem. Soc.* **1981**, *103*, 2436-2438. Nonplanar Alkenes and Carbonyls: a Molecular Distortion which Parallels Addition Stereoselectivity. b) P. Caramella, N. G. Rondan, M. N. Paddon-Row, K. N. Houk, *J. Am. Chem. Soc.* **1981**, *103*, 2438-2440. Origin of π-Facial Stereoselectivity in Additions to π-Bonds: Generality of the Anti-Periplanar Effect. c) K. N. Houk, N. G. Rondan, F. K. Brown, *Isr. J. Chem.* **1983**, *23*, 3-9. Electronic Structures and Reactivities of Pyramidal Alkenes and Carbonyls.

[69] a) D. A. Hrovat, W. T. Borden, *J. Am. Chem. Soc.* **1988**, *110*, 4710-4718. Ab Initio Calculations of the Olefin Strain Energies of Some Pyramidalized Alkenes. b) J. M. Smith, D. A. Hrovat, W. T. Borden, M. Allan, K. R. Asmis, C. Bulliard, E. Haselbach, U. C. Meier, *J. Am. Chem. Soc.* **1993**, *115*, 3816-3817. Synthesis and Spectroscopy of Tricyclo[3.3.3.0(3,7)]undec-3(7)-ene - Confirmation of Computational Predictions Regarding the Effects of Pyramidalization on Alkene Ionization Energies and Electron Affinities.

[70] K. Menke, H. Hopf, *Angew. Chem.* **1976**, *88*, 152-153; *Angew. Chem. Int. Ed.* **1976**, *15*, 165-166. Cyclopropanation of [2.2]Paracyclophanes.

[71] A. de Meijere, R. Näder, *Angew. Chem.* **1976**, *88*, 153-154; *Angew. Chem. Int. Ed.* **1976**, *15*, 166-167. Methylenation of [2.2]Paracyclophane-1,9-diene and [2.2]Paracyclophane.

[72] R. C. Haddon, *J. Am. Chem. Soc.* **1990**, *112*, 3385-3389. Measure of Nonplanarity in Conjugated Organic Molecules - Which Structurally Characterized Molecule Displays the Highest Degree of Pyramidalization.

[73] J. Cioslowski, 'Calculations on Fullerenes and Their Derivatives', Ed. D. G. Truhlar, Oxford University Press, New York, 1995.

[74] N. Matsuzawa, D. A. Dixon, T. Fukunaga, *J. Phys. Chem.* **1992**, *96*, 7594-7604. Semiempirical Calculations of Dihydrogenated Buckminsterfullerenes, $C_{60}H_2$.

[75] D. A. Dixon, N. Matsuzawa, T. Fukunaga, F. N. Tebbe, *J. Phys. Chem.* **1992**, *96*, 6107-6110. Patterns for Addition to C_{60}.

[76] J. Dias, *J. Chem. Educ.* **1989**, *66*, 1012-1015. A Facile Hückel Molecular Orbital Solution of Buckminsterfullerene Using Chemical Graph Theory.

[77] W. B. Brown, *Chem. Phys. Lett.* **1987**, *136*, 128-133. High Symmetries in Quantum Chemistry.

[78] P. W. Fowler, J. Woolrich, *Chem. Phys. Lett.* **1986**, *127*, 78-83. π-Systems in Three Dimensions.

[79] I. László, L. Udvardi, *Chem. Phys. Lett.* **1987**, *136*, 418-422. On the Geometrical Structure and UV Spectrum of the Truncated Icosahedral C_{60} Molecule.

[80] J. Feng, J. Li, Z. Wang, M. C. Zerner, *Int. J. Quantum Chem.* **1990**, *37*, 599-607. Quantum-Chemical Investigation of Buckminsterfullerene and Related Carbon Clusters (I) : The Electronic Structure and UV Spectra of Buckminsterfullerene, and Other C_{60} Cages.

[81] P. W. Fowler, P. Lazzeretti, R. Zanasi, *Chem. Phys. Lett.* **1990**, *165*, 79-86. Electric and Magnetic Properties of the Aromatic Sixty-Carbon Cage.

[82] S. H. Yang, C. L. Pettiette, J. Conceicao, O. Cheshnovsky, R. E. Smalley, *Chem. Phys. Lett.* **1987**, *139*, 233-238. UPS of Buckminsterfullerene and Other Large Clusters of Carbon.

[83] C. Brink, L. H. Andersen, P. Hvelplund, D. Mathur, J. D. Voldstad, *Chem. Phys. Lett.* **1995**, *233*, 52-56. Laser Photodetachment of C_{60}^- and C_{70}^- ions Cooled in a Storage Ring.

[84] L.-S. Wang, J. Conceicao, C. Jin, R. E. Smalley, *Chem. Phys. Lett.* **1991**, *182*, 5-11. Threshold Photodetachment of Cold C_{60}^-.

[85] Q. Xie, E. Perez-Cordero, L. Echegoyen, *J. Am. Chem. Soc.* **1992**, *114*, 3978-3980. Electrochemical Detection of C_{60}^{6-} and C_{70}^{6-} - Enhanced Stability of Fullerides in Solution.

[86] Y. Ohsawa, T. Saji, *J. Chem. Soc., Chem. Commun.* **1992**, 781-782. Electrochemical Detection of C_{60}^{6-} at Low Temperature.

[87] F. Paolucci, M. Marcaccio, S. Roffia, G. Orlandi, F. Zerbetto, M. Prato, M. Maggini, G. Scorrano, *J. Am. Chem. Soc.* **1995**, *117*, 6572-6580. Electrochemical Monitoring of Valence Bond Isomer Interconversion in Bipyridyl-C_{61} Anions.

[88] J. A. Zimmerman, J. R. Eyler, S. B. H. Bach, S. W. McElvany, *J. Chem. Phys.* **1991**, *94*, 3556-3562. Magic Number Carbon Clusters: Ionization Potentials and Selective Reactivity.

[89] D. L. Lichtenberger, K. W. Nebesny, C. D. Ray, D. R. Huffman, L. D. Lamb, *Chem. Phys. Lett.* **1991**, *176*, 203-208. Valence and Core Photoelectron Spectroscopy of C_{60}-Buckminsterfullerene.

[90] R. K. Yoo, B. Ruscic, J. Berkowitz, *J. Chem. Phys.* **1992**, *96*, 911-918. Vacuum Ultraviolet Photoionization Mass Spectrometric Study of C_{60}.

[91] J. de Vries, H. Steger, B. Kamke, C. Menzel, B. Weisser, W. Kamke, I. V. Hertel, *Chem. Phys. Lett.* **1992**, *188*, 159-162. Single-Photo Ionization of C_{60}^- and C_{70}^-Fullerene with Synchrotron Radiation: Determination of the Ionization Potential of C_{60}.

[92] Q. Xie, F. Arias, L. Echegoyen, *J. Am. Chem. Soc.* **1993**, *115*, 9818-9819. Electrochemically-Reversible, Single-Electron Oxidation of C_{60} and C_{70}.

[93] Y. Yang, F. Arias, L. Echegoyen, L. P. F.- Chibante, S. Flanagan, A. Robertson, L. J. Wilson, *J. Am. Chem. Soc.* **1995**, *117*, 7801-7804. Reversible Fullerene Electrochemistry: Correlation with the HOMO-LUMO Energy Difference for C_{60}, C_{70}, C_{76}, C_{78}, and C_{84}.

[94] H.-D. Beckhaus, C. Rüchardt, M. Kao, F. Diederich, C. S. Foote, *Angew. Chem.* **1992**, *104*, 69-70; *Angew. Chem. Int. Ed.* **1992**, *31*, 63-64. The Stability of Buckminsterfullerene C_{60} - Experimental Determination of the Heat of Formation.

[95] W. V. Steele, R. D. Chirico, N. K. Smith, W. E. Billups, P. R. Elmore, A. E. Wheeler, *J. Phys. Chem.* **1992**, *96*, 4731-4733. Standard Enthalpy of Formation of Buckminsterfullerene.

[96] T. Kiyobayashi, M. Sakiyama, *Fullerene Sci. Technol.* **1993**, *1*, 269-273. Combustion Calorimetric Studies on C_{60} and C_{70}.

[97] H. P. Diogo, M. E. Minas da Piedade, T. J. S. Dennis, J. P. Hare, H. W. Kroto, R. Taylor, D. R. M. Walton, *J. Chem. Soc., Faraday Trans.* **1993**, *89*, 3541-3544. Enthalpies of Formation of Buckminsterfullerene C_{60} and of the Parent Ions C_{60}^+, C_{60}^{2+}, C_{60}^{3+} and C_{60}^-.

[98] H.-D. Beckhaus, S. Verevkin, C. Rüchardt, F. Diederich, C. Thilgen, H.-U. ter Meer, H. Mohn, W. Müller, *Angew. Chem.* **1994**, *106*, 1033-1035; *Angew. Chem. Int. Ed.* **1994**, *33*, 996-998. C_{70} is More Stable than C_{60}: Experimental Determination of the Heat of Formation of C_{70}.

[99] C. K. Mathews, M. Sai Baba, T. S. Lakshmi Narasimhan, R. Balasubramanian, N. Sivaraman, T. G. Srinivasan, P. R. Vasudeva Rao, *J. Phys. Chem.* **1992**, *96*, 3566-3568. Vaporization Studies on Buckminsterfullerene.

[100] C. Pan, M. P. Sampson, Y. Chai, R. H. Hauge, J. L. Margrave, *J. Phys. Chem.* **1991**, *95*, 2944-2946. Heats of Sublimation from a Polycrystalline Mixture of C_{60} and C_{70}.

[101] R. D. Beck, P. S. John, M. M. Alvarez, F. Diederich, R. L. Whetten, *J. Phys. Chem.* **1991**, *95*, 8402-8409. Resilience of All-Carbon Molecules C_{60}, C_{70}, and C_{84}: A Surface-Scattering Time-of-Flight Investigation.

[102] a) N. L. Allinger, Y. H. Yuh, J.-H. Lii, *J. Am. Chem. Soc.* **1989**, *111*, 8551-8556. Molecular Mechanics. The MM3 Force Field for Hydrocarbons. 1. b) J.-H. Lii, N. L. Allinger, *J. Am. Chem. Soc.* **1989**, 8566-8575. Molecular Mechanics. The MM3 Force Field for Hydrocarbons. 2. Vibrational Frequencies and Thermodynamics. c) J.-H. Lii, N. L. Allinger, *J. Am. Chem. Soc.* **1989**, *111*, 8576-8582. Molecular Mechanics. The MM3 Force Field for Hydrocarbons. 3. The van der Waals' Potentials and Crystal Data for Ali phatic and Aromatic Hydrocarbons. d) N. Allinger, F. Li, L. Yan, *J. Comput. Chem.* **1990**, *11*, 848-867. Molecular Mechanics - The MM3 Force Field for Alkenes. e) N. L. Allinger, F. B. Li, L. Q. Yan, J. C. Tai, *J. Comput. Chem.* **1990**, *11*, 868-895. Molecular Mechanics (MM3) Calculations on Conjugated Hydrocarbons.

[103] J. M. Rudzinski, Z. Slanina, M. Togasi, E. Osawa, T. Iizuka, *Thermochim. Acta* **1988**, *125*, 155-162. Computational Study of Relative Stabilities of C_{60} (I_h) and C_{70} (D_{5h}) Gas-Phase Clusters.

[104] J. M. Schulman, R. L. Disch, M. A. Miller, R. C. Peck, *Chem. Phys. Lett.* **1987**, *141*, 45-48. Symmetrical Clusters of Carbon Atoms: The C_{24} and C_{60} Molecules.

[105] N. Matsuzawa, D. A. Dixon, *J. Phys. Chem.* **1992**, *96*, 6241-6247. Semiempirical Calculations of the Polarizability and Second-Order Hyperpolarizability of C_{60} , C_{70} , and Model Aromatic Compounds.

[106] M. Kolb, W. Thiel, *J. Comput. Chem.* **1993**, *14*, 37-44. MNDO Parameters for Helium - Optimization, Tests, and Application to Endohedral Fullerene Helium Complexes.

[107] D. Bakowies, W. Thiel, *J. Am. Chem. Soc.* **1991**, *113*, 3704-3714. MNDO Study of Large Carbon Clusters.

[108] R. L. Murry, J. R. Colt, G. E. Scuseria, *J. Phys. Chem.* **1993**, *97*, 4954-4959. How Accurate Are Molecular Mechanics Predictions for Fullerenes? A Benchmark Comparison with Hartree - Fock Self - Consistent Field Results.

[109] R. S. Ruoff, D. S. Tse, R. Malhotra, D. C. Lorents, *J. Phys. Chem.* **1993**, *97*, 3379-3383. Solubility of C_{60} in a Variety of Solvents.

[110] W. A. Scrivens, J. M. Tour, *J. Chem. Soc., Chem. Commun.* **1993**, 1207-1209. Potent Solvents for C_{60} and their Utility for the Rapid Acquisition of ^{13}C NMR Data for Fullerenes.

[111] R.S. Ruoff, R. Malhotra, D.L. Huestis, D.S. Tse, D.C. Lorents, *Nature (London)* **1993**, *362*, 140-141. Anomalous Solubility Behaviour of C_{60}.

[112] N. Sivaraman, R. Dhamodaran, I. Kaliappan, T. G. Srinivasan, P. R. Vasudeva Rao, C. K. Mathews, *J. Org. Chem.* **1992**, *57*, 6077-6079. Solubility of C_{60} in Organic Solvents.

[113] J. S. Murray, S. G. Gagarin, P. Politzer, *J. Phys. Chem.* **1995**, *99*, 12081-12083. Representation of C_{60} Solubilities in Terms of Computed Molecular Surface Electrostatic Potentials and Areas.

[114] A. L. Smith, E. Walter, M. V. Korobov, O. L. Gurvich, *J. Phys. Chem.* **1996**, *100*, 6775-6780. Some Enthalpies of Solution of C_{60} and C_{70}: Thermodynamics of the Temperature Dependence of Fullerene Solubility.

[115] D. Heymann, *Fullerene Sci. Technol.* **1996**, *4*, 509-515. Solubility of Fullerenes C_{60} and C_{70} in Seven Normal Alcohols and Their Deduced Solubility in Water.

[116] X. H. Zhou, J. B. Liu, Z. X. Jin, Z. N. Gu, Y. Q. Wu, Y. L. Sun, *Fullerene Sci. Technol.* **1997**, *5*, 285-290. Solubility of Fullerene C_{60} and C_{70} in Toluene *o*-Xylene, and Carbon Disulfide at Various Temperatures.

[117] M. T. Beck, G. Mandi, *Fullerene Sci. Technol.* **1997**, *5*, 291-310. Solubility of C_{60}; and references therein.

[118] N. Coustel, P. Bernier, R. Aznar, A. Zahab, J.-M. Lambert, P. Lyard, *J. Chem. Soc., Chem. Commun.* **1992**, 1402-1403. Purification of C_{60} by a Simple Crystallization Procedure.

[119] S. Leach, M. Vervloet, A. Desprès, E. Brèheret, J. P.- Hare, T. J. Dennis, H. W. Kroto, R. Taylor, D. R. W. Walton, *Chem. Phys.* **1992**, *160*, 451-466. Electronic Spectra and Transitions of the Fullerene C_{60}.

[120] Z. Gasyna, P. N. Schatz, J. P. Hare, T. J. Dennis, H. W. Kroto, R. Taylor, D. R. M. Walton, *Chem. Phys. Lett.* **1991**, *183*, 283-291. The Magnetic Circular Dichroism and Absorption Spectra of C_{60} Isolated in Ar Matrices.

[121] F. A. Cotten, 'Chemical Application of Group Theory', John Wiley & Sons, New York, 1990.

[122] J. Catalàn, J. L. Saiz, J. L. Laynez, N. Jagerovic, J. Elguero, *Angew. Chem.* **1995**, *107*, 86-88; *Angew. Chem. Int. Ed.* **1995**, *34*, 105-107. The Colors of C_{60} Solutions.

[123] O. Ermer, *Helv. Chim. Acta* **1991**, *74*, 1339-1351. 3:1 Molecular Complex of Hydroquinone and C_{60}.

[124] J. Catalàn, *New. J. Chem.* **1995**, *19*, 1233-1242. The Solvatochromism of C_{60} and its Color in Solution.

[125] T. Haino, M. Yanase, Y. Fukazawa, *Angew. Chem.* **1997**, *109*, 288-290. *Angew. Chem. Int. Ed.* **1997**, *36*, 259-260. New Supramolecular Complex of C_{60} Based on Calix[5]arene-Its Structure in the Crystal and in Solution.

[126] R. V. Bensasson, E. Bienvenüe, C. Fabre, J.-M. Janot, E. J. Land, V. Leboulaire, A. Rassat, S. Roux, P. Seta, *Chem. Eur. J.* **1998**, *4*, 270-278. Photophysical Properties of Three Methanofullerene Derivatives.

[127] L. Isaacs, F. Diederich, *Helv. Chim. Acta* **1993**, *76*, 2454-2464. Structures and Chemistry of Methanofullerenes - A Versatile Route into N-[(Methanofullerene)carbonyl]-Substituted Amino Acids.

[128] Y.-Z. An, J. L. Anderson, Y. Rubin, *J. Org. Chem.* **1993**, *58*, 4799-4801. Synthesis of α-Amino Acid Derivatives of C_{60} from 1,9-(4-Hydroxycyclohexano)- Buckminsterfullerene.

[129] N. Armaroli, F. Diederich, C. O. Dietrichbuchecker, L. Flamigni, G. Marconi, J. F. Nierengarten, J. P. Sauvage, *Chem. Eur. J.* **1998**, *4*, 406-416. A Copper(II)-Complexed Rotaxane with Two Fullerene Stoppers: Synthesis, Electrochemistry, and Photoinduced Processes.

[130] E. W. Godly, R. Taylor, *Pure Appl. Chem.* **1997**, *69*, 1411-1434. Nomenclature and Terminology of Fullerenes: A Preliminary Survey.

[131] T. Suzuki, Q. C. Li, K. C. Khemani, F. Wudl, *J. Am. Chem. Soc.* **1992**, *114*, 7301-7302. Dihydrofulleroid H_2C_{61} - Synthesis and Properties of the Parent Fulleroid.

[132] A. Curioni, P. Giannozzi, J. Hutter, W. Andreoni, *J. Phys. Chem.* **1995**, *99*, 4008-4014. $C_{61}H_2$ in Molecular and Solid Phases: Density-Functional Approach to Structural and Electronic Properties.

[133] F. Arias, L. Echegoyen, S. R. Wilson, Q. Lu, Q. Lu, *J. Am. Chem. Soc.* **1995**, *117*, 1422-1427. Methanofullerenes and Methanofulleroids have Different Electrochemical Behaviour at Negative Potentials.

[134] R. C. Haddon, *Nature (London)* **1995**, *378*, 249-255. Magnetism of the Carbon Allotropes.

[135] a) R. C. Haddon, L. F. Schneemeyer, J. V. Waszczak, S. H. Glarum, R. Tycko, G. Dabbagh, A. R. Kortan, A. J. Muller, A. M. Mujsce, M. J. Rosseinsky, S. M. Zahurak, A. V. Makhija, F. A. Thiel, K. Raghavachari, E. Cockayne, V. Elser, *Nature (London)* **1991**, *350*, 46-47. Experimental and Theoretical Determination of the Magnetic Susceptibility of C_{60} And C_{70}. b) R. S. Ruoff, D. Beach, J. Cuomo, T. McGuire, R. L. Whetten, F. Diederich, *J. Phys. Chem.* **1991**, *95*, 3457-3459. Confirmation of a Vanishingly Small Ring-Current Magnetic Susceptibility of Icosahedral C_{60}.

[136] A. Pasquarello, M. Schlüter, R. C. Haddon, *Science (Washington D.C.)* **1992**, *257*, 1660-1661. Ring Currents in Icosahedral C_{60}.

[137] A. Pasquarello, M. Schlüter, R. C. Haddon, *Physical Review A* **1993**, *47*, 1783-1789. Ring Currents in Topologically Complex Molecules : Application to C_{60}, C_{70}, and their Hexa-anions.

[138] R. Zanasi, P. W. Fowler, *Chem. Phys. Lett.* **1995**, *238*, 270-280. Ring Currents and Magnetisability in C_{60}.

[139] A. B. Smith III, R. M. Strongin, L. Brard, G. T. Furst, W. J. Romanow, K. G. Owens, R. J. Goldschmidt, R. C. King, *J. Am. Chem. Soc.* **1995**, *117*, 5492-

5502. Synthesis of Prototypical Fullerene Cyclopropanes and Annulenes. Isomer Differentiation via NMR and UV Spectroscopy.

[140] M. Prato, T. Suzuki, F. Wudl, V. Lucchini, M. Maggini, *J. Am. Chem. Soc.* **1993**, *115*, 7876-7877. Experimental Evidence for Segregated Ring Currents in C_{60}.

[141] M. Saunders, H. A. Jiménez-Vázquez, R. J. Cross, S. Mroczkowski, D. I. Freedberg, F. A. L. Anet, *Nature (London)* **1994**, *367*, 256-258. Probing the Interior of Fullerenes by ^{3}He NMR Spectroscopy of Endohedral ^{3}He@C_{60} and ^{3}He@C_{70}.

[142] M. Saunders, R. J. Cross, H. A. Jiménez-Vázquez, R. Shimshi, A. Khong, *Science (Washington D.C.)* **1996**, *271*, 1693-1697. Noble Gas Atoms Inside Fullerenes.

[143] M. Bühl, W. Thiel, H. Jiao, P. von Ragué Schleyer, M. Saunders, F. A. L. Anet, *J. Am. Chem. Soc.* **1994**, *116*, 6005-6006. Helium and Lithium NMR Chemical Shifts of Endohedral Fullerene Compounds: An ab Initio Study.

[144] J. Cioslowski, *Chem. Phys. Lett.* **1994**, *227*, 361-364. Endohedral Magnetic Shielding in Fullerenes. A GIAO CPHF Study.

[145] J. Cioslowski, *J. Am. Chem. Soc.* **1994**, *116*, 3619-3620. Endohedral Magnetic Shielding in the C_{60} Cluster.

[146] E. Shabtai, A. Weitz, R. C. Haddon, R. E. Hoffman, M. Rabinovitz, A. Khong, R. J. Cross, M. Saunders, ChengP.-C., L. T.Scott, *J. Am. Chem. Soc.* **1998**, *120*, 6389-6393. ^{3}He NMR of He@C_{60}^{6-} and He@C_{70}^{6-}. New Records for the Most Shielded and the Most Deshielded ^{3}He Inside a Fullerene.

[147] a) D. Cremer, E. Kraka, K. J. Szabo in 'The Chemistry of the Cyclopropyl Group', Ed. Z. Rappoport, John Wiley & Sons, 1995, p. 43-137. b) D. Cremer in 'The Chemistry of the Cyclopropyl Group', Ed. Z. Rappoport, John Wiley & Sons, 1995.

[148] A. B. Smith III, R. M. Strongin, L. Brard, W. J. Romanov, M. Saunders, H. A. Jiménez-Vázquez, R. J. Cross, *J. Am. Chem. Soc.* **1994**, *116*, 10831-10832. Synthesis and ^{3}He NMR Studies of C_{60} and C_{70} Epoxide, Cyclopropane, and Annulene Derivatives Containing Endohedral Helium.

[149] B. M. Trost, W. B. Herdle, *J. Am. Chem. Soc.* **1976**, *98*, 4080-4086. ^{13}C NMR and Ring Currents in Vinyl Cross-Linked Annulenes.

[150] L. T. Scott, M. S. Bratcher, S. Hagen, *J. Am. Chem. Soc.* **1996**, *118*, 8743-8744. Synthesis and Characterization of a $C_{36}H_{12}$ Fullerene Subunit.

[151] L. T. Scott, M. M. Hashemi, D. T. Meyer, H. B. Warren, *J. Am. Chem. Soc.* **1991**, *113*, 7082-7084. Corannulene. A Convenient New Synthesis.

[152] P. E. Hansen, *Org. Magn. Res.* **1979**, *12*, 109-142. The ^{13}C-NMR of Polycyclic Aromatic Compounds. A Review.

[153] R. D. Johnson, G. Meijer, J. R. Salem, D. S. Bethune, *J. Am. Chem. Soc.* **1991**, *113*, 3619-3621. 2D Nuclear Magnetic Resonance Study of the Structure of the Fullerene C_{70}.

[154] K.-A. Wang, A. M. Rao, P. C. Eklund, M. S. Dresselhaus, G. Dresselhaus, *Phys. Rev. B* **1993**, *48*, 11375-11380. Observation of Higher-Order Infrared Modes in Solid C_{60} Films.

[155] J-F. Nierengarten, T. Habicher, R. Kessinger, F. Cardullo, F. Diederich, V. Gramlich, J-P Gisselbrecht, C. Boudon, M. Gross, *Helv. Chim. Acta* **1997**, *80*, 2238-2276. Macrocyclisation on the Fullerene Core: Direct Regio- and Diastereoselective Multi-Functionalization of [60]Fullerene, and Synthesis of Fullerene-dendrimer Derivatives.

[156] L. Biczok, H. Linschitz, R. I. Walter, *Chem. Phys. Lett.* **1992**, *195*, 339-346. Extinction Coefficients of C_{60} Triplet Anion Radical, and One-Electron Reduction of the Triplet by Aromatic Donors.

[157] T. Ebbesen, K. Tanigaki, S. Kuroshima, *Chem. Phys. Lett.* **1991**, *181*, 501-504. Excited-State Properties of C_{60}.

[158] M. Wasielewski, M. O'Neil, K. Lykke, M. Pellin, D. Gruen, *J. Am. Chem. Soc.* **1991**, *113*, 2774-2776. Triplet States of Fullerenes C_{60} and C_{70} - Electron Paramagnetic Resonance Spectra, Photophysics, and Electronic Structures.

[159] M. Lee, Song O.-K., J.-C. Seo, D. Kim, Y. D. Su, S. M. Jin, S. K. Kim, *Chem. Phys. Lett.* **1992**, *196*, 325-329. Low-Lying Electronically Excited States of C_{60} and C_{70} and Measurement of their Picosecond Transient Absorption in Solution.

[160] B. Ma, Y.-P. Sun, *J. Chem. Soc., Perkin Trans. 2* **1996**, 2157-2162. Fluorescence Spectra and Quantum Yields of [60]Fullerene and [70]Fullerene under Different Solvent Conditions. A Quantitative Examination Using a Near Infrared-Sensitive Emission Spectrometer.

[161] J. W. Arbogast, A. P. Darmanyan, C. S. Foote, Y. Rubin, F. N. Diederich, M. M. Alvarez, S. J. Anz, R. L. Whetten, *J. Phys. Chem.* **1991**, *95*, 11-12. Photophysical Properties of C_{60}.

[162] P.-M. Allemand, G. Srdanov, A. Koch, K. Khemani, F. Wudl, Y. Rubin, F. Diederich, M. M. Alvarez, S. J. Anz, R. L. Whetten, *J. Am. Chem. Soc.* **1991**, *113*, 2780-2781. The Unusual Electron Spin Resonance of Fullerene C_{60}.

[163] Y. Zeng, L. Biczok, H. Linschitz, *J. Phys. Chem.* **1992**, *96*, 5237-5239. External Heavy Atom Induced Phosphorescence Emission of Fullerenes: The Energy of Triplet C_{60}.

[164] R. R. Hung, J. J. Grabowski, *J. Phys. Chem.* **1991**, *95*, 6073-6075. A Precise Determination of the Triplet Energy of C_{60} by Photoacoustic Calorimetry.

[165] M. Terazima, N. Hirota, H. Shinohara, Y. Saito, *J. Phys. Chem.* **1991**, *95*, 9080-9085. Photothermal Investigation of the Triplet State of C_{60}.

[166] J. W. Arbogast, C. S. Foote, M. Kao, *J. Am. Chem. Soc.* **1992**, *114*, 2277-2279. Electron Transfer to Triplet C_{60}.

[167] C. S. Foote, *Top. Curr. Chem.* **1994**, *169*, 347-363. Photophysical and Photochemical Properties of Fullerenes.

[168] A. S. Boutorine, H. Tokuyama, M. Takasugi, H. Isobe, E. Nakamura, C. Hélène, *Angew. Chem.* **1994**, *106*, 2526-2529; *Angew. Chem. Int. Ed.* **1994**, *33*, 2462-2465. Fullerene-Oligonucleotide Conjugates: Photoinduced Sequence-Specific DNA Cleavage.

[169] a) A. W. Jensen, S. R. Wilson, D. I. Schuster, *Bioorg. Med. Chem.* **1996**, *4*, 767-779. Biological Applications of Fullerenes. b) L. L. Dugan, D. M. Turetsky, C. Du, D. Lobner, M. Wheeler, C. R. Almli, C. K.-F. Shen, T.-Y. Luh, D. W. Choi, T.-S. Lin, *Proc. Natl. Acad. Sci. USA* **1997**, *94*, 9434-9439. Carboxyfullerenes as Neuroprotective Agents. c) Y. N. Yamakoshi, T. Yagami, S. Sueyoshi, N. Miyata, *J. Org. Chem.* **1996**, *61*, 7236-7237. Acridine Adduct of [60]Fullerene with Enhanced DNA-Cleaving Activity. d) K. Irie, Y. Nakamura, H. Ohigashi, H. Tokuyama, S. Yamago, E. Nakamura, *Biosci. Biotechnol. Biochem.* **1996**, *60*, 1359-1361. Photocytotoxicity of Water-Soluble Fullerene Derivatives.

[170] Y.-Z. An, C.-H. B. Chen, J. L. Anderson, D. S. Sigman, C. S. Foote, Y. Rubin, *Tetrahedron* **1996**, *52*, 5179-5189. Sequence-Specific Modification of Guanosine in DNA by a C_{60}^- Linked Deoxyoligonucleotide: Evidence for a Non-Singlet Oxygen Mechanism.

[171] A. Hirsch, 'The Chemistry of the Fullerenes', Thieme Verlag, Stuttgart, 1994 and references cited therein.

[172] R. Taylor, D. R. M. Walton, *Nature (London)* **1993**, *363*, 685-693. The Chemistry of Fullerenes.

[173] F. Diederich, L. Isaacs, D. Philp, *Chem. Soc. Rev.* **1994**, *23*, 243-255. Syntheses, Structures, and Properties of Methanofullerenes; and references cited therein.

[174] a) A. Hirsch, *Synthesis (Stuttgart)* **1995**, 895-913. Addition Reactions of Buckminsterfullerene (C_{60}) and references cited therein. b) A. Hirsch, *Angew. Chem.* **1993**, *105*, 1189-1192; *Angew. Chem. Int. Ed.* **1993**, *32*, 1138-1141. The Chemistry of the Fullerenes: An Overview. c) A. Hirsch, *Chem. unserer Zeit* **1994**, *28*, 79-87. Chemistry of Fullerenes.

[175] a) M. Iyoda, M. Yoshida, *J. Synth. Org. Chem. Jpn.* **1995**, *53*, 756-769. Chemistry of Fullerenes - The High Reactivity and New Developments. b) W. Sliwa, *Fullerene Sci. Technol.* **1995**, *3*, 243-281. Cycloaddition Reactions of Fullerenes. c) S. Eguchi, M. Ohno, S. Kojima, N. Koide, A. Yashiro, Y. Shirakawa, H. Ishida, *Fullerene Sci. Technol.* **1996**, *4*, 303-327. Synthesis of Heterocycle-Containing [60]Fullerene Derivatives.

[176] a) R. Taylor, *Phil. Trans. R. Soc. Lond. A* **1993**, *343*, 87-101. The Pattern of Additions to Fullerenes. b) R. Taylor, A. G. Avent, P. R. Birkett, T. J. S. Dennis, J. P. Hare, P. B. Hitchcock, J. H. Holloway, E. G. Hope, H. W. Kroto, G. J. Langley, M. F. Meidine, J. P. Parsons, D. R. M. Walton, *Pure Appl. Chem.* **1993**, *65*, 135-142. Isolation, Characterization, and Chemical Reactions of Fullerenes. c) A. G. Avent, P. R. Birkett, C. Christides, J. D. Crane, A. D. Darwish, P. B. Hitchcock, H. W. Kroto, M. F. Meidine, K. Prassides, R. Taylor, D. R. M. Walton, *Pure Appl. Chem.* **1994**, *66*, 1389-1396. The Fullerenes - Precursors for 21st Century Materials. d) A. G. Avent, P. R. Birkett, C. Christides, J. D. Crane, A. D. Darwish, P. B. Hitchcock, H. W. Kroto, M. F.

Meidine, K. Prassides, R. Taylor, D. R. M. Walton, *J. Mol. Struct.* **1994**, *325*, 1-11. The Structure of Buckminsterfullerene Compounds.

[177] W. Sliwa, *Transition Met. Chem.* **1996**, *21*, 583-592. Metallofullerenes.

[178] F. Diederich, C. Thilgen, *Science (Washington D.C.)* **1996**, *271*, 317-323. Covalent Fullerene Chemistry; and references cited therein.

[179] S. Samal, S. K. Sahoo, *Bull. Mater. Sci.* **1997**, *20*, 141-230. An Overview of Fullerene Chemistry.

[180] a) A. Hirsch, A. Soi, H. R. Karfunkel, *Angew. Chem.* **1992**, *104*, 808-810; *Angew. Chem. Int. Ed.* **1992**, *31*, 766-768. Titration of C_{60} A Method for the Synthesis of Organofullerenes. b) P. J. Fagan, P. J. Krusic, D. H. Evans, S. A. Lerke, E. Johnston, *J. Am. Chem. Soc.* **1992**, *114*, 9697-9699. Synthesis, Chemistry, and Properties of a Monoalkylated Buckminsterfullerene Derivative, *t*-BuC_{60} Anion.

[181] A. Hirsch, T. Grösser, A. Skiebe, A. Soi, *Chem. Ber.* **1993**, *126*, 1061-1067. Synthesis of Isomerically Pure Organodihydrofullerenes.

[182] a) H. L. Anderson, R. Faust, Y. Rubin, F. Diederich, *Angew. Chem.* **1994**, *106*, 1427-1429. Fullerene-Acetylene Hybrids: On the Way to Synthetic Molecular Carbon Allotropes. H. L. Anderson, R. Faust, Y. Rubin, F. Diederich, *Angew. Chem. Int. Ed.* **1994**, *33*, 1366-1368. Fullerene-Acetylene Hybrids: On the Way to Synthetic Molecular Carbon Allotropes. b) K.- Komatsu, Y. Murata, N. Takimoto, S. Mori, N. Sugita, T. S. M. Wan, *J. Org. Chem.* **1994**, *59*, 6101-6102. Synthesis and Properties of the First Acetylene Derivatives of C_{60}.

[183] M. Keshavarz-K., B. Knight, G. Srdanov, F. Wudl, *J. Am. Chem. Soc.* **1995**, *117*, 11371-11372. Cyanodihydrofullerenes and Dicyanodihydrofullerene: The First Polar Solid Based on C_{60}.

[184] F. Banim, D. J. Cardin, P. Heath, *Chem. Commun.* **1997**, 25-26. Proton Migration on the C_{60} Cage of 1-tert-butyl-1,4-dihydro[60]Fullerene to Yield the 1,2-Isomer.

[185] G. Vanlier, B. Safi, P. Geerlings, *J. Chem. Soc., Perkin Trans. 2* **1998**, 349-354. Charge Delocalisation in Hydrofullerenes and Substituted Hydrofullerenes: Effect of Deprotonation.

[186] Y. Murata, K. Motoyama, K. Komatsu, T. S. M. Wan, *Tetrahedron* **1996**, *52*, 5077-5090. Synthesis, Properties, and Reactions of a Stable Carbanion Derived from Alkynyldihydrofullerene: 1-Octynyl-C_{60} Carbanion.

[187] T. Kitagawa, T. Tanaka, Y. Takata, K. Takeuchi, K. Komatsu, *J. Org. Chem.* **1995**, *60*, 1490-1491. Regiospecific Coordination of tert-Butylfulleride Ion and 1,4-Dicyclopropyltropylium Ion. Synthesis of a Dialkyldihydrofullerene Having a Heterolytically Dissociative Carbon-Carbon σ-Bond.

[188] J. R. Morton, K. F. Preston, P. J. Krusic, S. A. Hill, E. Wasserman, *J. Phys. Chem.* **1992**, *96*, 3576-3578. ESR Studies of the Reaction of Alkyl Radicals with C_{60}.

[189] J. R. Morton, K. F. Preston, P. J. Krusic, S. A. Hill, E. Wasserman, *J. Am. Chem. Soc.* **1992**, *114*, 5454-5455. The Dimerization of RC_{60} Radicals.

[190] J. R. Morton, K. F. Preston, P. J. Krusic, E. Wasserman, *J. Chem. Soc., Perkin Trans. 2* **1992**, 1425-1429. Electron Paramagnetic Resonance Spectra of RC_{60} Radicals. Evidence for $RC_{60}C_{60}R$ Dimers.

[191] P. J. Krusic, D. C. Roe, E. Johnston, J. R. Morton, K. F. Preston, *J. Phys. Chem.* **1993**, *97*, 1736-1738. EPR Study of Hindered Internal Rotation in Alkyl-C_{60} Radicals.

[192] J. Morton, K. Preston, P. Krusic, L. Knight, *Chem. Phys. Lett.* **1993**, *204*, 481-485. The Proton Hyperfine Interaction in HC_{60}·, Signature of a Potential Interstellar Fullerene.

[193] P. N. Keizer, J. R. Morton, K. F. Preston, *J. Chem. Soc., Chem. Commun.* **1992**, 1259-1261. The EPR Spectra of Free Radical Adducts of C_{70}.

[194] M. A. Cremonini, L. Lunazzi, G. Placucci, P. J. Krusic, *J. Org. Chem.* **1993**, *58*, 4735-4738. Addition of Alkylthio and Alkoxy Radicals to C_{60} Studied by ESR.

[195] J. R. Morton, K. F. Preston, *J. Phys. Chem.* **1994**, *98*, 4993-4997. Hindered Internal Rotation in Perfluoroalkyl-C_{60} Radicals.

[196] J. R. Morton, F. Negri, K. F. Preston, G. Ruel, *J. Phys. Chem.* **1995**, *99*, 10114-10117. EPR Spectra of Partially Fluorinated Alkyl-C_{60} Radicals and a Theoretical Study of the Interactions on the C_{60} Sphere.

[197] J. R. Morton, F. Negri, K. F. Preston, G. Ruel, *J. Chem. Soc., Perkin Trans. 2* **1995**, 2141-2145. Electrostatic Effects on the C_{60} Surface of Alkyl-C_{60} Radicals.

[198] P. N. Keizer, J. R. Morton, K. F. Preston, P. J. Krusic, *J. Chem. Soc., Perkin Trans. 2* **1993**, 1041-1045. Electron Paramagnetic Resonance Spectra of RC_{60} Radicals part 2: Hindered Rotation in Alkyl- and Silyl-C_{60} Radicals.

[199] R. Borghi, L. Lunazzi, G. Placucci, P. J. Krusic, D. A. Dixon, N. Matsuzawa, M. Ata, *J. Am. Chem. Soc.* **1996**, *118*, 7608-7617. Addition of Aryl and Fluoroalkyl Radicals to Fullerene C_{70}: ESR Detection of Five Regioisomeric Adducts and Density Functional Calculations.

[200] P. W. Percival, S. Wlodek, *Chem. Phys. Lett.* **1992**, *196*, 317-320. The Structure of C_{60}Mu and other Fullerenyl Radicals.

[201] N. Matsuzawa, D. Dixon, P. Krusic, *J. Phys. Chem.* **1992**, *96*, 8317-8321. Semiempirical Calculations of C_{60} Derivatives: Addition to Double Bonds Radiating from a Five Membered Ring.

[202] J. R. Morton, F. Negri, K. F. Preston, *APPLIED MAGNETIC RESONANCE* **1996**, *11*, 325-333. ^{13}C Hyperfine Interactions in CD_3C_{60} and the Distribution of Unpaired Spin on the C_{60} Cage.

[203] J. R. Morton, R. Negri, K. F. Preston, *Acc. Chem. Res.* **1998**, *31*, 63-69. Addition of Free Radicals to C_{60}.

[204] J. R. Morton, F. Negri, K. F. Preston, *Can. J. Chem.* **1994**, *72*, 776-782. Addition of Alkyl Radicals to C_{60}. Part 3. The EPR Spectra of R_3C_{60} Radicals and a Theoretical Study of HC_{60} and H_3C_{60} Radicals.

[205] P. W. Percival, B. Addison-Jones, J.-C. Brodovitch, J. Feng, P. J. Horoyski, M. L. W. Tdhewalt, T. R. Anthony, *Chem. Phys. Lett.* **1995**, *245*, 90-94. ^{13}C Hyperfine Coupling Constants in MuC_{60}.

[206] P. J. Fagan, J. C. Calabrese, B. Malone, *Acc. Chem. Res.* **1992**, *25*, 134-142. Metal Complexes of Buckminsterfullerene C_{60}.

[207] a) J. M. Hawkins, T. A. Lewis, S. D. Loren, A. Meyer, J. R. Heath, Y. Shibato, R. J. Saykally, *J. Org. Chem.* **1990**, *55*, 6250-6252. Organic Chemistry of C_{60} (Buckminsterfullerene) - Chromatography and Osmylation. b) J. M. Hawkins, A. Meyer, S. Loren, R. Nunlist, *J. Am. Chem. Soc.* **1991**, *113*, 9394-9395. Statistical Incorporation of $^{13}C_2$ Units into C_{60}.

[208] T. J. Seiders, K. K. Baldridge, J. M. Oconnor, J. S. Siegel, *J. Am. Chem. Soc.* **1997**, *119*, 4781-4782. Hexahapto Metal Coordination to Curved Polyaromatic Hydrocarbon Surfaces: The First Transition Metal Corannulene Complex.

[209] H. Nagashima, M. Nakazawa, T. Furukawa, K. Itoh, *Chem. Lett.* **1996**, 405-406. Organopalladium and Platinum Complexes of C_{60} Bearing Isonitrile Ligands.

[210] M. Iyoda, Y. Ogawa, H. Matsuyama, *Fullerene Sci. Technol.* **1995**, *3*, 1-9. Synthesis and Properties of Platinum Complexes of Fullerenes C_{60} and C_{70}.

[211] C. Bingel, *Chem. Ber.* **1993**, *126*, 1957-1959. Cyclopropanierung von Fullerenen.

[212] H. J. Bestmann, D. Hadawi, T. Röder, C. Moll, *Tetrahedron Lett.* **1994**, *35*, 9017-9020. 6,6-Bridged Closed Methanofullerenes from C_{60} and Phosphonium Ylides.

[213] Y. Wang, J. Cao, D. I. Schuster, S. R. Wilson, *Tetrahedron Lett.* **1995**, *36*, 6843-6846. A Superior Synthesis of [6,6]-Methanofullerenes: The Reaction of Sulfonium Ylides with C_{60}.

[214] J.-F. Nierengarten, V. Gramlich, F. Cardullo, F. Diederich, *Angew. Chem.* **1996**, *108*, 2242-2244; *Angew. Chem. Int. Ed.* **1996**, *35*, 2101-2103. Regio- and Diastereoselective Bisfunctionalization of C_{60} and Enantioselective Synthesis of a C_{60} Derivative with a Chiral Addition Pattern.

[215] J.-F. Nierengarten, A. Herrmann, R. R. Tykwinski, M. Ruttimann, F. Diederich, C. Boudon, J.-P. Gisselbrecht, M. Gross, *Helv. Chim. Acta* **1997**, *80*, 293-316. Methanofullerene Molecular Scaffolding: Towards C_{60} Substituted Poly(triacetylenes) and Expanded Radialenes, Preparation of a C_{60}/C_{70} Hybrid Derivative, and a Novel Macrocyclization Reaction.

[216] X. Camps, A. Hirsch, *J. Chem. Soc., Perkin Trans. 1* **1997**, 1595-1596. Efficient Cyclopropanation of C_{60} Starting from Malonates.

[217] M. Keshavarz-K., B. Knight, R. C.- Haddon, F. Wudl, *Tetrahedron* **1996**, *52*, 5149-5159. Linear Free Energy Relation of Methanofullerene C_{61}-Substituents with Cyclic Voltammetry: Strong Electron Withdrawal Anomaly.

[218] P. Timmerman, H. L. Anderson, R. Faust, J. F. Nierengarten, T. Habicher, P. Seiler, F. Diederich, *Tetrahedron* **1996**, *52*, 4925-4947. Fullerene Acetylene Hybrids: Towards a Novel Class of Molecular Carbon Allotropes.

[219] J. F. Nierengarten, D. Felder, J. F. Nicoud, *Tetrahedron Lett.* **1998**, *39*, 2747-2750. Regioselective bisaddition to C_{60} with bis(.β.-keto esters).

[220] G.-W. Wang, K. Komatsu, Y. Murata, M. Shiro, *Nature (London)* **1997**, *387*, 583-586. Synthesis and X-Ray Structure of Dumb-Bell-Shaped C_{120}.

[221] G.-W. Wang, Y. Murata, K. Komatsu, T. S. M. Wan, *Chem. Commun.* **1996**, 2059-2060. The Solid-Phase Reaction of [60]Fullerene: Novel Addition of Organozinc Reagents.

[222] a) A. M. Rao, P. Zhou, K.-A. Wang, G. T. Hager, J. M. Holden, Y. Wang, W.-T. Lee, X.-X. Bi, P. C. Eklund, D. S. Cornett, M. A. Duncan, I. J. Amster, *Science (Washington D.C.)* **1993**, *259*, 955-957. Photoinduced Polymerization of Solid C_{60} Films. b) C. N. R. Rao, A. Govindaraj, H. N. Aiyer, R. Seshadri, *J. Phys. Chem.* **1995**, *99*, 16814-16816. Polymerization and Pressure-Induced Amorphization of C_{60} and C_{70}; and references cited therein.

[223] T. Ozaki, Y. Iwasa, T. Mitani, *Chem. Phys. Lett.* **1998**, *285*, 289-293. Elementary Processes in Pressure-Induced Polymerization of C_{60}; and references cited therein.

[224] W. Sliwa, *Fullerene Sci. Technol.* **1997**, *5*, 1133-1175. Diels Alder Reactions of Fullerenes.

[225] M. S. Meier, G.-W. Wang, R. C. Haddon, C. Pratt Brock, M. A. Lloyd, J. P. Selegue, *J. Am. Chem. Soc.* **1998**, *120*, 2337-2342. Benzyne Adds Across a Closed 5-6 Ring Fusion in C_{70}: Evidence for Bond Delocalization in Fullerenes.

[226] A. Chikama, H. Fueno, H. Fujimoto, *J. Phys. Chem.* **1995**, *99*, 8541-8549. Theoretical Study of the Diels-Alder Reaction of C_{60}. Transition-State Structures and Reactivities of C-C Bonds.

[227] a) M. Tsuda, T. Ishida, T. Nogami, S. Kurono, M. Ohashi, *J. Chem. Soc., Chem. Commun.* **1993**, 1296-1298. Isolation and Characterization of Diels-Alder Adducts of C_{60} with Anthracene and Cyclopentadiene. b) J. A.- Schlueter, J. M.- Seaman, S. Taha, H. Cohen, K. R. Lykke, H. H. Wang, J. M. Williams, *J. Chem. Soc., Chem. Commun.* **1993**, 972-974. Synthesis, Purification, and Characterization of the 1:1 Addition Product of C_{60} and Anthracene.

[228] a) F. Wudl, A. Hirsch, K. C. Khemani, T. Suzuki, P.-M. Allemand, A. Koch, H. Eckert, G.- Srdanov, H. M. Webb in 'Fullerenes: Synthesis, Properties and Chemistry of Large Carbon Clusters', Ed. G. S. Hammond, V. J. Kuck, American Chemical Society Symposium Series 481, 1992, p. 161-175. b) V. M. Rotello, J. B. Howard, T. Yadav, M. M. Conn, E. Viani, L. M. Giovane, A. L. Lafleur, *Tetrahedron Lett.* **1993**, *34*, 1561-1562. Isolation of Fullerene Products from Flames - Structure and Synthesis of the C_{60}-Cyclopentadiene Adduct. c) K. Komatsu, Y. Murata, N. Sugita, K. Takeuchi, T. S. M. Wan, *Tetrahedron*

Lett. **1993**, *34*, 8473-8476. Use of Naphthalene as a Solvent for Selective Formation of the 1:1 Diels-Alder Adduct of C_{60} with Anthracene.

[229] L. M. Giovane, J. W. Barco, T. Yadav, A. L. Lafleur, J. A. Marr, J. B. Howard, V. M. Rotello, *J. Phys. Chem.* **1993**, *97*, 8560-8561. Kinetic Stability of the C_{60}-Cyclopentadiene Diels-Alder Adduct.

[230] L. Isaacs. Dissertation No. 11247 Swiss Federal Institute of Technology. Zürich.

[231] I. Lamparth, C. Maichle-Mössmer, A. Hirsch, *Angew. Chem.* **1995**, *107*, 1755-1757; *Angew. Chem. Int. Ed.* **1995**, *34*, 1607-1609. Reversible Template Directed Activation of Equatorial Double Bonds of the Fullerene Framework: Regioselective Direct Synthesis, Crystal Structure, and Aromatic Properties of *Th* $C_{66}(COOEt)_{12}$.

[232] Y. Rubin, S. Khan, D. I. Freedberg, C. Yeretzian, *J. Am. Chem. Soc.* **1993**, *115*, 344-345. Synthesis and X-Ray Structure of a Diels-Alder Adduct of C_{60}.

[233] F. Diederich, U. Jonas, V. Gramlich, A. Herrmann, H. Ringsdorf, C. Thilgen, *Helv. Chim. Acta* **1993**, *76*, 2445-2453. Synthesis of a Fullerene Derivative of Benzo[18]crown-6 by Diels-Alder Reaction - Complexation Ability, Amphiphilic Properties, and X-Ray Crystal Structure of a Dimethoxy-1,9-(methano[1,2]benzenomethano)fullerene[60]Benzene Clathrate.

[234] P. Belik, A. Gügel, J. Spickermann, K. Müllen, *Angew. Chem.* **1993**, *105*, 95-97; *Angew. Chem. Int. Ed.* **1993**, *32*, 78-80. Reaction of Buckminsterfullerene with Ortho-Quinodimethane - A New Access to Stable C_{60} Derivatives.

[235] S. I. Khan, A. M. Oliver, M. N. Paddon-Row, Y. Rubin, *J. Am. Chem. Soc.* **1993**, *115*, 4919-4920. Synthesis of a Rigid 'Ball-and-Chain' Donor Acceptor System through Diels-Alder Functionalization of Buckminsterfullerene C_{60}.

[236] P. Belik, A. Gügel, A. Kraus, J. Spickermann, V. Enkelmann, G. Frank, K. Müllen, *Adv. Mater.* **1993**, *5*, 854-856. The Diels-Alder Adduct of C_{60} and 4,5-Dimethoxy-*o*-quinodimethane - Synthesis, Crystal Structure, and Donor-Acceptor Behavior.

[237] a) B. Kräutler, M. Puchberger, *Helv. Chim. Acta* **1993**, *76*, 1626-1631. On Diels-Alder reactions of the C_{60}-Fullerene. b) S. R. Wilson, Q. Lu, *Tetrahedron Lett.* **1993**, *34*, 8043-8046. Electrospray MS Studies of C_{60} Diels-Alder Chemistry - Characterization of a C_{60} Adduct with the Danishefsky Diene. c) Y.-Z. An, A. L. Viado, M.-J. Arce, Y. Rubin, *J. Org. Chem.* **1995**, *60*, 8330-8331. Unusual Regioselectivity in the Singlet Oxygen Ene Reaction of Cyclohexenobuckminsterfullerenes. d) M. Ohno, T. Azuma, S. Kojima, Y. Shirakawa, S. Eguchi, *Tetrahedron* **1996**, *52*, 4983-4994. An Efficient Functionalization of [60]Fullerene. Diels-Alder Reaction Using 1,3-Butadienes Substituted with Electron-Withdrawing and Electron-Donating (Silyloxy) Groups. e) B. Kräutler, J. Maynollo, *Tetrahedron* **1996**, *52*, 5033-5042. Diels-Alder Reactions of the [60]Fullerene - Functionalizing a Carbon Sphere with Flexibly and with Rigidly Bound Addends. f) G. Torres-Garcia, H. Luftmann, C. Wolff, J. Mattay, *J. Org. Chem.* **1997**, *62*, 2752-2756. A Versatile Route to Substituted 1,4 Diazine Fused [60]Fullerenes.

[238] Y.-Z. An, G. A. Ellis, A. L. Viado, Y. Rubin, *J. Org. Chem.* **1995**, *60*, 6353-6361. A Methodology for the Reversible Solubilization of Fullerenes.

[239] M. Prato, T. Suzuki, H. Foroudian, Q. Li, K. Khemani, F. Wudl, J. Leonetti, R. D. Little, T. White, B. Rickborn, S. Yamago, E. Nakamura, *J. Am. Chem. Soc.* **1993**, *115*, 1594-1595. [3 + 2] and [4 + 2] Cycloadditions of C_{60}.

[240] a) S. Yamago, H. Tokuyama, E. Nakamura, M. Prato, F. Wudl, *J. Org. Chem.* **1993**, *58*, 4796-4798. Chemical Derivatization of Organofullerenes through Oxidation, Reduction, and C-O and C-C Bond-Forming Reactions. b) H. Tokuyama, M. Nakamura, E. Nakamura, *Tetrahedron Lett.* **1993**, *34*, 7429-7432. [1+2] and [3+2] Cycloaddition Reactions of Vinylcarbenes with C_{60}.

[241] a) M. Maggini, G. Scorrano, M. Prato, *J. Am. Chem. Soc.* **1993**, *115*, 9798-9799. Addition of Azomethine Ylides to C_{60} - Synthesis, Characterization, and Functionalization of Fullerene Pyrrolidines. b) X. Zhang, M. Willems, C. S. Foote, *Tetrahedron Lett.* **1993**, *34*, 8187-8188. 1,3-Dipolar Cycloaddition of N-Benzyl Azomethine Ylide to C_{60} - Formation of a C_{60}-Fused N-Benzylpyrrolidine. c) M. Maggini, A. Karlsson, L. Pasimeni, G. Scorrano, M. Prato, L. Valli, *Tetrahedron Lett.* **1994**, *35*, 2985-2988. Synthesis of N-Acylated Fulleropyrrolidines: New Materials for the Preparation of Langmuir-Blodgett Films Containing Fullerenes. d) M. Maggini, G. Scorrano, A. Bianco, C. Toniolo, R. P. Sijbesma, F. Wudl, M. Prato, *J. Chem. Soc., Chem. Commun.* **1994**, 305-306. Addition Reactions of C_{60} Leading to Fulleroprolines.

[242] N. Jagerovic, J. Elguero, J.-L. Aubagnac, *J. Chem. Soc., Perkin Trans. 1* **1996**, 499. Cycloaddition of Tetracyanoethene Oxide with [60]Fullerene.

[243] a) M. S. Meier, M. Poplawska, *J. Org. Chem.* **1993**, *58*, 4524-4525. Addition of Nitrile Oxides to C_{60} - Formation of Isoxazoline Derivatives of Fullerenes. b) H. Irngartinger, C.-M. Kohler, U. Huber-Patz, W.- Krätschmer, *Chem. Ber.* **1994**, *127*, 581-584. Functionalization of C_{60} with Nitrile Oxides to 4,5-Dihydroisoxazoles and their Structure Determination. c) H. Irngartinger, A. Weber, T. Escher, *Liebigs Ann.* **1996**, 1845-1850. Cycloaddition of Functionalized Nitrile Oxides and Fulminic Acid to C_{60}. d) M. S. Meier, M. Poplawska, *Tetrahedron Lett.* **1996**, *52*, 5043-5052. The Addition of Nitrile Oxides to C_{60}. e) T. Da Ros, M. Prato, F. Novello, M. Maggini, M. De Amici, C. De Micheli, *Chem. Commun.* **1997**, 59-60. Cycloaddition of Nitrile Oxides to [60]Fullerene.

[244] a) S. Muthu, P. Maruthamuthu, R. Ragunathan, P. R. V. Rao, C. K. Mathews, *Tetrahedron Lett.* **1994**, *35*, 1763-1766. Reaction of Buckminsterfullerene with 1,3-Diphenylnitrilimine - Synthesis of Pyrazoline Derivatives of Fullerene. b) Y. Matsubara, H. Tada, S. Nagase, Z. Yoshida, *J. Org. Chem.* **1995**, *60*, 5372-5373. Intramolecular Charge Transfer Interaction in 1,3-Diphenyl-2-Pyrazoline Ring-Fused C_{60}. c) Y. Matsubara, H. Muraoka, H. Tada, Z. Yoshida, *Chem. Lett.* **1996**, 373-374. Functionalization of C_{60} with 1,3-Nitrilimine Dipole: Synthesis of 2-Pyrazoline Ring-Fused C_{60} Derivatives.

[245] a) L.-H. Shu, W.-Q. Sun, D.-W.- Zhang, S.-H. Wu, H.-M.- Wu, J.-F. Xu, X.-F.-Lao, *Chem. Commun.* **1997**, 79-80. Phosphine Catalised [3+2] Cycloadditions of Buta-2,3-dienoates and But-2-ynoates to [60]Fullerene. b) B. F. O'Donovan, P. B. Hitchcock, M. F. Meidine, H. W. Kroto, R. Taylor, D. R. M. Walton, *Chem. Commun.* **1997**, 81-82. Phosphine-Catalyzed Cycloaddition of Buta-2,3-dienoates and But-2-ynoates to [60]Fullerene.

[246] D. Brizzolara, J. T. Ahlemann, H. W. Roesky, K. Keller, *Bull. Soc. Chim. Fr.* **1993**, *130*, 745-747. Reactions of Buckminsterfullerene C_{60} with Sulfinimides

and $(CF_3)_2NO$, the First Access to Fullerenes Containing Perfluorinated Substituents.

[247] T. Suzuki, Li Q., K. C. Khemani, F. Wudl, Ö. Almarsson, *Science (Washington D.C.)* **1991**, *254*, 1186-1188. Systematic Inflation of Buckminsterfullerene C_{60}: Synthesis of Diphenyl Fulleroids C_{61} to C_{66}.

[248] F. Wudl, *Acc. Chem. Res.* **1992**, *25*, 157-161. The Chemical Properties of Buckminsterfullerene C_{60} and the Birth and Infancy of Fulleroids.

[249] F. Diederich, L. Isaacs, D. Philp, *J. Chem. Soc., Perkin Trans. 2* **1994**, 391-394. Valence Isomerism and Rearrangements in Methanofullerenes.

[250] a) E. Vogel, *Pure Appl. Chem.* **1969**, *20*, 237-262. Perspektiven der Cycloheptatrien-Norcaradien-Valenztautomerie. b) E. Vogel, *Pure Appl. Chem.* **1982**, *54*, 1015-1039. Recent Advances in the Chemistry of Bridged Annulenes. c) E. Vogel, *Isr. J. Chem.* **1980**, *20*, 215-224. Bridged Annulenes. d) E. Vogel, *Pure Appl. Chem.* **1993**, *65*, 143-152. The Porphyrins from the 'Annulene Chemist's' Perspective. e) R. Arnz, J. W. de M. Carneiro, W. Klug, H. Schmickler, E. Vogel, R. Breuckmann, F.-G. Klärner, *Angew. Chem.* **1991**, *103*, 702-704; *Angew. Chem. Int. Ed.* **1991**, *30*, 683-686. σ-Homoacenaphthylene and π-Homoacenaphthene.

[251] a) A. B. Smith III, R. M. Strongin, L. Brard, G. T. Furst, W. J. Romanow, K. G. Owens, R. C. King, *J. Am. Chem. Soc.* **1993**, *115*, 5829-5830. 1,2-Methanobuckminsterfullerene $C_{61}H_2$, the Parent Fullerene Cyclopropane - Synthesis and Structure. b) A. B. Smith III, R. M. Strongin, L. Brard, G. T. Furst, W. J. Romanow, K. G. Owens, R. J. Goldschmidt, *J. Chem. Soc., Chem. Commun.* **1994**, 2187-2188. $C_{71}H_2$ Cyclopropanes and Annulenes: Synthesis and Characterization.

[252] T. A. Keith, R. F. W. Bader, *Chem. Phys. Lett.* **1993**, *210*, 223-231. Calculation of Magnetic Response Properties Using a Continuous Set of Gauge Transformations.

[253] R. González, J. C. Hummelen, F. Wudl, *J. Org. Chem.* **1995**, *60*, 2618-2620. The Specific Acid-Catalyzed and Photochemical Isomerization of a Robust Fulleroid to a Methanofullerene.

[254] R. A. J. Janssen, J. C. Hummelen, F. Wudl, *J. Am. Chem. Soc.* **1995**, *117*, 544-545. Photochemical Fulleroid to Methanofullerene Conversion via the Di-π-methane (Zimmerman) Rearrangement.

[255] M. Eiermann, F. Wudl, M. Prato, M. Maggini, *J. Am. Chem. Soc.* **1994**, *116*, 8364-8365. Electrochemically Induced Isomerization of a Fulleroid to a Methanofullerene.

[256] J. C. Hummelen, B. W. Knight, F. LePeq, F. Wudl, J. Yao, C. L. Wilkins, *J. Org. Chem.* **1995**, *60*, 532-538. Preparation and Characterization of Fulleroid and Methanofullerene Derivatives.

[257] Z. Li, P. B. Shevlin, *J. Am. Chem. Soc.* **1997**, *119*, 1149-1150. Why is the Rearrangement of [6,5] Open Fulleroids to [6,6] Closed Fullerenes Zero Order?

[258] M. Prato, V. Lucchini, M. Maggini, E. Stimpfl, G. Scorrano, M. Eiermann, T. Suzuki, F. Wudl, *J. Am. Chem. Soc.* **1993**, *115*, 8479-8480. Energetic

Preference in 5,6 and 6,6-Ring Junction Adducts of C_{60} - Fulleroids and Methanofullerenes.

[259] A. Skiebe, A. Hirsch, *J. Chem. Soc., Chem. Commun.* **1994**, 335-336. A Facile Method for the Synthesis of Amino Acid and Amido Derivatives of C_{60}.

[260] J. Osterodt, M.- Nieger, P.-M. Windscheif, F. Vögtle, *Chem. Ber.* **1993**, *126*, 2331-2336. Crowned Fullerenes.

[261] Z. Z. Li, K. H. Bouhadir, P. B. Shevlin, *Tetrahedron Lett.* **1996**, *37*, 4651-4654. Convenient Syntheses of 6,5 Open and 6,6 Closed Cycloalkylidenefullerenes.

[262] I. Fleming, 'Frontier Orbitals and Organic Chemical Reactions', John Wiley & Sons, New York.

[263] a) S. Shi, K. C. Khemani, Q. C. Li, F. Wudl, *J. Am. Chem. Soc.* **1992**, *114*, 10656-10657. A Polyester and Polyurethane of Diphenyl-C_{61} - Retention of Fulleroid Properties in a Polymer. b) Y.-P. Sun, B. Liu, D. K. Moton, *Chem. Commun.* **1996**, 2699-2700. Preperation and Characterization of a Highly Water Soluble Pendant Fullerene Polymer.

[264] M. Prato, *J. Mater. Chem.* **1997**, *7*, 1097-1109. [60] Fullerene Chemistry for Materials Science Applications; and references cited therein.

[265] H. L. Anderson, C. Boudon, F. Diederich, J.-P. Gisselbrecht, M. Gross, P. Seiler, *Angew. Chem.* **1994**, *106*, 1691-1694; *Angew. Chem. Int. Ed.* **1994**, *33*, 1628-1632. 61,61-Bis(trimethylsilylbutadiynyl)-1,2-dihydro-1,2-Methanofullerene[60]: Crystal Structure at 100 K and Electrochemical Conversion to a Conducting Polymer.

[266] a) K. L.- Wooley, C. J. Hawker, J. M. J. Fréchet, F. Wudl, G. Srdanov, S. Shi, C. Li, M. Kao, *J. Am. Chem. Soc.* **1993**, *115*, 9836-9837. Fullerene-Bound Dendrimers - Soluble, Isolated Carbon Clusters. b) X. Camps, H. Schonberger, A. Hirsch, *Chem. Eur. J.* **1997**, *3*, 561-567. The C_{60} Core: A Versatile Tecton for Dendrimer Chemistry.

[267] U. Jonas, F. Cardullo, P. Belik, F. Diederich, A. Gügel, E. Harth, A. Herrmann, L. Isaacs, K. Müllen, H. Ringsdorf, C. Thilgen, P. Uhlmann, A. Vasella, C. A. A. Waldraff, M. Walter, *Chem. Eur. J.* **1995**, *1*, 243-251. Synthesis of a Fullerene[60] Cryptate and Systematic Langmuir-Blodgett and Thin-Film Investigations of Amphiphilic Fullerene Derivatives ; and references cited therein.

[268] a) F. Diederich, C.- Dietrich-Buchecker, J.-F. Nierengarten, J.-P. Sauvage, *J. Chem. Soc., Chem. Commun.* **1995**, 781-782. A Copper(I)-Complexed Rotaxane with Two Tullerene Stoppers. b) D. Armspach, E. C. Constable, F. Diederich, C. E. Housecroft, J. F. Nierengarten, *Chem. Commun.* **1996**, 2009-2010. Bucky-Ligands: Fullerene-Substituted Oligopyridines for Metallosupramolecular Chemistry.

[269] P. R. Asthon, F. Diederich, M. Gómez-López, J.-F. Nierengarten, J. A. Preece, F. M. Raymo, J. F. Stoddart, *Angew. Chem.* **1997**, *109*, 1611-1614; *Angew. Chem. Int. Ed.* **1997**, *36*, 1448-1451. Self-Assembly of the First Fullerene-Containing [2]Catenane .

[270] a) S. H. Friedman, D. L. DeCamp, R. P. Sijbesma, G. Srdanov, F. Wudl, G. L. Kenyon, *J. Am. Chem. Soc.* **1993**, *115*, 6506-6509. Inhibition of the HIV-1 Protease by Fullerene Derivatives - Model Building Studies and Experimental Verification. b) M. Prato, A. Bianco, M. Maggini, G. Scorrano, C. Toniolo, F. Wudl, *J. Org. Chem.* **1993**, *58*, 5578-5580. Synthesis and Characterization of the First Fullerene Peptide. c) C. Toniolo, A. Bianco, M. Maggini, G. Scorrano, M. Prato, M. Marastoni, R. Tomatis, S. Spisani, G. Palú, E. D. Blair, *J. Med. Chem.* **1994**, *37*, 4558-4562. A Bioactive Fullerene Peptide.

[271] M. Prato, Q. C. Li, F. Wudl, V. Lucchini, *J. Am. Chem. Soc.* **1993**, *115*, 1148-1150. Addition of Azides to C_{60} - Synthesis of Azafulleroids.

[272] T. Grösser, M. Prato, V. Lucchini, A. Hirsch, F. Wudl, *Angew. Chem.* **1995**, *107*, 1462-1464; *Angew. Chem. Int. Ed.* **1995**, *34*, 1343-1345. Ring Expansion of the Fullerene Core by Highly Regioselective Formation of Diazafulleroids.

[273] B. Nuber, F. Hampel, A. Hirsch, *Chem. Commun.* **1996**, 1799-1800. X-Ray Structure of 1'-(2-methoxyethoxymethyl)triazolinyl[4', 5' :1,2]-1,2-dihydro[60]Fullerene.

[274] I. Lamparth, A. Herzog, A. Hirsch, *Tetrahedron* **1996**, *52*, 5065-5075. Synthesis of [60]Fullerene Derivatives with an Octahedral Addition Pattern.

[275] J. Averdung, J. Mattay, *Tetrahedron* **1996**, *52*, 5407-5420. Exohedral Functionalization of [60]Fullerene by [3+2] Cycloadditions: Syntheses and Chemical Properties of Triazolino-[60]Fullerenes and 1,2-(3,4-dihydro-2H-pyrrolo)-[60]Fullerenes.

[276] J. C. Hummelen, M. Prato, F. Wudl, *J. Am. Chem. Soc.* **1995**, *117*, 7003-7004. There is a Hole in my Bucky.

[277] J. C. Hummelen, M. Keshavarzk-K, J. L. J. Vandongen, R. A. J. Janssen, E. W. Meijer, F. Wudl, *Chem. Commun.* **1998**, 281-282. Resolution and Circular Dichroism of an Asymmetrically Cage-Opened [60]Fullerene Derivative.

[278] J. C. Hummelen, B. Knight, J. Pavlovich, R. González, F. Wudl, *Science (Washington D.C.)* **1995**, *269*, 1554-1556. Isolation of the Heterofullerene $C_{59}N$ as its Dimer $(C_{59}N)_2$.

[279] M. Keshavarz, R. González, R. G. Hicks, G. Srdanov, V. I. Srdanov, T. G. Collins, J. C. Hummelen, C. Bellavia-Lund, J. Pavlovich, F. Wudl, K. Holczer, *Nature (London)* **1996**, *383*, 147-150. Synthesis of Hydroazafullerene $C_{59}HN$, the Parent Hydroheterofullerene.

[280] C. Bellavia-Lund, R. Gonzáles, J. C. Hummelen, R. G. Hicks, A. Sastre, F. Wudl, *J. Am. Chem. Soc.* **1997**, *119*, 2946-2947. Synthesis of $C_{59}(CHPh_2)N$ from $(C_{59}N)_2$ and $C_{59}HN$. The First Derivatization of $C_{59}N$.

[281] B. Nuber, A. Hirsch, *Chem. Commun.* **1998**, 405-406. Facile Synthesis of Arylated Heterofullerenes $ArC_{59}N$.

[282] C. K. F. Shen, H. H. Yu, C. G. Juo, K. M. Chien, G. R. Her, T. Y. Luh, *Chem. Eur. J.* **1997**, *3*, 744-748. Synthesis of 1,2,3,4 Bisiminofullerene and 1,2,3,4 Bis(Triazolino)fullerene: on the Mechanism of the Addition Reactions of Organic Azides to [60]Fullerene.

[283] C. J. Hawker, K. L. Wooley, J. M. J. Fréchet, *J. Chem. Soc., Chem. Commun.* **1994**, 925-926. Dendritic Fullerenes - A New Approach to Polymer Modification of C_{60}.

[284] C. J. Hawker, P. M. Saville, J. W. White, *J. Org. Chem.* **1994**, *59*, 3503-3505. The Synthesis and Characterization of a Self-Assembling Amphiphilic Fullerene.

[285] N. Wang, J. Li, D. Zhu, T. H. Chan, *Tetrahedron Lett.* **1995**, *36*, 431-434. A C_{60}-Derivatized Dipeptide.

[286] M. Takeshita, T. Suzuki, S. Shinkai, *J. Chem. Soc., Chem. Commun.* **1994**, 2587-2588. Synthesis and Spectroscopic Properties of C_{60} Functionalized Calix[8]arene (Calixfullerene).

[287] T. Akasaka, W. Ando, K. Kobayashi, S. Nagase, *J. Am. Chem. Soc.* **1993**, *115*, 1605-1606. Reaction of C_{60} with Silylene, the First-Fullerene Silirane Derivative.

[288] A. Vasella, P. Uhlmann, C. A. A. Waldraff, F. Diederich, C. Thilgen, *Angew. Chem.* **1992**, *104*, 1383-1385; *Angew. Chem. Int. Ed.* **1992**, *31*, 1388-1390. Fullerene Sugars: Oreparation of Enantiomerically Pure, Spiro-Linked C-Glycosides of C_{60}.

[289] P. Uhlmann, E. Harth, A. B. Naughton, A. Vasella, *Helv. Chim. Acta* **1994**, *77*, 2335-2340. Glycosylidene Carbenes Part 20: Synthesis of Deprotected, Spiro-Linked C-Glycosides of C_{60}.

[290] a) M. Tsuda, T. Ishida, T. Nogami, S. Kurono, M. Ohashi, *Tetrahedron Lett.* **1993**, *34*, 6911-6912. $C_{61}Cl_2$ - Synthesis and Characterization of Dichlorocarbene Adducts of C_{60}. b) T. Ishida, T. Furudate, T. Nogami, M. Kubota, T. Hirano, M. Ohashi, *Fullerene Sci. Technol.* **1995**, *3*, 399-409. .

[291] a) J. Osterodt, F. Vögtle, *Chem. Commun.* **1996**, 547-548. $C_{61}Br_2$: A New Synthesis of Dibromomethanofullerene, and Mass Spectrometric Evidence of the Carbon Allotropes C_{121} and C_{122}. b) A. M. Benito, A. D. Darwish, H. W. Kroto, M. F. Meidine, R. Taylor, D. R. M. Walton, *Tetrahedron Lett.* **1996**, *37*, 1085-1086. Synthesis and Characterisation of the Methanofullerenes, $C_{60}(CHCN)$ and $C_{60}(CBr_2)$.

[292] W. W. Win, M. Kao, M. Eiermann, J. J. McNamara, F. Wudl, D. L. Pole, K. Kassam, J. Warkentin, *J. Org. Chem.* **1994**, *59*, 5871-5876. Methyl 1,2-dihydrofullerenecarboxylate.

[293] Y.-Z. An, Y. Rubin, C. Schaller, S. W. McElvany, *J. Org. Chem.* **1994**, *59*, 2927-2929. Synthesis and Characterization of Diethynylmethanobuckminsterfullerene, a Building Block for Macrocyclic and Polymeric Carbon Allotropes.

[294] C. A. Merlic, H. D. Bendorf, *Tetrahedron Lett.* **1994**, *35*, 9529-9532. Cyclopropanation of C_{60} via a Fischer Carbene Complex.

[295] M. R. Banks, J. I. G. Cadogan, I. Gosney, P. K. G. Hodgson, P. R. R. Langridge-Smith, D. W. H. Rankin, *J. Chem. Soc., Chem. Commun.* **1994**, 1365-

1366. Bis-Functionalisation of C_{60} via Thermal Rearrangement of an Isolable Fulleroaziridine Bearing a 'Solubilising' Supermesityl Ester Moiety.

[296] G. Schick, T. Grösser, A. Hirsch, *J. Chem. Soc., Chem. Commun.* **1995**, 2289-2290. The Transannular Bond in [5,6]-NCO_2R-Bridged Monoadducts of [60]Fullerene is Open.

[297] J. Averdung, J. Mattay, D. Jacobi, W. Abraham, *Tetrahedron* **1995**, *51*, 2543-2552. Addition of Photochemically Generated Acylnitrenes to C_{60}. Synthesis of Fulleroaziridines and Thermal Rearrangement to Fullerooxazoles.

[298] M. Yan, S. X. Cai, J. F. W. Keana, *J. Org. Chem.* **1994**, *59*, 5951-5954. Photochemical and Thermal Reactions of C_{60} with N-Succinimidyl 4-Azido-2,3,5,6-Tetrafluorobenzoate: A New Method for Functionalization of C_{60}.

[299] M. R. Banks, J. I. G. Cadogan, I. Gosney, P. K. G. Hodgson, P. R. R. Langridge-Smith, J. R. A. Millar, A. T. Taylor, *J. Chem. Soc., Chem. Commun.* **1995**, 885-886. Aziridino[2',3':1,2][60]Fullerene.

[300] J. Averdung, H. Luftmann, J. Mattay, K.-U. Claus, W.- Abraham, *Tetrahedron Lett.* **1995**, *36*, 2957-2958. Synthesis of 1,2-(2,3-dihydro-1H-azirino)-[60]Fullerene, the Parent Fulleroaziridine.

[301] S.- Kuwashima, M. Kubota, K. Kushida, T. Ishida, M. Ohashi, T. Nogami, *Tetrahedron Lett.* **1994**, *35*, 4371-4374. Synthesis and Structure of Nitrene-C_{60} Adduct, $C_{(60)}$NPhth (*Phth* = *phthalimido*).

[302] M. R. Banks, J. I. G. Cadogan, I. Gosney, P. K. G. Hodgson, P. R. R. Langridgesmith, J. R. A. Millar, A. T. Taylor, *Tetrahedron Lett.* **1994**, *35*, 9067-9070. Chemical Transformations on the Surface of [60]Fullerene: Synthesis of [60]Fullereno[1',2':4,5]oxazolidin-2-one.

[303] J. Averdung, C. Wolff, J. Mattay, *Tetrahedron Lett.* **1996**, *37*, 4683-4684. Syntheses of Urethano-, Amido- and Sulfonamido[60]Fullerenes by Nucleophilic Substitutions with 1,2-(2,3-dihydro-1H-azirino)-[60]Fullerene.

[304] J. Averdung, H. Luftmann, I. Schlachter, J. Mattay, *Tetrahedron* **1995**, *51*, 6977-6982. Aza-Dihydro[60]Fullerene in the Gas Phase. A Mass Spectrometric and Quantumchemical Study.

[305] M. R. Banks, J. I. G. Cadogan, I. Gosney, A. J. Henderson, P. K. G. Hodgson, W. G. Kerr, A. Kerth, P. R. R. Langridgesmith, J. R. A. Millar, A. R. Mount, J. A. Parkinson, A. T. Taylor, P. Thornburn, *Chem. Commun.* **1996**, 507-508. Unprecedented Ring Expansion of [60]Fullerene: Incorporation of Nitrogen at an Open 6,6-ring Juncture by Regiospecific Reduction of Oxycarbonylaziridino-[2'3':1,2][60]Fullerenes. Synthesis of 1a-aza-1(6a)-homo[60]Fullerene, $C_{60}H_2NH$.

[306] A. Hirsch, I. Lamparth, H. R. Karfunkel, *Angew. Chem.* **1994**, *106*, 453-455; *Angew. Chem. Int. Ed.* **1994**, *33*, 437-438. Fullerene Chemistry in Three Dimensions - Isolation of Seven Regioisomeric Bisadducts and Chiral Trisadducts of C_{60} and Di(Ethoxycarbonyl)Methylene.

[307] A. Hirsch, I. Lamparth, G.- Schick, *Liebigs Ann.* **1996**, 1725-1734. Regioselectivity of Multiple Cyclopropanations of C_{60} and Introduction of a General Bond-Labeling Algorithm for Fullerenes and their Derivatives.

[308] L. Isaacs, P. Seiler, F. Diederich, *Angew. Chem.* **1995**, *107*, 1636-1639; *Angew. Chem. Int. Ed.* **1995**, *34*, 1466-1469. Solubilized Derivatives of C_{195} and C_{260}: The First Members of a New Class of Carbon Allotropes $C_{n(60+5)}$.

[309] P. J. Fagan, J. C. Calabrese, B. Malone, *J. Am. Chem. Soc.* **1991**, *113*, 9408-9409. A Multiply - Substituted Buckminsterfullerene (C_{60}) with an Octahedral Array of Platinum Atoms.

[310] A. Hirsch, I. Lamparth, T. Grösser, H. R. Karfunkel, *J. Am. Chem. Soc.* **1994**, *116*, 9385-9386. Regiochemistry of Multiple Additions to the Fullerene Core: Synthesis of a T_h-Symmetric Hexakisadduct of C_{60} with Bis(ethoxycarbonyl)methylene.

[311] G. Schick, A. Hirsch, H.- Mauser, T. Clark, *Chem. Eur. J.* **1996**, *2*, 935-943. Opening and Closure of the Fullerene Cage in *cis*-1-Bisimino Adducts of C_{60}: The Influence of the Addition Pattern and the Addend.

[312] F. Djojo, A. Herzog, I. Lamparth, F. Hampel, A. Hirsch, *Chem. Eur. J.* **1996**, *2*, 1537-1547. Regiochemistry of Twofold Additions to [6,6] Bonds in C_{60}: Influence of the Addend-Independent Cage Distortion in 1,2 Monoadducts.

[313] C. C. Henderson, C. M. Rohlfing, R. A. Assink, P. A. Cahill, *Angew. Chem.* **1994**, *106*, 803-805; *Angew. Chem. Int. Ed.* **1994**, *33*, 786-788. $C_{60}H_4$ - Kinetics and Thermodynamics of Multiple Addition to C_{60}.

[314] M. S. Meier, B. R. Weedon, H. P. Spielmann, *J. Am. Chem. Soc.* **1996**, *118*, 11682-11683. Synthesis and Isolation of One Isomer of $C_{60}H_6$.

[315] R. Taylor, *J. Chem. Soc., Perkin Trans. 2* **1993**, 813-824. C_{60}, C_{70}, C_{76}, C_{78} and C_{84}: Numbering, π-Bond Order Calculations and Addition Pattern Considerations.

[316] J. Baker, P. W. Fowler, P. Lazzeretti, M. Malagoli, R. Zanasi, *Chem. Phys. Lett.* **1991**, *184*, 182-186. Structure and Properties of C_{70}.

[317] A. Rathna, J. Chandrasekhar, *Fullerene Sci. Technol.* **1995**, *3*, 681-705. Structures, Stabilities and Strain in C_{60} and C_{70} Derivatives.

[318] B. Kräutler, J. Maynollo, *Angew. Chem.* **1995**, *107*, 69-71; *Angew. Chem. Int. Ed.* **1995**, *34*, 87-88. A Highly Symmetric Sixfold Cycloaddition Product of Fullerene C_{60}.

[319] A. L. Balch, J. W. Lee, B. C. Noll, M. M. Olmstead, *J. Am. Chem. Soc.* **1992**, *114*, 10984-10985. A Double Addition Product of C_{60}: $C_{60}Ir(CO)Cl(PMe_2Ph)_2$2. Individual Crystallization of Two Conformational Isomers.

[320] A. L. Balch, J. W. Lee, B. C. Noll, M. M. Olmstead, *Inorg. Chem.* **1994**, *33*, 5238-5243. Multiple Additions of Vaska-Type Iridium Complexes to C_{60}: Preferential Crystallization of the "Para" Double Addition Products $C_{60}Ir(CO)Cl(PMe_3)_2$2•2C_6H_6 and $C_{60}Ir(CO)Cl(PEt_3)_2$2•C_6H_6.

[321] B. Kräutler, T. Müller, J. Maynollo, K. Gruber, C. Kratky, P. Ochsenbein, D. Schwarzenbach, H.-B. Bürgi, *Angew. Chem.* **1996**, *108*, 1294-1296; *Angew. Chem. Int. Ed.* **1996**, *35*, 1204-1206. A Topochemically Controlled, Regiospecific Fullerene Bisfunctionalization.

[322] M. Rasinkangas, T. T. Pakkanen, T. A. Pakkanen, M. Ahlgrén, J. Rouvinen, *J. Am. Chem. Soc.* **1993**, *115*, 4901. Multimetallic Binding to Fullerenes - $C_{60}(Ir_2Cl_2(1,5\text{-COD})_2)_2$ - A Novel Coordination Mode to Fullerenes.

[323] H.-F. Hsu, J. R. Shapley, *J. Am. Chem. Soc.* **1996**, *118*, 9192-9193. $Ru_3(CO)_9(\mu_3\text{-}\eta^2,\eta^2,\eta^2\text{-}C_{60})$: A Cluster Face-Capping, Arene-like Complex of C_{60}.

[324] I. J. Mavunkal, Y. Chi, S.-M. Peng, G.-H. Lee, *Organometallics* **1995**, *14*, 4454-4456. Preparation and Structure of $Cp^*2Ru_2(\mu\text{-}Cl)(\mu\text{-}X)(C_{60})$, X=H and Cl. Novel Dinuclear Fullerene Complexes with and without Direct Ruthenium-Ruthenium Bonding.

[325] I. Lamparth, B. Nuber, G. Schick, A. Skiebe, T. Grösser, A. Hirsch, *Angew. Chem.* **1995**, *107*, 2473-2476; *Angew. Chem. Int. Ed.* **1995**, *34*, 2257-2259. $C_{59}N^+$ and $C_{69}N^+$: Isoelectronic Heteroanalogues of C_{60} and C_{70}.

[326] B. Nuber, A. Hirsch, *Chem. Commun.* **1996**, 1421-1422. A New Route to Nitrogen Heterofullerenes and the First Synthesis of $(C_{69}N)_2$.

[327] M. Kawaguchi, A. Ikeda, S. J. Shinkai, *J. Chem. Soc., Perkin Trans. 1* **1998**, 2, 179-184. Synthesis and Metal-Binding Properties of [60]Fullerene - Linked Calix[4]arenes : An Approach to "Exohedral Metallofullerenes".

[328] G.-X. Dong, J.-S. Li, T.-H. Chan, *J. Chem. Soc., Chem. Commun.* **1995**, 1725-1726. Reaction of [60]Fullerene with Diethyl Diazidomalonate: A Doubly Bridged Fulleroid.

[329] L.-L. Shiu, K.-M. Chien, T.-Y. Liu, T.-I. Lin, G.-R. Her, T.-Y. Luh, *J. Chem. Soc., Chem. Commun.* **1995**, 1159-1160. Bisazafulleroids.

[330] C. K.-F. Shen, K.-M. Chien, C.-G. Juo, G.-R. Her, T.-Y. Luh, *J. Org. Chem.* **1996**, *61*, 9242-9244. Chiral Bisazafulleroids.

[331] M.-J. Arce, A. L. Viado, Y.-Z. An, S. I. Khan, Y. Rubin, *J. Am. Chem. Soc.* **1996**, *118*, 3775-3776. Triple Scission of a Six-Membered Ring on the Surface of C_{60} via Consecutive Pericyclic Reactions and Oxidative Cobalt Insertion.

[332] P. J. Krusic, E. Wasserman, P. N. Keizer, J. R. Morton, K. F. Preston, *Science (Washington D.C.)* **1991**, *254*, 1183-1185. Radical Reactions of C_{60}.

[333] G. A. Olah, I. Bucsi, C. Lambert, R. Aniszfeld, N. J. Trivedi, D. K. Sensharma, G. K. S. Prakash, *J. Am. Chem. Soc.* **1991**, *113*, 9385-9387. Chlorination and Bromination of Fullerenes - Nucleophilic Methoxylation of Polychlorofullerenes and Their Aluminum Trichloride Catalyzed Friedel-Crafts Reaction with Aromatics to Polyarylfullerenes.

[334] O. V. Boltalina, V. Y. Markov, R. Taylor, M. P. Waugh, *Chem. Commun.* **1996**, 2549-2550. Preparation and Characterization of $C_{60}F_{18}$.

[335] O. V. Boltalina, A. Y. Borschevskii, L. N. Sidorov, J. M. Street, R. Taylor, *Chem. Commun.* **1996**, 529-530. Preparation of $C_{60}F_{36}$ and $C_{70}F_{36/38/40}$.

[336] a) A. A. Gakh, A. A. Tuinman, J. L. Adcock, R. A. Sachleben, R. N. Compton, *J. Am. Chem. Soc.* **1994**, *116*, 819-820. Selective Synthesis and Structure Determination of $C_{60}F_{48}$. b) O. V. Boltalina, L. N. Sidorov, V. F. Bagryantsev, V. A. Seredenko, A. S. Zapol'skii, J. M. Street, R. Taylor, *J. Chem. Soc., Perkin Trans. 2* **1996**, 2275-2278. Formation of $C_{60}F_{48}$ and Fluorides of Higher Fullerenes.

[337] P. R. Birkett, P. B. Hitchcock, H. W. Kroto, R. Taylor, D. R. M. Walton, *Nature (London)* **1992**, *357*, 479-481. Preparation and Characterization of $C_{60}Br_6$ and $C_{60}Br_8$.

[338] F. N. Tebbe, R. L. Harlow, D. B. Chase, D. L. Thorn, G. C. Campbell Jr., J. C. Calabrese, N. Herron, R. J. Young Jr., E. Wasserman, *Science (Washington D.C.)* **1992**, *256*, 822-825. Synthesis and Single-Crystal X-Ray Structure of a Highly Symmetrical C_{60} Derivative, $C_{60}Br_{24}$.

[339] P. R. Birkett, A. G. Avent, A. D. Darwisch, H. W. Kroto, R. Taylor, D. R. M. Walton, *J. Chem. Soc., Chem. Commun.* **1993**, 1230-1232. Preparation and ^{13}C NMR Spectroscopic Characterisation of $C_{60}Cl_6$.

[340] A. G. Avent, P. R. Birkett, J. D. Crane, A. D. Darwish, G. J. Langley, H. W. Kroto, R. Taylor, D. R. M. Walton, *J. Chem. Soc., Chem. Commun.* **1994**, 1463-1464. The Structure of $C_{60}Ph_5Cl$ and $C_{60}Ph_5H$, Formed via Electrophilic Aromatic Substitution.

[341] A. K. Abdulsada, A. G. Avent, P. R. Birkett, H. W. Kroto, R. Taylor, D. R. M. Walton, *J. Chem. Soc., Perkin Trans. 1* **1998**, 393-395. A Hexaallyl[C_{60}]Fullerene, $C_{60}(CH_2CH{=}CH_2)_6$.

[342] M. Sawamura, H. Iikura, E. Nakamura, *J. Am. Chem. Soc.* **1996**, *118*, 12850-12851. The First Pentahaptofullerene Metal Complexes.

[343] Y. Murata, M. Shiro, K. Komatsu, *J. Am. Chem. Soc.* **1997**, *119*, 8117-8118. Synthesis, X-Ray Structure and Properties of the First Tetrakisadduct of Fullerene C_{60} Having a Fulvene π-System on the Spherical Surface.

[344] L. Isaacs, R. F. Haldimann, F. Diederich, *Angew. Chem.* **1994**, *106*, 2434-2437. Tether-Directed Remote Functionalization of Buckminsterfullerene: Regiospecific Hexaadduct Formation. L. Isaacs, R. F. Haldimann, F. Diederich, *Angew. Chem. Int. Ed.* **1994**, *33*, 2339-2342. Tether-directed Remote Functionalization of Buckminsterfullerene: Regiospecific Hexaadduct Formation.

[345] a) R. Breslow, *Acc. Chem. Res.* **1980**, *13*, 170-177. Biomimetic Control of Chemical Selectivity. b) R. Breslow, *Chemtracts: Org. Chem.* **1988**, *1*, 333-348. Biomimetic Regioselective Template-Directed Functionalizations. c) R. Breslow, *Acc. Chem. Res.* **1995**, *28*, 146-153. Biomimetic Chemistry and Artificial Enzymes: Catalysis by Design.

[346] R. Breslow, M. A. Winnik, *J. Am. Chem. Soc.* **1969**, *91*, 3083-3084. Remote Oxidation of Unactivated Methylene Groups.

[347] J. J. P. Stewart, *J. Comput. Chem.* **1989**, *10*, 209-220. Optimization of Parameters for Semiempirical Methods I. Methods.

[348] L. Isaacs, F. Diederich, R. F. Haldimann, *Helv. Chim. Acta* **1997**, *80*, 317-342. Mutilple Adducts of C_{60} by Tether Directed Remote Functionalization and Synthesis of Soluble Derivatives of New Carbon Allotropes $C_{(60+5)n}$.

[349] S. H. Friedman, G. L. Kenyon, *J. Am. Chem. Soc.* **1997**, *119*, 447-448. A Computational Strategy for the Design of Regiospecific Syntheses of Fullerene Derivatives.

[350] C. Boudon, J.-P. Gisselbrecht, M. Gross, L. Isaacs, H. L. Anderson, R. Faust, F. Diederich, *Helv. Chim. Acta* **1995**, *78*, 1334-1344. Electrochemistry of Mono- through Hexakis-Adducts of C_{60}.

[351] P. Seiler, L. Isaacs, F. Diederich, *Helv. Chim. Acta* **1996**, *79*, 1047-1058. The X-Ray Crystal Structure and Packing of a Hexakis-Adduct of C_{60}: Temperature Dependence of Weak C-H O Interactions.

[352] F. Cardullo, P. Seiler, L. Isaacs, J. F. Nierengarten, R. F. Haldimann, F. Diederich, T. Mordasini-Denti, W. Thiel, C. Boudon, J. P. Gisselbrecht, M. Gross, *Helv. Chim. Acta* **1997**, *80*, 343-371. Bis- through Tetrakis-Adducts of C_{60} by Reversible Tether-Directed Remote Functionalization and Systematic Investigation of the Changes in Fullerene Properties as a Function of Degree, Pattern, and Nature of Functionalization.

[353] M. J. S. Dewar, E. G. Zoebisch, E. F. Healy, J. J. P. Stewart, *J. Am. Chem. Soc.* **1985**, *107*, 3902-3909. AM1: A New General Purpose Quantum Mechanical Molecular Model.

[354] P. R. Birkett, A. G. Avent, A. D. Darwish, H. W. Kroto, R. Taylor, D. R. M. Walton, *J. Chem. Soc., Chem. Commun.* **1995**, 1869-1870. Holey Fullerenes! A Bis-lactone Derivative of [70]fullerene with an Eleven-Atom Orifice.

[355] M. L. Mihailovic, Z. Cekovic in 'Encyclopedia of Reagents for Organic Synthesis', Ed. L.A. Paquette, John Wiley & Sons Ltd., West Sussex, England, 1995, p. 2949-2954.

[356] T. Weiske, T. Wong, W. Krätschmer, J. K. Terlouw, H. Schwarz, *Angew. Chem.* **1992**, *104*, 242-244. *Angew. Chem. Int. Ed.* **1992**, *31*, 183-185. The Neutralization of HeC_{60}^+ in the Gas Phase - Compelling Evidence for the Existence of an Endohedral Structure for $He@C_{60}$.

[357] M. Saunders, H. A. Jiménez-Vázquez, R. J. Cross, W. E. Billups, C. Gesenberg, A. Gonzalez, W. Luo, R. C. Haddon, F. Diederich, A. Herrmann, *J. Am. Chem. Soc.* **1995**, *117*, 9305-9308. Analysis of Isomers of the Higher Fullerenes by ^{3}He NMR Spectroscopy.

[358] M. Saunders, H. A. Jiménez-Vázquez, B. W. Bangerter, R. J. Cross, S. Mroczkowski, D. I. Freedberg, F. A. L. Anet, *J. Am. Chem. Soc.* **1994**, *116*, 3621-3622. ^{3}He NMR - a Powerful New Tool for Following Fullerene Chemistry.

[359] M. Saunders, H. A. Jiménez-Vázquez, R. J. Cross, S. Mroczkowski, M. L. Gross, D. E. Giblin, R. J. Poreda, *J. Am. Chem. Soc.* **1994**, *116*, 2193-2194.

Incorporation of Helium, Neon, Argon, Krypton, and Xenon into Fullerenes using High Pressure.

[360] D. M. Guldi, H. Hungerbühler, K.-D. Asmus, *J. Phys. Chem.* **1995**, *99*, 9380-9385. Redox and Excitation Studies with C_{60} Substituted Malonic Acid Diethyl Esters.

[361] D. M. Guldi, K.-D. Asmus, *J. Phys. Chem. A* **1997**, *101*, 1472-1481. Photophysical Properties of Mono- and Multiply-Functionalized Fullerene Derivatives.

[362] T. Hamano, K. Okuda, T. Mashino, M. Hirobe, K. Arakane, A. Ryu, S. Mashiko, T. Nagano, *Chem. Commun.* **1997**, 21-22. Singlet Oxygen Production from Fullerene Derivatives: Effect of Sequential Functionalization of the Fullerene Core.

[363] R. J. Cross, H. A. Jiménez-Vázquez, Q. Lu, M. Saunders, D. I. Schuster, S. R. Wilson, H. Zhao, *J. Am. Chem. Soc.* **1996**, *118*, 11454-11459. Differentiation of Isomers Resulting from Bisaddition to C_{60} Using ^3He NMR Spectroscopy.

[364] F.-G. Klärner, 'Topics in Stereochemistry', 1985, 1-42.

[365] F.-G. Klärner, V. Glock, J. L. Hemmes, *Chem. Ber.* **1990**, *123*, 1869-1879. Mechanism of the Cyclopropane Walk Rearrangement - Syntheses and Properties of 2-Diazopropane Arene Adducts - A Regiospecific N_2 Elimination.

[366] F.-G. Klärner, R. Band, V. Glock, W. A. Konig, *Chem. Ber.* **1992**, *125*, 197-208. Mechanism of the Cyclopropane Walk Rearrangement - Synthesis and Properties of an Optically Active Diazoalkane-Toluene Adduct - A Highly Stereoselective N_2 Elimination.

[367] M. J. S. Dewar, *Angew. Chem.* **1971**, *83*, 850-866; *Angew. Chem. Int. Ed.* **1971**, *10*, 761-776. Aromaticiy and Pericyclic Reactions.

[368] H. E. Zimmermann, *Acc. Chem. Res.* **1971**, *4*, 272-280. The Möbius-Hückel Concept in Organic Chemistry. Application to Organic Molecules and Reactions.

[369] R. Herges, H. Jiao, P. v. R. Schleyer, *Angew. Chem.* **1994**, *106*, 1441-1443; *Angew. Chem. Int. Ed.* **1994**, *33*, 1376-1378. Magnetic Properties of Aromatic Transition States: The Diels-Alder Reactions.

[370] H. Jiao, P. v. R. Schleyer, *Angew. Chem.* **1993**, *105*, 1833-1835; *Angew. Chem. Int. Ed.* **1993**, *32*, 1763-1765. Detailed Theoretical Analysis of the 1,7-Sigmatropic Hydrogen Shift - the Möbius Character of the Eight-Electron Transition Structure.

[371] V. Barone, R. Arnaud, *J. Chem. Phys.* **1997**, *106*, 8727-8732. Diels-Alder Reactions: An Assessment of Quantum Chemical Procedures.

[372] U. Salzner, S. M. Bachrach, Mulhearn. D. C., *J. Comput. Chem.* **1997**, *18*, 198-210. Ab Initio Investigation of the Diels-Alder Reaction Between 2H-Phosphole and Phosphaethene: A model for Phosphole Dimerization.

[373] F. Jensen, *J. Am. Chem. Soc.* **1989**, *111*, 4643-4647. The Walk Rearrangement in Bicyclo[2.1.0]pent-2-ene. An MCSCF Study.

[374] a) K. N. Houk, Y. Li, J. D. Evanseck, *Angew. Chem.* **1992**, 711-738; *Angew. Chem. Int. Ed.* **1992**, *31*, 682-708. Transition Structures of Hydrocarbon Pericyclic Reactions. b) Y. Li, K. N. Houk, *J. Am. Chem. Soc.* **1993**, *115*, 7478-7485. Diels-Alder Dimerization of 1,3-Butadiene - an Ab Initio CASSCF Study of the Concerted and Stepwise Mechanisms and Butadiene Ethylene Revisited. c) K. N. Houk, J. Gonzalez, Y. Li, *Acc. Chem. Res.* **1995**, *28*, 81-90. Pericyclic Reaction Transition States: Passions and Punctilios, 1935-1995.

[375] a) W. R. Roth, O. Adamczak, R. Breuckmann, H. W. Lennartz, R. Boese, *Chem. Ber.* **1991**, *124*, 2499-2521. Resonance Energy Calculation - The MM2ERW Force Field. b) W. R. Roth, F.-G. Klärner, G. Siepert, H. W. Lennartz, *Chem. Ber.* **1992**, *125*, 217-224. Heats of Hydrogenation: Homoaromaticity in Norcaradiene and Cycloheptatriene.

[376] R. F. W. Bader, T. A. Keith, *J. Chem. Phys.* **1993**, 3683. Properties of Atoms in Molecules: Magnetic Susceptibilities.

[377] P. W. Fowler, E. Steiner, *J. Phys. Chem. A* **1997**, *101*, 1409-1413. Ring Currents and Aromaticity of Monocyclic π-Electron Systems C_6H_6, $B_3N_3H_6$, $B_3O_3H_3$, $C_3N_3H_3$, $C_5H_5^-$, $C_7H_7^+$, $C_3N_3F_3$, and C_6F_6.

[378] Z. Zsótér, T. Eszenyi, T. Tímár, *J. Org. Chem.* **1994**, *59*, 672-673. TLC Mesh Column Chromatography - Facile Combination of Vacuum-Driven and Low-Pressure Methods.

[379] A. L. Goodson, C. L. Gladys, D. E. Worst, *J. Chem. Inform. Comput. Sci.* **1995**, *35*, 969-978. Numbering and Naming of Fullerenes by Chemical Abstracts Service.

[380] B. F. Duerr, Y.-S. Chung, W. Czarnik, *J. Org. Chem.* **1988**, *53*, 2120-2122. Syntheses of 9,10-Disubstituted Anthracenes Derived from 9,10-Dilithioanthracene.

Curriculum Vitae

1969	Born on July 6, in Geneva, Switzerland.
1976 - 1982	Primary School in Rüschlikon (ZH).
1982 - 1984	Secondary School in Rüschlikon (ZH).
1984 - 1988	High School at the 'Wirtschaftsgymnasium' in Enge (ZH).
1989 - 1994	Undergraduate chemistry studies at the ETH in Zürich. Diploma thesis with the title "Tether-Directed Functionalisation of Buckminsterfullerene (C_{60})" carried out under the supervision of *L. Isaacs* in the group of Prof. Dr. F. Diederich.
since 1994	Ph.D. studies in organic chemistry in the group of Prof. Dr. F. Diederich.

Zürich, September 1998 Richard F. Haldimann